Ultra-stable ring-type organosilicas with click modifiable groups: application as catalytic support and HPLC packing.

Sander Clerick

Promotors: Prof. dr. Pascal Van Der Voort, Prof. dr. Frederic Lynen.
IOF Advisor: dr. Bart Hommez.

Dissertation submitted in fulfillment of the requirements for the degree of Doctor (PhD) in Sciences: Chemistry

Department of Chemistry
Faculty of Sciences
Ghent University
Academic year 2017-2018

GHENT UNIVERSITY

FACULTY OF SCIENCES

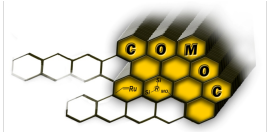

Part of this research was supported by the UGhent Industrial Research Fund (IOF) - F2015 IOF STARTT 104

Promotors

Prof. dr. Pascal Van Der Voort
Department of Chemistry

Prof. dr. Frederic Lynen
Department of Organic and Macromolecular Chemistry

Members of the examination committee

Chair

Prof. dr. Klaartje De Buysser (Universiteit Gent)

Examination Committee

Prof. dr. Damien Debecker (Université catholique de Louvain)
dr. Els De Canck (Recticel Insulation)
Prof. dr. ir. Wim De Malsche (Vrije Universiteit Brussel)
dr. Leszek Gora (Agilent Technologies)
Prof. dr. ir. Christian Stevens (Universiteit Gent)
Prof. dr. ir. Paul Van der Meeren (Universiteit Gent)
Prof. dr. Isabel Van Driessche (Universiteit Gent)

Dankwoord

Aan iedereen die heeft meegeholpen, bedankt! Aan iedereen die niet heeft meegeholpen, ook bedankt!

De Burgemeester

Het is een cliche zo hoog als een huis, maar een doctoraat is niet het werk van één enkele persoon. Ook dit doctoraat kon enkel en alleen tot stand komen door de hulp en steun van vele mensen rondom mij. Hoe vlot het schrijven van dit werk ook mocht verlopen, des te moeilijker is het om iedereen die rechtstreeks of indirect een rol heeft gespeeld in deze 4 jaar op een passende manier te bedanken. Sta mij toe dat ik het toch probeer.

Allereerst wil ik graag mijn promoter Pascal bedanken om mij de mogelijkheid te geven dit onderzoek te verrichten binnen COMOC. Qua financiering is het een vrij hobbelig parcours geweest, maar toch kreeg ik steeds voldoende vrijheid om onderzoek te voeren naar mijn interesses en ideeën. Heel erg bedankt voor dit geschonken vertrouwen.

Daarnaast bedank ik ook Frederic om als co-promotor mee te stappen in het IOF project en mij te voorzien van de nodige begeleiding. Ook wil ik via deze weg Bart van harte bedanken om mee dit project mogelijk te maken en mij op sleeptouw te nemen doorheen het business-gedeelte hiervan. Dit gaf me de mogelijkheid om boeiende ervaringen op te doen naast het wetenschappelijk onderzoek. Ook al werd het uiteindelijk een verhaal van net niet, je geloof in het welslagen van het project en het vertrouwen dat je in me stelde werkte zeer motiverend.

Furthermore, I would like to thank all members of the examination committee for their valuable time and constructive comments. This was of great help to further increase the quality of this work. Next to this, also the invested time and work of the chair is much appreciated.

Also, all of my co-authors are greatly thanked for the fluent collaboration and valued input in (future) publications.

Having a lot of pleasant colleagues makes work no longer feel like an effort and it definitely makes work a lot of fun. Thanks to all of you to provide the unique S3 atmosphere, especially in and around the coffee room which sort of became my second habitat. I'm pretty sure there are not a lot of places around where working is that enjoyable and I genuinely hope it stays this way. It was my pleasure to share the building with you. Of course, I wish everyone the best, but some people I would like to mention more specific.

Eerst en vooral bedankt aan de COMOC collega's die er van in het begin bij waren (toen de schuif minder bestendig was tegen de hitte dan verwacht). Els (intussen al uw 3^e vermelding zeker?), merci om mij vanaf dag 1 onder uw vleugels te nemen. Hannes, Kevin, we zijn als 3 musketiers gestart, en zo zullen we ook ons doctoraat afronden. Jeroen, Judith, Isabelle, Wannes, Thomas, Matthias, Karen,... het moet vreselijk geweest zijn om dag in dag uit naar mijn gezwans, gezwets, gezever, gezaag en geroddel te moeten luisteren, maar het feit dat de meesten van jullie het bureau niet ontvlucht zijn betekent ergens dat het toch nog een leutige periode moet geweest zijn, niet? Ik heb alleszins, voorlopig dan toch, de tijd van mijn leven gehad.

Bedankt ook aan het ATP voor de familiale sfeer en om er voor te zorgen dat ik überhaupt iets kon uitrichten in het labo. Hoewel, er is gelukkig ook veel tijd verloren gegaan aan aangename babbels. Ik wens jullie het volgende toe: Pierre, dat ge nog veel "Allez jong"moogt roepen in de aanwezigheid van alle verse doctoraatstudentjes. Sorry, maar mijn antwoord op uw vraag blijft "Euhm, neen". Kathleen, ik hoop voor u dat bovenstaande zich een beetje blijft gedragen. Het is en blijft immers een instelling. Tom, ik hoop uit de grond van mijn hart de uw pelouze gespaard blijft van mollen en roste plekken. Pat, dat er nog veel dozen in uw bureau gedropt mogen worden en succes met uw handeltje in namaak-Gucci's. Bart (of was het BALT?), leg u nog goed plat in de bochten, maar niet te plat, en als ge plat hebt gelegen, laat u goed soigneren. Funda, sterkte tussen al die charels ginder. Hou het schip recht. Katrien, nog veel fermenteerplezier bij de boerinnenbond en bedankt voor de TEM-beeldjes. Ilse, mogen uw taartjes en cakes nog velen verblijden. Philip, ik hoop dat de printer al uw werk nog lang volhoudt. Els B, hopelijk neemt het aantal PhDs om practica onder te verdelen snel toe. Bernard, dat je nog veel van de voorgaanden onder je vleugels mag nemen en entertainen met boeiende wetenschappelijk babbeltjes tijdens de practica. Chokri, bedankt om samen met uw vrouwke de boel een beetje proper te houden, het zou anders nogal een bende worden.

Ook enkele andere collega's, intussen uitgegroeid tot vrienden, wil ik niet sparen: JJ, brejen, met u ga ik geen spel zoeken na al uw work-outs in de fitness en uw fors toegenomen biceps. Vanzeel, hopelijk kleuren veel oranje zieltjes uw bolleke in 2018, en anders bel ik wel eens met de grote voorzitter voor uw plekje op de lijst in 2019. Hannes R, merci voor uw FIB-SEM plaatje maar geeft uwen bal af, ah neen, sorry, ok, ge hebt gescoord. Glenn, Kenny, Jonas Feys, Joni, Fady, bedankt voor de kameraderie, het lawaai in de coffeeroom, een fanatastisch thesisjaar, de schone filmkes op Whatsapp, shoulder massages, etc. Mieke, Katrien, bedankt om samenwerken met sommige bovenstaanden toch enigszins draaglijk te maken. Mathijs en Pieter, bedankt om steeds klaar te staan om te antwoorden op mijn spervuur van vragen.

Naast een doctoraat is er natuurlijk ook tijd voor ontspanning. Bedankt aan alle vrienden bij wie ik steeds terecht kon voor amusement. De Sportclub "Pilleuh Kopeuh", PJ, de Wurtel, de Tettegem-gang, hoog tijd dat we nog eens iets gaan drinken, een traktatie wacht op jullie. Daarnaast ook merci aan mijn voetbalploegen, Steaua ('t volgende rondje Tongerlo van't vat is van mij), Car Wash, Meeting en de zondagsresereven van Tenstar, om de nodige sportiviteit te voorzien.

Tenslotte, wil ik ook mijn ouders, Carine en Alex, meme Lucienne, Diane en Robert, Greta en Ignace, en mijn tantes, nonkels, neven en nicht(en) bedanken voor de familiale warmte die ik altijd heb mogen ervaren. Ma, Pa, ik vermoed dat jullie ergens wel trots zijn op wat ik bereikt heb, maar weet dat dit grotendeels komt door jullie. Bedankt voor jullie goede zorgen en om mij een goede, verstandige en rationele mentaliteit en ingesteldheid mee te geven.

En dan rest mij enkel nog Ianthe te bedanken, als allerbelangrijkste, om ettelijke keren alleen ons huis te kuisen, veelvuldig alleen naar de winkel te moeten en telkens zonder hulp het eten te moeten maken terwijl ik dit boekje aan het schrijven was. Maar vooral, zonder melig te worden, te zijn wie je bent, me steeds te steunen. Merci, liefje loetie poepie zoetie!

I'm so glad that I know more than I knew then
Gonna keep on tryin'
Till I reach my highest ground

Steveland Hardaway Judkins

Sander Clerick
Gent, 5 december 2017

Outline

This dissertation is split up into three parts which are further subdivided in introductory, experimental and concluding chapters.

In **Part I**, the development of a novel organosilane precursor is discussed, which might offer a solution for issues currently associated with organosilica research. Within this first part, (Periodic) Mesoporous Organosilicas or PMOs are introduced as an advanced class of porous materials, with special focus on their synthesis and limitations. With this in mind, we propose the synthesis of a novel organosilane precursor with high potential in terms of stability and versatility.

In **Part II**, this 'ultimate' precursor is applied for the synthesis of a PMO optimized as catalytic support. After introducing the use of PMOs in catalysis, we recommend click chemistry for the modification of the pore surface into a 'solid ligand'. Thereafter, a Ru(III)-complex is anchored and the porous material is used as a highly stable, non-leaching heterogeneous catalyst in an aqueous oxidation reaction.

In **Part III**, synthesis pathways are explored to transform the newly developed precursor into an ultra-stable chromatographic packing. First, the fundamentals of chromatography are presented to raise awareness for the specifications organosilica particles should possess to be applicable as HPLC stationary phase. Synthetic approaches for silica-based materials are described and initial efforts to produce such organosilica particles are given. In **Chapter 7**, a co-template co-solvent method is investigated to obtain fully porous particles, while in **Chapter 8** the synthesis of core-shell type particles is attempted. Finally, in **Chapter 9**, a water-in-oil emulsion is exploited to generate spherical porous particles and chromatographic experiments with emphasis on stability are performed.

Contents

Summary

Organosilicas or polysilsesquioxane frameworks are attractive alternatives for commonly applied silica-based materials. Due to their increased hydrolytic stability and embedded organic functionalities, organosilicas have successfully been applied in many fields of research. In this work, a deliberate suggestion towards an ultimate organosilica precursor in terms of versatility and stability is made. Regarding the difficulties and somewhat trial and error approach inherent to the synthesis of organosilicas and their ordered counterparts (Periodic Mesoporous Organosilicas or PMOs), one single precursor is desirable. As a start, and to obtain maximum hydrolytic stability, the $[Si(CH_2)]_3$ ring or 1,1,3,3,5,5-hexaethoxy-1,3,5-trisilacyclohexane (HETSCH) precursor is selected as the base. Although this molecule is known to provide unprecedentedly high stability, it is clear that it has one major drawback. It has no useful functionality. Therefore, if a distinct functional group is required, one would need to revert to grafting of the silanols. This is not favorable, as such grafted group is removed at low pH, which, as a result, renders the material useless in such conditions. Instead, the attachment of a functionality onto the methylene-bridged ring allows to circumvent the grafting approach.

Functionalization of the $[Si(CH_2)]_3$ ring precursor is obtained through the deprotonation of the methylene group with t-butyl lithium (tBuLi) and reacting this with a functional electrophile. The aim of this work is to develop one single precursor in which a reactive functional handle is incorporated. An allyl group is a useful choice, as this would allow many options for hydrolytically stable post-modifications. All taken in consideration, by combining a base structure recognized for its stability and attaching a versatile functionality, 2-allyl-1,1,3,3,5,5-hexaethoxy-1,3,5-trisilacyclohexane (AHETSCH) has the potential to yield highly adaptable materials with exceptional hydrolytic and hydrothermal stability.

This novel precursor is employed to develop the ultimate catalytic support for organic reactions in water. Such support would require large, or-

dered pores and a high surface area together with high structural stability and leach-proof functionalities. We present the hydrothermal synthesis of an AHETSCH-based 100% monoallyl ring-type PMO (mAR) optimized for catalytic applications, using P123 as pore generating surfactant to create uniform and large ordered pores. Via thiol-ene click chemistry and employing reagents of the form $HS-(CH_2)_2-X$, with X = NH_2, OH, SH, the allyl groups protruding in the pores are transformed into three distinct bidentate thioether ligands.

Experiments and theoretical calculations confirm the heterogenization of a Ru(III)-complex onto these solid ligands. Although protonation of the amine group in the acidic catalytic medium causes leaching for mAR-SNH_2-Ru; mAR-SOH-Ru and mAR-SSH-Ru are successfully applied as selective, truly heterogeneous catalysts in the oxidation of cyclohexanol in water at 25°C. Moreover, the hydrophobic/hydrophilic reaction environment and ordered pores of the mAR-support enable high catalytic activity for a poorly water-soluble and sterically very challenging substrate such as (±)-menthol.

For application in chromatography, the AHETSCH organosilica precursor gives rise to materials that inherently have a high hydrolytic stability, combining unprecedented resistance against high pH and providing stability at elevated temperatures. Again, the incorporated allyl group grants the opportunity for stable and efficient click modification of the particle surface. Hereby, also modifications, such as functional and chiral groups, which are not easily anchored through classic chemistries are easily accessible. The challenge remains, however, the synthesis of materials with all appropriate specifications, preferably tunable, in terms of morphology, porosity and mechanical stability to be suitable for HPLC.

In this dissertation, three methods are explored to obtain AHETSCH organosilica particles with the aim to be highly resemblant of current commercial materials while taking tunability, adaptability and ease of the synthesis into account. Monodisperse spherical particles of 3 to 5 μm with large mesopores are targeted to allow chromatographic evaluation with a common HPLC set-up.

Employing a co-template co-solvent system, the synthesis of fully porous AHETSCH spheres is attempted, but, despite of a plethora of experiments, we were not able to obtain particles that satisfy the stringent properties we have set out. Porous organosilica shell - SiO_2 core particles, in turn, benefit from the uniform morphology of the core material. However, the instability of the SiO_2 cores and the simultaneous control

of porosity and morphology remained insurmountable.

Using a water-in-oil emulsion, we have developed a new method to obtain micron-sized spheres of mesoporous organosilicas. Herein, it is clear that the emulsion droplet acts as a micro-environment, which controls size and shape of the synthesized particle, while an organosilica gel is formed inside the droplet. By means of stirring rate, we show a very easy way to control the particle size, which would allow application of the spheres from UHPLC to preparative LC. Various organic functionalities can be incorporated within the particle framework, some of which bear reactive groups allowing further modification of the pore surface with other functional groups of interest. Finally, we show that not only the particle size is tunable, but that porosity can readily be engineered by either the amount of precursor added or the amount of acid catalyst used. Altogether, the flexibility and versatility of this novel synthesis procedure allows the creation of tailor-made hybrid materials providing opportunities primarily as chromatographic packing, but also as catalytic carrier or controlled drug release matrix.

Based on the above method, we have developed a prosperous chromatographic packing using a 50-50 precursor mixture of HETSCH and AHETSCH. The embedded allyl functionalities of the latter allowed for the click modification with a C18 group, commonly used for reverse phase HLPC. Separation of complex mixtures was successful and high hydrolytic stability was demonstrated at high temperatures and over an unprecedentedly broad pH range at elevated temperatures. This shows that not only the particle framework, but also the clicked surface modification is stable from at least pH 0.85 to pH 12 and up to 140°C at pH 7 under analytical column pressures. Moreover, in vitro investigations of unmodified $[Si(CH_2)]_3$-ring particles indicate that pH stability might potentially be as high as pH 0 and pH 12.5, while under neutral conditions analysis temperatures of up to 160°C might be reachable.

Click modification of the organosilica surface offers the chance to create stationary phases with a plethora of different bonded functionalities, e.g. highly polar or ionic groups, chiral moieties, etc., that are unachievable through classic grafting of the silanols. Given that the thioether functionality is stable under the harsh conditions applied, this might offer opportunities for the development of completely new chromatograpic methods and specialized separations. Next to this, the exceptional hydrothermal stability of the packing permits ultra-fast separations ($<$ 2 min) which might, in the long term, turn HPLC to an almost instantaneous analysis technique.

Samenvatting

Organosilicas of polysilsesquioxane netwerken zijn aantrekkelijke alternatieven voor veel gebruikte silica gebaseerde materialen. Door hun verhoogde hydrolytische stabiliteit en ingebouwde functionaliteiten zijn organosilicas reeds succesvol ingezet in vele onderzoeksdomeinen. In dit werk wordt eerst een weloverwogen suggestie gedaan naar de ultieme organosilica precursor inzake stabiliteit en veelzijdigheid. Gezien de moeilijkheden en de *trial en error* methode inherent aan de synthese van organosilica's en PMO's, wordt één enkele precursor beoogd. Als start, en om een zo groot mogelijke hydrolytische stabiliteit te verkrijgen, wordt de $[Si(CH_2)]_3$ ring of 1,1,3,3,5,5-hexaethoxy-1,3,5-trisilacyclohexaan (HETSCH) precursor gekozen als basis. Hoewel deze molecule ervoor gekend staat een ongekende stabiliteit te voorzien, heeft deze een duidelijk gebrek, zijnde de afwezigheid van een toegevoegde functionaliteit. Daarom, indien een uitgesproken functionele groep nodig is, moet men teruggrijpen naar het modificeren van de silanol groepen. Dit is niet gewenst, daar dergelijke groep verwijderd wordt bij lage pH, met als gevolg dat het materiaal zijn functionaliteit verliest bij deze condities. In plaats daarvan staat het verankeren van een functionele groep aan de methyleen-brug van de ring toe om dit type modificatie te omzeilen.

Functionalizatie van de $[Si(CH_2)]_3$ ring precursor wordt verkregen door de deprotonering van de methyleen groep met t-butyl lithium en dit te reageren met een functioneel electrofiel. Aangezien het de bedoeling is één enkele precursor te ontwikkelen en dus een reactief functioneel handvat in te voeren, is een allyl groep een goede keuze, aangezien deze een velerlei aan hydrolytisch stabiele modificaties toelaat. Alles samen, heeft 2-allyl-1,1,3,3,5,5-hexaethoxy-1,3,5-trisilacyclohexane (AHETSCH), verkregen door de combinatie van een stabiele basisstructuur en de aanhechting van een veelzijdige groep, het potentieel om sterk aanpasbare materialen te verkrijgen met uitzonderlijke hydrolytische en hydrothermale stabiliteit.

Deze nieuwe precursor is gebruikt om de ultieme katalytische drager

voor organische reacties in water te ontwikkelen. Dergelijke drager behoeft grote en geordende poriën en een groot oppervlak, samen met een grote structurele stabiliteit en uitloog-bestendigde functionaliteiten. Wij stellen de hydrothermale synthese van een AHETSCH-gebaseerde 100% monoallyl ring-type PMO (mAR) voor, dewelke geoptimaliseerd is voor katalytische toepassingen door het gebruik van P123 als porie genererend surfactant voor grote geordende poriën. Met behulp van thiol-een click chemie en reagentia van de vorm $HS-(CH_2)_2-X$, met $X = NH_2$, OH, SH, worden de allyl groepen die in de poriën aanwezig zijn, getransformeerd in drie uitgesproken thioether liganden.

Experimenten en theoretische berekeningen bevestigen de heterogenizatie van een Ru(III)-complex aan deze vaste liganden. Hoewel protonering van de amine groep bij mAR-SNH_2-Ru ervoor zorgt dat uitloging veroorzaakt wordt in het zuur katalytisch medium, zijn mAR-SOH-Ru en mAR-SSH-Ru succesvol gebruikt als selectieve en heterogene katalysatoren in de oxidatie van cyclohexanol in water bij 25°C. Bovendien zorgen de reactieomgeving en geordende poriën ervoor dat hoge kataytische activiteit optreedt zelfs voor beperkt wateroplosbare en sterisch uitdagende substraten zoals (±)-menthol.

Voor gebruik in chromatografie geeft AHETSCH eveneens aanleiding tot materialen met een grote hydrolytische stabiliteit door combinatie van ongeziene resistentie tegen hoge pH en verhoogde temperaturen. Opnieuw staat de geïncorporeerde allyl groep stabiele en efficiënte modificatie van het porie oppervlak toe. Hierdoor zijn ook modificaties mogelijk die niet eenvoudig te verankeren zijn op de klassieke manier. De uitdaging blijft nu de synthese van materialen met alle benodigde specificaties, het liefst aanpasbaar, inzake morfologie, porositeit en mechanische stabiliteit, om inzetbaar te zijn in HPLC.

In dit proefschrift worden drie methodes onderzocht om AHETSCH organosilica partikels te verkrijgen met als doel om sterk gelijkend te zijn op huidige commerciële materialen, terwijl rekening gehouden wordt met aanpasbaarheid en eenvoud van synthese. Monodisperse sferische partikels van 3 tot 5 μm met grote mesoporiën worden beoogd om chromatografische analyze toe te staan met een doorsnee HPLC opstelling.

Gebruik makend van een co-templaat co-solvent systeem werd de synthese van volledig poreuze AHETSCH partikels gepoogd, maar, desondanks vele experimenten, zijn we er niet in geslaagd aan de strenge eisen te voldoen. Poreuze organosilica schil - silica kern partikels daarentegen profiteren van de uniforme morfologie van deze laatste, hoewel de instabiliteit van de SiO_2 kernen en de gelijktijdige controle van porositeit en

morfologie onoverkomelijk bleek.

Door een water in olie emulsie te gebruiken daarentegen, hebben we een nieuwe methode ontwikkeld om organosilica microsferen te maken. Hierbij is het duidelijk dat de emulsie druppels optreden als microreactoren die de vorm en grootte van de partikels controleren, terwijl een organosilica gel gevormd wordt binnenin. Met de roersnelheid tonen we een erg eenvoudige manier aan om de partikel grootte te wijzigen. Dit laat mogelijk toe de partikels te gebruiken van UHPLC tot preparatieve LC. Verschillende organische functionaliteiten kunnen worden geïncorporeerd in het skelet van het partikel. Sommigen daarvan dragen reactieve groepen dewelke verdere modificatie toestaan met andere interessante functionaliteiten. Tenslotte tonen we aan dat niet enkel de partikelgrootte aanpasbaar is, maar ook dat de porositeit gemakkelijk kan gemanipuleerd worden door middel van de hoeveelheid gebruikte precursor of de hoeveelheid gebruikte katalysator. Alles samen staat de flexibiliteit van deze nieuwe methode toe om op maat gemaakte hybride materialen aan te maken dewelke mogelijkheden bieden als vooral als chromatografische pakking, maar ook als katalytisch drager of als matrix voor de gecontroleerde afgifte van medicijnen.

Gebaseerd op de bovenstaande methode hebben we voort een veelbelovend chromatografisch materiaal ontwikkeld uitgaande van een 50-50 precursor mengsel van HETSCH en AHETSCH. Dit laat toe om de ingebouwde allyl groepen te click modificeren met een C18 groep welke standaard gebruikt wordt in omkeerfase HPLC. Scheiding van complexe mengsels was succesvol en een hoge hydrolytische stabiliteit werd aangetoond bij zeer hoge analyse-temperaturen en over een onuitgegeven breed pH gebied bij verhoogde temperatuur. Dit toont aan dat niet enkel het partikel zelf maar ook de verankerde groep stabiel is tenminste van pH 0.85 tot pH 12 en tot 140°C, bij analytische druk van de kolom. Meer nog, onderzoek *in vitro* van ongemodificeerde $[Si(CH_2)]_3$-ring partikels toonde aan dat de pH stabiliteit potentieel van pH 0 tot pH 12.5 ligt, terwijl bij neutrale pH analyze temperaturen tot 160°C mogelijk moeten zijn.

Click modificatie van het organosilica oppervlak reikt de mogelijkheid aan om stationaire fasen te creëren met een overvloed aan verschillende gebonden groepen zoals sterk polaire, ionische of chirale groepen, dewelke niet beschikbaar zijn door klassieke silanol verankering. Gegeven dat de thioether groep stabiel is onder de harde condities die toegepast werden, opent dit mogelijkheden voor de ontwikkeling van volledig nieuwe chromatografische methoden en gespecialiseerde scheidingen. Hiernaast staat de uitzonderlijk hydrothermale stabiliteit van de pakking toe om

ultra-snelle scheidingen (< 2 min) uit te voeren, dewelke er op termijn toe kunnen leiden dat HPLC een bijna ogenblikkelijke analyse-techniek wordt.

List of Publications

The contents of this work have been published as followed:

- S. Clerick, E. De Canck, K. Hendrickx, V. Van Speybroeck and P. Van Der Voort, "Heterogeneous Ru(III) oxidation catalysts via 'click' bidentate ligands on a periodic mesoporous organosilica support", *Green Chemistry* **2016**, 59, 6035-6045
- S. Clerick, E. De Canck, S. Lanke, J. Trébosc, O. Lafon, F. Lynen and P. Van Der Voort, "Porosity control and hydrolytic study of water-in-oil emulsion based spherical mesoporous organosilica particles", ready for submission.
- S. Clerick, M. Baert, J. Ouwehand, E. De Canck, P. Van Der Voort and F. Lynen, "A robust W/O emulsion method for the synthesis of spherical organosilica gel particles: Evaluation of a C18 HPLC stationary phase under extreme pH and temperatures.", ready for submission.
- S. Clerick, E. De Canck, K. Hendrickx, V. Van Speybroeck and P. Van Der Voort, "Heterogeneous Ru(III) oxidation catalysts via 'click' bidentate ligands on a periodic mesoporous organosilica support", Oral presentation, Multifunctional, Hybrid and Nanomaterials (HYMA 2016), March 6-10, 2016, Lisbon, Portugal

The author also contributed to the following works:

- S. Clerick, W. Libbrecht, O. van den Berg, E. De Canck, J. De Clercq and P. Van Der Voort, "A novel malonamide Periodic Mesoporous Organosilica (PMO) for tuneable ibuprofen release", *Advanced Porous Materials* **2014**, 2, 1-8
- A. Ryzhikov, T.J. Daou, H. Nouali, J. Patarin, J. Ouwehand, S. Clerick, E. De Canck, P. Van Der Voort, J.A. Martens, "Periodic mesoporous organosilicas as porous matrix for heterogeneous

lyophobic systems", *Microporous and Mesoporous Materials* **2018**, 260, 166-171.

- W.Y. Hernandez, K. De Vlieger, S. Clerick, P. Van Der Voort, A. Verberckmoes, "One-pot preparation of Ni-Cu nanoparticles supported on γ-Al_2O_3 as selective and stable catalyst for the Guerbet reaction of 1-octanol", *Catalysis Communications* **2017**, 98, 94-97

- G. Pollefeyt, S. Clerick, P. Vermeir, P. Lommens, K. De Buysser and I. Van Driessche, "Influence of Aqueous Precursor Chemistry on the Growth Process of Epitaxial $SrTiO_3$ Buffer Layers", *Inorganic Chemistry* **2014**, 53, 10, 4913-4921

- G. Pollefeyt, S. Clerick, P. Vermeir, J. Feys, R. Huhne, P. Lommens and I. Van Driessche, "Ink-jet printing of $SrTiO_3$ buffer layers from aqueous solutions", *Superconductor Science and Technology* **2014**, 27, 9, 095007

- S. Clerick, W. Libbrecht, O. van den Berg, E. De Canck, J. De Clercq and P. Van Der Voort, "A novel malonamide Periodic Mesoporous Organosilica (PMO) for tuneable Ibuprofen release", Poster presentation, Meeting of the Dutch Zeolite Association (DZA 2014), October 7, 2014, Ghent, Belgium

- S. Clerick, W. Libbrecht, O. van den Berg, E. De Canck, J. De Clercq and P. Van Der Voort, "A novel malonamide Periodic Mesoporous Organosilica (PMO) for tuneable Ibuprofen release", Poster presentation, Advanced Complex Nanoporous Materials (ACIN 2015), July 13-17, 2015, Namur, Belgium

List of Abbreviations

α	Separation factor, selectivity
AAS	Atomic Absorption Spectroscopy
AH	Auto-hydrophobization
AHETSCH	2-allyl-1,1,3,3,5,5-hexaethoxy-1,3,5-trisilacyclohexane
AlPO	Aluminophosphate
APTES	3-aminopropyltriethoxysilane
ARHH	Hydrothermally and hydrolytically treated allyl-ring particles
ARHHC18	C18 modified, ARHH particles
BSSE	Basis Set Superposition Error
BTEB	Bis(triethoxysilyl)benzene
BTEE	Bis(triethoxysilyl)ethane
BTEEe	Bis(triethoxysilyl)ethane
C18SH	1-Octadecanethiol
CHNS	Carbon Hydrogen Nitrogen Sulphur
CIP	Cleaning in Place
COF	Covalent Organic Framework
CP-MAS	Cross-Polarization Magic Angle Spinning
CSmAR	Core-shell monoallyl ring particle
CTAB	Cetyltrimethylammonium bromide
$D_{90/10}$	Size dispersion
$d_{p,BJH}$	Pore diameter following Barrett-Joyner-Halenda
d_{part}	Particle diameter
DDA	Dodecylamine
DFT	Density Functional Theory
DMDA	N,N-dimethyldecylamine
DMPA	2,2-dimethoxy-2-phenylacetophenone
DRIFTS	Diffuse Reflectance Infrared Fourier Transform Spectroscopy
DTAB	Dodecyltrimethylammonium bromide
EDX	Energy Dispersive X-ray
EISA	Evaporation Induced Self-Assembly
EXAFS	Extended X-ray Absorption Fine Structure
FCC	Fluid Catalytic Cracking
FWHM	Full Width at Half Maximum
GC	Gas Chromatography
H	Plate height
HETSCH	1,1,3,3,5,5-hexaethoxy-1,3,5-trisilacyclohexane
HF	Hot filtration
HLB	Hydrophilic-Lipophilic Balance

HILIC	Hydrophilic Interaction Liquid Chromatography
HMDS	Hexamethyldisilazane
(U)HPLC	(Ultra) High Performance Liquid Chromatography
ICP-MS	Inductively Coupled Plasma Mass Spectrometry
IEC	Ion-exchange Chromatography
K	Nernst partitioning factor
k	Retention factor
LbL	Layer by layer
mAR	Monoallyl ring-type PMO
MCM	Mobil Composition of Matter
MOF	Metal Organic Framework
MPS	Mesoporous silica
N	Plate number
NMR	Nuclear Magnetic Resonance
NP	Nanoparticle
NP-LC	Normal-phase Liquid Chromatography
OTAC	Octadecyltrimethylammonium chloride
PEG	Polyethyleneglycol
PEO	Polyethyleneoxide
PES	Polyethoxysiloxane
PMO	Periodic Mesoporous Organosilica
PPO	Polypropyleneoxide
PREP	Preparative
R_s	Resolution
RP-LC	Reverse-phase Liquid Chromatography
S_μ	Micropore surface area
S_{BET}	Specific surface area following Brunauer-Emmett-Teller
SAPO	Silico-aluminophosphate
SBA	Santa Barbara Amorphous
SDA	Structure Directing Agent
SDS	Sodiumdodecylsulfate
SEC	Size Exclusion Chromatography
SEM	Scanning Electron Miscroscope
sphmAR	Spherical mono allyl ring particle
ST80	Mixture of SPAN80 and TWEEN80
t_R	Retention time
TEA	Triethylamine
TEM	Transmission Electron Microscope
TEOS	Tetraethylorthosilicate
TFA	Trifluoroacetic acid
TLC	Thin Layer Chromatography
TMB	1,3,5-Trimethylbenzene
TMOS	Tetramethylorthosilicate
TMS	Tetramethylsilane
TOF	Turnover Frequency
TON	Turnover Number
TPR	Temperature-Programmed Reduction
V_p	Pore volume
XANES	X-ray Absorption Near Edge Structure
XPS	X-ray Photoelectron Scattering
XRF	X-Ray Fluorescence Spectroscopy
XR(P)D	X-Ray Powder Diffraction

Part I

Development of a novel ring-type organosilane precursor with allylic functional handle

Chapter 1

Introduction on (Periodic) Mesoporous Organosilicas

1.1 Preface on porous materials

In our day to day life, porous materials are all around us with diapers, cat litter, sponges and filters to name a few. Less obvious, many other daily life products and objects have encountered porous materials during its life cycle or manufacturing process, albeit indirectly, as many raw materials in the chemical industry are made using a porous catalyst.

Perhaps the most important example is the Fe_3O_4/FeO/Fe-catalyst used in the Haber-Bosch process, which has a porous surface generated by the reduction of a solid magnetite particle. A second process of primordial importance is Fluid Catalytic Cracking (FCC) to transform crude oil into shorter carbon chains (e.g. petrol or polymer feedstocks). For this reaction, at very large scale, zeolites, an early 'class' of porous materials, are commonly employed. Zeolites are simple, cheap and available in bulk. However, for more advanced applications in catalysis, separation, adsorption, etc., their properties (microporous, no organic functionality,...) do not suffice. Researchers have therefore developed a plethora of other, advanced materials, e.g. Metal Organic Frameworks (MOFs), Covalent Organic Frameworks (COFs), mesoporous carbon, metal oxides and silica, as valuable alternatives (**Figure 1.1**). All have significant benefits but also bear disadvantages in common, mainly cost and scalability. Furthermore most of these examples suffer from material specific drawbacks such as stability.

From these, mesoporous silicas (MPS) are especially intriguing. MPS chemically resemble zeolites to a certain extent but, they have significantly larger and tunable mesopores (2-50 nm). Hereby, they are able to accommodate far larger (bio)molecules, allowing for applications which are impossible to perform within the micropores of zeolites. Furthermore, distinct organic functionalities of interest can be attached to target specific applications in adsorption, separation or catalysis. Despite their high versatility, adaptability and resolved (well-known) structure, the silica framework of MPS lacks hydrolytic stability. As a consequence, MPS can typically not be employed in boiling water, nor at a high or very low pH [1, 2]. But that was about to change with the discovery of Mesoporous Organosilica materials (bridged polysilsesquioxanes) in 1989 [3] and of Periodic Mesoporous Organosilicas (PMOs) ten years later [4–6].

From the plethora of porous materials existing nowadays, Mesoporous Organosilicas, and their counterpart with ordered pores, Periodic Mesoporous Organosilicas (PMOs), are some of the most versatile and advanced. These 'hybrid' organic-inorganic materials differ from their MPS predecessors through the embedment of an organic functionality inside the silica framework making the organic group a structural part of the material. Often referred to as organic 'bridge', the functionality of choice, determined by the selection of silane precursor, is effectively located as a bridge in between two silicon atoms. This renders a polysilsesquioxane $[RSiO_{3/2}]_n$ framework, in which R is the incorporated organic group, instead of a siloxane network SiO_2 (**Figure 1.2**). Next to functionality,

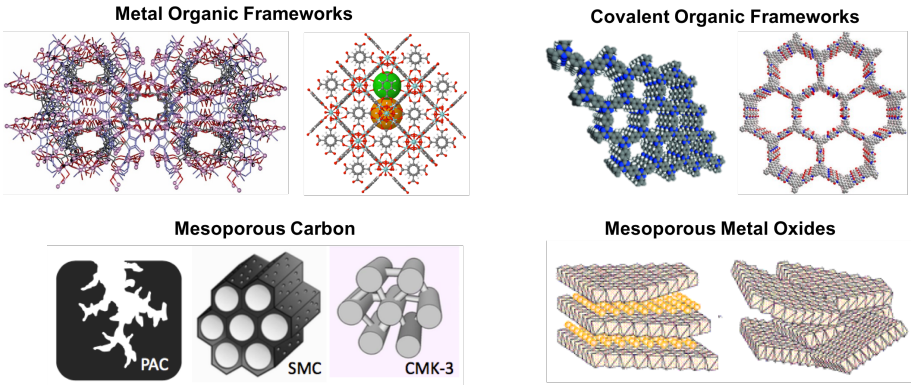

Figure 1.1: Graphic representation of present-day porous materials: MOFs (top left), COFs (top right), mesoporous carbon (bottom left) and mesoporous metal oxides (bottom right).

this latter R group also introduces very attractive properties for envisaged applications. Therefore, in applications where a combination of high stability, adaptability and functionality is required, organosilicas are emerging as relevant alternatives for current technologies (**Figure 1.3**). Accordingly, they have been applied as catalysts or catalytic supports (Part II) and as chromatographic phases (Part III) but also as low-k materials, adsorbents, membranes,...

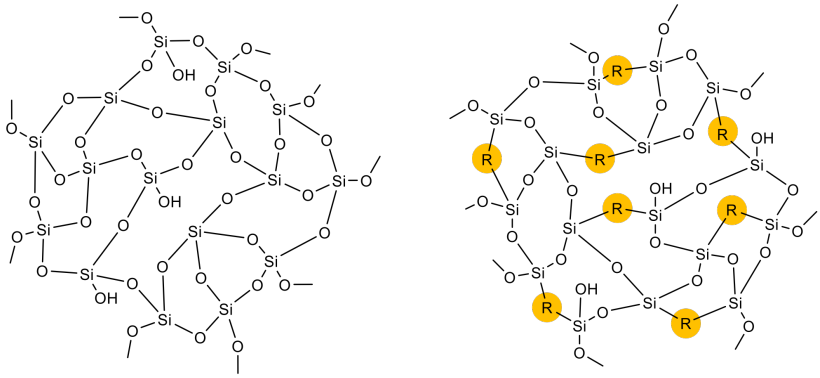

Figure 1.2: Chemical structure of a siloxane SiO_2-network (left) and a polysilsesquioxane $[RSiO_{3/2}]_n$-framework with incorporated R-groups.

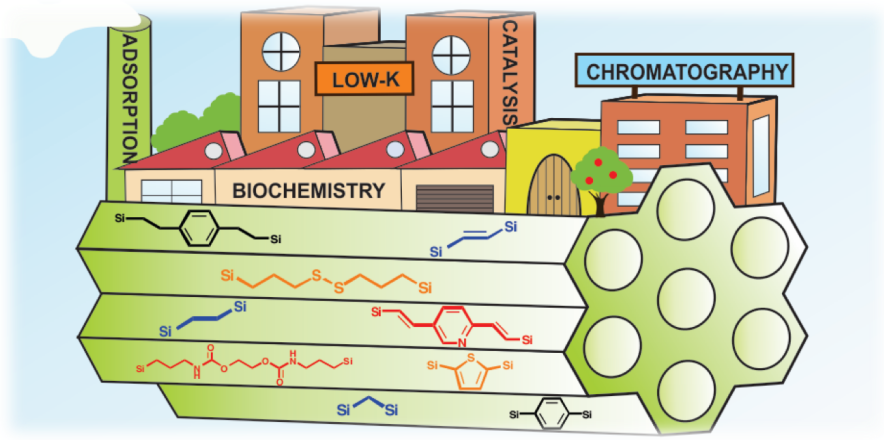

Figure 1.3: Overview: the fields of application for organosilica materials [7].

In what follows, the general sol-gel synthesis of Mesoporous Organosilicas and PMOs will be described and some possibilities for property control during the synthesis are provided. Furthermore, an overview of the most

important or intriguing functional bridges will be given together with some selected applications. However, the aim of this introduction is not to give a comprehensive overview of all existing materials, syntheses, adaptations or applications, as many high level reviews have been published on this matter [7–18]. Instead, by explaining all concepts concerning porous organosilicas, here the final aim is to eventually define our suggestion for the ultimate organosilica precursor and its successive porous solid(s).

1.2 Polysilsesquioxane frameworks or Mesoporous Organosilicas through sol-gel chemistry

The sol-gel chemistry driving the formation of silicate materials and silica gels is almost known for a century [19–22]. However, only in 1989, Shea et al. were the first to employ bis-silanes ($X_3Si{-}R{-}SiX_3$, with X denoting a hydrolysable group, usually ethoxy or methoxy groups and R the functional organic linker) as silicon source, to obtain a porous polysilsesquioxane framework with aryl-bridges [3]. In a first step, the precursor is (partially) hydrolyzed with the formation of a hydroxysilyl (Si−OH) group (**Figure 1.4**). In a second step, such hydroxysilyl group reacts with another hydroxysilyl group from a second precursor molecule with the formation of a siloxane bond (Si−O−Si) and a water molecule. Alternatively, the Si−OH group may immediately react with a Si-X bond, again forming a siloxane bond and a compound HX, an alcohol if an alkoxy precursor was chosen. Once the siloxane or polysilsesquioxane polymer exceeds a certain molecular weight, phase separation occurs and a gel is formed in which all reaction solvent is incorporated [8, 9, 23].

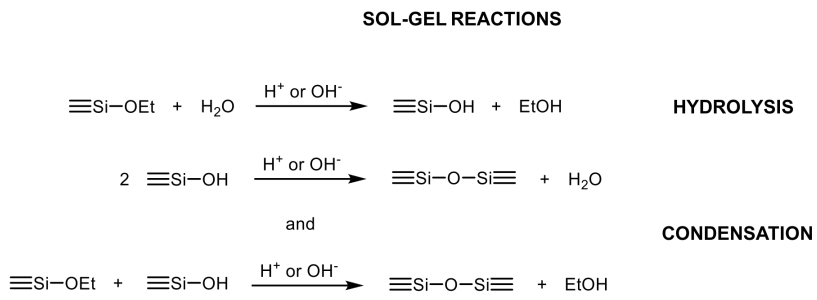

Figure 1.4: Summary of the reactions involved in the sol-gel polymerization of (ethoxy)silanes.

Both reactions are catalyzed by addition of an acid or base catalyst. At low pH the rate of hydrolysis is higher than the condensation rate, while at high pH hydrolysis becomes the rate determining step [19, 24]. This implies that, under acidic conditions, more weakly branched long polymeric networks are formed, while under basic conditions, highly branched, dense networks are formed (**Figure 1.5**). As a first result, acid catalyzed gels are obtained as transparent monoliths, while with base catalysis white, opaque materials are found. Next to this, also a nucleophile e.g. the fluorine anion, is known to catalyze the sol-gel reaction. This often results in different structural properties e.g. porosity, due to different reaction kinetics of the sol-gel reaction [25, 26]. In all cases, prolonged treatment of the formed gels or aging also influences its final properties. Hereby, the network can obtain a higher degree of condensation and/or restructuring of the framework can occur through redeposition [27].

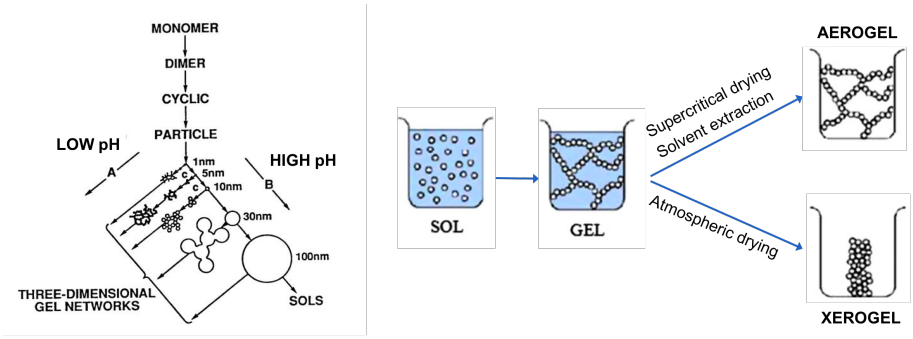

Figure 1.5: Polymerization behavior of silica as a function of catalyst (left, taken from [19]). Processing of a wet gel to obtain an aero- or xerogel (right).

Typically, after condensation of the bis-silane precursor, the polysilsesquioxane framework is found as a wet gel in which all reaction solvents (H_2O, EtOH, THF,...) are still incorporated. Only solvent removal exposes the materials' porosity and this can be pursued in two ways (**Figure 1.5**). Most commonly, the gels are dried in an air atmosphere, sometimes at elevated temperatures, retrieving a xerogel. During the drying step, shrinkage (up to 95 vol%) takes place causing the initially monolithic wet gels to crack over time. As in many applications monoliths are not required, these xerogels are often crushed to speed up the solvent removal. If needed, cracking of xerogels during shrinkage can be avoided by addition of a solvent (e.g. dimethylformamide) that slows down the evaporation of the other solvents. A second approach to dry the wet organosilica gels is supercritical drying with CO_2 yielding an aerogel

with the same volume and structure of the wet gel monolith. Classic organosilica aerogels are extremely porous, yet unpractically brittle. To circumvent the brittleness, Nakanishi's group was successful in preparing flexible, sponge-like aerogel monolith using adapted $MeX_2Si{-}R{-}SiX_2Me$ precursors [28–30]. Furthermore, the same group succeeded in the synthesis of polysilsesquioxane frameworks with bimodal macro- and mesopores by using nonionic amphiphilic polymeric templates [31].

In terms of functional groups embedded, the very first report uses phenyl, biphenyl, and terphenyl linkers or spacers [3]. These aryl functionalities were soon followed by materials derived from 9,10-bis(triethoxysilyl)-anthracene and bis(triethoxysilyl)ethyne [32]. Later, bridged -yne groups were exploited to perform a post-synthesis pore size modification or expansion. To do so, the materials are treated with methanol and water in the presence of 2.0% of ammonium fluoride. Such procedure effectively breaks the Si-C(≡C) bonds [33, 34] inside the polysilsesquioxane framework, which in turn results in enlarged pores. Thereafter, alkyl chains of different length were also shown to be incorporated in organosilica gels, but it was shown impossible to retrieve porous materials with bridges containing more than 6 aliphatic carbons due to excessive flexibility [35, 36]. Few of these early materials found application but, following these initial efforts, many other bis-, tris- and poly-alkoxysilyl precursors were developed, allowing incorporation of a plethora of organic groups e.g. crown-ethers, chromophores, metal-coordinating sites and organic acids and bases [8, 10, 11].

1.3 PMOs: Pore ordering via the use of a surfactant as soft template

Following the discovery of surfactant templated mesoporous silicas (MPS), e.g. MCM-41 [37, 38] and SBA-15 [39], the synthesis of porous organosilicas using bis-silanes ($X_3Si{-}R{-}SiX_3$), immediately focussed on similar synthesis strategies to result in Periodic Mesoporous Organosilicas (PMOs). Here, the bis-silane precursor is hydrolyzed and subsequently condensed around surfactant micelles acting as a soft-template by acid or base catalysis (**Figure 1.6**). Similar to their non-hybrid counterparts, PMOs have a high surface area, but this is now combined with uniform and ordered mesopores as a result of the templated synthesis. On top of this, however, the embedment of an organic group inside the pore walls leads to improved hydrolytic and mechanical stability as the surface is

more hydrophobic with less labile siloxane bonds present throughout the entire material [2, 40, 41] (see also Section 1.4).

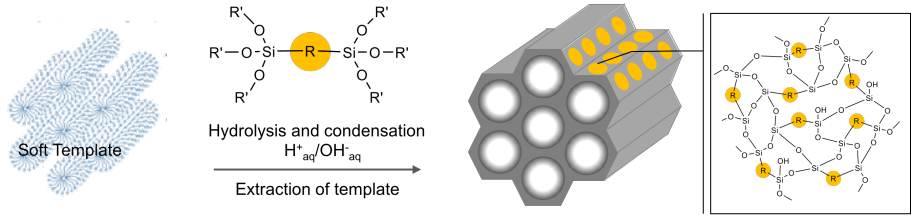

Figure 1.6: Schematic overview of a general PMO synthesis yielding 2D hexagonal ($P6mm$) ordered pores.

In the first reports on PMOs in 1999, simultaneously by the research groups of Inagaki, Ozin and Stein, the initial synthesis procedure highly resembled the preparation of the Periodic Mesoporous Silicas known at that time [4–6]. Herein, a cationic surfactant (cetyltrimethylammonium bromide, CTAB or octadecyltrimethylammonium chloride, OTAC) is employed to form micelles in an aqueous solution. After addition of a base catalyst and the bis-silane precursor, the resulting PMOs have relatively small, cylindrical pores (2 - 4 nm, in function of the template size) with multiple types of pore ordering, which is in turn depending on the stoichiometry, synthesis conditions and the type of surfactant used. Later, applying a synthesis adapted from SBA-type mesoporous silicas [39, 42], larger non-ionic templates such as Pluronic P123, F127, Brij-56 or Brij-76 (**Figure 1.7**), were used to obtain 4 - 12 nm pores. These again can show various pore geometries e.g. 2D hexagonal ($P6mm$) or 3D cubic ($Im3m$, $Pm3m$).

The formation mechanism of PMOs is rather complex, and the smallest of variations in terms of conditions or stoichiometry can have an enormous effect on the resulting mesostructure. Most of the following mechanistic insights have been postulated for MPS-type materials. However, one must definitely take into account the fact that bis-silanes are inherently different from commonly applied precursors for MPS, e.g. tetraethyl- and tetramethylorthosilicate (TEOS, TMOS). Compared to the latter, PMO precursors are in gereral more hydrophobic, bear organic functionalities and have different rates of hydrolysis and condensation. Although proven for silicas, these mechanistic insights must be taken as a guideline, and more often than not, synthesis of a new PMO is very much subject of trial and error.

1.3.1 Surfactants as lyotropic liquid crystals

The surfactants or structure directing agents (SDAs) used in the synthesis of mesoporous materials can roughly be divided in two types, ionic surfactants and non-ionic ones (**Figure 1.7**). The first form micelles in water through a hydrophilic head group consisting of a cationic or anionic moiety, e.g. CTAB and sodiumdodecylsulfate (SDS) respectively, combined with a lipophilic tail, typically a long aliphatic group. The second type of surfactants is generally comprised of a block co-polymer in which one part is more hydrophilic than the other e.g. Pluronic-type surfactants with hydrophilic polyethyleneoxide (PEO) moieties spaced by a hydrophobic polypropylene block (PPO).[1]

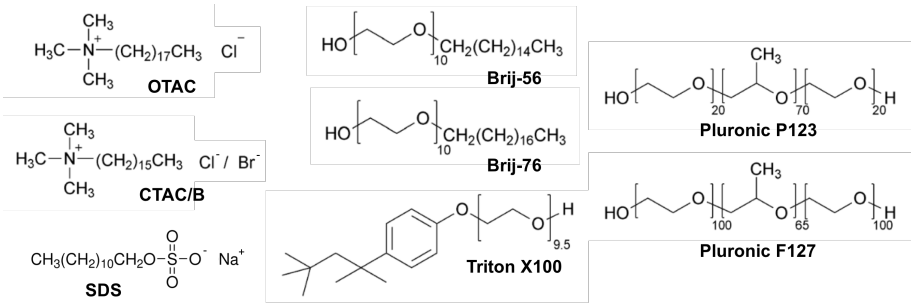

Figure 1.7: List of ionic and non-ionic surfactants commonly applied in the synthesis of MPSs and PMOs.

For both types of templates, the concentration of the template in the water/oil phase plays the most important role in the formation of a liquid crystal phase and for the most common surfactants phase diagrams are readily available. Typically, at low surfactant concentration but above the critical micelle concentration, high curvature is favored and thus randomly distributed spherical micelles are formed. With increasing concentration, less curved rod-like micelles are formed or the spherical micelles become cubic packed. Going further, liquid crystal phase transition is witnessed from 2D hexagonal cylindrical micelles over to 3D $Im3m$ organized micelles until at high concentration, a lamellar phase is obtained (**Figure 1.8**). It must be noted that the amount of oil phase, temperature and additives (salts, pore swellers) also play a critical role in micelle and liquid crystal formation.

1. All Pluronic-type surfactants are denoted by a letter-number code. Herein, the letter indicates the appearance of the polymer, L = Liquid, P = Paste and F = Flake whereas the first one or two digits x 100 stand for the approximate molecular mass of the PPO core, and the last digit x 10 gives the percentage PEO content.

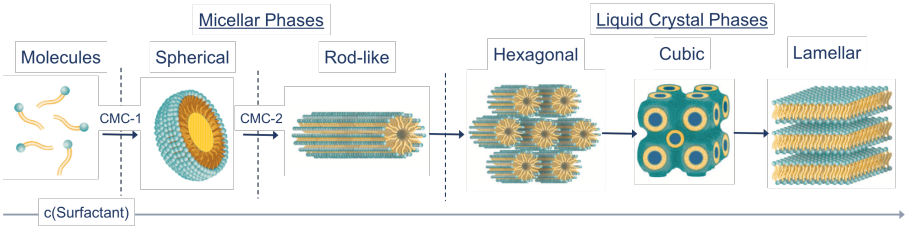

Figure 1.8: Generic micelle and liquid crystal formation of surfactants with increasing concentration in a monophasic water/oil mixture with a fixed ratio.

For non-ionic templates, specific mesostructures can be favored by the hydrophilic/lipophilic volume ratio (V_H/V_L) of the surfactant. Again, this is most readily explained with the Pluronic-type surfactant, but the reasoning is transferable to other templates. P123 and F127 have a similar hydrophobic PPO chain lenght (M_w = 12000). However, F127 has 70 w% of PEO-chains, where P123 only consists of 30 w% PEO. Now, a high V_H/V_L, as is the case for F127, comes with an increase in the curvature of the surfactant layer towards water. Thus, F127 favors the formation of cubic caged-like mesostructures with a high surface curvature (SBA-16) in a relatively wide range of conditions [42]. Block copolymers with medium V_H/V_L ratios (P123) on the other hand, tend to favor the formation of mesostructures with medium curvatures such as 2D-hexagonal ordering (SBA-15). Of course, when conditions are specifically selected to do so, P123 is still able to form a 3D cubic system ($Ia3d$) and F127 can give rise to 2D cylindrical micelles [43].

1.3.2 Hydrolysis and condensation around a pore generating soft-template - Directing the sol-gel reaction

Once a suitable surfactant system is found or selected, the next step in preparing the porous material can be considered, being the sol-gel reaction of a the silica source around the soft-template. In order to form a silica-based framework around the template, interaction between the surfactant and the condensing silica species is critical. Dependent of the selected template system, multiple precursor-template interactions are differentiated that are involved in the mesostructure formation. Here, the pH of the reaction medium is again majorly involved as it determines the charge of the precursor during synthesis. In MCM-41 type materials surfactant (S) - precursor (P) interaction is achieved through ionic attraction of the cationic head group of the surfactant and the negatively charged precursor at high pH (S^+P^- interaction). For an

anionic surfactant (SDS), synthesis at low pH is preferred to obtain S^-P^+ interactions. Counterions (C), coming from the catalyst or intentionally added, can also mediate in $S^+C^-P^+$ or $S^-C^+P^+$ systems (**Figure 1.9**).

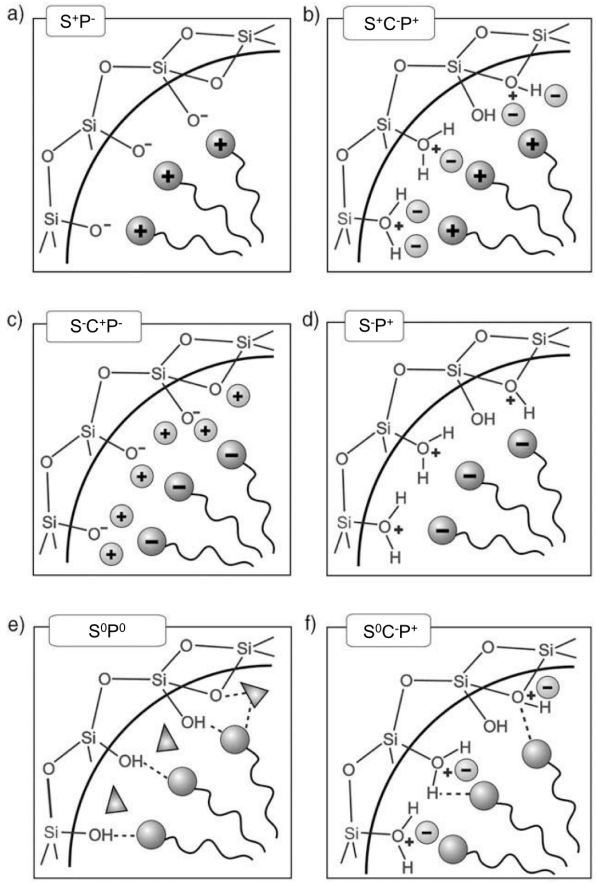

Figure 1.9: Possible precursor (P) - surfactant (S) interactions during MPS (or PMO) synthesis in acidic (P^+) or basic (P^-) media, or at the isoelectric point (P^0) of the precursor with cationic (S^+), anionic (S^-) or neutral (S^0) SDAs, mediated by counterions (C^+ or C^-) or hydrogen bonding mediators (triangles) [17].

Changing to a system with a non-ionic template, the precursor/surfactant interaction gets even more complex and debatable. Commonly, SBA-15 type materials are successfully synthesized in very acidic conditions as it is believed that in this regime a $S^0H^+C^-P^+$ or a $S^0C^-P^+$ interaction emerges. Also, it is experimentally witnessed that addition of metal-chloride (M-Cl) salts is beneficial for the final ordering of the mesopores, with larger cations having a more drastic effect [44]. It is believed that

extra attraction arises from $S^0M^+Cl^-P^+$ interactions as the metal salt nestles itself in and around the PEO-chains of the surfactant. Around the isoelectric point of silica (pH 2-3), hydrogen bonding between PEO and uncharged hydroxysilyl groups (P^0) might explain the good quality of the SBA-materials investigated. However, above the isoelectric point (pH $>$ 4) unordered, worm-like pores are found, except when special mediators such as NH_4F are added.

It is easily recognized that the surfactant not only determines the ordering of the pores, but that it also controls the size of the pores. For ionic surfactants, pore enlargement is easily done by using a longer alkyl chain ($C_{12} < C_{16} < C_{18} < C_{20}$). With non-ionic surfactants, an increase in the pore size is less straightforward through raising the M_w of the whole polymer or the lipophilic part as the use of a different block co-polymer, unfortunately, often gives rise to a different liquid crystal phase if the same conditions are applied [45, 46]. Pore size expansion up to 20 nm, both for ionic and non-ionic surfactants, can elegantly be implemented by adding hydrophobic molecules or pore swellers e.g. 1,3,5-trimethylbenzene (TMB) which dissolve inside the lipophilic micelle core and effectively swell these parts [47]. However, this procedure should be executed with care, because once a threshold is exceeded, phase transition of the liquid crystal phase can occur, up until hollow organosilica nanospheres are obtained (**Figure 1.10**) [48–51].

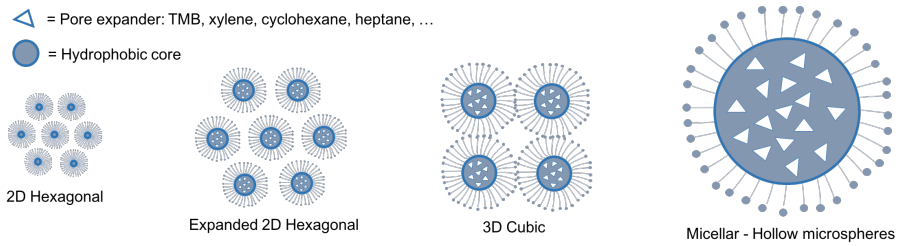

Figure 1.10: Influence of the addition of a hydrophobic molecule as pore expander.

One would also expect that non-ionic templates, being significantly larger than ionic ones, would give rise to much larger pore sizes, however, this is not the case. This can be attributed to the following: where the hydrophobic part (e.g. PPO) of the non-ionic surfactant completely entangles into the non-water soluble core of the micelle, the hydrophilic side-chains are still suspended in the aqueous phase. Condensation of the silica precursor now takes place at the hydrophobic/hydrophilic interface which results in the PEO-chain being encased. After removal of the soft-

template[2], a 'bimodal' pore system is obtained, where the hydrophobic core has generated mesoporosity with micropores connecting the mesopores as a result of the hydrophilic chains protruding the pore walls (**Figure 1.11**). This also implies that SBA-type materials have thicker pore walls, which turn them far more hydrolytically stable than MCM-type materials, and that materials (e.g. mesoporous carbons) casted inside SBAs (hard templating) possess a structural stability (CMK-3 [52]), in contrast to MCM casted materials. Increased synthesis temperature and addition of salts, are known to influence this bimodal porosity. Both cause dehydration of the hydrophilic chains, turning them more hydrophobic. As a result, larger mesopores are formed and/or microporosity is reduced [53–55].

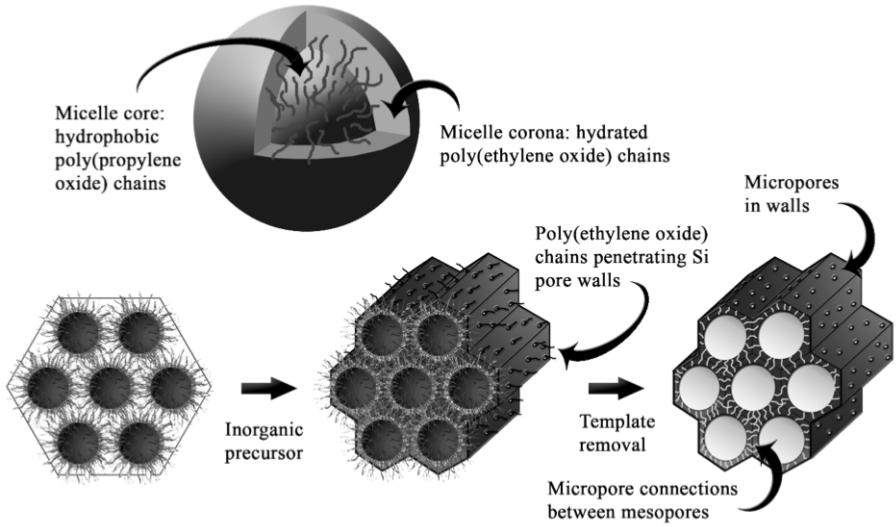

Figure 1.11: P123-surfactant: PPO-chains make up the micelle core whereas PEO-chains of the micelle corona penetrate the pore walls and generate micropores and connectivity between the mesopores [56].

From all the above, it is clear that all synthesis parameters are entangled, which makes the synthesis of a templated porous material a complicated subject. Moreover, for PMOs, even more uncertainty is added into the equation as less is known considering the specific bis-silane precursors.

2. To obtain the MPS or PMO, the template needs to be removed. Where this can easily be done by calcining the MPS material at high temperature ($> 300°C$), this method cannot be applied for PMOs as the organic bridge would be destroyed. Therefore surfactant removal via solvent extraction is preferred. Refluxing the material in acidified ethanol is most effective for MCM-type PMOs, where Soxhlet extraction with acetone is apt for the removal of non-ionic templates.

In many reports, new bridged functionalities are proposed which are transformed into their subsequent PMOs. However, dependent of the structure of the R-group, the isoelectric point can differ, hydrolysis and condensation speed varies, the precursor is more (or less) hydrophobic and other chemical functionalities are incorporated. All of the preceding has an enormous impact on the organization of the precursor around the template and precursor/surfactant interactions (e.g. PMOs have typically smaller pores and thicker walls compared to MPS as the precursor hydrophobicity leads to condensation closer to the hydrophobic core). Every other type of organic bridge is different and as a result, synthesis conditions need to be optimized repeatedly.[3]

Finally, next to the classical hydrothermal approach yielding powders, PMOs can also be prepared as thin porous films. This is performed by depositing a solution of catalyst, precursor and surfactant in an excess of evaporative solvent (EtOH) and H_2O on a substrate via spin- or dip-coating. As the excess solvent evaporates, self-assembly of the precursor around the micelles occurs as the sol-gel reaction takes places (Evaporation Induced Self-Assembly or EISA). This results in an ordered porous thin film (**Figure 1.12**) [58, 59].

1.4 On the hydrolytic and mechanical stability of organosilicas

Comprised completely out of siloxane (Si-O-Si) bonds, mesoporous silicas show both poor hydrolytic and mechanical stability. When treated in boiling water or subjected to elevated mechanical pressure, all types of MPS gradually lose their structural ordering and porosity. Where MCM-type materials are known to disintegrate completely in boiling water or even to lose their structural properties in humid air over time, SBA-15 can endure somewhat more drastic hydrothermal conditions as

3. In practice, optimization of the PMO synthesis with a new bis-silane precursor is often started from a robust synthesis of a comparable precursor. A second option is via a system in which precipitation of a solid and interaction is maximized, using high concentration of catalyst and addition of a salt. Two practical parameters can help during optimization. a. Before adding the bis-silane precursor one might want to visually check the quality of the surfactant micelles. From experience with P123, reaction media with a blueish opaque color often lead to nicely 2D hexagonal ordered PMOs. b. Materials for which the induction time (t_I), the time between adding of the precursor and the first visual precipitation, lies around 30 min, tend to have satisfying properties as this allows enough time for the condensing precursors to organize around the SDA. This latter is based on the Colloidal Phase Separation Mechanism proposed by D. Zhao's group [57].

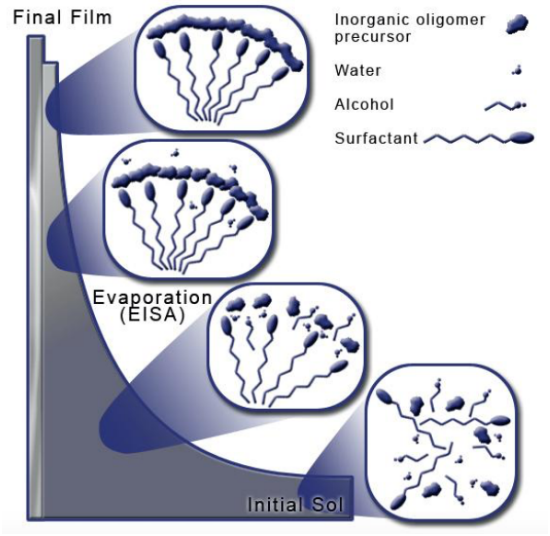

Figure 1.12: Schematic representation of the Evaporation Induced Self Assembly (EISA) process for the preparation of thin films [60].

a result of its thicker pore wall. However, in the end, SBAs also succumb over time. The low mechanical stability of porous silicas on the other hand can be directly linked to the surface hydrophilicity as even small traces of adsorbed water can break the framework siloxane bonds at high mechanical pressure. One can increase the mechanical stability by end-capping the surface silanol with hexamethyldisilazane (HMDS) (**Figure 1.13**). This technique effectively hydrophobizes the surface as the silanol-groups are terminated by a trimethylsilyl functionality, which repels the water causing hydrolytic cleavage of the framework [61]. However, if such materials are subjected to treatment in boiling water or to a pH < 2, the trimethylsilyl groups are removed, and the material is once again prone to mechanical stress [41]. Ultimately, the rate of dissolution of pure silica (dependent of its synthesis, precursor, calcination step and purity) increases dramatically above pH 8 [19].

As already suggested in this dissertation, next to functionality, the second asset to organosilicas and PMOs is their exceptional hydrolytic, hydrothermal and mechanical stability. This sharp difference with MPS can be ascribed to multiple factors. Firstly, polysilsesquioxane frameworks just contain fewer labile siloxane bonds as at least one Si-O-Si bond is replaced with a stable Si-C bond. Secondly, the organic bridge incorporated induces hydrophobicity in the framework, thus the

framework itself is able to obstruct water from attacking the Si-O-Si bond. Thirdly, as compared to MPS, PMOs have drastically thicker pore walls which is also adding to the improved stability. As a result, most organosilicas exposed to boiling water, elevated pH (12 - 13) or high mechanical stress (> 250 MPa), endure this treatment without structural deformation [40, 41, 62–64]. The stability of some concrete examples can be found in Section 1.6.1.

1.5 Clarifying a misconception: hybrid silica vs. organosilica

Because of the similarity between MPS and PMO materials, confusion often arises between the terms 'hybrid silica' and 'organosilica', with 'hybrid' denoting a combined organic/inorganic material. To immediately set things straight, a PMO is per definition a hybrid silica, but, not all hybrid silicas can be designated as organosilica or PMO.

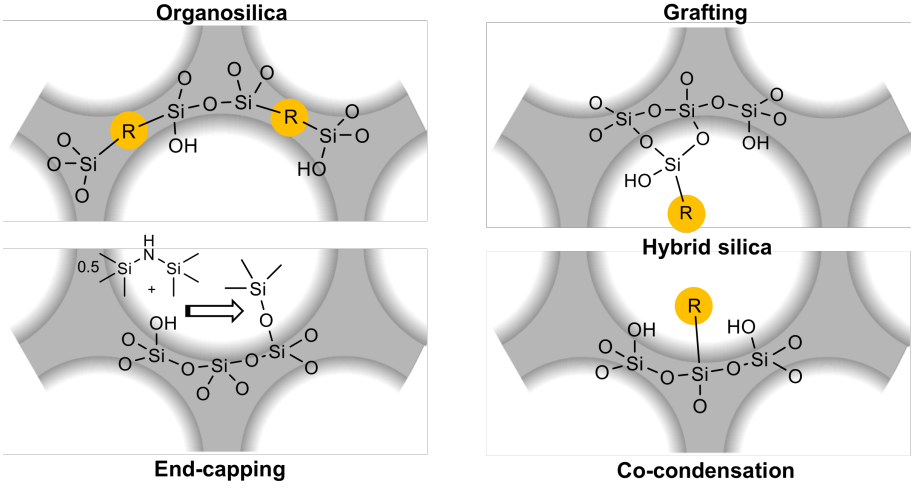

Figure 1.13: Overview of hybrid silicas: organosilica, X_3SiR grafted silica, X_3SiR co-condensed hybrid silica and end-capped (hydrophobized) silica.

Next to PMOs, there are two pathways to obtain a hybrid mesoporous silica that are not organosilicas. In a first method, an organic group R can be attached or grafted onto the pore walls of a MPS by silylation of the hydrolyzed yet uncondensed silanol (Si−OH) groups of MPS with a silane of the form X_3SiR with X a hydrolyzable group (**Figure 1.13**) [17, 65, 66]. Secondly, a X_3SiR-silane can be co-condensed with a silica precursor

(e.g. TEOS), again resulting in a dangling functional R-group, now with a local silsesquioxane $[RSiO_{3/2}]_n$ framework [67–70]. However, for both materials (grafted and co-condensed hybrid silicas) it is clear that the structural framework still consists of pure SiO_2 with hydrolytically labile siloxane bonds. Thus, although being a hybrid silica, the final properties of these hybrid silicas are similar to 'pure' MPS.

As indicated earlier, for organosilicas, the organic group is part of the siloxane framework, where it actively contributes to its properties, and these properties are what clearly discriminate hybrid silicas from organosilicas. First of all, the functionality of interest (R-group) is rigidly embedded in the framework with Si-C bonds and no longer through labile siloxane bonds. As a result, in conditions where Si-O-Si bonds are cleaved (e.g. pH $<$ 2), grafted hybrid silicas lose their functionality, where organosilicas remain intact. Secondly, organosilicas attain an extremely high loading of functional groups as the R-bridges are present throughout to whole material. In contrast, a maximum of 40 mol% of X_3SiR-silane can be intermixed in hybrid silicas via co-condensation before all structural properties are lost (**Figure 1.14**) [17].[4] Finally, as mentioned before, the R-group introduces hydrophobicity in the pore walls, which, combined with the presence of fewer labile siloxane bonds, results in a dramatically increased hydrolytic and mechanical stability of organosilicas as compared to the hybrid silica materials [40].

1.6 The bridged organic functionality: from simple systems to application-driven design

Next to variation of synthesis conditions and the choice of the soft template, probably the most significant source of versatility in organosilicas is the organic functionality. Over the years, many bridging R-groups have been proposed via different templating and synthesis methods resulting in a plethora of materials. Here, some of the most common, important or remarkable functionalities are concisely portrayed and some of their applications will be highlighted. Since the properties of organosilicas are determined primarily by the nature of the organic bridge, special focus will lay on the stability of the materials. Applications of organosilicas in catalysis and chromatography will be covered in Part II and III re-

4. Not withstanding that the addition of a tetravalent silica precursor is required to to obtain a structural polysiloxane, the trifunctional X_3SiR-silanes can undergo the sol-gel process on their own. This however only forms a polyhedral silsesquioxane oligomers (**Figure 1.14**) [8].

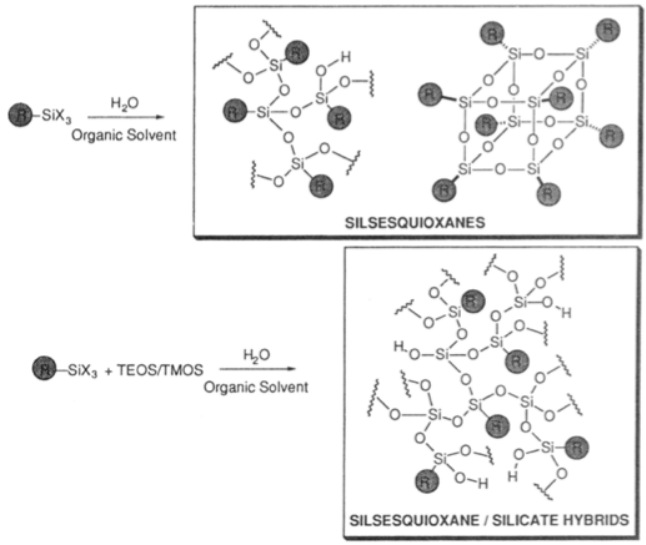

Figure 1.14: Condensation of X_3SiR-silanes yields silsesquioxane oligomers whereas a polysilsesquioxane/siloxane framework is formed upon addition of a a tetravalent silica precursor. Image taken from [8].

spectively. For a more extensive overview of PMO functionalities and applications, the review by Van Der Voort et al. (2013) is a very good start [7].

1.6.1 The early years of PMOs: applications profiting from simple functionalities

Back in 1999, all PMOs from the first three reports consisted of very simple organic bridges. Inagaki et al. describe two ethylene-bridged ($-CH_2-CH_2-$) PMOs having a uniform pore size distribution. Pore diameters of 31 and 27Å with 2D hexagonal ($P6mm$, MCM-41) and 3D hexagonal pore ordering (SBA-2, SBA-12) and high surface areas of 750 and 1170 m^2/g respectively, are obtained by variation of the precursor: surfactant(OTAC):NaOH:H_2O ratio. This clearly indicates the importance of the synthesis conditions [4]. Interestingly, 1,2-bis(trichlorosilyl)-ethane is transformed to 1,2-bis(trimethoxysilyl)ethane by adding the former to a $NaOCH_3$ solution (28 w% in methanol), assumingly to reduce the reactivity of the precursor and avoid the formation of inconvenient HCl as byproduct in the hydrolysis reaction. Since this very first report, nearly all future PMOs are prepared with alkoxy-based precursors. Materials containing other functionalities such as methylene ($-CH_2-$),

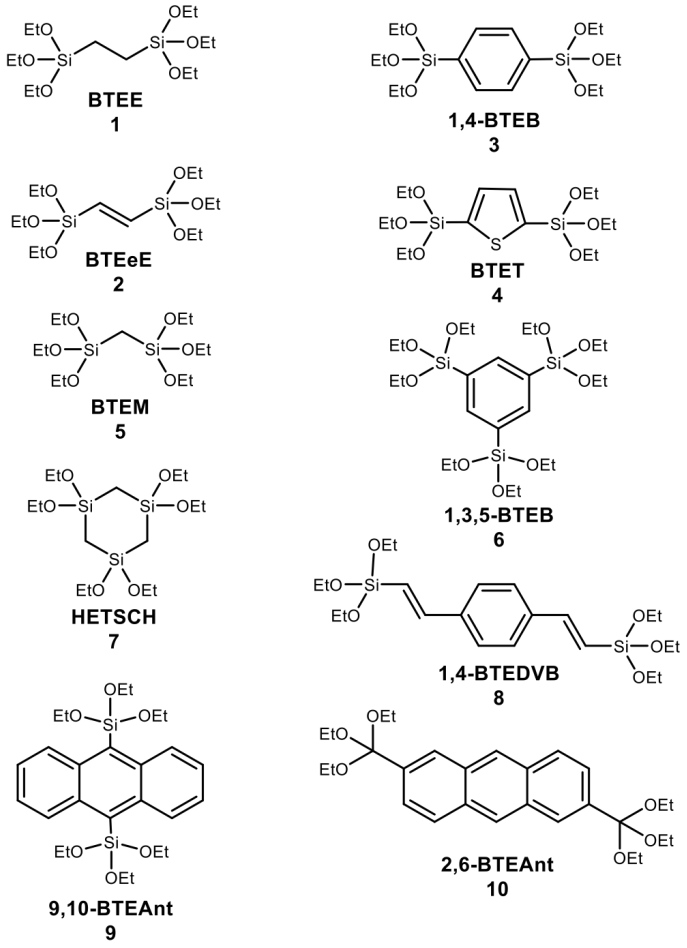

Figure 1.15: Overview of the simple-bridged PMO precursors described further: bis(triethoxysilyl) -ethane (BTEE), -ethene (BTEeE), -methane (BTME); 1,4-bis(triethoxysilyl) -benzene (1,4-BTEB), -thiophene (BTET), -divinylbenzene (1,4-BTEDVB); 1,3,5-tris(triethoxysilyl)benzene (1,3,5-BTEB); 1,1,3,3,5,5-hexethoxy-1,3,5-trisilacyclohexane (HETSCH); 2,6-bis(triethoxysilyl)anthracene (2,6-BTEAnt) and 9,10-bis(triethoxysilyl)anthracene (9,10-BTEAnt).

phenylene ($-C_6H_4-$), and vinylene/ethenylene ($-CH=CH-$) groups in their silicate networks, are suggested but not disclosed in this report, however, these are the subject of the very first PMO-patent [71].

The Inagaki report was immediately followed by Melde et al. disclosing the synthesis of both an ethylene- and vinylene-bridged organosilica [6]. Although the synthesis using CTAB, H_2SO_4 (hydrolysis of precursors) and NaOH (condensation agent) yielded materials with uniform pores, these had a disordered worm-like morphology. Finally, and very short after, Ozin et al. reported an optimized CTAB-based synthesis of ethene PMOs, either with or without addition of TEOS, resulting in 2D hexagonal ordering of the pores [5]. Both groups performed a bromination reaction of the double bond to show that the embedded groups are still reactive.

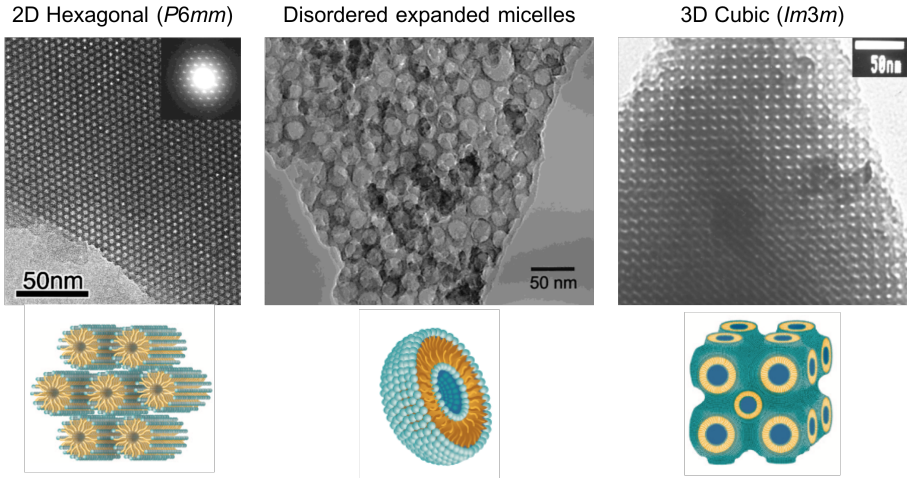

Figure 1.16: TEM images of ethane-bridged PMOs following Inagaki [4] ([001]-axis, left), Burleigh [72] (middle) and Guo [73] ([100-axis], right).

In an effort to enlarge the pores of PMOs, M. Fröba's group were among the first to use a non-ionic surfactant, P123, for the synthesis of an ethylene-bridged PMO [74]. This SBA-15 type synthesis resulted in a material with 6.5 nm pores, larger than all of the earlier PMOs yet still significantly smaller than SBA-15 (see also Section 1.3.2). Shortly thereafter Burleigh et al. reported the pore expanded version (TMB/P123) of this PMO, having pores up to 20 nm [72]. Pore ordering, however, is lost as the addition of TMB causes a phase transition of the cylindrical P123 micelles towards spherical micelles. The ethane-bridged PMO was also published using F127 as SDA, resulting in an SBA16-type ($Im3m$) pore structure with 9.8 nm pores [73]. An $Ia3d$ 3D cubic pore structure

(cfr. FDU-5 silica) with > 6.0 nm pores was obtained using P123 under specially selected conditions [43]. All these reports nicely illustrate the malleability of PMO synthesis. And indeed, typically, once a new bis-silane precursor is found, researchers start playing with the synthesis conditions and template system to find new shapes and porosities to suit their envisaged application. Other examples are the reports of P123 templated ethenylene-bridged PMOs from Vercaemst et al. Initially, the use of a pure E-diastereoisomer of bis(triethoxysilyl)ethene led to nicely 2D hexagonal ordered pores of 5.9 nm in a unprecedentedly fast synthesis through the addition of butanol [75, 76]. Also, template removal efficiency was studied in this work. In a follow up paper materials with highly expanded 28.3 nm pores are disclosed. Due to a high TMB/P123 ratio, again spherical pores are formed but in contrast to the Burleigh paper, these were found as an ordered array of pores (**Figure 1.17**) [50].

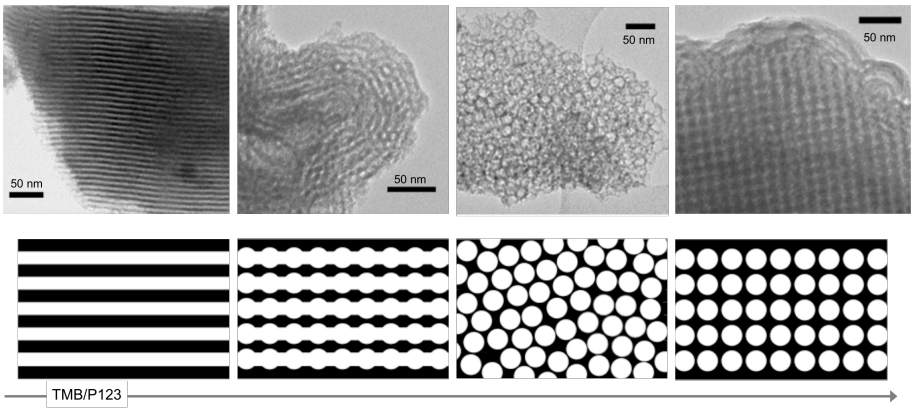

Figure 1.17: TEM images of ethene-bridged PMOs following Vercaemst et al. [50]. Addition of TMB causes the original 2D hexagonal pores ([110-axis], left) to expand into nodular strings, foam-like material and finally ordered spherical pores (right).

Still in 1999, Ozin's group reported on 1,4-phenylene- and thiophene-bridged PMOs following a synthesis using cetylpyridinium chloride (CPCl) as the surfactant to obtain uniform, ordered pores of an undisclosed size [77]. Strikingly, when the synthesis conditions are optimized for slow hydrolysis and condensation, and when the bis(triethoxysilyl)benzene precursor is added slowly, not only a highly ordered mesostructure is obtained, but crystal-like pore walls are observed due to $\pi-\pi$ interactions of the incorporated aromatic benzene moieties [78]. Similar molecular scale periodicity was found for a divinylbenzene-bridged PMO [79]. Both the 1,4-phenylene- and thiophene-bridged PMO have also been prepared with other templates and pore expanders [51, 80, 81]. Other incorporated

aromatic functionalities are, among many others, 1,3,5-benzene [82] and anthracene [83]. Finally, the very first PMO thin films were reported with these benzene and thiophene (and ethene) functionalities [84].

The simplest of organic bridges is the methylene ($-CH_2-$) group. At first sight, this group does not look very interesting in terms of functionality, however it is appealing in terms of stability. Ozin and coworkers described the self-hydrophobisation of a methylene-PMO through rearrangement of the siloxane framework (**Figure 1.18**) by treatment of the material in air at 400-700°C, rendering a more hydrolytically stable material [85]. This restructuring was also found later to occur for other PMOs [41, 86–88].

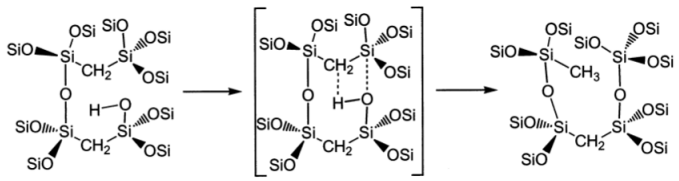

Figure 1.18: Thermal framework rearrangement of the methylene-PMO leading to methyl groups terminally bonded to silicon, taken from [85].

A particularly interesting variation of the methylene-bridge is found in the 1,3,5-trisilacyclohexane group from the HETSCH precursor first synthesized by Brondani et al. [89]. Such interconnected $[Si(CH_2)]_3$ ring-PMOs were first published as powder and oriented films with $<$ 4 nm pores using CTAB and NH_3 [87]. After a treatment similar to the one reported for methylene PMOs (500°C, N_2), the materials were found extremely hydrophobic as a result of the same silanol terminating framework rearrangement. These PMOs were found having a low relative permittivity (ϵ_r) or dielectric constant (κ = 2.1-3.6) and good mechanical stability, making this material especially attractive for microelectronic applications [90]. Due to their hydrophobicity, these PMO films make good low-(κ) layers, as they repel H_2O which has a detrimental effect on the insulating properties (high dielectric constant of water). Moreover, the porosity ensures that pockets of air (lowest κ-value, approx. 1.00) are contained inside the PMO layer, thus lowering the total dielectric constant of the material, if the pores are properly sealed (**Figure 1.19**) [91, 92]. Using a poly(N,N-dimethylacrylamide)-block-poly(styrene) block copolymer, the mesopores of ring-PMO layers were enlarged to 23 nm, resulting in a dielectric constant as low as 1.2 [93]. Finally, the $[Si(CH_2)]_3$ ring-PMOs are hydrolytically more stable compared to most other organosilicas as an additional Si-C bond is

present, replacing a hydrolytically labile Si-O bond. Because of the high carbon/oxygen ratio in the silica network, these materials were shown to withstand steaming at 130°C, a mechanical compression of 272 MPa and a treatment with 1M NaOH for 2.5 h [41].

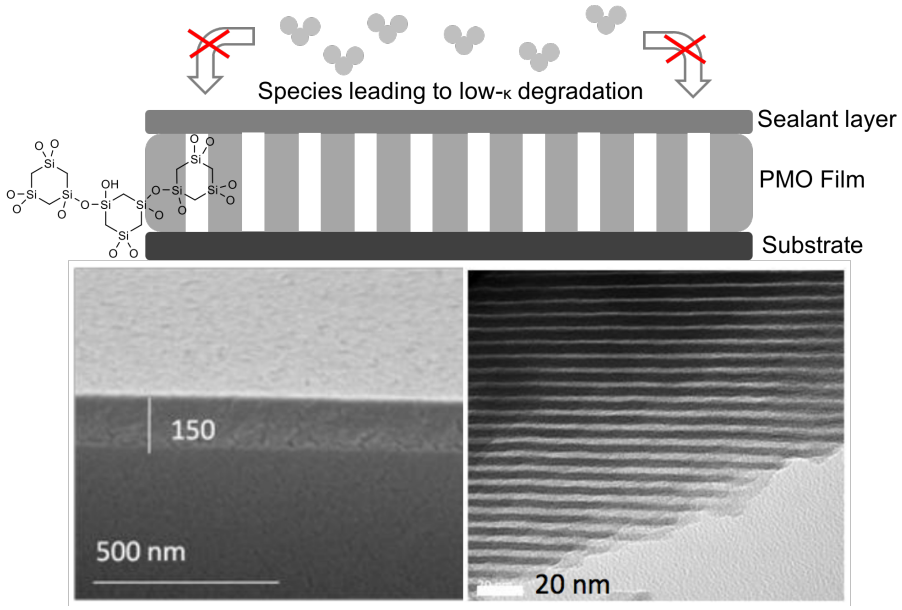

Figure 1.19: Schematic representation of a PMO thin film and the dense sealant layer avoiding penetration of species that may deteriorate the low-κ properties. SEM and TEM image of a $[Si(CH_2)]_3$ ring-PMO layer. Image adapted from [92].

Despite their lack of true reactive or interacting functionality, simple mesoporous organosilicas and PMOs were found attractive in applications where stability, hydrophobicity and/or a confined porosity is key. Similar to described above, a variety of PMO thin films were synthesized via spin-coating of BTEM, BTEE, BTEeE, 1,4-BTEB and 1,3,5-BTEB and tested as low-κ materials [58]. Particularly, ethane-, methane-, and $[Si(CH_2)]_3$ ring-PMOs show impressive water repellency (water contact angle) after a post-treatment at 350°C, combined with high mechanical stability (Young's modulus $>$ 10 GPa) and κ-values $<$ 2 [63].

Next to this, a Brij-76 templated ethane-PMO (S_{BET} = 891 m^2/g, d_p = 4.8 nm) was shown useful for protein refolding courtesy of its hydrophobic (ethane-bridge) and hydrophilic (Si-OH) regions inside the material combined with the uniform porosity (**Figure 1.20**) [94]. Also, ethane- and benzene-PMOs with large cage-like pores, realized using Pluronic P123 as a template and 1,3,5-trimethylbenzene (TMB) as a

pore expander, were used to efficiently immobilize (adsorb) enzymes [95]. Alternatively, benzene-PMOs were shown good adsorbentia for aromatic compounds due to $\pi - \pi$ interactions [96–98].

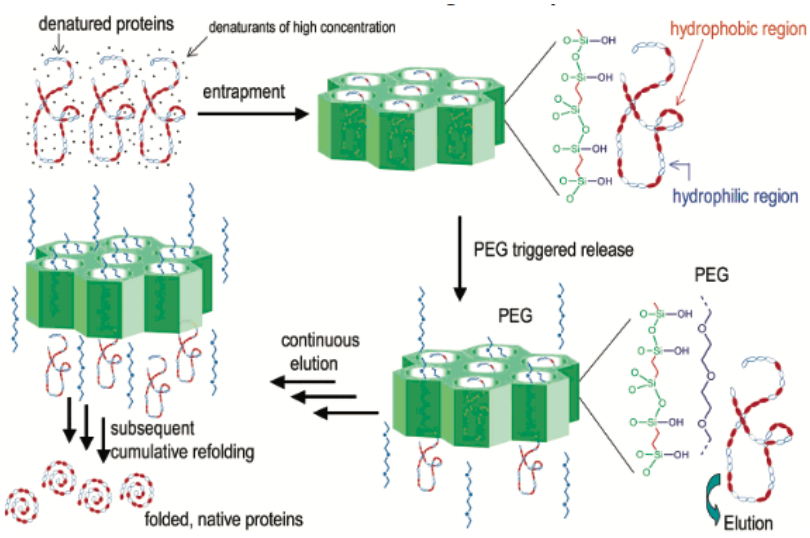

Figure 1.20: Protein refolding assisted by the hydrophillic-hydrophobic surface of an ethane-bridged PMO. Image from [94].

The exceptional hydrothermal stability of organosilicas is also illustrated and exploited by membrane technology. Although arguably porous on its own, bis(triethoxysilyl)ethane (BTEE) is deposited onto a microporous alumina membrane via dip-coating and applied for molecular separation. The hybrid composite membrane is found stable in the dehydration of n-butanol at 150°C for almost two years, combining a high resistance against water at elevated temperatures with a high separation factor and permeance [99, 100]. Furthermore, ethane-bridged polysilsesquioxane coated membranes are used for separation of water-isopropanol and water-butanol mixtures [101, 102]. Therefore, such membranes are deemed to have high potential for energy-efficient molecular separation under industrial conditions, including the separation and dehydration of organic solvents.

Finally, organosilicas with simple functionalities are commonly employed as chromatographic media, both as porous particles and monoliths. This application is subject of Part III of this dissertation.

1.6.2 Specialized materials: rational design of the organic bridges

At the time of their discovery, the R group of PMOs consisted mainly of simple ethane, methane, ethene or benzene groups. However, increasingly complex functionalities, connecting to the same trend in Mesoporous Organosilicas, were designed for progressively advanced applications.

As a first method, evidently, more advanced bis-silane precursors are used in the PMO synthesis. These can be acquired through several reactions with a bifunctional variant of the desired functionality and reacting this with a compatible silane (**Figure 1.21**). Nice examples are the Grignard reaction of dibromo-aryl compounds with TEOS to obtain a bis(triethoxysilyl)aryl precursor [3, 82, 103], and more advanced, the Heck coupling of triethoxyvinylsilane and a dibromo-aryl compound [79, 104, 105] and the silylation of aryl iodides and bromides with triethoxysilane $HSi(OEt)_3$ in the presence of NEt_3 and a Rh-catalyst [106]. Through this latter method PMOs have been reported with e.g. carbazole [107], 2,6- and 9,10-anthracene [83], stilbene [108] and (chiral) biphenyl functionalities [109]. A range of alkyl-chain precursors can be synthesized via the hydrosilylation of the corresponding endstanding alkyldienes with $HSi(OEt)_3$ employing chloroplatinic acid H_2PtCl_6. Other reactions yielded disulfide [110], isocyanurate [111], amide [112] and diurea groups [113, 114] to specially target specific applications. This opened up many possibilities for rational design of precursors and materials that are well-suited for the envisaged application.

For instance, the latter two materials, with amide and diurea functionalities, can act as controlled drug delivery agents as a result of predicted hydrophobic-hydrophobic and hydrogen bonding interactions with drug molecules such as ibuprofen or 5-fluorouracil. Dependent on the amount of functionality incorporated or pH of the release medium, different release profiles or triggered release are witnessed. Furthermore, aniline groups were incorporated especially to allow peptide synthesis inside the confined PMO pores [105]. A final example (excluding catalytic supports and chromatographic media) of rational design is the incorporation of extended aromatic systems inside the PMO pore walls as chromophore or light harvesting groups [104, 115–118]. Many other examples of rational PMO design can be found for PMOs as (organo)catalyst or catalytic support. These will be described in Part II of this dissertation.

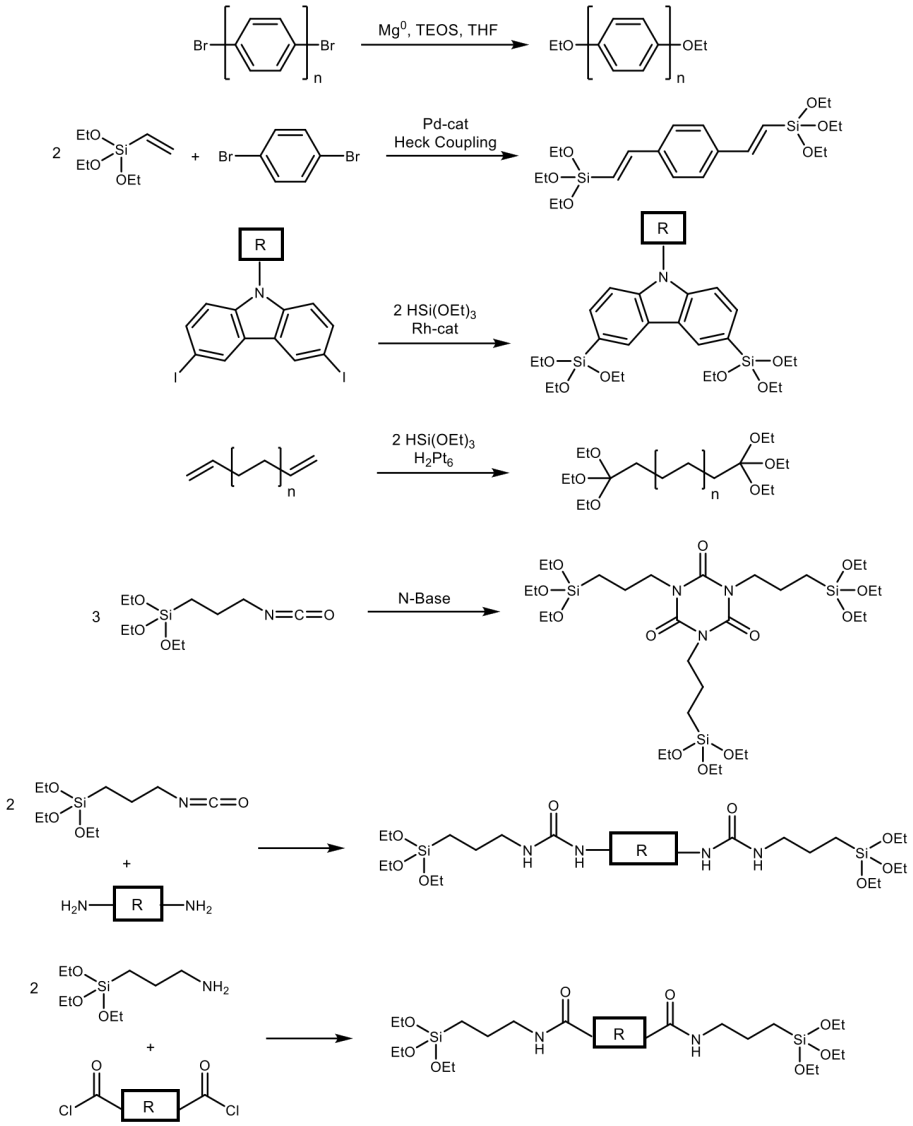

Figure 1.21: Overview of some reactions used to introduce functional bridges in PMO synthesis.

1.6.3 Encountering the limitations

Unfortunately, the increase in complexity of the bridged functionality does not come without drawbacks [15]. As a result of their size and rotational freedom, large aliphatic R-groups need to be co-condensed or 'diluted' with small, non-interacting precursors (e.g. BTEE, BTEB) or TEOS to ensure structural stability [119]. Fixation of the R-group in between two Si-framework atoms was described to induce faulty orientation and conformation of the bridged organic functionality, which is especially undesired for bidentately and chirally interacting groups [120]. Finally, and perhaps most importantly, every novel precursor is inherently different causing it to interact differently in the templated sol-gel reaction (Section 1.3.2). Every new precursor thus requires a time consuming reoptimization of the PMO synthesis.

Therefore, a second pathway can be pursued to obtain PMOs with a more intricate functionality. Borrowed from polymer chemistry and Staudinger's groundbreaking work, this 'post-modification' approach comprises the incorporation of functional groups in the framework or 'polymer' which can be reacted with either many or specially selected chemistries to yield other functionalities [121, 122]. For PMOs, this method was already proposed in the very first reports, where reactive groups incorporated within the PMO-framework are subsequently modified after the PMO synthesis. The bromination reaction used to prove the reactivity of the bridged ethene-group in the reports of Melde and Ozin, can already be considered as the first PMO post-modification reaction [5, 6, 69].

Clearly the post-modification method has advantages compared to the classical incorporation of functionality through the precursor. First and foremost, only the material synthesis of the PMO carrying the reactive group needs to be optimized and all possible variations in functionality are attached to this support. Therefore, also long, flexible functionalities can be bound to the PMO surface. Moreover, their rotational freedom is no longer hampered as the functionality is (mostly) anchored via one bond only, causing the functionality to dangle inside the pore cavity. In turn, this causes ensured accessibility of the functional group in a suitable solvent[5]. Finally, the organic group is attached via a C-C or a C-heteroatom bond, which are typically more stable in hydrolytic conditions compared to grafted hybrid silicas.

5. Depending on the functionality, chain length, surface polarity and solvent, functional groups are known to bend towards or fall back on the pore surface through specific intramolecular interaction e.g. H-bonding [123, 124].

On the flip-side, care needs to be taken when selecting the post-modification reaction. High yielding, selective reactions (e.g. the Diels-Alder reaction) are preferred for two main reasons. One, the post-modification of a PMO is a heterogeneous reaction. This means that the reagents are not molecularly mixed and that in practice, post-modification reactions take longer to finish or have lower yields compared to the homogeneous variant. Two, every side reaction that occurs, sticks to the material, without any possibility for purification. Furthermore, the reaction conditions cannot be too harsh as the structural properties of the PMO itself could be influenced (e.g. ozonolysis of an ethene-PMO causes the complete removal of the organic bridge [125]). Also, bulky reagents, catalysts or intermediates should be avoided as the risk arises they might not be able to penetrate the pores. One should also bear in mind that the remaining silanol groups on the surface are acidic, thus they can also participate in a reaction cycle. At the time of writing, relatively few reactive functionalities have been incorporated in PMOs, that are able to undergo modification via several types of reactions. Examples of these are described below.

The most exploited functionality for post-modification is the ethene-group. After a bromination reaction, the bromine groups introduced are known as a good leaving groups for nucleophilic substitution (S_N2) reactions, allowing for further modification. This resulted, for example, in PMOs with various, dangling amine chains for CO_2 adsorption and a thiol-containing PMO for Hg adsorption [126, 127]. Furthermore, the double bond can be epoxidized. The resulting oxirane ring can subsequently be opened with an amine, alcohol or water to obtain other functionalities or a diol group [128]. Also, it was shown that the Diels-Alder reaction can be employed efficiently for the addition of benzocyclobutene or functionalized dienes to the ethene group with the silicon atoms behaving as electron withdrawing groups [129, 130].

The benzene-PMO can undergo direct sulfonation with a 25% SO_3/H_2SO_4 solution or chlorosulfonic acid as sulfonating agent [78, 131]. Next to this, the benzene-PMO can be nitrated using a solution of sulfuric acid and nitric acid. After reduction of the nitro-groups with HCl and $SnCl_2$ an aniline-PMO was obtained [132].

Possibly the most interesting group of reactions to post-modify solids is 'click' chemistry (for details see Part II, Section 3.3). In this light, one particular PMO, bearing accessible thiol-groups in its pore walls is especially noteworthy as the SH-group offers a functional handle to attach all sorts of olefinic compounds via a very straightforward and efficient thiol-ene 'click' reaction [133].

1.7 A stable and versatile organosilica precursor: a ring-type organosilane precursor with allylic functional handle

With the knowledge of all the above, a deliberate suggestion for the ultimate organosilica precursor in terms of versatility and stability can be made. First and foremost, regarding the difficulties and somewhat trial and error approach inherent to organosilica and PMO synthesis, one single precursor is desirable. As a start, and to obtain maximum hydrolytic stability, the $[Si(CH_2)]_3$ ring or 1,1,3,3,5,5-hexaethoxy-1,3,5-trisilacyclohexane (HETSCH) precursor is selected as the base. Although this molecule is known to provide unprecedentedly high stability, it is clear that it has one major drawback. It has no added functionality. Therefore, if a distinct functionality is required, one would need to revert to grafting of the silanols. This is not favorable, as such grafted group is removed at low pH, which, as a result, renders the material useless in such conditions. Instead, the attachment of a functionality onto the methylene-bridged ring allows to circumvent the grafting approach.

Further functionalization of the $[Si(CH_2)]_3$ ring precursor was suggested through the deprotonation of the methylene group with t-butyl lithium (tBuLi) [58], and indeed interlinked rings were obtained when deprotonated rings were reacted with a bifunctional electrophile (Br-R-Br) [90]. If a mono-functional electrophile is selected, attachment without connection of two ring structures is obtained. In theory, reaction of the deprotonated rings with allylbromide is enhanced by $\pi - \pi*$ backbonding of the S_N2-intermediate in the nucleophilic addition reaction. Now, the aim of this work is to develop one single precursor and incorporate a reactive functional handle. An allyl group is a useful choice, as this would allow many options for hydrolytically stable post-modifications. All taken in consideration, by combining a base structure recognized for its stability and attaching a versatile functionality, 2-allyl-1,1,3,3,5,5-hexaethoxy-1,3,5-trisilacyclohexane (AHETSCH) has the potential to yield highly adaptable materials with exceptional hydrolytic and hydrothermal stability.

Chapter 2

Synthesis of the AHETSCH precursor

2.1 Synthetic approaches

Following chemicals were used as received:
1,1,3,3,5,5-hexaethoxy-1,3,5-trisilacyclohexane (HETSCH, 95%, ABCR), tBuLi (1.7 M in pentane, Sigma-Aldrich), allylbromide (99%, Sigma-Aldrich), anhydrous THF (≥99.9%, 250 ppm BHT as inhibitor, Sigma-Aldrich), anhydrous Et_2O (≥99.9%, Sigma-Aldrich), silica gel (60Å, 60-200 μm, ROCC), EtOAc (99%, Carl Roth), hexane (mixture of isomers, Acros Organics).

To obtain the 2-allyl-1,1,3,3,5,5-hexaethoxy-1,3,5-trisilacyclohexane (AHETSCH, **3**) or allylated ring silane precursor, two similar synthetic pathways can be followed, both comprising the nucleophilic S_N2 addition of deprotonated 1,1,3,3,5,5-hexaethoxy-1,3,5-trisilacyclohexane (HETSCH, **1**) to allylbromide.

In a first procedure (**Figure 2.1**), developed by Ide et al., 0.12 mol of HETSCH is dissolved in 150 mL Et_2O under inert atmosphere. Then, 1 eq. of t-Butyllithium (t-BuLi) is added drop-wise to this solution to deprotonate a methylene group of the ring, while the mixture is stirred heavily at -78.5°C. This temperature is obtained through addition of dry CO_2 to isopropanol in a cooling bath.[1] After 30 minutes of stirring,

1. The reason for this setup is two-fold. Firstly, the reaction temperature needs to stay below -78.5°C to avoid deprotonation of the solvent(s), which in turn lead to undesired side-products. Secondly, the safety of doing this reaction is majorly improved given that iPrOH does not catch fire if tBuLi would accidentally be spilled, as compared to other solvents employed in similar cooling baths (e.g. acetone, -77°C).

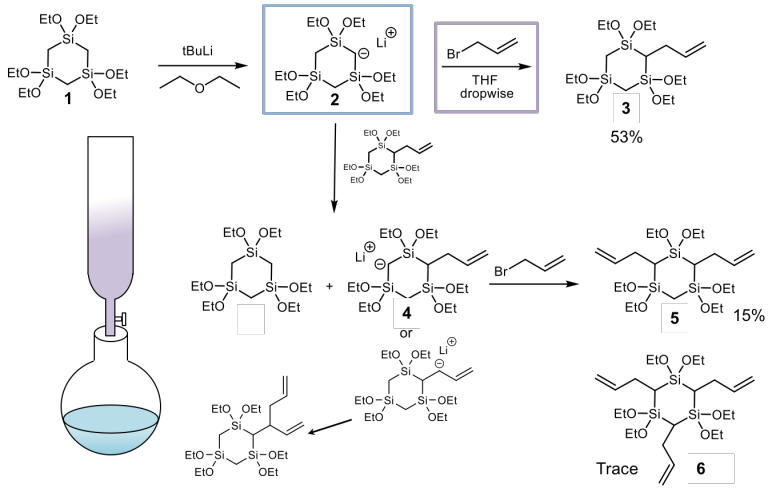

Figure 2.1: Reaction scheme of the AHETSCH **3** synthesis (Procedure 1).

the deprotonated ring silane is found as a white precipitate in Et_2O. Now, 1 eq. of 3-bromo-1-propene (allylbromide) in 200 ml THF is added drop-wise through the same adding funnel and stirred for 15 h while the temperature is gradually raised to room temperature. The allyl ring precursor (AHETSCH) is washed and purified with 4 x 50 ml Et_2O, 2 x 50 ml 1 w% $NaHCO_3$ solution and 3 x 50 ml H_2O in a separation funnel. The organic phase is recuperated and solvents are evaporated until a yellow oil is obtained.

In a second, adapted procedure (**Figure 2.2**), 10 ml of HETSCH is dissolved in 30 ml of anhydrous THF under Ar. This solution is heavily stirred at -78.5°C; 1 eq. or 1.5 eq. of t-BuLi is added dropwise over 30 min and the mixture is stirred for another 30 min. By means of a syringe cooled with dry CO_2, the HETSCH solution is added over 30 min to a separate flask containing 2.2 ml allylbromide (1.07 eq.) in 20 ml of anhydrous THF, also cooled to -78.5°C. The reaction is left to stir overnight with the temperature gradually increasing to room temperature. The resulting yellow solution is subsequently washed with 25 ml of a 0.2 w% $NaHCO_3$ solution and 2 x 50 ml of water. Thereafter, the THF-fraction is recuperated and the solvents are evaporated under reduced pressure until a faint yellow oil is obtained.

To direct the reaction towards a maximized yield for the mono-allylated ring silane, stoichiometric control of the reaction is attempted in both methods. It is clear from **Figure 2.1** that the formation of compound **4** needs to be prevented. Therefore, an excess of the deprotonated ring **2** in the reaction with allylbromide is highly undesired as may give rise

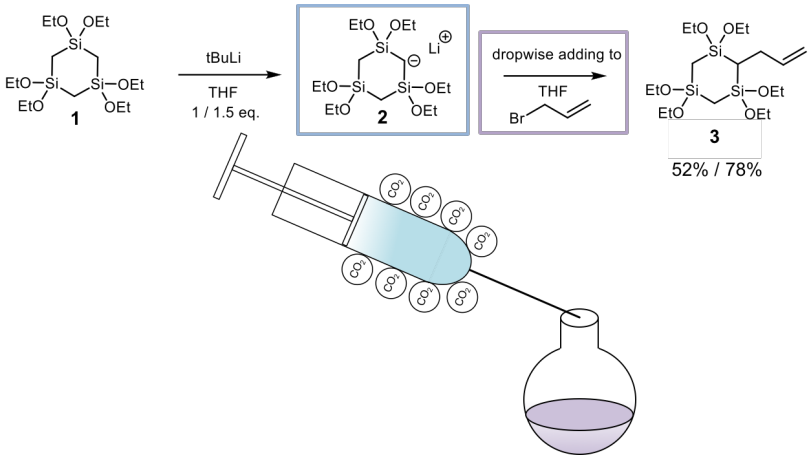

Figure 2.2: Reaction scheme of the AHETSCH **3** synthesis (Procedure 2).

to the formation of **4** and thus the bis-(**5**), and tris-(**6**) allylated ring species. Pathways to other side-products are also accessible, yet the true nature of the latter is not investigated.

Procedure 1, following Ide et al., was developed to maximize safety and the ease of execution given this procedure requires fewer handling of substances under inert atmosphere. The different solubility of the deprotonated compound **2** is exploited to obtain stoichiometric control of the reaction. **2** is insoluble in Et_2O, illustrated by the formation of a white precipitate, while **2** readily dissolves in THF. In theory, when adding a solution of allylbromide in THF, compound **2** is no longer present in excess, as only part of **2** dissolves in the small amount of THF added (while the precipitated **2** remains unreactive until more THF is added).

However, when considering the GC determined conversion and yield of this reaction (**Table 2.1**), still a significant amount (15%) of **5** is found, together with 53% of the desired mono-allyl ring **3** and traces of tris-(**6**) allylated ring and THF adduct side products (GC-MS). The total conversion for procedure 1 is 68%, without considering that 15% of species **1** is formed by the reaction. Purification of all reaction products is possible via meticulous column chromatography employing hexane:EtOAc 20:1 as eluent. On a 50 x 4 cm column packed with silica gel, as much as 15 ml of precursor mixture can be separated (elution sequence: **6**, **5**, **3**; HETSCH and THF adducts do not elute).

In procedure 2, a more direct approach is taken to ensure an excess of allylbromide. Using a CO_2 cooled syringe, **2** is added to a separate flask

Table 2.1: Results of the nucleophilic S_N2 addition of deprotonated 1,1,3,3,5,5-hexaethoxy-1,3,5-trisilacyclohexane (HETSCH) to allylbromide.

Procedure	tBuLi [eq.]	Conv. [%][a]	Yield (**3**) [%][a]	Yield (**5**) [%][a]
1	1.0	68[b]	53	15
2	1.0	52	52	0
2	1.5	88[b]	78	10

[a]Determined via GC. [b]Conversion determined on the amount of HETSCH in final reaction mixture.

filled with the allylbromide solution. The results are satisfying; a yield of 52% **3** is found and no side reaction is observed when 1 eq. of t-BuLi is used. In an attempt to increase the conversion, 1.5 eq. of t-BuLi is applied in the reaction. Unfortunately, or logically, the side reaction to **5** and **6** is observed again. This can be ascribed to the presence of unreacted tBuLi during the S_N2 reaction, insufficient cooling of the syringe and/or too fast adding of the **2**-solution. Despite the relatively low yield of the reaction with 1 eq. of tBuLi, its selectivity allows for a faster and more straightforward purification of AHETSCH through column chromatography. As compounds **5** and **6** are no longer present, 'flash' chromatography with hexane:EtOAc 10:1 can be employed to elute AHETSCH, while leaving HETSCH on the silica column. After separation, HETSCH can be recuperated by changing the solvent to 100% EtOAc.

The ^{1}H NMR spectrum of pure AHETSCH is provided in **Figure 2.3** and ^{13}C NMR spectrum in **Figure 2.4**. ^{1}H NMR (300 MHz, $CDCl_3$) δ = 6.01 (ddt, J=17.0, 9.9, 7.0, 1H, CH_2CH=CH_2), 5.00 (ddd, J=17.0, 3.6, 1.4, 1H, CH=CH_2), 4.87 (ddd, J=10.0, 2.1, 1.0, 1H, CH=CH_2), 3.85 - 3.71 (m, 12H, OCH_2), 2.41 - 2.32 (m, 2H, CHCH_2CH=CH_2), 1.26 - 1.16 (m, 18H, OCH_2CH_3), 0.38 (t, J=6.4, 1H, CH(Si)$_2$(CH_2CH=CH_2)), 0.20 - 0.02(m, 4H, SiCH_2Si). ^{13}C NMR (400 MHz, $CDCl_3$) δ = 142.82 (CH_2CH=CH_2), 114.89 (CH=CH_2), 59.84 - 59.67 - 59.65 - 59.55 (OCH_2), 29.47 (CHCH_2CH=CH_2), 19.85 - 19.81 (OCH_2CH_3), 15.66 (CH(Si)$_2$(CH_2-CH=CH_2)), 0.00 (SiCH_2Si). In both spectra * denotes signals originating from $CDCl_3$ (NMR solvent). The #-signal can be attributed to leftover THF (reaction solvent). x indicates the tetramethylsilane (TMS) NMR-standard.

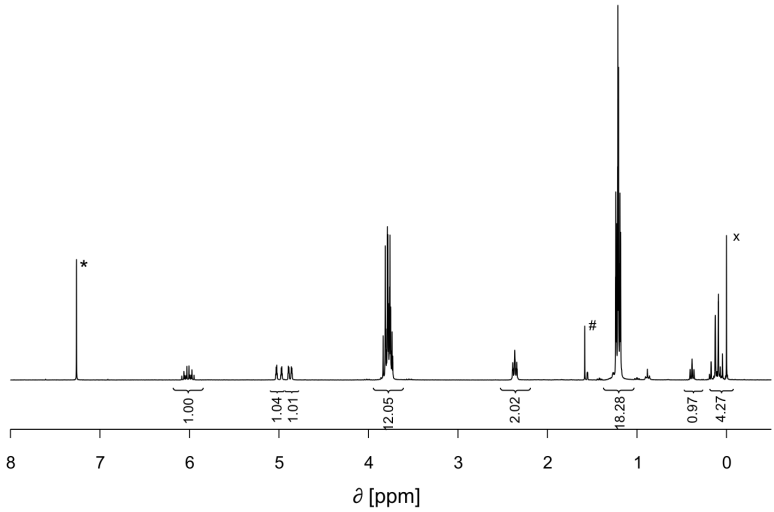

Figure 2.3: ^1H NMR spectrum of pure 2-allyl-1,1,3,3,5,5-hexaethoxy-1,3,5-trisilacyclohexane (AHETSCH).

2.2 Conclusion and outlook

We have explored two pathways to obtain the desired AHETSCH precursor. Approach 1, in which allylbromide is added to the deprotonated $[Si(CH_2)]_3$ ring is easier and arguably safer to perform. However, this sequence of addition gives rise to impurities as the double solvent system is not sufficient to avoid side-reactions. As a result, a more meticulous work-up and purification is required to obtain AHETSCH. A second approach, in which the deprotonated ring is added to a solution allylbromide, results in reduced yield yet higher selectivity. Purification of the precursor therefore becomes more straightforward.

The allyl-group can be modified as precursor, however, this is not studied in this work as the aim is to develop one robust material synthesis procedure and exploit the reactivity of the allyl-group in post-modification reactions. These post-modification reactions, producing hydrolytically stable functionalization of the pore surface, can comprise first and foremost thiol-ene 'click' reactions with any thiol-group containing molecule, yet many other reactions are suited. The same reactions used to modify ethene-bridged materials can be employed for the allyl-group with the latter being more reactive in certain reactions due to its asymmetrical substitution. Furthermore, the allyl group has rotational freedom and

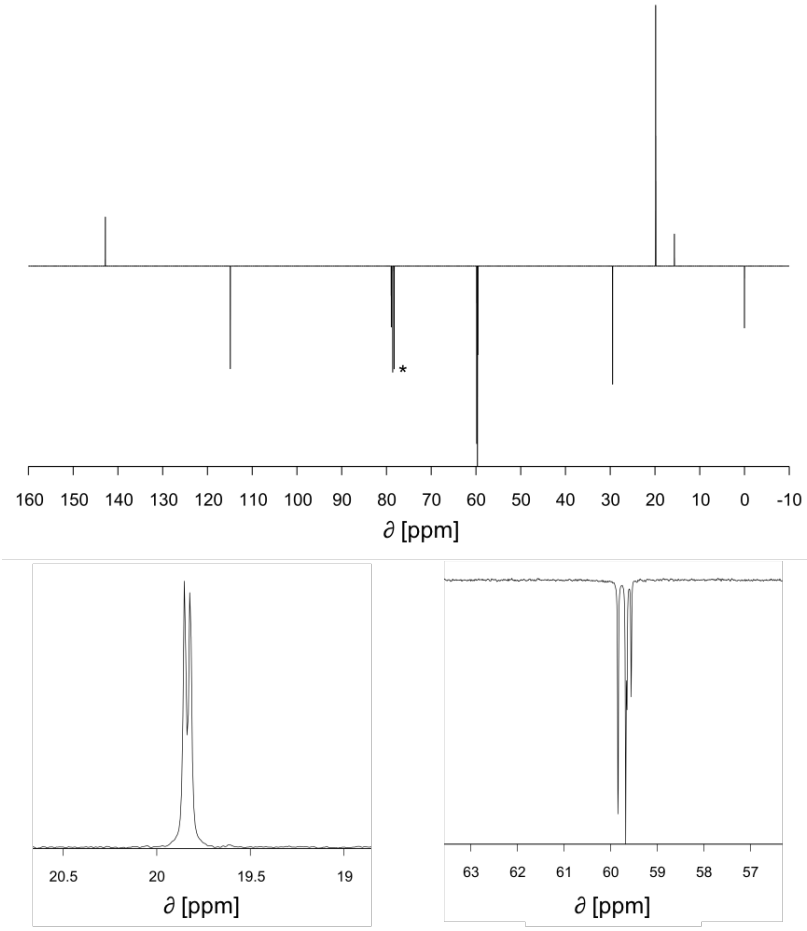

Figure 2.4: ^{13}C NMR spectrum of pure 2-allyl-1,1,3,3,5,5-hexaethoxy-1,3,5-trisilacyclohexane (AHETSCH).

is probably easier to reach as it will supposedly dangle in the pores. Some examples of possible post-modifications are depicted in **Figure 2.5**, with hydroboration, epoxidation, (anti-) Markovnikov addition of HBr and Mn-mediated radical addition of acetylacetone to name a few options.

In what follows, the AHETSCH precursor will be transformed into a catalytic support (Part II) and as chromatographic packing (Part III). In both applications, the hydrolytic stability of the organosilica, combined with the possibility to introduce various functionalities is key to success.

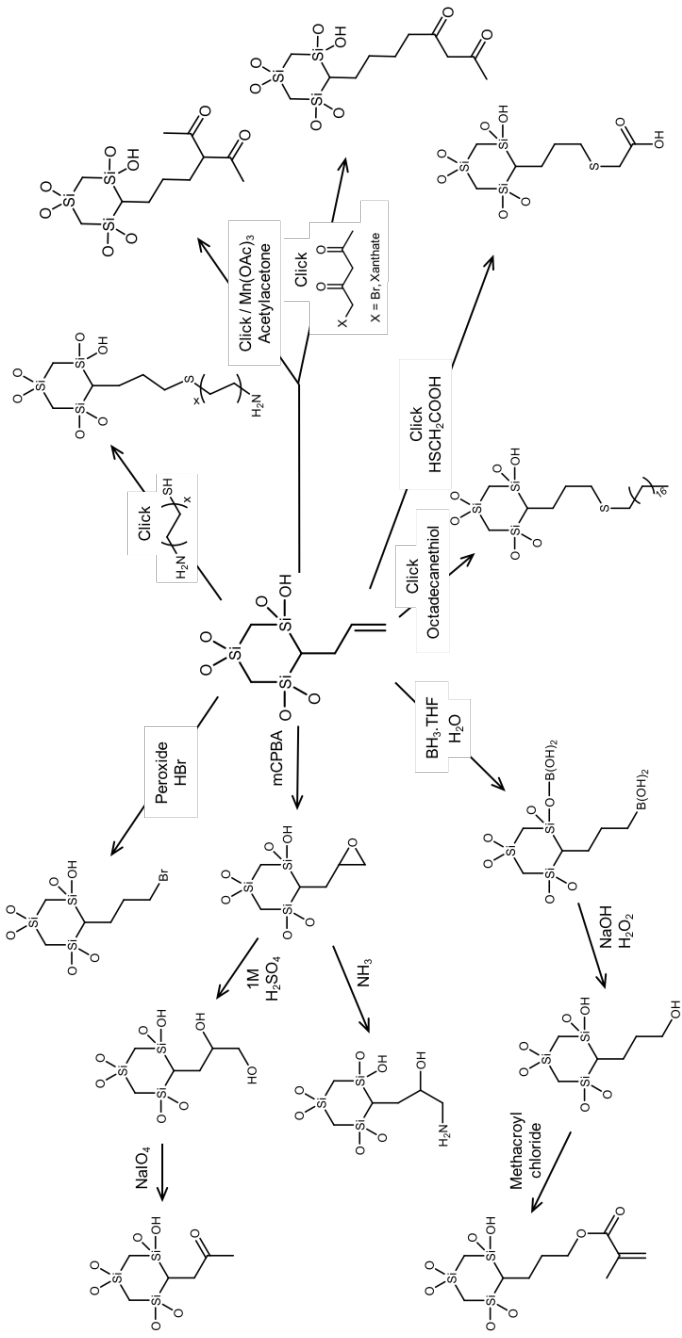

Figure 2.5: Overview of possible post-modifications of the allyl-group.

Part II

A stable catalytic support and its application as heterogeneous Ru(III) catalyst for "green" oxidations

Chapter 3

Introduction: PMOs as catalytic support

3.1 (Heterogeneous) Catalysis

Per definition, a catalyst is a compound which accelerates a chemical reaction by participating in the reaction while not being consumed by the reaction. It does so by providing an alternative pathway for the reaction to occur. Herein, more favorable transition states for the reagents (lowering the activation energy of the reaction, E_a) are achievable as they interact with the catalyst (**Figure 3.1**). Once a catalytic reaction is finished, the products detach from the catalyst, and the latter becomes available again for further reaction. Therefore, only low amounts of catalyst are sufficient to transform reagents or substrates to the reaction products. However, a catalyst only influences the kinetics of a chemical reaction, not the chemical equilibrium (ΔG unchanged). So, if a reaction is thermodynamically unfavorable, a catalyst does not help, as both the forward and reverse reaction are sped up to the same extend.

Catalysts can be divided into three categories: homogeneous catalysts, biocatalysts and heterogeneous catalysts. As the nomenclature already suggests, homogeneous catalysts such as metal complexes, acids or bases, are present in the same phase as the reactants, i.e. in the gas or, more commonly, the liquid phase. This implies that both are mixed at the molecular scale, resulting in high activity and selectivity of the catalyst combined with efficient heat transfer. On the down-side, separation and recycling of the catalyst is a rather expensive task. This is, however, required to obtain pure reaction products or to avoid losses of often expensive catalysts. Furthermore, homogeneous catalysts are not suited

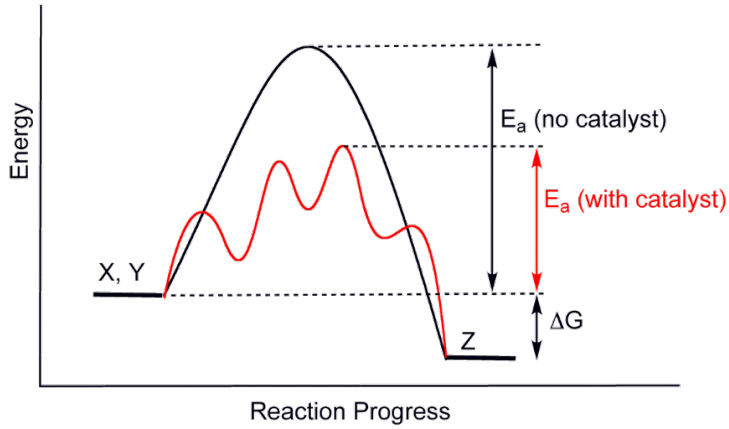

Figure 3.1: Potential energy diagram illustrating the effect of a catalyst in a chemical reaction, X + Y to give Z.

for continuous processes as the catalyst can not readily be separated from the reagent flow.

Bio-catalysts or enzymes evolved in nature to perform very specific tasks with extremely high activity. As a result of their extremely high activity and selectivity, bio-catalysts are distinguished from synthetic homogeneous catalysts. Unfortunately, their biggest asset, specialization, is also their most important drawback as enzymes can only carry out a single type of reaction while it is difficult to design them for other applications.

A heterogeneous catalyst is a solid which mediates in gas or liquid phase reactions where reactions take place at the catalysts surface. Being solid, it allows easy and fast separation of the catalyst from the reaction mixture and it permits continuous flow reactions as the solid can be packed into catalyst beds. Therefore, heterogeneous catalysts are often applied in industrial-scale reactions. However, due to the fact that catalysis only occurs at the solid-gas or solid-liquid interface, the activity of heterogeneous catalysts is usually reduced as compared to their homogeneous counterparts. To make up for this, heterogeneous catalysts are often developed as materials having a high surface area e.g. as nanoparticles or as porous materials.

3.1.1 Characterization and evaluation of heterogeneous catalysts [134]

Three important parameters prevail when a catalyst is generally assessed: activity, selectivity and stability. Activity is a quantitative measure of

the reaction rate or, in other words, how fast a catalyst works. Some catalysts show both catalytic activity towards the desired product and undesired side-products. The ratio of these catalytic activities is referred to as selectivity. Basically, selectivity describes the catalyst's ability to direct the chemical reaction towards the correct end-product. Combined, activity and selectivity determine the yield of the catalytic reaction. From this, it is appreciated that both high activity and selectivity are preferred, yet in many cases, selectivity is of primordial importance as high selectivity reduces the need for a costly work-up of the obtained reaction products.

Where selectivity is easily determined via analysis of the formed products, determination of the activity requires a more practical measure than reaction rate. For that reason, Turnover Number (TON) and Turnover Frequency (TOF), are commonly used in batch conditions. TON is defined as the amount of substrate in moles, that one mole of catalyst can convert before becoming inactive, while TOF is the TON per unit of time. Both definitions are up for debate as it is hard to exactly determine when a catalyst turns inactive and because catalyst activity is not constant over time due to reduction of the amount of substrate in batch. As a general agreement, TON is often described at maximum conversion and TOF is reported at the maximum speed of the catalysis. For catalysis under continuous flow, two other measures are introduced; space velocity (SV) and space time (τ), indicative for the amount of reactor volumes that can be treated in a set time and the time it takes to handle one reactor volume, respectively.

Loss of catalyst activity is often associated with catalyst poisoning or (in)stability. Poisoning refers to either the irreversible bonding of feedstock impurities to the catalytic site or to hampered detachment of a reaction product from the catalyst. Both render the catalyst unable to perform any further reaction. Stability issues can arise if catalysis proceeds at too harsh conditions. Examples are: thermal decomposition of metal complexes or organic catalysts, aggregation of nanoparticles, pseudomorphization or amorphization of a crystalline compound, etc. Also attrition and abrasion can be taken into account when assessing a heterogeneous catalyst.

Furthermore, heterogeneous catalysts require an extra experiment to evaluate the heterogeneity of the catalyst. During reaction, the possibility arises that the catalytic site detaches or leaches from the solid and turns to a homogeneous catalyst. This, of course, needs to be avoided as this results in product impurities, catalyst deactivation over time and loss of reaction control if, for example, the solid itself plays a role in

product selectivity. This leaching can be examined via a hot filtration test. Herein, the solid is filtered off from the reaction after a set reaction time and the catalytic activity of the filtrate is further evaluated. If the catalytic conversion of the substrate stops abruptly after the removal of the catalyst, one can consider the reaction as truly heterogeneous. On the other hand, if no change is witnessed in the reaction profile, the catalyst has leached in the reaction medium.

In terms of characterization of the active site, there is a clear contrast between homogeneous and heterogeneous catalysts. Given that the former dissolves, many liquid phase analysis methods such as NMR, IR and UV-VIS spectroscopy are in place to investigate the pure compound. The characterization of the catalytic sites of a solid is often less trivial and highly dependent on the amount of active sites. More advanced techniques are mandatory to investigate or get an idea of how the catalytic site looks like. Raman and IR spectroscopy can be employed, albeit the latter through Diffuse Reflectance with Fourier transformation (DRIFTS), while also CP-MAS solid-state NMR can be used. Catalyst loading can be determined via quantitative methods such as CHNS elemental analysis, X-Ray Fluorescence Spectroscopy (XRF), Atomic Absorption Spectroscopy (AAS) or (Inductively Coupled Plasma) Mass Spectrometry (ICP-MS). Characterization of metal sites on the other hand, requires techniques such as X-Ray Photoelectron Scattering (XPS), Temperature-Programmed Reduction (TPR) or synchrotron methods such as X-ray Absorption Near Edge Structure (XANES) and Extended X-ray Absorption Fine Structure (EXAFS) to determine the oxidation state, redox behavior, and neighboring atoms. SEM and TEM provide insight in the morphology of heterogeneous catalysts, and, when combined with an EDX detector, both techniques can provide information on the distribution of catalytic sites. Finally, optical light microscopy combined with catalysis towards a fluorescent compound allows mapping of the reaction sites of a heterogeneous catalyst [135], while more advanced techniques were developed to spatially resolve reactions at the nanometer scale [136].

3.1.2 Advances in heterogeneous catalysts: trend for Green and Sustainable Chemistry

In recent years, much time and effort has been invested in the sustainable or green revolution of the chemical industry. And rightly so, given that ecology and economy are becoming more and more entangled. Within this movement, referred to as Green Chemistry, catalysis is one of the

pillars as it is involved in at least 8 out of the 12 principles (italic) proclaimed by Anastas and Warner [137]:

1. *It is better to prevent waste than to treat or clean up waste after it is formed.*
2. *Synthetic methods should be designed to maximize the incorporation of all materials used in the process into the final product.*
3. *Wherever practicable, synthetic methodologies should be designed to use and generate substances that possess little or no toxicity to human health and the environment.*
4. Chemical products should be designed to preserve efficacy of function while reducing toxicity.
5. *The use of auxiliary substances (e.g. solvents, separation agents, etc.) should be made unnecessary wherever possible and innocuous when used.*
6. *Energy requirements should be recognized for their environmental and economic impacts and should be minimized. Synthetic methods should be conducted at ambient temperature and pressure.*
7. *A raw material or feedstock should be renewable rather than depleting wherever technically and economically practicable.*
8. Reduce derivatives: unnecessary derivatization (blocking group, protection/deprotection, temporary modification) should be avoided whenever possible.
9. *Catalytic reagents (as selective as possible) are superior to stoichiometric reagents.*
10. Chemical products should be designed so that at the end of their function they do not persist in the environment and break down into innocuous degradation products.
11. Analytical methodologies need to be further developed to allow for real-time, in-process monitoring and control prior to the formation of hazardous substances.
12. *Substances and the form of a substance used in a chemical process should be chosen to minimize potential for chemical accidents, including releases, explosions, and fires.*

From what is already hinted above, catalysis offers new pathways in chemical reactions. This has led to major improvements of existing chemical reactions or design of new ones, thereby avoiding the use of (harmful) auxiliary substances, eliminating by-products, opening access to new feedstocks, etc. Furthermore, catalysts reduce the energy of activation needed to start a reaction which, in turn, reduces energy requirements and its associated pollution and costs.

The benefits of heterogeneous catalysis have already been exploited by industry for many years, where zeolites are widely applied. These microporous materials comprise aluminosilicates (e.g. ZSM-5, FAU-X), acting as strong solid acids after cation exchange, which combined with their confined pores, has led to their use in, for example, Fluid Catalytic Cracking (FCC), isomerisation and alkylation reactions. Titanosilicates such as TS-1 are employed as efficient epoxidation catalysts. All zeolites are very easily prepared, are available in bulk and are cheap. This latter signifies that, although zeolites are perhaps not the ideal catalyst for an industrial process [138], they are certainly the most cost-efficient. Furthermore, many years of economy-driven process development have turned large-scale industrial reactions even more efficient.

Typically, the E-factor, a measure for the efficiency and environmental impact of a reaction suggested by Sheldon, of a reaction producing a bulk chemical ($10^4 - 10^8$ tons/year) lies somewhere below 5 kg waste/kg of product [139]. In oil refining, this figure even drops to below 0.1 kg/kg due to highly optimized processes using highly specific zeolite catalysts. On the other hand, the amount of waste produced in the synthesis of fine chemicals or pharmaceuticals lies 10- to 100-fold higher, leaving plenty of room for improvement. To reduce the E-factor in these latter markets, zeolites are not able to contribute significantly. Principally, their micropores only allow catalysis with molecules < 8.5Å or < 13Å if aluminophosphates (AlPOs) and silico-aluminophosphates (SAPOs) are taken into account, which clearly restricts the use of zeolites for catalysis of large functional compounds or bio-molecules. Moreover, the catalytically active sites of zeolites are restricted to defect metal sites in the zeolite's lattice, providing redox active or Lewis acid-base sites. Because of this lack of functionality, zeolites are only known as solid acid/base or redox catalysts.

With the opportunities in fine chemical catalysis in mind, researchers developed a multitude of new promising materials, especially focussing on increasing the pore size. This research has, over many years, led to the development of a plethora of mesoporous (2-50 nm pores) metaloxides such as Al_2O_3, CaO, Fe_2O_3, TiO_2, ZrO_2 and SiO_2 using templating

methods [140–142]. From these examples, silica immediately gained a lot of interest as the SiO_2-surface is well-known and easily modified with organic functionalities. Furthermore, it was quickly shown possible to obtain ordered arrays of mesopores (Part I, Section 1.3). Straight pores with a large diameter have an attractive effect on catalysis as the mass transfer of both reagents and products is enhanced [143].

3.2 PMOs: advanced hybrid materials as catalytic supports or solid organocatalysts

3.2.1 Mesoporous silica as catalytic support

Ordered mesoporous silicas such as MCM and SBA-type materials have some unique structural properties that have made them highly interesting for catalysis [138]. Firstly, MPS have a high surface area, which maximizes contact and thus activity between the solid catalyst and the reagents in gas or liquid phase. Furthermore, the templated synthesis approach yields mesopores of tunable size that are easily able to accommodate large molecules, typical for fine chemical synthesis and biological applications. Moreover, these large pores, combined with the ordering, allow for reduced mass transfer limitations and efficient diffusion of reagents inside the material. On the other hand, MPS only have silanol (Si-OH) decorating the surface and are therefore barely[1] to not active, yet they are ideal as inert catalytic support as the surface can be modified via 3 pathways: isomorphic substitution, silanization or co-condensation.

Isomorphic substitution refers to the replacement of silicon atoms within the silicate framework with other metals such as Al, Ti or Zr without altering the framework nor pore structure. This substitution can either be performed during synthesis or post-synthesis (impregnation) and results in materials that are chemically similar to zeolites albeit with the benefits of mesoporosity. Reactions with these materials are widely studied [146] and some examples include the Friedel-Crafts alkylation of benzene using Al-MCM-41, -MCM-48 and -KIT-5 [147], the epoxidation of olefins using Ti-MCM-41 [148, 149] and the photocatalytic generation of hydrogen on Zr-MCM-41 [150, 151].

1. The silica surface is known to co-catalyze some reactions like the aldol condensation. For this acid-base tandem reaction a base site is introduced within the silica, while the mildly acidic silanol group acts as acid catalyst (pKa of isolated silanol is 4.5, vicinal and geminal is 8.5) [144, 145].

Nonetheless, at this point, one might argue that these MPS-based catalysts lack functionality just like zeolites do. However, via grafting and co-condensation, the interesting possibility has risen to incorporate distinct functionalities in the material. This allows the generation of defined heterogeneous catalysts, often used in synthesis of fine chemicals, supported by the MPS [152]. These defined catalysts are either organocatalysts or metal complexes, which can be anchored through the incorporation of ligands. For the anchoring of metal complexes, two methods can further be discriminated. As illustrated below, either a multidentate ligand is attached or multiple monodentate ligands are used to coordinate the metal center. Although often more synthesis steps are needed to obtain a tetherable multidentate ligand, this approach is slightly preferred above the second. Using only monodentate ligands, the distance between two ligands (surface loading) and the ligands size (linker) needs to be optimized as a function of the pore size to obtain a stabilized complex (**Figure 3.2**), which can be a difficult and time-consuming task [124, 153].

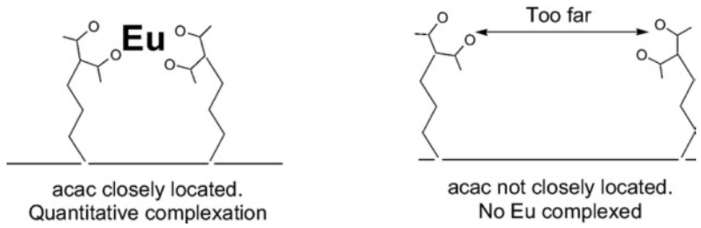

Figure 3.2: Effect of the surface functionalization on catalyst loading. Figure adapted from [153].

Many grafting or co-condensation procedures to obtain a hybrid silica employ commercially available silanes, which are further modified on the solid. For instance, grafting or co-condensation of aminopropyl-triethoxysilane or other amine-silanes introduces an organic base functionality [145], but can also be modified to obtain an attached Mn-Salen complex [154], a Rh-BINAP-complex [155] or a triphenylphosphine ligand for the heterogenization of $Pd(OAc)_2$ [156]. Grafted or co-condensed mercaptopropyl-triethoxysilane can be oxidized into a catalytically active sulfonic acid group [157], yet the original thiol groups can also coordinate and tether a Pd-complex for the Suzuki reaction [158]. Furthermore, the thiol groups are ideal functional handles for post-modification via thiol-ene chemistry, as illustrated by the attachment of natural quinine for asymmetric Michael additions [159] or by the attachment of allyl-modified Salen ligands [160].

As a final note, mesoporous silicas, because of their uniform and controllable pore size, have been used to synthesize and support monodisperse nanoparticles (NPs) in which the SiO_2 support avoids agglomeration thereof. Common examples of such supported NPs are TiO_2 and Fe_2O_3, where the size and bandgap of these NPs can be controlled via selection of the pore size of the support [161–164].

3.2.2 Why PMOs?

PMOs are probably the most advanced support materials for catalysis known today. In contrast with MPS, these hybrids bear covalently bound organic functionalities embedded in the pore walls of the silsesquioxane framework, which overcomes leaching issues as compared to classical silanol functionalization methods [152]. Furthermore, PMOs have ordered mesopores, a high degree of hydrophobicity and a high surface area, which contributes to improved mass transfer of organics, hydrolytic stability and the amount of accessible functional groups. As a result, PMOs combine all important technical properties for a catalytic support in one material and do not suffer from drawbacks other advanced materials experience[2]. Furthermore, the hydrophobic/hydrophilic interface arising from the organic bridges combined with silanol groups is shown to further promote catalytic activity of organics in water as a green solvent [165–169].

Because of their versatility, an incredible amount of PMOs have been developed through rational design of its functional bridge [7, 170]. As a result of the often high functional complexity and large size of the bridged bis-silanes used, multiple strategies exist to obtain ordered porous materials (**Figure 3.3**). As it is more difficult to organize such bulky precursors around the soft-template, a popular and easy option is to co-condense the functional bis-silane with TEOS (Type 0). Although such materials are often claimed to be PMOs, the framework structure more resembles that of a pure silica. Therefore they lack the hydrophobicity and stability which differentiate PMOs from MPS.

A second approach is to graft the catalytic functionality of interest onto a pre-made PMO with simple bridges (Type 1A), or to co-condense a functional silane with the bis-silanes presented in Part I, Section 1.6.1 (Type 1B). Strictly seen, it is correct to call such Type 1 materials PMOs, however, these materials are more prone to leaching as siloxane bonds are more readily cleaved, with grafted functionalities being more susceptible

2. Except for the cost price

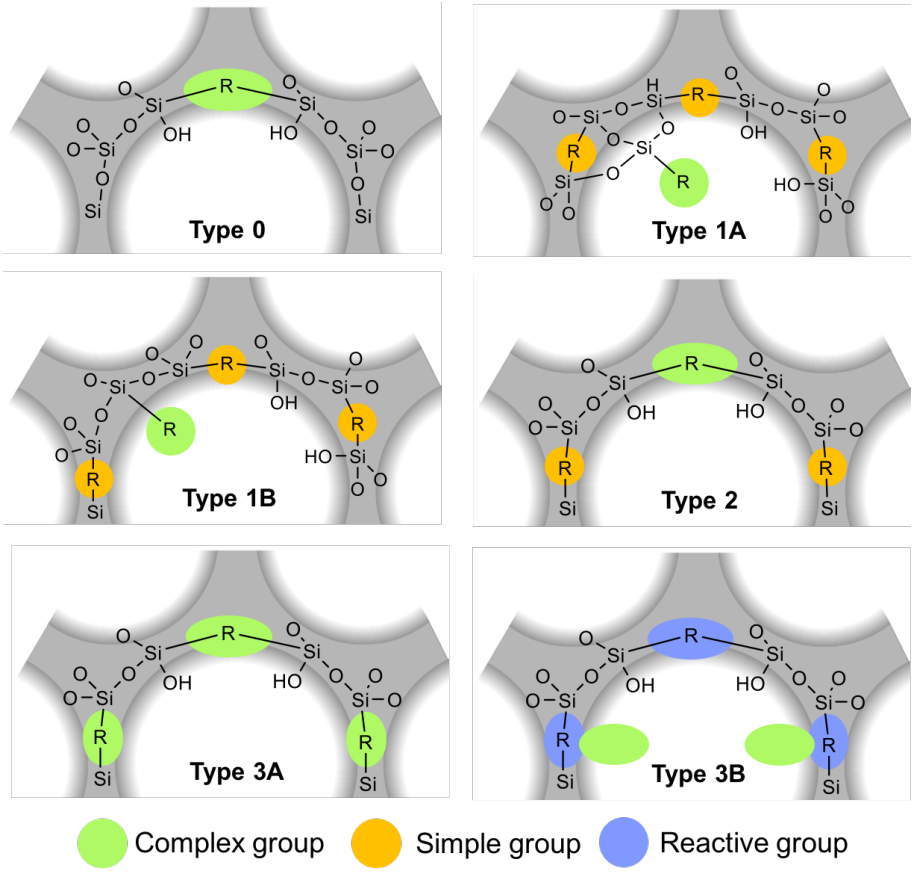

Figure 3.3: Overview of strategies to obtain PMOs with complex bridges. Type 0: Complex bis-silane condensed together with TEOS. Type 1A: Simple bridged PMO with grafted complex functionality. Type 1B: Co-condensation of a simple bis-silane and a complex silane. Type 2: Co-condensation of a simple with a complex bis-silane. Type 3A: PMO consisting completely of the complex functionality. Type 3B: PMO consisting completely of a reactive functionality, which is post-modified into the complex functionality.

than co-condensed ones [171]. Nonetheless, if reaction conditions are mild, and very intricate functionalities are present (bulky organic groups, chiral ligands), Type 0 and Type 1 materials have already shown great promise in catalysis.

A third method is based on the same idea of Type 0, but, instead of TEOS, a simple bis-silane is co-condensed in various ratios with the bis-silane of interest. These Type 2 materials, are without any doubt PMOs per definition, as they completely consist of a polysilsesquioxane framework with functionalities embedded inside the pore walls. Unfortunately, this latter fact, is known to introduce faulty orientation of the incorporated groups and limits the rotational freedom. This is in contrast with grafted or co-condensed functionalities which are dangling inside the pore voids. Especially troublesome is the incorporation of non-rigid multidentate ligands inside the pore wall, as the risk is high these lose their chelating properties due to a more restricted conformation. Furthermore, dependent of the complexity of the functionality, the loading of this latter is often lower than 25%.

In some unique cases PMOs are prepared for which the complex functionality makes up the whole organosilica structure (Type 3A), however, due to the issues with all the above strategies a final method is becoming increasingly popular (Type 3B). Herein, a 100% bis-silane PMO with short, yet reactive bridge is synthesized (e.g. ethene, thio-ethane). Post-modification of these groups has the potential to deliver stable, covalently bound, dangling organocatalysts or ligands, which are easy to reach and possess conformational freedom.

Similar to MPS, PMO-based catalysts can be divided into catalysts with undefined metal sites, defined organocatalysts and 'solid ligands' for metal-complex based catalysis.

3.2.3 Catalysis by metal sites in PMOs

In line with the isomorphic substitution proposed for MPS, PMO can also be synthesized in combination with other hydrolyzable metal precursors to incorporate isolated tetrahedral metal sites in the polysilsesquioxane framework. Mainly ethane-bridged bissilanes were used for the synthesis of Ti, Al, Sn, V and Nb substituted PMOs. Again, this generates only redox active or Lewis acid-base sites, but, these materials now enjoy the benefits of the hydrophobicity of the PMO. Therefore, in general, the activity per metal center is higher, than their silica counterparts. Also, the metal substituted PMOs are usually more hydrolytically stable, even though metal leaching (particularly, V and Cr) is an issue.

Some examples of reported reactions promoted by these PMO-types are: the epoxidation of different olefins with H_2O_2 as oxidant using a Ti-PMO [172], Sn-PMO [173], V-PMO [174] and Nb-PMO (**Figure 3.4**) [175]. Ti-PMOs and Nb-PMOs are furthermore shown excellent catalysts for the ammoximation of cyclic ketones [176]. Al-PMOs, having an acidic site, are used for the alkylation of 2,4-di-tert-butylphenol with cinnamyl alcohol and showed higher selectivity and conversion than Al-MCM-41 [177].

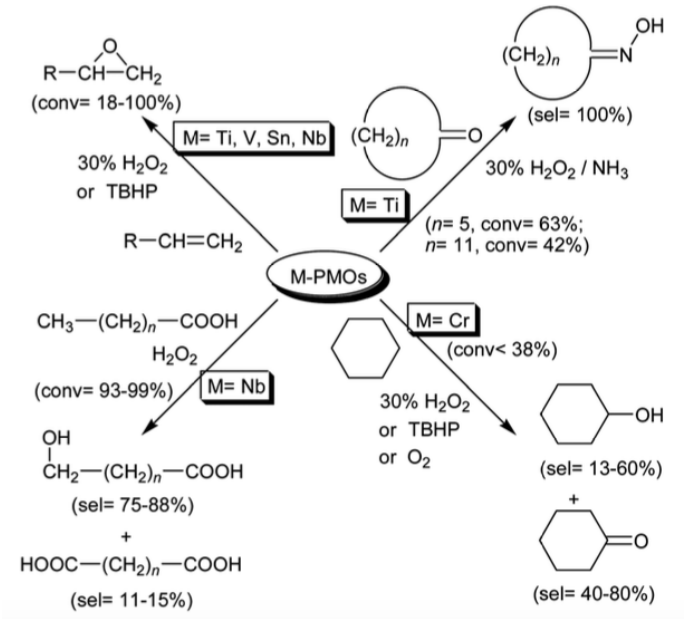

Figure 3.4: Overview of reactions carried out with isomorphically substituted PMOs [7].

3.2.4 PMOs as solid organocatalysts

Catalytically interesting Brønsted acid sites have been widely investigated on PMOs by introducing sulfonic acid (SO_3H)-groups, with a comprehensive overview given elsewhere [7]. In order to prepare such solid acid PMO, all strategies (Type 0 to 3) described earlier have been applied, and in many cases, the hydrophobicity of sulfonated PMOs plays a key role in their increased activity and stability compared to their MPS versions. The most interesting examples are those materials prepared as Type 3 and these can be, among other methods, obtained via direct sulfonation of benzene or biphenyl PMOs (**A**) (**Figure 3.5**) [178].

PMO-**B** was prepared using a Diels-Alder reaction on the ethene-bridged PMO, followed by a sulfonation reaction. This material was shown 30% more active than commercial solid (SO_3H-)catalysts (Amberlyst-15, Nafion) in the pinacol-pinacolone rearrangement due to its higher acid strength [129]. A similar conclusion was found for a perfluorinated sulfonic acid PMO (Type 1, **C**) in the self-condensation of heptanal [179]. Materials **D** and **E** are other examples of the use of the Diels-Alder reaction and subsequent sulfonation to obtain solid acid PMOs to be used as catalysts for the esterification between acetic acid and ethanol [130]. Another SO_3H-PMO was obtained through the Friedel-Crafts addition of the ethene-PMO to benzene and subsequent sulfonation (**F**) [180]. A final material was elegantly synthesized in-situ by adding H_2O_2 during the synthesis of a PMO with 1-thiol-1,2-bis(triethoxysilyl)ethane (TBTEE) as precursor (**G**). In this report, the functional loading was easily adapted by varying the ratio of thiol to ethane precursor. The resulting materials showed four times higher TOF values than Amberlyst-15 for the esterification of acetic acid with benzyl alcohol [181]. Other reactions catalyzed by SO_3H-PMOs include: etherifications, Friedel-Crafts reactions, hydrolysis, dehydration and dimerization reactions [7].

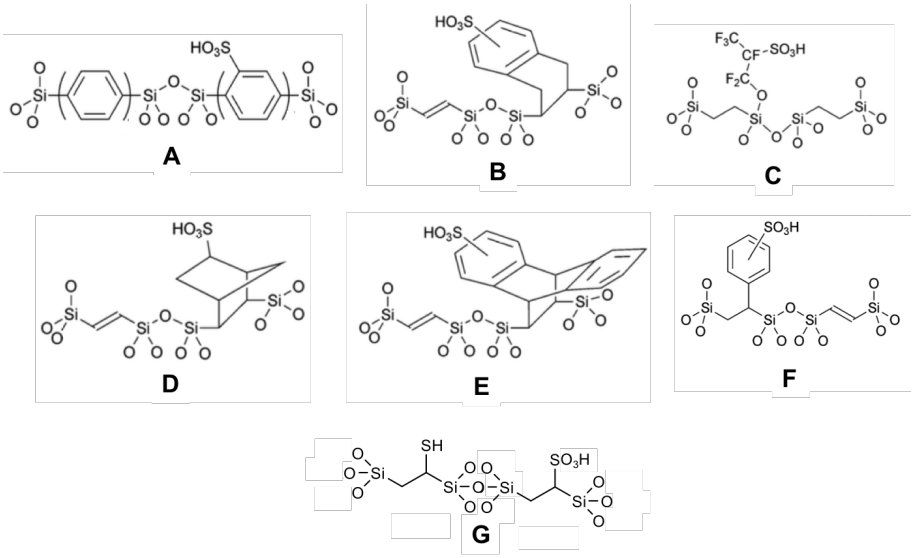

Figure 3.5: Overview of PMOs bearing sulfonic acid (SO_3H)-groups as Brønsted acid sites within their structure.

Base catalysis is far less explored on PMOs, and often materials are obtained employing 3-aminopropyltriethoxysilane (APTES) in a co-condensation procedure (Type 1), although it is possible to modify a benzene-PMO

into an aniline one via a two step procedure [132]. Another particular Type 3 PMO was prepared using tris(3-(trimethoxysilyl)propyl)-amine as precursor, resulting in tertiary amines inside the pore walls. These groups are highly active as catalysts for the Knoevenagel condensation of malononitrile and benzaldehyde and for the benzaldehyde-nitroethane Henry reaction [182].

Combining both an acid and base catalytic site in one PMO material gives rise to a bifunctional material that can be of interest to perform multistep or tandem reactions. This is implemented with multiple synthesis steps such as co-condensing a benzene or disulfide bis-silane with APTES, protecting the amine group (NBoc) while oxidizing the disulfide or sulfonating of the benzene and finally deprotecting the NH_2-group [183, 184]. Others provide routes based on the ethene-PMO, where the double bond is either treated with $NaHSO_3$ or epoxidized and opened with NH_3 to obtain a bridged SO_3H- or NH_2-group, respectively. Bifunctionality is introduced by co-condensation with the complementary catalytic site (**Figure 3.6**) [128]. Next to this, combinations of PMO supported nanoparticles (NPs) with a Brønsted acid or base site can also be considered as bifunctional catalysts [185].

Recently, chiral proline and proline derivatives grafted onto MPSs and PMOs gained high interest as these combine acid-base properties together with enantioselectivity in asymmetric aldol condensation reactions, however no reports of covalently bound PMO systems are reported [152]. Alternatively, cysteine-derivatives and cysteamine have been clicked onto ethene-bridged PMOs, yet low activity is observed when the acidic silanol groups do not promote the acid catalyzed reaction [169, 186]. Next to this, cinchona alkaloids and imidazolidinone compounds (MacMillan catalysts) are promising enantioselective organocatalysts which have been supported on silica gel or PMOs via grafting [186, 187]. These examples show that still a lot of possibilities are around in this field of PMO research and that major improvements are yet to be implemented. Finally, a somewhat underexploited area is enzymatic catalysis supported on PMOs considering that hydrophobic mesopores are attractive to accommodate these bulky groups [188].

3.2.5 PMOs as support for metal complexes

Metal complexes are an ever increasing group of homogeneous catalysts, which are particularly interesting as they are known to promote some of the most important reactions in fine chemical synthesis, e.g. Suzuki and Heck reaction, olefin metathesis, Phauson-Khand reaction, ... Many of

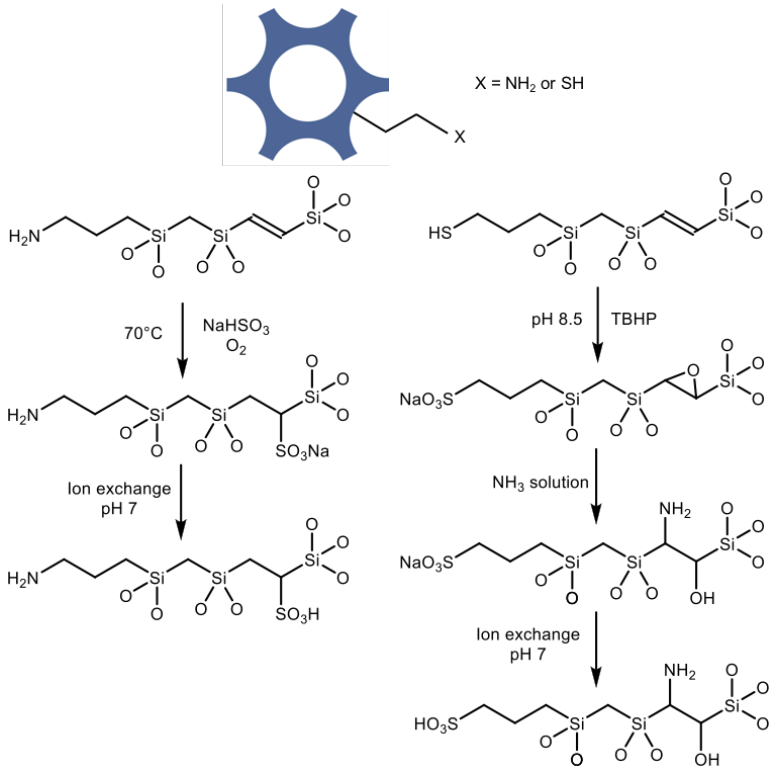

Figure 3.6: Synthesis procedure for bifunctional acid-base catalysts as developed by [128].

these metal catalyzed reactions are very selective and chiral ligands can induce enantioselectivity in the reaction products. Being homogeneous, however, separation and recycling of the catalyst is troublesome. Loss of catalyst is especially critical when expensive metals such as Ru, Pd, Au, Rh and Ir are used together with intricate chiral ligands. Heterogenization of the active site on a PMO support is an elegant method, often explored nowadays, to obtain a catalyst that can be easily separated from the medium by filtration. Such PMO is basically a solid ligand which after anchoring of a metal ion delivers a solid metal complex.[3] Several synthesis methods are possible to obtain such material.

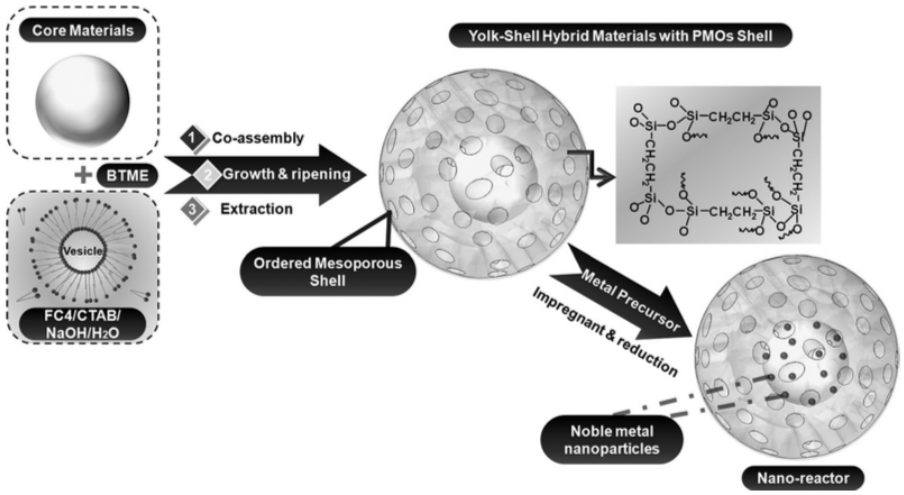

Figure 3.7: Synthesis and structure of PMO yolk-shell hybrid materials with supported metal NPs, taken from reference [190].

In general, ligands are relatively bulky and flexible groups, which require co-condensation of ligand-bridged bis-silanes with TEOS to obtain a structurally robust PMO (Type 0 PMOs, **Figure 3.8**). In a second synthesis step, the metal ion of interest is attached. This method especially allowed the incorporation of some important yet bulky ligands such as a chiral tartrate (Sharpless-Kagan) ligand for Ti-catalyzed asymmetric sulfoxidations into a porous solid (**A**) [191]. A Ru-BINAP solid ligand

3. Apart from supports for metal-complexes, PMOs have also been disclosed a supports for NP-based catalysis. Typically, an organic functionality of the PMO is used as a site for seeded growth of the particle confined inside the pores e.g. sulfur containing PMOs for Au-NP growth [189]. Another architecture is to grow a hollow PMO sphere around solid silica particle on which NPs are formed after impregnation and reduction. This is reported using a fluorocarbon (FC-4) as surfactant to yield Au, Pt and Pd yolk-shell particles as catalytic nano-reactors (**Figure 3.7**) [190].

PMO is employed in the asymmetric hydrogenation of β-ketoesters (**B**) [192]. Pd-mediated Wacker oxidation of styrene with H_2O_2 is described on a β-diketimine-PMO, while the Suzuki reaction is investigated using an imidazolium chloride ionic liquid-PMO (**C, D**) [193, 194]. Furthermore via this approach, a heterogeneous diimine-Ni complex is used for ethylene polymerization inside the PMO pores, which led to confined polyethylene particles (**E**) [195]. Finally, Type 0 PMOs were developed bearing N-heterocyclic carbene (NHC) and porphyrin groups inside the pore walls (**F, G**)[196, 197]. Next to the reduced stability compared to pure PMOs and the relatively low loading resulting from TEOS co-condensation, these materials have another not ignorable drawback. As the ligand is fixed in between two silicon atoms, the rotational freedom of the ligand is hampered, which may result in a reduced ability or incapability to bind metal ions after the synthesis of the PMO or which may result in a different conformation of chiral ligands as compared to their homogeneous analogues [120].

To circumvent this latter issue, PMOs have been synthesized immediately using metal-complex bridged precursors (**Figure 3.9**). Again, these are rather bulky groups and generally the use of TEOS is required. Examples include a $Rh(PPh_2X)Cl$ with $X = (EtO)_3Si(C_2H_4)$ PMO used for the hydrogenation of alkenes (**H**), a ferrocene bridged PMO (**J**) and vanadyl-acac bridged PMO (**I**) for benzene hydroxylation with H_2O_2 [198–200]. This approach, however, is also not without risk as the bridged complex needs to be stable in the synthesis conditions (acid or base) used to prepare the material.

All of the above examples of solid ligand PMOs are not 100% polysilsesquioxane frameworks but next to these, also Type 1 and 2 materials, with their specific benefits and drawbacks, have been reported (**Figure 3.10**). For Type 1, a benzene bridged PMO was grafted with a chiral bisoxazoline-Cu complex (**L**)[201]. Type 2 examples comprise a NHC-IMes bis-silane co-condensed with BTEE (**K**) and a BINAP-PMO using a biphenyl-bridged precursor (**M**) which were employed in Pd catalyzed Suzuki cross-couplings and Rh catalyzed hydrogenations respectively [202, 203]. Furthermore, the same $Rh(PPh_2X)Cl$ materials as described earlier, were prepared using BTEB as co-condensation precursor instead of TEOS [204].

Reports of Type 3A PMOs with bridging ligands are scarce and heavily rely on rigid aromatic precursors (**Figure 3.11**). Kuschel et al. describe acac-like mesoporous organosilica monoliths as interesting oxygen-donor ligands starting from a 1,5-diphenyl-propane-2,4-dione precursor (**P**) [205]. Periodicity, however, was not obtained. Waki and co-workers,

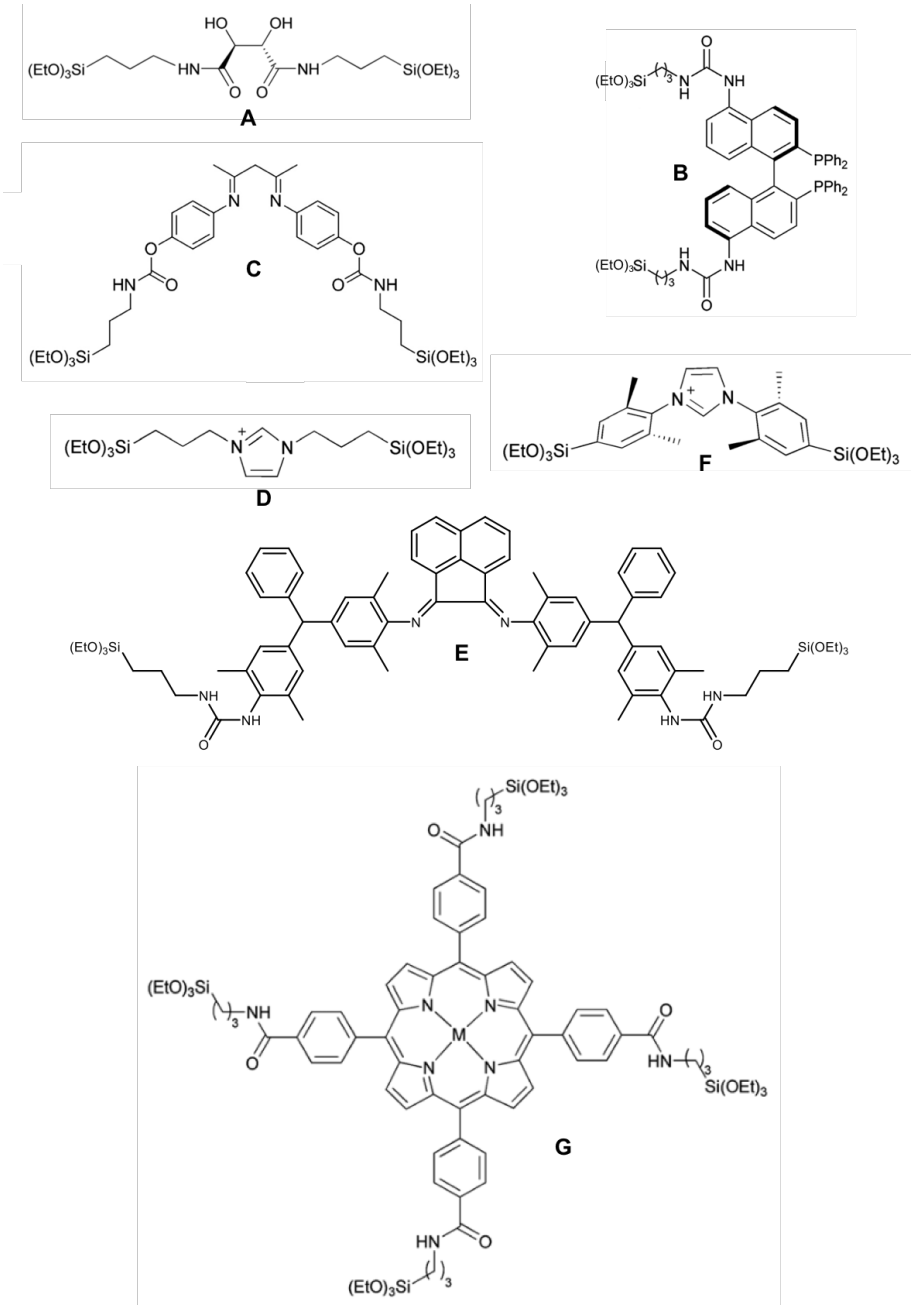

Figure 3.8: Examples of bis-silane precursors with coordinative properties used in Type 0 PMO synthesis.

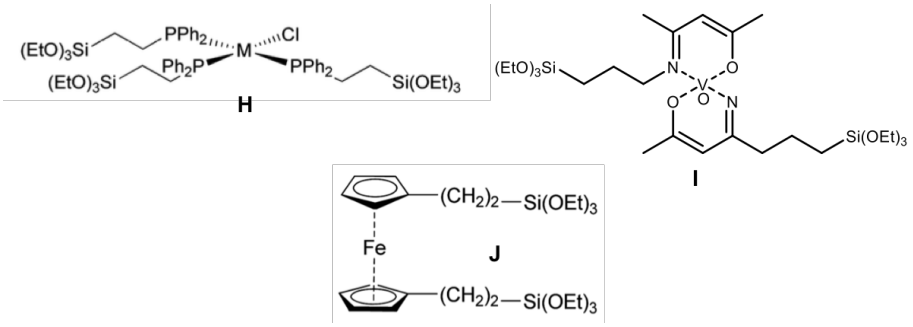

Figure 3.9: Examples of bis-silane precursors consisting of a metal complex used in Type 0 PMO synthesis.

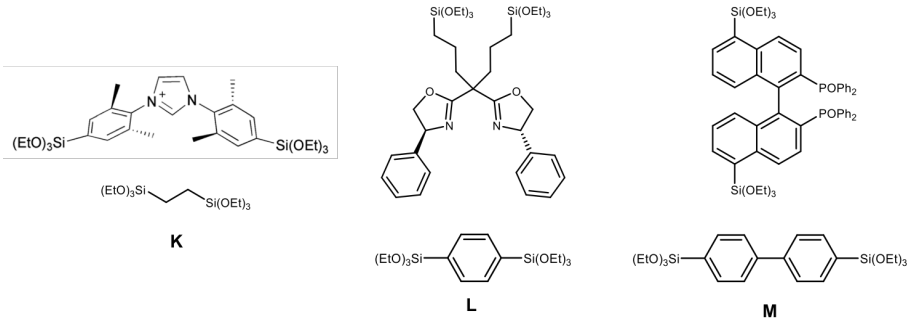

Figure 3.10: Examples of bis-silane precursors with coordinative properties used in Type 1 and Type 2 PMO synthesis.

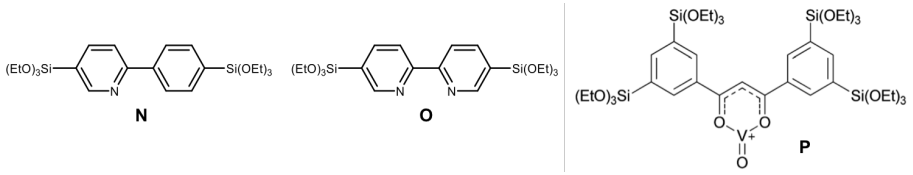

Figure 3.11: Examples of bis-silane precursors with coordinative properties used in Type 3A PMO synthesis.

on the other hand, were successful in the synthesis of 100% 2-phenylpyridine (**N**) and bipyridine PMOs (**O**) with crystal-like pore walls [117, 206]. Both are good solid ligands to anchor Ir, Rh, Ru, Re and Pd complexes to the PMOs, which were subsequently used as catalysts for the direct C-H borylation of arenes (Ir-PMO). Unfortunately, most popular ligands are not as rigid as these examples.

For this reason, the intention here is to transform a 100% PMO with a reactive group into a solid ligand via post-modification. Such Type 3B PMO has the potential to deliver the ultimate catalytic support. The stability of the PMO is hereby combined with a (multidentate) ligand which is covalently bound to the support. Moreover it is, free from conformational restrictions as it dangles accessibly in the pores. Inspired by the clicking of ligands on thiol-modified MPS, the thiol-ene reaction is very apt to perform this post-modification as it is highly efficient and tolerates many functional groups.

3.3 Click chemistry for decoration of the pore surface

The term click chemistry was first coined by Sharpless in 1998 (Nobel Prize in 2001) and includes a range of intriguing chemical reactions which, by definition are [207]:

- modular: one reaction type should tolerate many or all organic functional groups.
- wide in scope: the reaction should be applicable from molecular reactions to polymer and materials science.
- resulting in high chemical yields.
- only generating inoffensive byproducts.

- stereospecific: yet enantioselectivity is not explicitly required.
- physiologically stable.
- 'spring-loaded': reactions should exhibit a large thermodynamic driving force (Δ G $>$ 84 kJ/mol) to favor a selective reaction with a single product.
- highly atom efficient: as much of the initial reagents as possible should be incorporated in the end-product to reduce waste.

On top of this, with the concepts of Green Chemistry in mind, these reactions are preferably:

- easy to perform, with simple reaction conditions and requirements.
- using readily available reagents.
- solvent-free or using a benign (H_2O) or easily removable solvent.
- providing straightforward product isolation (non-chromatographic).

These requirements describe the ideal click reaction, however, in practice it is unlikely that one single reaction suits every situation and application. Nonetheless, a couple of reactions come relatively close to ticking all of the above boxes. Widely investigated and applied are [3+2] cycloadditions, with the Cu-catalyzed Huisgen 1,3-dipolar cycloaddition as the most renown reaction (**Figure 3.12**, a). Although this reaction is very efficient, the Cu(I) used is toxic, and as the triazole formed is able to coordinate Cu(I), metal impurities, often undesired in materials science, can be introduced. This reaction can be performed Cu-free, but then requires activation of the alkyne via ring strain, limiting the amount of substrate molecules (b). Furthermore, working with azides always comes with explosion hazards.

Other reactions that live up to the definition include the Diels-Alder reaction (e), the Schotten-Baumann reaction between acid chlorides and amines (f), the reaction between isocyanates and amines to form ureas (g) and nucleophilic substitution to small strained rings like epoxy (h) and aziridine (i) groups (**Figure 3.13**). The Diels-Alder reaction, however, is often listed as click-reaction, yet its presence is debatable as typically, a high excess of diene or dienophile is required to obtain high yields. Nonetheless, all the above reactions have been described in Part I to either synthesize new bis-silane precursors or to perform post-modifications. This clearly indicates the relevance and potential of click

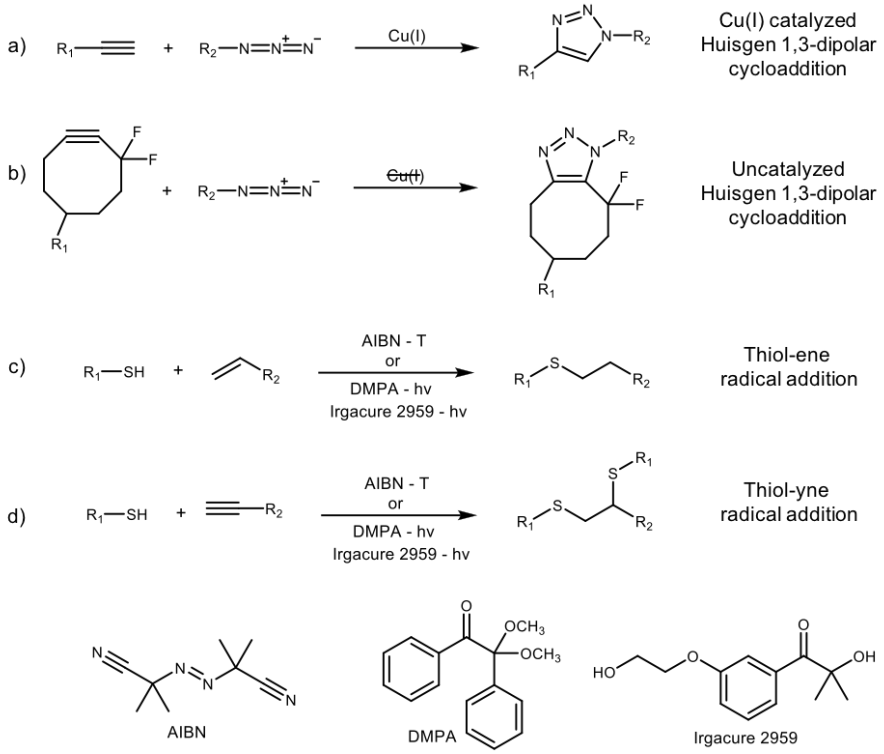

Figure 3.12: Click chemistry: chemical representation of the Huisgen 1,3-dipolar cycloaddition and the radical thiol-ene/yne reaction. Bottom: Molecular structure of commonly applied UV radical initiators.

reactions in organosilica research. Perhaps the most attractive click reaction is the radical addition of thiols to alkene or alkyne groups (thiol-ene/yne click) (**Figure 3.12**, c and d) [208, 209]. This reaction is induced by a radical initiator (thermal or light)[4] and results in quantitative yields of the anti-Markovnikov product[5] with no by-products (**Figure 3.14**). The thiol-ene reaction is carried out in mild conditions, tolerates many functional groups, is water-compatible and can be performed solvent free.

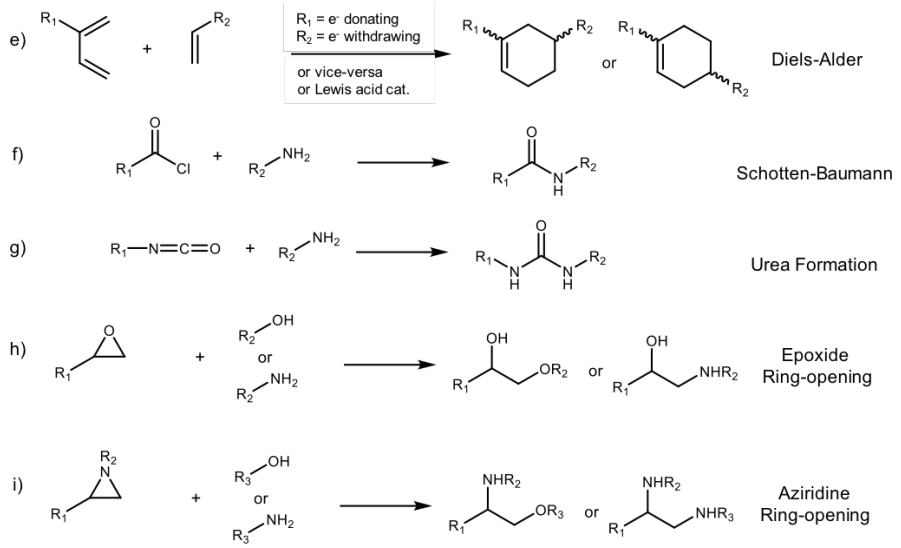

Figure 3.13: Click chemistry: a selection of other reactions that can be defined as click chemistry.

Because of all the above, click chemistry, is highly attractive for modification of the surface of porous solids. Furthermore, given its modularity, it is a very useful tool for attaching chelating agents via one single covalent bond to a support. Such covalent attachment is inherently more stable (in water) than conventional but leach-prone grafting of a trialkoxysilane ($(XO)_3SiR$) onto free silanol groups of MPS or PMOs. Moreover, click chemistry yields a more homogeneous distribution of the functionalities within the porous scaffolds, resulting in augmented catalytic activity [187, 211].

4. A typical thermal radical initiator is azobisisobutyronitril (AIBN). This compound forms a radical upon decomposition above 65°C and is safer to use than benzoylperoxide. Common photoinitiators are dimethoxy-2-phenylacetophenon (DMPA) and Irgacure 2959, which are used solvent-free and in water respectively.
5. As a consequence, vinyl and allyl groups are more reactive in the thiol-ene reaction than more substituted olefins [210].

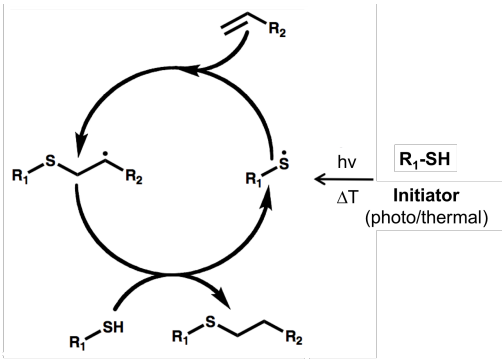

Figure 3.14: Thiol-ene click chemistry: reaction mechanism.

Specially designed alkyne or azide organosilicas, either PMOs (Type 1) or MPSs co-condensed with $(XO)_3Si(CH_2)_3N_3$, can easily be transformed by Cu(I) catalyzed azide-alkyne cycloaddition, into a desired functionality, e.g., dyes, adsorbent moieties or catalysts [152, 186, 187, 211–214]. Next to this, thiol-ene click chemistry, which can be performed solely in water at room temperature using an appropriate UV-active radical initiator (as compared to the water/THF mixture used in CuAAC) has also been applied in organosilica research. The reaction is readily performed both on ethenylene-bridged organosilica precursors in solution [133] as well as on porous materials having accessible thiol groups. The latter post-modification was shown in the attachment of catalytically active chiral quinine, proline or vanadyl-Salen complexes on 3-mercaptopropyl functionalized SBA-15 [120, 159, 215], in the modification of a thiol bearing PMO with Rose Bengal [216], in organosilane coatings [217] and in the attachment of organosilica nanoparticles on glass [218]. Only recently, ethenylene-bridged PMOs have been modified by thiol-ene reactions for the first time. Such PMOs, clicked with cysteine and cysteamine, were successfully used in the aldol condensation of 4-nitrobenzaldehyde and acetone [169].

An allyl-functionalized interconnected $[CH_2Si]_3$ ring-type PMO based on AHETSCH, shows great promise for click modification as the dangling and highly reactive allyl moieties of this material are easily accessible for post-modification. Furthermore, to our knowledge, there are no reports exploiting the thioether functionality inherently created by a thiol-ene click reaction. Given that the sulphur atom is generally known to interact strongly with late transition metals e.g. Ru, Rh, Pd, clicking a functional group provides a straightforward pathway to a bidentate solid ligand (see Section 3.5).

3.4 Ru-based oxidation reactions

The oxidation of primary alcohols to aldehydes and carboxylic acids and the oxidation of secondary alcohols to ketones are widely recognized among the most important reactions in organic synthesis. In classic chemistry this reaction is very often performed with stoichiometric oxidants such as $KMnO_4$ and CrO_3 combined with H_2SO_4 in the Jones-oxidation. Not only are these reagents present in the same phase as the products, they also produce waste in the form of salts after the reaction and are harmful or toxic. In recent days, with processes needing to live up to far more stringent ecological standards, new environmentally benign methods are being developed, with emphasis on heterogeneous catalysts. Therefore, the oxidation reaction is heavily studied and all sorts of catalysts have been found for this reaction. The main focus of alcohol oxidation reactions lies on the usage of O_2 or air as green oxidants. Several mixed metal catalysts especially using Pt, Pd, Au, Co, Cu and V supported on carbon, alumina or titania are known to promote this aerobic oxidation [219–222]. Although these are highly promising and relatively simple and cheap catalysts, supported metal catalysts have undefined catalytic sites and more often than not deactivation is witnessed. This latter is generally caused by metal leaching, poisoning of the catalytically active centers at the surface through irreversible adsorption of products, or clustering of the metal sites as a result of Ostwald ripening when subjected to harsh reaction conditions.

Also for ruthenium, both in homo- or heterogeneous catalysis, research aims on the use of O_2 or air as benign oxidants [223–230]. Unfortunately, in almost all reports the reaction is performed at elevated temperatures, in toluene or a halogenated solvent (e.g. trifluorotoluene) and often a co-oxidant is used. All of this is clearly undesired in green chemistry. High yields are witnessed for aromatic substrates in which the oxidation is driven by expansion of the aromatic system (e.g. oxidation of benzylalcohol to benzaldehyde). Switching to non-aromatic substrates, however, the yield becomes moderate.

On the other hand, catalytic systems have been described where this Ru-oxidation is performed in water and at room temperature [231]. The trade-off is that periodic acid, H_5IO_6 is used as sacrificial oxidant. However, this cheap, non-toxic oxidant is safe and easy to handle and can be recovered via electrochemistry. In the same report, a $[Ru(CH_3CN)_2(acac)_2]PF_6$-complex is heterogenized on MPS via an NH_2-group and used for the selective oxidation of alcohols. Many substrates are investigated, but leaching and recycling tests are not considered.

3.5 Heterogeneous Ru(III) oxidation catalysts via click bidentate ligands on a periodic mesoporous organosilica support

The aim of this work is to develop our suggestion for the ultimate catalytic support in terms of stability and versatility for organic reactions in water. Such support would require large, ordered pores and a high surface area together with high structural stability and leach-proof functionalities. Therefore, as indicated earlier, AHETSCH is a suitable candidate. This precursor has already been developed into particles with spherical morphology and has been applied as a HPLC packing [232]. The material's versatility is illustrated by the straightforward thiol-ene modification of the allyl groups with a C18-chain. Furthermore, it exhibited a exceptional hydrolytic stability ($>$ pH 12 and $>$ 150°C), in analogy with similar ring-structured PMOs [41, 87].

The AHETSCH-based materials from this report are, however, not optimized for catalysis as they possess unstructured pores of 3.1 nm given that the slightest disorder of mesopores already has a significant adverse impact on the diffusion of molecules within these pores [143] and that such small pores cannot easily accommodate large complexes and reagents. Furthermore, a mixture of ring and allylated ring precursors was used which results in hampered reproducibility of the synthesis and varying functional loading.

Here, we present the hydrothermal synthesis of an AHETSCH-based 100% monoallyl ring-type PMO (mAR) optimized for catalytic applications, using P123 as SDA to create uniform and large ordered pores (**Figure 3.15**). The allyl groups are one-step post-modified with reagents of the form HS$-(CH_2)_2-$X, with X = NH_2, OH, SH, to obtain a heterogeneous bidentate ligand in a green and facile manner by using thiol-ene click chemistry. These ligands are attached via a single thioether bond, allowing ensured coordination of complexes without leaching of the functionality at low or high pH (cfr. grafted functionalities). The stable thioether bond is further exploited as part of the bidentate ligand, given its affinity for late transition metals. Finally, a Ru(III)-complex is anchored onto the chelating ligands inside the PMO pores. The resulting well-defined heterogeneous Ru-catalyst is then tested in the oxidation of carefully selected alcohols in water at room temperature while recycling and catalyst-leaching assessments are performed.

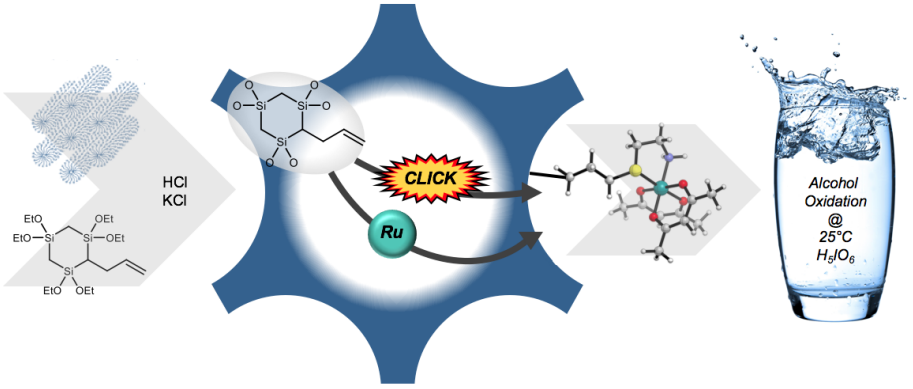

Figure 3.15: Graphical overview of the synthesis of an AHETSCH-based 100% monoallyl ring-type PMO, click post-modification into solid ligands, anchoring of a Ru(III)-complex and catalytic assessment.

Chapter 4

Experimental

Following chemicals were used as received: Pluronic P123 (Mn = 5800, Sigma-Aldrich), KCl (≥99.5%, Carl Roth), HCl (37%, Carl Roth), 2-hydroxy-4'-(2-hydroxyethoxy)-2-methylpropiophenone (Irgacure 2959, 98 %, Sigma-Aldrich), 2-aminoethanethiol (>95%, TCI Europe), 2-mercaptoethanol (99%, Acros), 1,2-ethanedithiol (≥98%, Sigma-Aldrich), ruthenium(III)-acetylacetonate (99%, STREM), acetonitrile (anhydrous, 99.8%, Sigma-Aldrich), H_2SO_4 (96%, Carl Roth), n-pentane (≥99%, Carl Roth), CH_2Cl_2 (≥99.5%, Carl Roth) toluene (anhydrous, 99.8%, Sigma-Aldrich), ammonium hexafluorophosphate (99%, STREM), H_5IO_6 (99%, ABCR), benzylalcohol (99-100.5%, Sigma-Aldrich), cyclohexanol (99%, Sigma-Aldrich), (±)-menthol (>98%, TCI Europe).

4.1 Hydrothermal synthesis of mono-allyl ring-PMO (mAR)

In a 50 ml flask, a mixture is made with molar composition AHETSCH: H_2O:P123:HCl:KCl 1:500:0.0517:8.62:23.5. First, 0.375 g of Pluronic P123 is dissolved in 11.25 ml H_2O. Subsequently, 0.9 ml of HCl (37%) and 2.19 g of KCl is added and the solution is stirred (800 RPM) until a clear blue solution is obtained. Under continued stirring, the reaction mixture is heated to 45°C after which 0.5625 g AHETSCH is added at once. 3 h later, stirring is switched off and the temperature is raised to 95°C in order to promote further condensation of the AHETSCH precursor for 24 h (ageing step). A white precipitate is filtered off and washed with 3 x 25 ml H_2O and 3 x 25 ml acetone. The template (P123) is removed during a 6 h Soxhlet extraction in acetone and afterwards, the powder

is dried overnight at 120°C under vacuum. The amount of allyl groups is determined gravimetrically by bromination of the double bonds [127].

4.2 Click post-modification of mAR to mAR-SX (X = NH_2, OH, SH)

The accessible allyl groups in the pores of mAR react with 2-aminoethanethiol, 2-mercaptoethanol or 1,2-ethanedithiol to obtain solid bidentate ligands, i.e., an amine- (mAR-SNH_2), hydroxyl- (mAR-SOH) or thiol- (mAR-SSH) functionalized thioether, respectively (**Figure 4.1**). In a general procedure, 3 eq. of thiol per double bond (see also Section 5.2) are mixed with 0.75 eq. of Irgacure 2959 in 20 ml of H_2O and flushed with Ar. 0.5 g of mAR is added and the suspension is stirred at room temperature in a home-made UV reactor (λ = 360 nm) for 1h. The products are filtered as off-white powders and resuspended in H_2O at reflux temperature to remove any leftover reagents. Finally the powders are dried at 110°C for 24 h and loading is determined via CHNS elemental analysis.

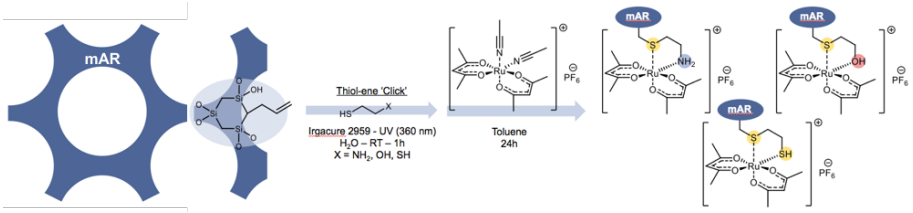

Figure 4.1: Schematic representation of the thiol-ene click post-modification and anchoring of $[Ru(acac)_2(CH_3CN)_2]PF_6$ onto the solid bidentate thioether ligands.

4.3 Synthesis of $[Ru(acac)_2(CH_3CN)_2]PF_6$ and anchoring onto mAR-SX

As adapted from literature [233], $[Ru(acac)_2(CH_3CN)_2]PF_6$ is prepared by dissolving 1 g of $Ru(acac)_3$ in 100 ml of a 1.5% H_2SO_4 solution in anhydrous acetonitrile and stirring this at room temperature until the red solution turns deep blue (approx. 5 h). Next, 90% of the solution is evaporated and cooled to 0°C. $[NH_4PF_6$ (0.409 g, 1.5 eq.) in 10 ml of H_2O is added under stirring and the solution is left to stand for 30 min. $[Ru(acac)_2(CH_3CN)_2]PF_6$ (85%) is obtained as a blue precipitate which

is filtered, washed (2 x 10 ml of ice water, 2 x 10 ml of pentane) and dried for 24 h under vacuum.

Subsequently, $[Ru(acac)_2(CH_3CN)_2]PF_6$ is heterogenized by stirring mAR-SX with 0.5 eq. of complex per bidentate ligand in toluene (100 ml/g mAR-SX) for 24 h at room temperature (**Figure 4.1**). The solids (mAR-SX-Ru) are obtained as purple powders after filtration, washing with minimal amounts of CH_2Cl_2 and vacuum drying overnight at 30°C.

4.4 Synthesis of aminopropyl grafted SBA-15 and anchoring of $[Ru(acac)_2(CH_3CN)_2]PF_6$

4 g of P123 is dissolved in 120 ml of a 2 M HCl solution and 30 ml H_2O at 45°C. 9.1 ml TEOS is added at once and the solution is stirred heavily for 5 h at 45°C. Then, stirring is stopped and temperature is raised to 90°C and the solution is left to stand for 18 h. Hereafter, the white solid is filtered off and washed with 3 x 10 ml H_2O. Finally the SBA-15 powder is calcined for 6 h at 550°C with a heating rate of 2°C/min (S_{BET} = 670 m_2/g). 0.5 g of SBA-15 is suspended in 10 ml of dry toluene and 1.427 ml of aminopropyl-(triethoxy)silane (APTES) is added. The mixture is then reacted for 24 h at reflux temperature. The product is filtered off and washed with 3 x 10 ml CH_2Cl_2 and dried under vacuum at 120°C. $[Ru(acac)_2(CH_3CN)_2]PF_6$ is anchored in the same conditions as for the PMOs.

4.5 Alcohol oxidation: catalytic procedure

1 mmol of substrate (benzylalcohol, cyclohexanol, (±)-menthol) is weighed off in a 15 ml reactor; 10 ml of H_2O and the supported catalyst (0.06 mol% Ru in respect to the substrate) are added, together with 0.1 g of toluene as a standard with similar low solubility as the analytes in water. An extraction efficiency factor is determined for all analytes to compensate for extraction losses. To start the reaction, 1.1 eq. of H_5IO_6 is added while stirring and the reaction is kept at 25°C for 3 h. Then, the solid catalyst is filtered off and the filtrate is extracted 3 times with 25 ml of diethylether. Finally, the samples are analysed by means of gas chromatography. For recycling tests, the catalyst is washed with H_2O and acetone and dried at 30°C overnight. Catalytic profiles are constructed by taking 1 ml aliquots at set times. To test the heterogeneity of the catalyst, the solid is filtered off (0.45 μm membrane)

after 10 min of reaction time and the catalytic activity of the filtrate is further evaluated (hot filtration test).

4.6 Characterization and analysis

X-ray powder diffraction (XRPD) patterns of all mAR-PMOs are recorded on a Thermo Scientific ARL X'TRA X-ray diffractometer using Cu Kα radiation of 40 kV and 30 mA. A Micromeretics Tristar II is used for N_2-sorption experiments at 77 K to obtain the internal surface area (S_{BET}) and pore size distribution (d_{BJH}) making use of the BET and BJH theory, respectively. Diffuse Reflectance Infrared Fourier Transform Spectroscopy (DRIFTS) is performed using a Thermo Nicolett 6700 FT-IR spectrometer equipped with a Greasby-Specac diffuse reflectance cell, modified to measure samples at 20 - 300°C under vacuum. For CHNS elemental analysis, a Thermo Flash 200 elemental analyser is used with V_2O_5 as catalyst. Transmission electron microscopy (TEM) images are taken on a JEOL JEM 2200-FS TEM and scanning electron microscopy (SEM) images on a JEOL JSM 7600F FEG SEM. Ru loadings (Kα) are determined by X-ray fluorescence (XRF) on a Rigaku NEX CG with an Al source and compared to Sr-Kα as internal standard. All catalytic tests are analyzed with an ultrafast TRACE GC (Thermo, Interscience) equipped with a flame ionisation detector and a 5% diphenyl / 95% poly-dimethylsiloxane column (10 m x 0.10 mm) using He as carrier gas at 0.8 mL/min.

4.7 Computational methodology

All calculations are performed within the Gaussian09 (G09) package [234] using Density Functional Theory (DFT). Calculations are performed using the B3LYP [235, 236] and OPBE [237–240] functionals and a Def2-TZVP polarized split-valence triple-ε basis set [241, 242]. Dispersion corrections are added using Grimme's DFT-D3 version [243] with Becke-Johnson damping [244] The coefficients for the OPBE calculations are taken from Goerigk et al. [245] (S8 = 3.3816, a_1 = 0.5512 and a_2 = 2.9444) and defined manually in the Gaussian program. Furthermore, a correction energy for the Basis Set Superposition Error (BSSE) is calculated using the Boys and Bernardi Counterpoise correction [246].

Chapter 5

Results and discussion

5.1 mAR-PMO as a stable and multifunctional catalytic support

The synthesis and work-up of AHETSCH as the PMO-precursor is successfully optimized, yielding a pure compound and no longer a mixture of mono-, bis- and trisallylated HETSCH (**Figure 5.1**) as described before.

The importance of this purification is seen in the X-Ray diffractograms (**Figure 5.2**) of mAR and a PMO, denoted mixAR, synthesized in the same conditions as mAR but using the unpurified precursor mixture. For mAR, an intense (100) reflection peak is distinguished, together with less intense second order (110) and (200) peaks, which are indicative for the 2D hexagonal ($P6mm$) ordered pore structure of the material. The diffractogram of mixAR is however lacking the second order peaks, indicating the loss of long-range ordering.

These results are clearly confirmed in the TEM images of both materials (**Figure 5.2**) where ordering is found throughout the entire rod-shaped mAR particles (**Figure 5.3**). The mixAR-PMO only shows patches of

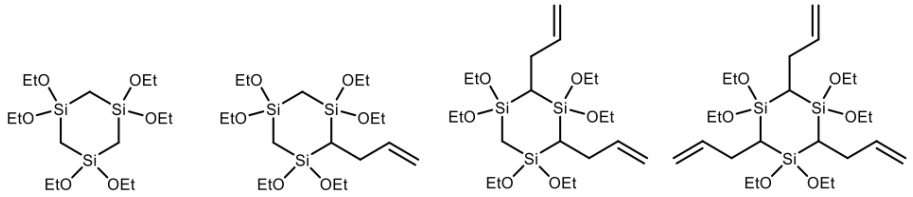

Figure 5.1: Mixture of HETSCH and AHETSCH precursors used in the synthesis of mixAR.

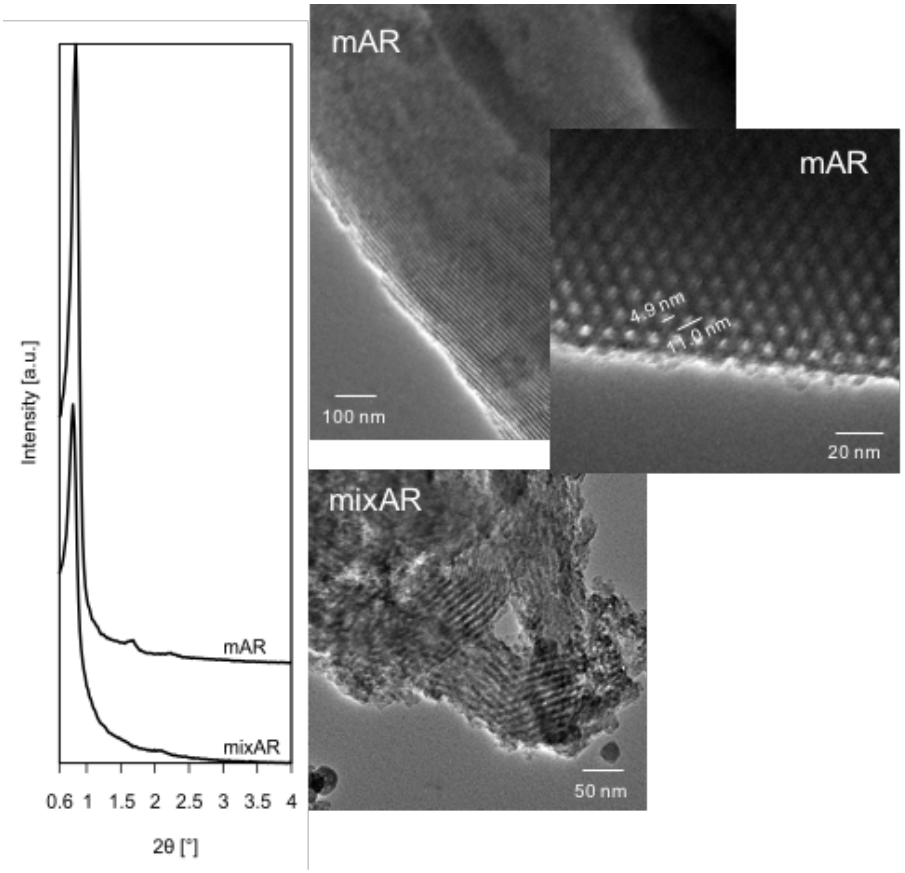

Figure 5.2: XRD diffractograms of the 100% monoallyl PMO (mAR, top) and the mixed precursor PMO (mixAR, bottom). TEM images confirm the ordered pore geometry of mAR.

ordered pores with variable alignment. The major enhancement of pore ordering for mAR is ascribed to a more uniform rate of hydrolysis and condensation of purified AHETSCH. Approximately the same unit cell parameter (a_0) for mAR is seen in the images as calculated via XRD (**Table 5.1**).

In terms of porosity similar differences are also observed. N_2-sorption experiments (**Figure 5.4**) show type IV isotherms with sharp H1 hysteresis for mAR, typical for highly ordered mesoporous materials with uniform cylindrical pores (SBA-15 like). mAR shows a high internal surface area ($S_{BET} = 536$ m^2/g) with 5.0 nm pores (d_{BJH}) in accordance with TEM images. Comparable results are obtained for mixAR ($S_{BET} = 472$ m^2/g, $d_{BJH} = 5.1$ nm) but the pore size distribution is broadened,

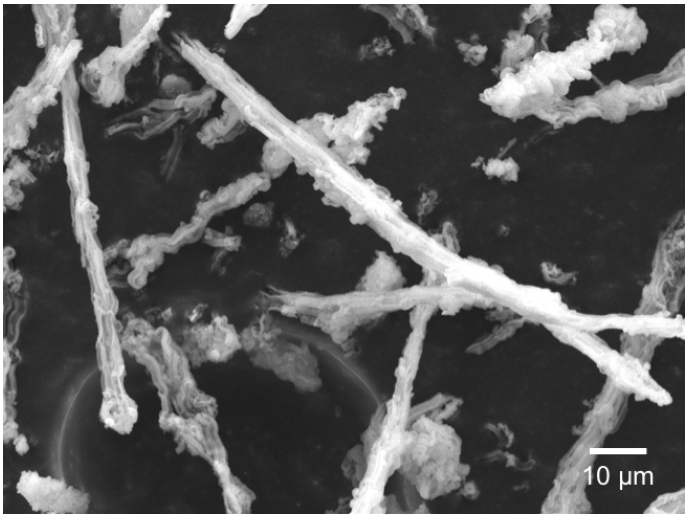

Figure 5.3: SEM image of mAR particles.

Table 5.1: Structural properties of the synthesized PMO materials.

	S_{BET} [m^2/g]^a	V_p [ml/g]^b	$d_{p,BJH}$ [nm]^c	a_0 [nm]^d
mAR	536	0.48	5.0	12.1
mAR-SNH_2	400	0.45	5.1	12.1
mAR-SNH_2-Ru	271	0.32	4.8	12.0
mAR-SOH	343	0.44	5.0	12.0
mAR-SOH-Ru	309	0.39	5.0	11.9
mAR-SSH	304	0.46	5.1	11.9
mAR-SSH-Ru	208	0.28	5.1	11.8

[a]Specific surface area determined via Brunauer-Emmett-Teller theory. [b]Mesoore volume determined via the BJH theory (adsorption isotherm). [c]Pore size calculated from desorption branch following Barrett-Joyner-Halenda theory. [d]XRD unit cell parameter ($a_0 = 2d_{100}/\sqrt{3}$) for $P6mm$ 2D hexagonal ordering.

the mesopore volume is decreased (V_p =0.48 ml/g vs. 0.41 ml/g) and increased macroporosity, attributed to irregular, disordered areas, is witnessed. Given that the slightest disorder of mesopores already has a significant impact on the diffusion of molecules within these pores [143], results of this structural assessment clearly indicate the superior quality of mAR as a catalytic support.

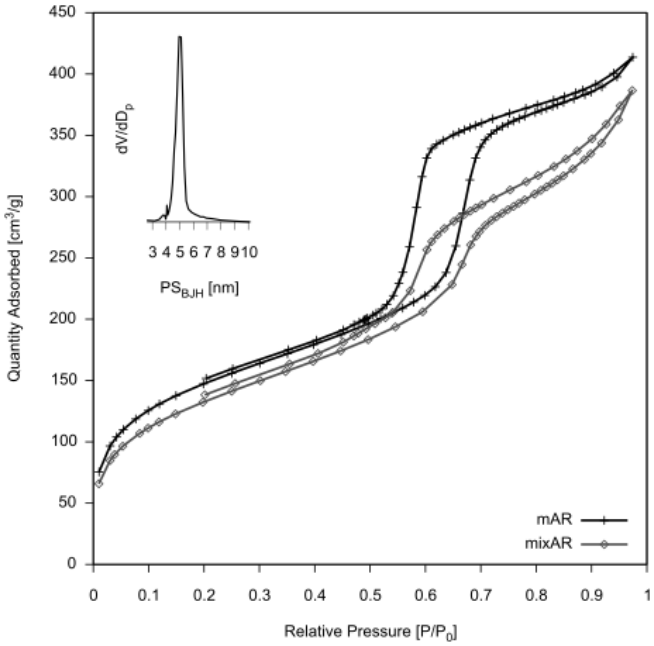

Figure 5.4: N_2-sorption isotherms of mAR and mixAR. Inset: BJH pore size distribution plot of mAR.

Furthermore, we have tested the hydrolytic stability of mAR-PMOs by stirring the material in a 1M HCl solution and a 0.1M NaOH solution at room temperature. In order to perform these tests, a new batch of mAR was prepared. The XRD diffractogram, S_{BET} and d_{BJH} (**Figure 5.5, Table 5.2**) of this sample are similar, 529 m^2/g and 5.0 nm respectively, to the initial mAR material, indicating a highly reproducible synthesis. After acid treatment at pH 0, the XRD and N_2 sorption show no structural change, although the pore volume has slightly dropped. Also, the material remains unaffected after 3 h in strong basic medium. Only after 24h at pH 13 mAR starts to show the first signs of deterioration, indicated by a small drop in surface area and pore size.

This exceptional hydrolytic stability compared to other silicas makes

mAR highly suitable for reactions requiring extreme pH in water. The hydrophobicity of mAR not only explains its stability as we experienced before [41, 232] but might also enhance mass transport of organics towards the catalytic support in water (see catalytic tests).

Table 5.2: N_2 sorption data of hydrolytically treated mAR

	pH	t [h]	S_{BET} [m^2/g][a]	$d_{p,BJH}$ [nm][b]
mAR (Reference)[c]			529	5.0
mAR-pH13-3h	13	3	539	5.0
mAR-pH13-24h	13	24	461	4.7
mAR-pH0-24h	0	24	540	5.0

[a]Specific surface area determined via Brunauer-Emmett-Teller theory. [b]Pore size calculated from desorption branch following Barrett-Joyner-Halenda theory. [c]A new batch of mAR (Reference) and the same material treated at 25°C for 3 h with a 0.1M NaOH solution (pH13-3h), 24 h 0.1M NaOH solution (pH13-24h) and treated for 24 h with a 1M HCl solution (pH0-24h).

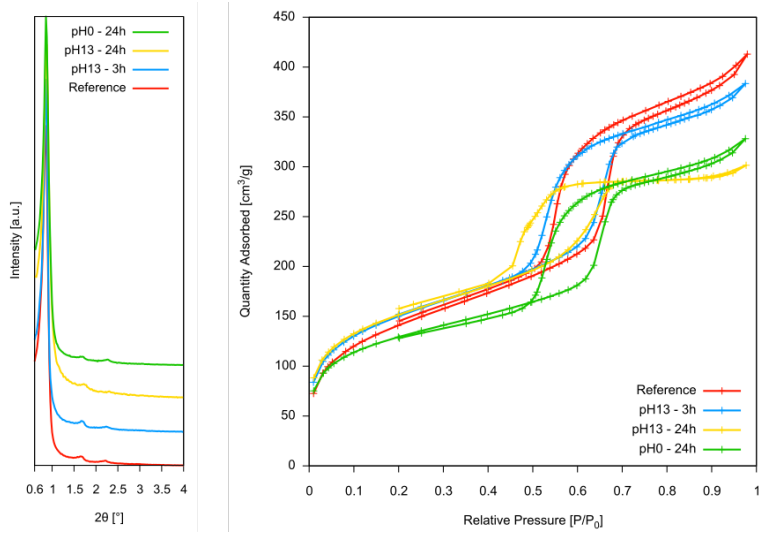

Figure 5.5: XRD diffractograms and N_2 sorption isotherms of hydrolytically stressed mAR (Reference).

5.2 Click post-modification of the allyl functional handles

The allyl groups of mAR are readily transformed into any organic functionality of interest via thiol-ene click chemistry. The amount of accessi-

Table 5.3: Functional loading of the ligand and the Ru-complex after click post-modification and Ru anchoring.

	mAR-SNH_2-Ru	mAR-SOH-Ru	mAR-SSH-Ru
Lig. [mmol/g][a]	0.73	1.70	1.72
Ru [mmol/g][b]	0.204	0.049	0.040
%[c]	27	2.9	2.3

[a]Ligand loading determined from S-content in CHNS elemental analysis. [b]Ru loading determined via XRF. [c]Amount of ligands functionalized with Ru(III).

ble double bonds is gravimetrically estimated at 2.4 mmol/g by performing a gas-phase bromination reaction [127]. The functional loading of the resulting materials (CHNS) after click reaction with 2-aminoethanethiol (mAR-SNH_2), 2-mercaptoethanol (mAR-SOH) and 1,2-ethanedithiol (mAR-SSH) on mAR is found in (**Table 5.3**). Treatment of 1 h in the UV reactor (λ = 360 nm) already leads to high functional loading (ca. 1.7 mmol/g) for mAR-SOH and mAR-SSH. No further increase of functionality is observed for a reaction time of 3 h or even 24 h. The click reaction of 2-aminoethanethiol is shown to be less effective (0.73 mmol/g). For all post-modification steps, a drop in S_{BET} is observed as a result of the mass increase of the material and the decoration of the pore walls with the functionalities (**Table 5.1**). Furthermore, no structural degradation is observed in the XRD diffractograms after functionalization (**Figure 5.6**).

The infrared spectrum (DRIFTS) of mAR is given in **Figure 5.7**. Next to C-H and 2 Si-O-Si stretch vibrations, in the region 2950-2800 cm^{-1}, 1200-1000 cm^{-1} and 800 cm^{-1}, respectively. Distinct peaks show up at 3070, 1640 and 890 cm^{-1} testimonial for the allyl-groups (olefin C-H stretch, C=C stretch and olefin C-H out of plane deformation). Vibrations in the 1475-1280 cm^{-1} region are typical for the modified ring structure. After bromination reaction (mAR-Br_2), it is clear that all C=C vibrations (1640 cm^{-1}) have disappeared (**Figure 5.7, zoom**), implying that Br_2 gas, due to its small size, reacts with allyl groups in the micropores and/or penetrates inside the pore walls. This makes us believe that the gas-phase bromination reaction overestimates the amount of reachable double bonds inside the material. During the functionalization process in water, the thiols cannot reach all of these allyl groups, indictated by the persisting C=C peaks in the IR spectrum. In accordance with a lower loading (CHNS), a less drastic decrease is observed for mAR-SNH_2, however, the primary amine gives rise to the appearance of new vibration peaks at 1607 and 1502 cm^{-1} (NH_2 bend and C-N stretch). O-H stretches (mAR-SOH) are not observed due to

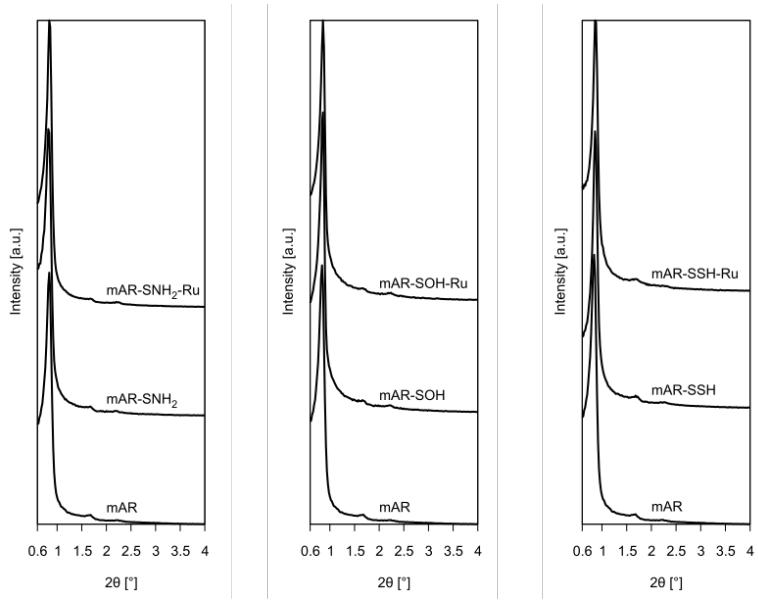

Figure 5.6: XRD diffractograms after thiol-ene click post-modification and anchoring of $[Ru(acac)_2(CH_3CN)_2]PF_6$.

overlap with residual adsorbed water. S-H vibrations (mAR-SSH) are distinguished at 2570 cm^{-1} in the RAMAN spectrum (**Figure 5.8**).

Table 5.3 also shows the amount of $[Ru(acac)_2(CH_3CN)_2]PF_6$ anchored onto the bidentate ligands created on the PMO. In mAR-SNH_2, Ru is attached to up to 27% of the SNH_2 ligands. In DRIFTS, the characteristic peaks of $[Ru(acac)_2(CH_3CN)_2]PF_6$, e.g. acac carbonyl stretches at 1544 and 1523 cm^{-1}, are superimposed on the mAR-SNH_2 spectrum to form mAR-SNH_2-Ru (**Figure 5.9**). Given the meticulous washing step, this indicates that anchoring of the Ru-complex is successful. As a 10 fold less Ru gets anchored to the SOH and SSH ligands, the Ru-complex peaks can no longer be identified. After anchoring, the PF_6^- counter ion remains present as confirmed by XRF.

Unfortunately, DRIFTS does not provide sufficient evidence of the exact complex formation once the Ru-complex is heterogenized. Furthermore, other techniques (e.g. XPS) proved insufficient because of the low Ru loading compared to the PMO matrix. Therefore, we conducted a computational study on a simplified ligand-Ru(III) model to explain the nature of complex formation.

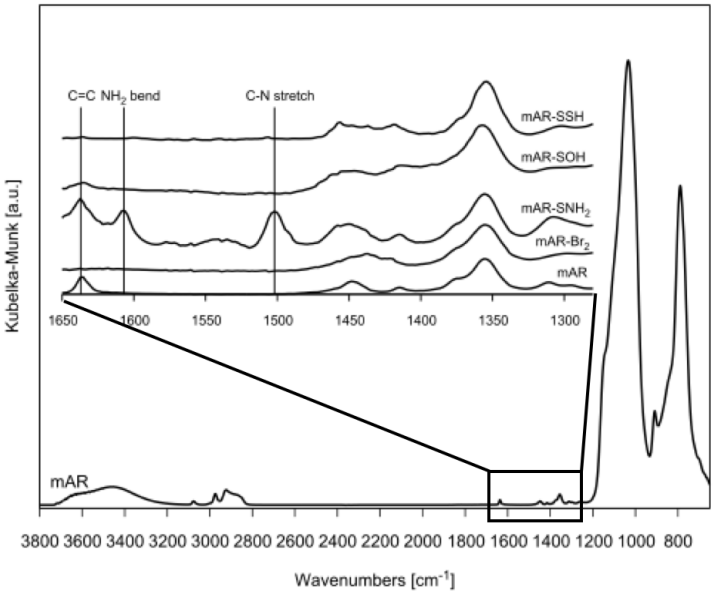

Figure 5.7: DRIFT spectrum of mAR. Inset: Zoom of the region of interest for reaction on the allyl groups.

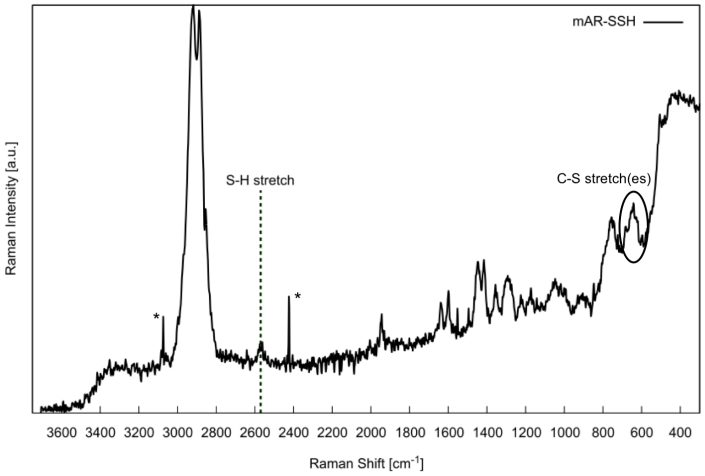

Figure 5.8: Raman spectrum of mAR-SSH (Laser power 0.45W, 4200 scans). S-H stretch Raman signal of free thiol groups is observed at 2570 cm^{-1}. Signals arising from the sulfide stretch can be seen around 700 - 620 cm^{-1}. Sharp peaks (*) arise from the glass vial in which the spectrum was recorded.

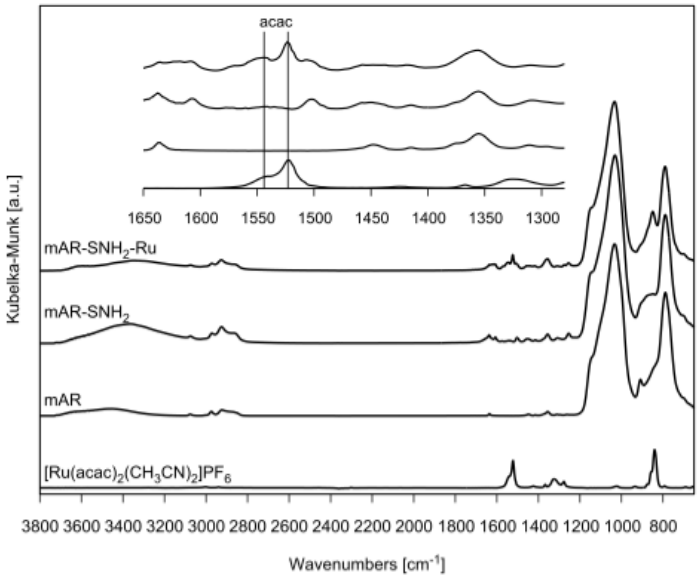

Figure 5.9: DRIFT spectrum of the homogeneous $[Ru(acac)_2(CH_3CN)_2]$-PF_6 complex, mAR, mAR-SNH_2 and mAR-SNH_2-Ru.

5.3 Computational study of complex formation

To study the complexation process of the Ru catalyst to the PMO anchored ligands, a simplified model system is constructed (**Figure 5.10**). This model comprises the Ru center, surrounded by two acac groups and the ligand of interest, terminated by a methyl group. We assume that the large pore diameter of 5 nm gives a large curvature and hence limited interactions with the pore wall are expected. Therefore, the PMO environment is neglected during the calculations [169] This simple model system allows us to investigate whether the complexation to the ligand is thermodynamically favoured, compared to the original $[Ru(acac)_2(CH_3CN)_2]^+$ complex, and hence corroborate that the complex is anchored to the PMO.

In detail, two separate fragments are considered: the ligand (Fragment 1) and the ruthenium cluster (Fragment 2). Fragment 1 has a zero charge and a singlet spin state, except when the protonated ligand is considered (charge +1, see later). Fragment 2 comprises the ruthenium centre and two acac ligands. The ruthenium is in a 3+ state and thus has a d^5 configuration. The two possible spin states (doublet and sextuplet) have been examined and both DFT-functionals indicate that the expected

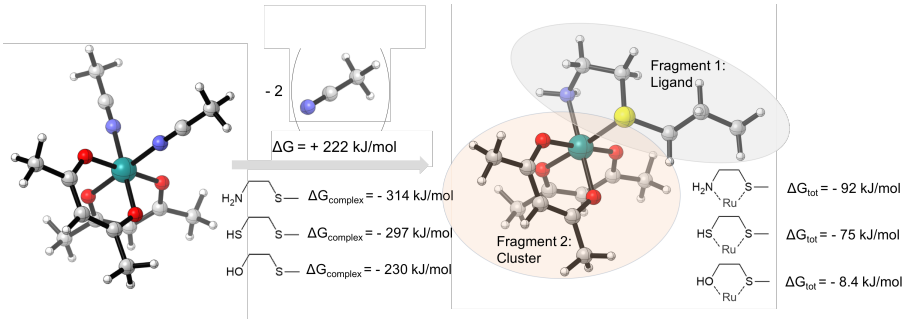

Figure 5.10: Computational model with two fragments indicated. Total charge of the system is +1 and it has a doublet spin state.

doublet state is the most stable. Since the two acac groups are negatively charged, the charge of this cluster is +1. The total fragment has a charge of +1 and a doublet spin state. The complexation free energies are calculated using the following equation:

$$\Delta G_{complex} = \Delta G_{total} - [\Delta G_{Fragment1} + \Delta G_{Fragment2} + CP]$$

with ΔG_{total} the free energy of the total system ($Ru(acac)_2SX$) and $\Delta G_{Fragment}$ the energies of the separate fragments. CP is the counterpoise correction energy for the BSSE error. Next to this value, we calculated the free energy cost to remove 2 CH_3CN groups (**Figure 5.10**) and added this to the free energy of complexation.

Open shell transition metal systems are notoriously difficult for DFT methods to predict correct spin states and geometries. Recent studies have shown that the OPBE functional performs very well for transition metal complexes [247, 248]. For comparison, B3LYP calculations are also performed, since this widely tested functional still proves to be very robust for organic systems [249]. Both functionals gave the same qualitative understanding of the system and predict complexation energies that are in the same range.

The calculations (**Figure 5.10, Table 5.4**) show that the bidentate linkers can effectively bind the complex with large interaction strength for every type of ligand.

In conclusion, theoretical calculations support that the complex formation with the bidentate ligand is thermodynamically favourable compared to the starting complex. Furthermore, the amine ligand has the strongest interaction with the Ru complex, which supports the higher Ru loading of mAR-SNH_2-Ru. In order to have a more physically correct

Table 5.4: Computational data for the ligand-Ru complexation energies determined via the B3LYP and OPBE functional.

	B3LYP		OPBE		
Ligand	$\Delta E_{el}{}^{a}$	ΔG^{b}	$\Delta E_{el}{}^{a}$	ΔG^{b}	CP^{c}
S-NH_2	-389	-331	-385	-314	9.2
S-SH	-347	-293	-360	-297	5.9
S-OH	-310	-247	-293	-230	8.8
CH_3CN	-134	-88	-142	-100	4.2

All energy differences are expressed in [kJ/mol] and include dispersion corrections. [a]Purely electronic energy with zero-point energy correction (same as eq.1, without CP correction and free energy contribution). [b]Gibbs free energy calculated from the frequency analysis (via eq.1, without CP correction). [c]Counterpoise correction term.

point of view, we compared the anchored ruthenium to the original complex as a reference system, which is schematically represented in (**Figure 5.10**). Here, we first calculate the energy cost to 'remove' both acetonitrile groups and the consecutive stabilization caused by the recomplexation to the new ligand, representative for the actual experimental exchange process. Using this approach, we find that the anchoring to the new ligand is thermodynamically favoured by 8.4 - 92 kJ/mol depending on the ligand (an order of $NH_2 > SH > OH$ is found).

5.4 Catalytic alcohol oxidation in water

For catalytic tests, we retained three different materials: mAR-SOH-Ru, mAR-SSH-Ru with relatively low Ru loading and mAR-NH_2-Ru with a relatively high Ru loading. Although the pore walls of these PMOs are relatively hydrophobic, all catalysts are homogeneously dispersed in water courtesy of the remaining silanol groups. In our initial experiments, we performed the oxidation of benzylalcohol, as this is the substrate of choice in many reports on Ru catalyzed oxidation reactions [229, 231]. However, in our system, we already observe full conversion of benzylalcohol to benzaldehyde without addition of a Ru-catalyst (blank reaction). We assume that benzylalcohol and similar substrates are easily oxidized as expansion of the π-system pushes the reaction towards full conversion.

Therefore, we selected cyclohexanol as non-aromatic substrate, which does not benefit from conjugation after oxidation. Catalytic results are represented in (**Table 5.5**). All considered Ru-catalysts show full

Table 5.5: Oxidation of cyclohexanol. Entry 1-2: Homogeneous complex, entry 3-5: supported catalyst.

Entry	Catalyst	Ru [mol%]	Conversion [%][a]	Yield [%][a]
1	$[Ru(acac)_2(CH_3CN)_2]PF_6$	5	>99	>99
2	$Ru(acac)_3$	2.5	93	88
3	mAR-SNH_2-Ru	0.06	>99	95
4	mAR-SOH-Ru		>99	81
5	mAR-SSH-Ru		>99	80
6	Blank	0	12	12

[a] GC-determined conversion and yield after 180 min; toluene as internal standard

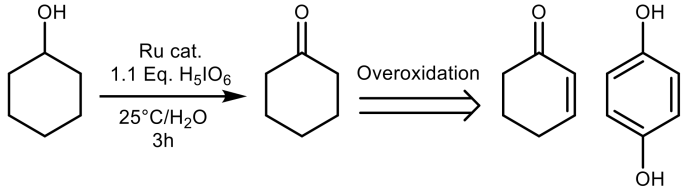

conversion of cyclohexanol after 180 min, whereas for the blank reaction only 12% is observed. This reaction is roughly four times faster compared to $[Ru(acac)_2(CH_3CN)_2]PF_6$ anchored on an aminopropyl grafted silica [231], which nicely illustrates the enhanced diffusion of organics in water towards the hydrophobic PMO materials [165–169]. The results, however, show a discrepancy between $[Ru(acac)_2(CH_3CN)_2]PF_6$ and the solid PMO catalysts in terms of selectivity. A similar loss in selectivity is seen if homogeneous $Ru(acac)_3$ is used as catalyst. Here, a vacant reaction site must be created by the expulsion of an acac-ligand, which causes a tendency for overoxidation (by-products were determined as cyclohexenone and hydroquinone). Overreaction does not occur when the weakly bound CH_3CN ligands of $[Ru(acac)_2(CH_3CN)_2]PF_6$ are removed. This fact thus suggests that Ru is indeed anchored to mAR-SX by exchange of the weak acetonitrile ligands corroborating with the assumption made in the computational study.

Next, we constructed reaction profiles for mAR-SOH-Ru, mAR-SSH-Ru and mAR-SNH_2-Ru and performed 'hot-filtration' tests (**Figure 5.11**) to determine whether the catalysis takes place exclusively on the PMO surface. Given the reaction profiles of mAR-SOH-Ru and mAR-SSH-Ru, the optimum reaction time is 40 min with a high TOF_{10min} of 1.53 s^{-1} and 1.47 s^{-1}, respectively. At this optimum, all cyclohexanol is selectively oxidized into cyclohexanone and only thereafter further

oxidation products are formed as a result of continuing β-elimination reactions [250]. The dashed line in **Figure 5.11** shows the reaction profile during the hot filtration (HF) test. For both materials, separation of the catalyst from the reaction mixture occurred after 10 min. No further reaction is witnessed in the filtrates but the blank reaction. This, combined with the fact that no leaching of Ru was observed in the filtrate at ppm level (XRF) shows that the reaction occurs on the pore surface of the PMO and that we have developed non-leaching, fully heterogeneous and recyclable catalysts. This also proofs that the S-X ligands remain bound at reaction pH (∼1.4).

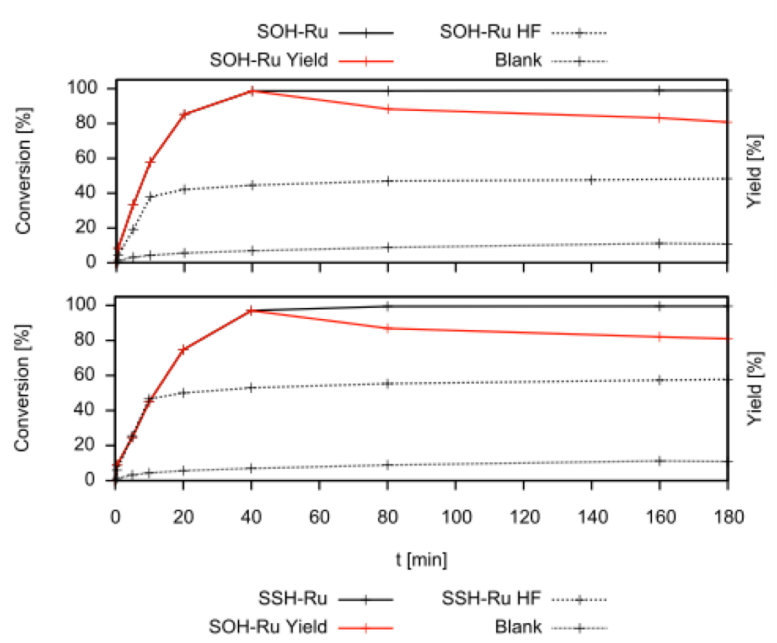

Figure 5.11: Reaction profiles of mAR-SOH-Ru (top) and mAR-SSH-Ru (bottom). A hot filtration test (HF) is performed with filtration at t = 10 min (dashed).

The latter statement is demonstrated in **Figure 5.12**, where catalyst-recycling experiments for mAR-SOH-Ru show a similar activity for 3 consecutive catalytic runs of 180 min, without loss of structural ordering of the support (**Figure 5.13**). The total reactant conversion is similar for all runs. However, as seen in the reaction profiles, the occurring reaction is sequential (-ol to -one to enone/hydroquinone). The lower yield of cyclohexanone in Run 1 and 3 is accompanied by an increase of the overoxidation products. We believe that the variability in the yield of cyclohexanone during run 2 is due to uncontrolled external factors

causing changes in the kinetics of the reaction. Given that Run 1 and 3 are similar, however, one can assume recyclability of the catalyst.

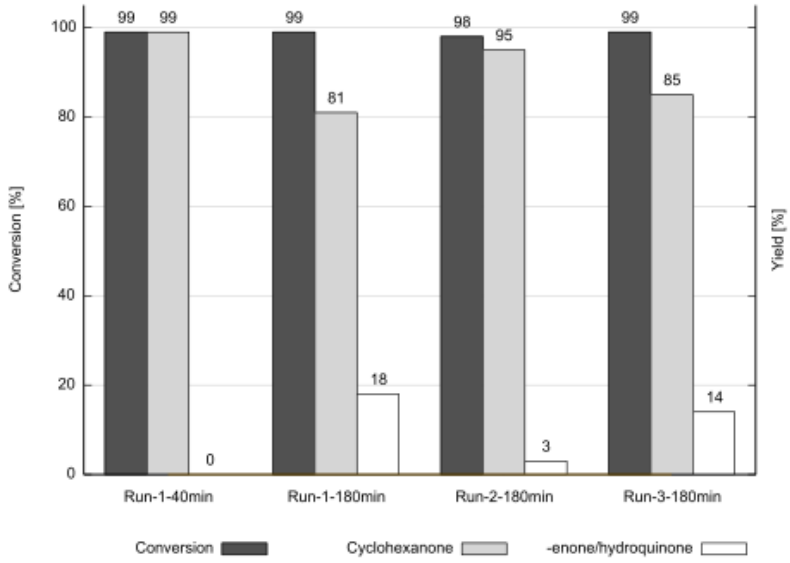

Figure 5.12: Catalyst recycling experiment for mAR-SOH-Ru, with conversion of cyclohexanol (dark grey), yield of cyclohexanone (grey) and formation of the byproducts, cyclohexenone and hydroquinone (white).

However, when immersing mAR-SNH_2-Ru in the reaction medium and filtering off the catalyst after 10 min, we observed further reaction in the filtrate. The conversion of cyclohexanol in the filtrate increased from 35% at the time of filtration, to 83%, significantly more than expected for the blank reaction. This indicates that the Ru-complex is detached from the support and partially leaches into the medium, where it can no longer be recovered. Via XRF, the Ru-leaching is determined at 30% after 3 catalytic runs. To ensure this leaching is not loading related, we prepared a mAR-SNH_2-Ru sample for which the anchoring was executed in acetone, to obtain a catalyst with similar Ru-loading (0.037 mmol/g) to mAR-SOH-Ru and mAR-SSH-Ru. Again, the hot filtration test was unsuccessful. The very different behaviour of mAR-SNH_2-Ru can be explained by taking into account the reaction medium. H_5IO_6 not only acts as the oxidant, it can also readily protonate the NH_2-group of the ligand, whereas -OH and -SH remain unaltered.

This is confirmed in our computational study. The acidic environment created by the periodic acid (pKa 3.29) is sufficiently strong to protonate the amine group of the ligand (approx. pKa 10). This leads to a

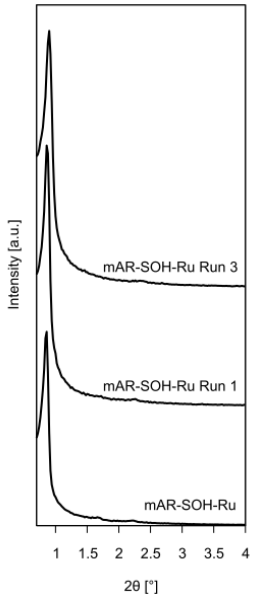

Figure 5.13: XRD diffractograms of mAR-SOH-Ru as fresh catalyst (bottom), after 1 run (middle) and after 3 runs (top).

subsequent change in the conformation of the complex as is shown in **Figure 5.14**. The now positively charged amine group turns away from the Ru center, and only a weak interaction of the sulphur lone electron pair (about 25 kJ/mol) remains, not sufficient to retain the complex in that position.

The hydroxyl group (approx. pKa -2) and the thiol group (approx. pKa -7) of the other ligands cannot be protonated in this reaction environment and therefore stay in the same conformation. These results explain why ruthenium leaching is only observed for the amine-based ligand, notwithstanding that this ligand has the strongest affinity to bind the ruthenium complex.

As a control experiment, we prepared an aminopropyl grafted SBA-15 and subsequently anchored $[Ru(acac)_2(CH_3CN)_2]PF_6$. For this catalyst, the Ru is no more stabilized by the sulphur atom after protonation of the amine group. Here, up to 50% of Ru is leached after 1 catalytic run, whereas for mAR-SNH_2-Ru 30% of Ru leaching is observed after 3 runs. These results prove that the amine group indeed causes leaching by protonation in the acidic medium. Also, the small stabilizing effect of the lone sulphur atom is witnessed given the less pronounced leaching for mAR-SNH_2-Ru.

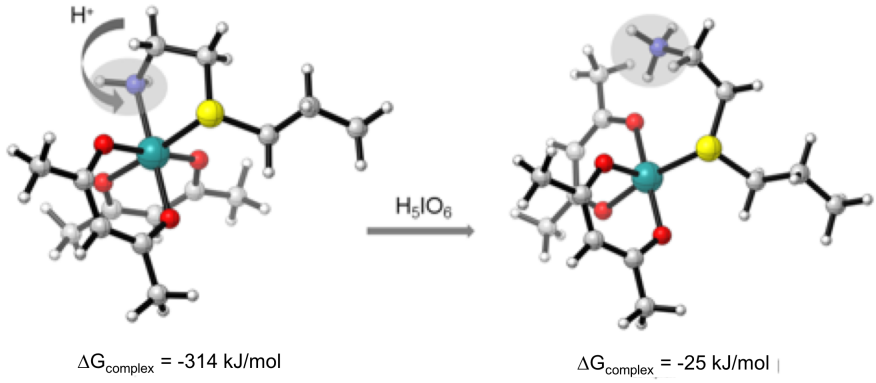

Figure 5.14: In an acidic environment, the amine group can be easily protonated. The remaining S-Ru interaction is rather weak and as a consequence, the complex leaches out.

5.5 Mechanistic insights

In **Figure 5.15**, a mechanism for this catalytic oxidation is proposed. In our system at 25°C, the acidity of H_5IO_6 is needed to expel an acac-ligand and to create vacant Ru-sites as indicated by the catalytic activity of $Ru(acac)_3$. Furthermore, we did not observe conversion if $NaIO_4$ is used as neutral oxidant at room temperature, demonstrating that the acidity is decisive for catalytic activity. It is generally accepted that alcohols undergo β-elimination in the presence of late transition metals, which is often regarded as the rate-determining step [221, 222, 226, 227]. Here, the resulting $Ru-H_2$ is readily oxidized by the periodate anion. Although the latter is consumed during reaction, electrochemical regeneration is straightforward. By-products of the cyclohexanol oxidation, cyclohexenone and hydroquinone, are the result of extended β-elimination. This side-reaction is far less favourable as these products are only formed after full conversion to cyclohexanone. We believe the selectivity of the reaction arises from selective coordination of cyclohexanol to vacant Ru sites followed by β-elimination. Given the reaction profile, cyclohexanone, the reaction product, must only be able to coordinate to the vacant sites after all cyclohexanol is consumed to yield cyclohexenone.

Finally, we attempted cyclohexanol oxidation with either H_2O_2 or O_2 as the oxidant at low pH to promote the removal of the acac group. No conversion of the substrate was observed after 180 min. This results

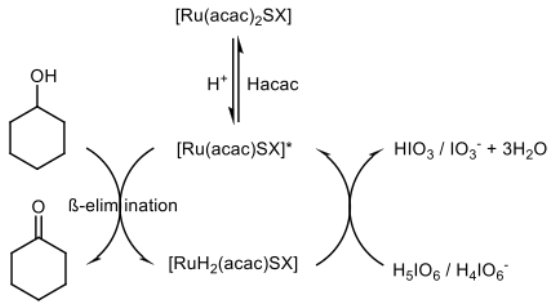

Figure 5.15: Schematic mechanism of H_5IO_6 heterogeneous cyclohexanol oxidation. X = OH, SH denote the anchored ligand on mAR.

from the lower oxidation potential of H_2O_2 and O_2 compared to H_5IO_6, which is insufficient to regenerate the active Ru(III)-species. Arguably, in all performed catalytic reactions, H_5IO_6 is used as a sacrificial oxidant. However, after filtration of the Ru catalysts and subsequent extraction of the reaction products, only an aqueous phase containing HIO_3 remains. In potential applications, this latter can be reconverted into a H_5IO_6 solution within the same medium via an electrochemical procedure in a separate cycle. This, combined with the catalyst recycling, the use of water as a solvent and performing the reaction at room temperature, provides a sustainable alternative to current aerobic oxidation reactions at elevated temperature in organic solvents.

5.6 Oxidation of poorly water-soluble alcohols

As a final experiment, we selected (±)-menthol as a sterically hindered, poorly water-soluble substrate. Such substrates are notoriously hard to oxidize in water/RT and no selective, complete conversion is reported even after reaction for over 12 h [224, 231]. Despite the poor solubility of (±)-menthol in water, we obtain full conversion after 6 hours, with >99% selectivity towards menthone with our PMO catalyst (mAR-SOH-Ru) (**Figure 5.16**). This remarkable behaviour must be attributed to the properties of the mAR-PMO support. Sequential hydrophobic/hydrophilic 'zones' in the PMO material, originating from the organic bridges and siloxane/silanol functionalities, create an ideal reaction environment for the reaction of hydrophobic molecules in water [130, 165, 166, 169, 251]. Therefore, reactants are locally enriched and/or reaction products are repelled which, combined with an ordered pore structure, results in high catalytic activity ($TOF_{30min} = 0.54\ s^{-1}$). No further β-elimination

products are found, which implies that steric hindrance of the isopropyl and methyl groups prevent overreaction.

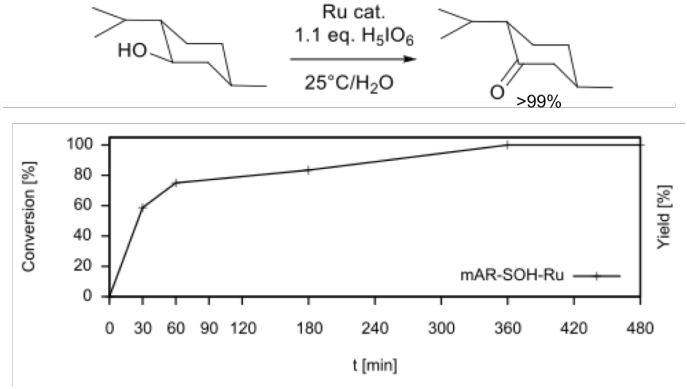

Figure 5.16: Reaction profile for (±)menthol oxidation with mAR-SOH-Ru as catalyst.

5.7 Conclusion

We have developed a novel 100% monoallyl ring-type PMO (mAR) of which structure and porosity (536 m^2/g, 5.0 nm pores) are optimized to serve as a catalytic support material. Via thiol-ene click chemistry, the allyl groups protruding in the pores are transformed into three distinct bidentate thioether ligands (SNH_2, SOH, SSH). Experiments and theoretical calculations confirm the heterogenization of a Ru(III)-complex onto these solid ligands. Although protonation of the amine group in the acidic catalytic medium causes leaching for mAR-SNH_2-Ru, mAR-SOH-Ru and mAR-SSH-Ru are successfully applied as selective, truly heterogeneous catalysts in the oxidation of cyclohexanol in water at 25°C. Compared to the same complex anchored on an MPS [231], we show a significant shortening of the reaction time towards full conversion of cyclohexanol, using a recyclable catalyst. The hydrophobic/hydrophilic reaction environment and ordered pores of the mAR-support enable high catalytic activity for a poorly water-soluble and sterically very challenging substrate such as (±)-menthol. Full conversion to menthone is obtained after only 6 h whereas no selective, complete conversion is reported even after reaction for over 12 h in [231]. As a remark, one should consider carefully what might happen when any homogeneous complex is attached to a solid. As illustrated here, the anchoring of

the homogeneous $[Ru(acac)_2(CH_3CN)_2]PF_6$ complex has led to loss of selectivity.

Next to this application, we show that the mAR-PMOs are exceptionally stable hybrid silicas in hydrolytically harsh conditions as they show no structural change at pH 0 and at pH 13 only small signs of deterioration are witnessed after 24 h. Therefore, mAR is highly suitable for reactions requiring extreme pH in water. In this work, thiol-ene click chemistry is used only to attach small ligands in such manner that they do not leach at low pH. In theory, the thiol-ene reaction is able to attach several popular chiral ligands and organocatalysts on our mAR-PMO support, given a thiol functionalization of the catalytic functionality of interest. The use of this support instead of MPS will definitely allow more harsh conditions that may be beneficial for the reaction to be catalyzed or allow reactions deemed impossible to perform with a silica-based material. Moreover, the unique PMO environment will possibly result in higher reaction rates in aqueous solvents.

Part III

Hydrolytically stable and versatile organosilica particles for chromatography

Chapter 6

Introduction: Organosilicas in High Performance Liquid Chromatography (HPLC)

In many fields of chemical research, separation of compounds is essential. For example, newly synthesized drugs need to be isolated from possibly harmful side-products, while organic pollutants in waste water, food, etc., can only be analyzed when separated from complex mixtures. Also in biochemistry, compounds obtained from enzymatic digests require separation before analysis. Where many other methods e.g. precipitation, distillation and extraction, fail or take much time, chromatography is far more potent while the process can be automated. Therefore it has become an important techniques in chemical analysis. In general, chromatography is a group of methods that allow separation of closely related compounds and complex mixtures by using a mobile phase (gas, liquid or supercritical fluid) to carry the components to be analyzed along or through a stationary phase, often a cylindrical column. If the mobile and stationary phases are carefully chosen, the components distribute themselves between the mobile and stationary phase. Hereby a dynamic equilibrium takes place along mobile/stationary phase interface, thus over the length of the column. As a result, compounds with high affinity for the stationary phase (high retention) move only slowly with the flow of the mobile phase as they reside longer within the stationary phase. Compounds with a low affinity for the stationary phase (low retention) will elute faster as they reside longer in the mobile phase. This physically separates the components over time allowing qualitative and quantitative analysis and recuperation of the pure compounds (**Figure 6.1**).

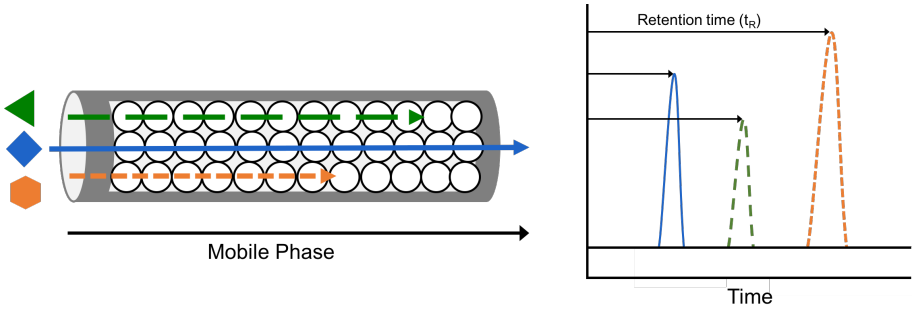

Figure 6.1: Illustration of the chromatographic process separating 3 components with a different partitioning factor over time. Retention time is the time between the injection of the analytes in the mobile phase and the time of elution or detection.

From all chromatographic methods, high performance liquid chromatography (HPLC) is the most used technique world-wide because of its high versatility (see Section 6.1.3). Currently, HPLC is heavily reliant on spherical particles of porous silica for separations with high efficiency. Since chromatography is in essence a diffusion controlled process, silica stationary phases benefit from their high surface area, mechanical stability, a modifiable surface and uniform morphology. However, as mentioned before, the poor hydrolytic stability of silica is a serious drawback especially given the user-driven demand for water-based separations at extreme pH and temperature. Therefore, organosilicas are gaining increasingly more interest, not only in academia but also in industry.

Over the years, however, HPLC has evolved dramatically in search for increasingly higher resolution, separation efficiency and analysis speed. Next to improvements in instrumentation, the stationary phase has always been the center of new developments and has become increasingly advanced going from irregular shaped silica particles to state-of-the-art highly uniform spherical particles of hybrid silica. As a result, synthesis of such stationary phases has become more challenging and complex (see Sections 6.3 and 6.4), while specifications of a good chromatographic packing material have become very stringent (see Section 6.2). Seen the exceptional stability and functional versatility of AHETSCH organosilicas, these materials are inherently well-suited for application in HPLC where they potentially allow separation in unprecedented conditions. Stability at very low and high pH provides opportunities to perform efficient separation of organic acids and bases e.g. pharmaceuticals, whereas high temperature stability opens the pathway to ultra-fast chromatography (see Section 6.2.6). In this part, existing and new methods for

obtaining porous and spherical silicas and organosilicas will be explored to transform the AHETSCH precursor into such theoretically ultimate stationary phase for HPLC.

6.1 Principles of HPLC [252–255]

In brief, HPLC comprises the following steps to obtain a chromatogram:

- Applying a certain flow of a chosen mobile phase along or through the selected stationary phase.
- The injection of a sample comprising the analytes to be determined.
- Separation of the compounds.
- Detection of the analytes at the end of the stationary phase or column by means of refractive index, UV-VIS, mass spectrometry, etc.

In this section some important fundamental concepts of chromatography in general and HPLC are introduced. Later, this will help appreciate the influence of the stationary phase on the chromatographic performance.

6.1.1 The fundamentals of chromatography

As described earlier, separation in all types of chromatography is dependent of the distribution of the analytes between the immiscible stationary and mobile phase. This distribution process can be considered the dynamic equivalent of consecutive separations in a separation funnel. Decent partitioning of the analytes is true only if the process occurs fast enough and if analyte concentrations are relatively low. In these conditions the distribution can be described with the Nernst partitioning factor K.

$$K = C_S/C_M$$

with C_S: concentration of the analyte interacting with the stationary phase and C_M: the concentration of the analyte in the mobile phase.

In a chromatographic column the distribution constant translates into the retention factor k.

$$k = M_S/M_M$$

with M_S being the mass of the component in the stationary phase and M_M the mass of the component in the mobile phase.

The distribution constant K and the retention factor k are correlated by the phase ratio, β:

$$K = k\beta$$

with β a fixed column characteristic describing the ratio of the total volume of mobile phase (V_M) over the total volume of stationary phase (V_s) in the column.

Interestingly, the distribution coefficient is temperature dependent, which in HPLC causes decreased retention with higher temperatures. Aside from this, k and β are independent from the column length and the velocity of the mobile phase.

In practice, the retention factor k is obtained from the chromatogram as it describes the ratio of the time an analyte spends in the stationary phase compared to the time it resides in the mobile phase. This gives the following equation:

$$k = \frac{(t_R - t_0)}{t_0} = \frac{t'_R}{t_0}$$

with t_R the time between sample injection and elution of the analyte, t_0 the time of elution of an unretained component and t'_R the effective retention time, where a correction is made for the dead time of the column. t'_R and thus k are influenced by the composition of mobile and stationary phase, the analyte and temperature. A higher elution strength of the mobile phase will cause lower values for both t'_R and k, while choosing a column with more affinity for the analytes will have the opposite effect.

The quality of a separation can be deducted from the broadness of the resulting peaks in the chromatogram, with sharper peaks indicating a higher separation efficiency. As a measure, the plate number (N) is generally calculated from the peak width and the retention time through the following equation:

$$N = 5.54 \left(\frac{t_R}{W_{FWHM}} \right)^2$$

where t_R and W_{FWHM} are the retention time and the peak width at half of the maximum. Since the total number of theoretical plates depends upon the column length, it is useful to express column performance otherwise. The height of a theoretical plate H or plate height is related

to N in such a manner that a column is divided into N segments of length H, with H corresponding to the distance in the column over which the the equilibrium of distribution is reached.

$$H = L/N$$

As a rule of thumb to make a quick estimation for the theoretical maximum plate height of a column packed with fully porous spherical particles the following equation is often used:

$$N_{max} = \frac{L}{2d_p}$$

and also:

$$H_{min} = 2d_p$$

Herein L denotes the length of the column and d_p is the mean diameter of the particles packed in the column. Comparison of the theoretical plate number or height N_{max} or H_{min} and the experimental plate number or height gives an estimation of the quality of the column (packing efficiency, particle shape effects, ...). Only well packed columns with state-of-the-art materials run at optimal linear velocity are able to approximate these values. This estimation is true for completely porous particles, yet lower plates heights than theoretically expected can be found for particles with a solid core - porous shell architecture. Next to this, it can be appreciated from the equation that the column diameter has no influence on the efficiency. Therefore smaller column diameters can be employed to reduce solvent consumption or flow while maintaining the same efficiency and linear velocity of the mobile phase. Furthermore, it cannot be unseen that elongation of columns indeed raises the total plate number, however, column back-pressure is also increased with column length. This makes that the application of longer columns is not necessarily the best way to optimize the column efficiency.

The separation factor or selectivity (α) describes how good two analytes (1 and 2) are separated from each other under given chromatographic conditions. The larger α becomes, the greater the solute retentions differ:

$$\alpha = \frac{t'_{R2}}{t'_{R1}} = \frac{k_2}{k_1}$$

The selectivity factor is a very valuable parameter as it depends on the properties of the solutes, the stationary phase, the mobile phase and temperature. However, as it is influenced by many factors, this complex factor is hard to predict and is the main cause why the optimization of

a separation often requires a trial-and-error approach with screening of different column types, eluents and conditions.

The key parameter in chromatography is resolution (R_s), which defines the degree of the separation between two adjacent peaks. Peaks can be considered fully resolved when no more than 5% of the two signals are still overlapping. Resolution combines all of the above in the following master equation of chromatography:

$$R_s = \frac{\sqrt{N}}{4}\left(\frac{\alpha - 1}{\alpha}\right)\left(\frac{k}{k+1}\right)$$

Herein, three major trends for optimization of a chromatographic separation can be identified (**Figure 6.2**). Firstly, the resolution increases with the square root of the plate number (N). Doubling the resolution thus requires a fourfold increase of the plate number, which indicates that raising the plate number is only a finite solution. Next to this, it can be appreciated that the retention factor has limited effect on the resolution once it becomes larger than 5. One should also bear in mind that temperature also influences k. Finally, it is clear that selectivity is the key parameter in HPLC, exerting the strongest influence on the resolution. Again, the arduous control of the selectivity explains why more often than not trial-and-error is used in the development of novel HPLC methods.[1]

In practice, the plate height (H) is minimized by the application of the optimal linear velocity (u) of the mobile phase[2], which is dictated by the Van Deemter curves (**Figure 6.4**), the most often used model to describe peak broadening in chromatography:

$$H = A + \frac{B}{u} + Cu$$

with

$$A = 2\lambda d_p$$

$$B = 2\gamma D_M$$

$$C = C_M + C_S$$

1. To develop a new isocratic chromatographic method, commonly a range of mobile phase ratios is explored under isocratic conditions at the same flow rate. Thereafter, the optimal flow rate is sought for and/or solvent mixtures are run under gradient to optimize the separation in terms of efficiency and speed (**Figure 6.3**).
2. $u = F/S$ where F is the solvent flow rate and S is relative to the column cross-section times the porosity.

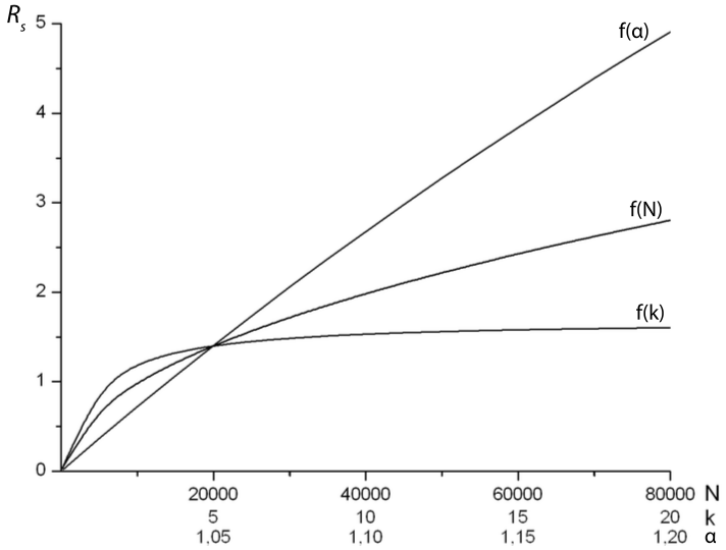

Figure 6.2: Influence of the plate number (N), the selectivity factor (α) and the retention factor (k) on the resolution (R_s) .

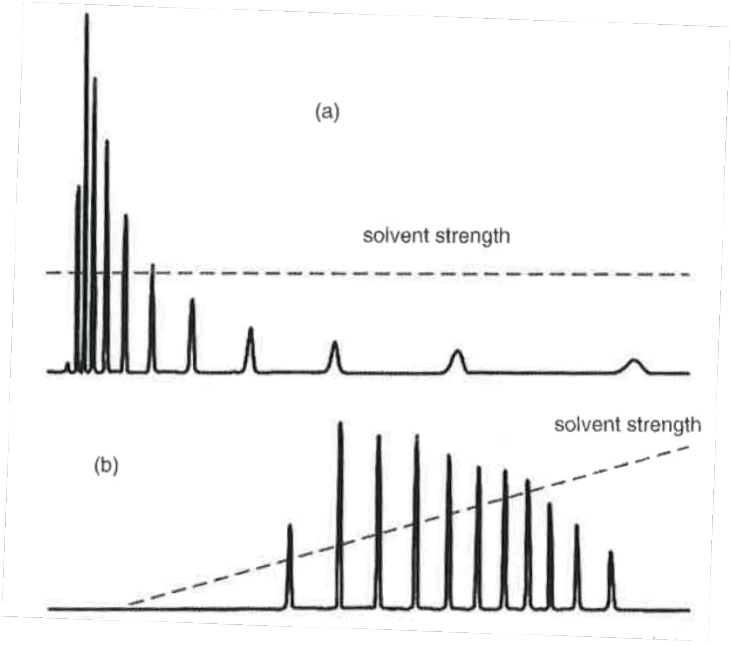

Figure 6.3: Illustrative example of the effect of gradient conditions on peak shape and separation efficiency. Taken from [256].

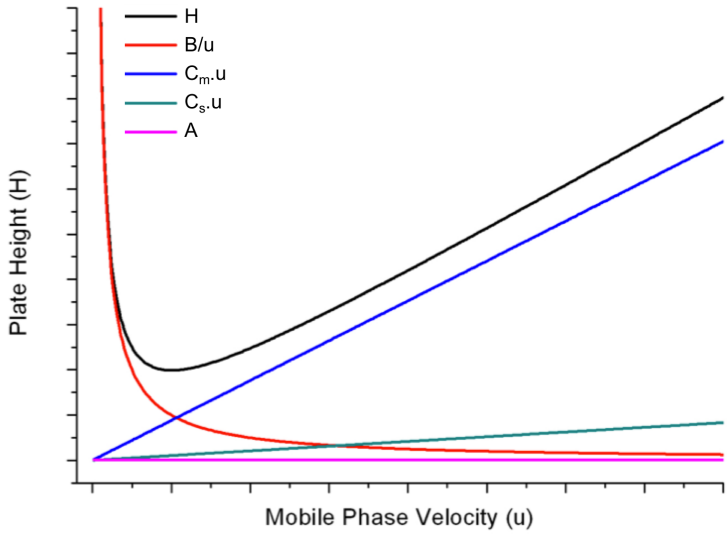

Figure 6.4: An illustration of the Van Deemter model composed of its separate A, B and C terms showing the plate height (H) as a function of the linear mobile phase velocity (u).

From these equations it is clear that band broadening and thus loss of efficiency and resolution within the column originates from three different effects two of which are linked to the flow rate of the mobile phase:

The Eddy diffusion term (A), dependent of the diameter of the packed particles (d_p) and a packing efficiency term (λ), describes peak broadening as a result of the variable residence time of analyte molecules (**Figure 6.5**). The latter can follow multiple paths with different length through the column which leads to broadening of the signal. Therefore, an efficient column must provide percolation pathways that are as uniform as possible. This term is independent from the mobile phase velocity but is mainly determined by the quality of the column. For a packed column, the packing efficiency and particle morphology are crucial to reduce the A-term (see Section 6.2.1).

The longitudinal diffusion term (B/u) refers to 'natural' diffusion effects of analytes (**Figure 6.6**). When injected, these molecules occupy a small part of the column with relatively high concentration. Over time, and independent from the flow rate, these migrate both along and opposed to the direction (longitudinal diffusion term D_M) of the mobile phase flow, thereby causing peak broadening. Diffusion is partly hindered by the stationary phase, thus an obstructive factor γ (typically 0.6 for packed columns) is introduced. The longitudinal diffusion term is inversely

proportional to the mobile phase velocity. This is logical as diffusion effects will be less pronounced the shorter the analytes reside in the column.

Finally, the mass transfer coefficients (C_s and C_m) also influence separation efficiency (**Figure 6.7**). Time is required for the partitioning equilibrium to take place. As time is also needed for the solute molecules to diffuse from inside the stationary or mobile phase to the interface where transfer occurs, no equilibrium can take place when the flow rate is too high with widening of the analyte peak as a result. C_m is influenced by d_p, u, D_m, k, the viscosity of the mobile phase, the porosity of the stationary phase, and the temperature; C_s is a function of d_p, u, the quality of the stationary phase, the diffusion coefficient in the stationary phase (D_s), k and the temperature.

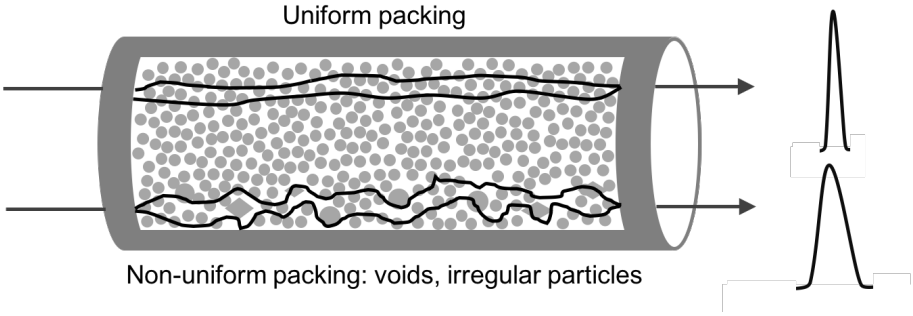

Figure 6.5: Graphical representation of the Eddy diffusion term throughout a column. Uniform pathways result in narrow peaks (top), poor quality of the column causes peak broadening (bottom).

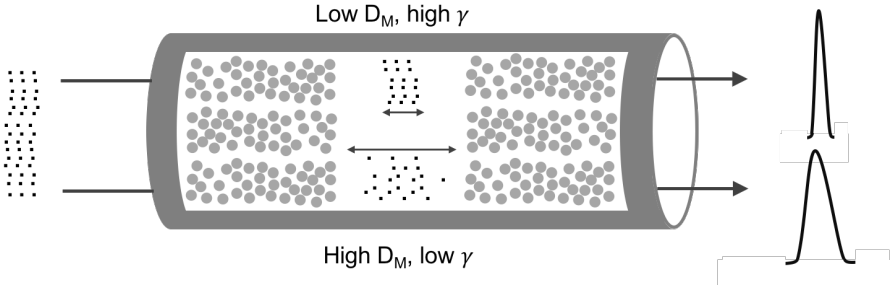

Figure 6.6: The longitudinal diffusion term B/u: with a low longitudinal diffusion term D_M and/or high obstructive factor well-resolved peaks are obtained while high D_M and low γ result in broad peaks.

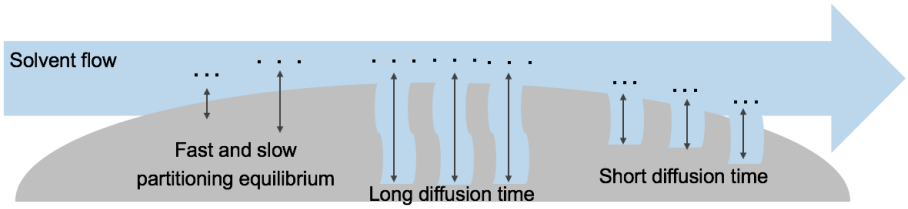

Figure 6.7: The mass transfer coefficient C: Long diffusion paths and slow partitioning equilibrium cause peak broadening at increased velocity of the mobile phase.

6.1.2 The stationary phase in HPLC: column types

The stationary phases in HPLC can be subdivided in planar columns, packed columns, monolithic columns and chips.

In **planar chromatography** capillary forces mobilize the solvent along paper or a thin layer of silica on a glass plate in, aptly named, paper and thin layer chromatography (TLC) respectively. After the development of a spot of analytes, the separated components can be visualized using UV-light, $KMnO_4$,... This type of chromatography is very basic yet it is often employed in lab environments for the optimization of column chromatography. On the other hand, this type of chromatography can hardly be automated and lacks efficiency.

Open tubular columns are a second type of columns in which a layer of stationary phase is coated on the inner wall of a narrow tube or capillary (**Figure 6.8**, right). Although widely applied for GC, these capillaries have limited use in liquid chromatography as the diffusion coefficients in the liquid phase are up to three magnitudes lower than in gas phase. Where gas phase diffusion gives GC a clear advantage in terms of maximum efficiency, this same gas phase also limits GC by nature. Volatile solutes are needed while not every analyte is volatile or can be made volatile without decomposition.

Most widely used are **packed columns** which are basically metal cylinders generally packed with silica-based particles. Columns are loaded with particles at high pressure, by pumping a slurry of particles in an empty column provided with a frit to contain the particles. A constant pressure is maintained for a certain amount of time by pumping extra solvent or a driving solvent through the freshly packed column. Although subject of research, the many variables such as the slurry solvent and density, particle chemistry and morphology, column diameter and length, packing pressure and time, etc., make the packing of column more

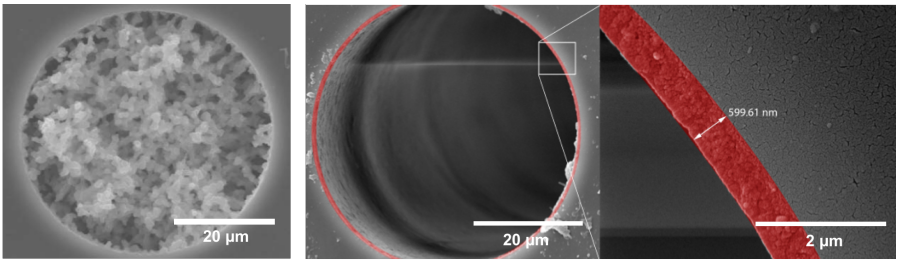

Figure 6.8: SEM images of the cross-section of a monolithic column (left, from [257]), an open tubular column (center) and a zoom of the coated layer on inside the capillary (right, from [60]).

craftsmanship than exact science.[3] Nonetheless, working with particles has clear advantages as these are readily synthesized in a reproducible way. Furthermore, it is straightforward to apply fairly uniform surface modifications on these powdery materials before packing.

As a main alternative for packed columns, **monolithic columns** are marketed. Herein, the column, typically a capillary, is filled with one porous piece of silica or polymeric material having macropores (**Figure 6.8**, left) [259]. This highly interconnected architecture can handle high loading capacity of analytes and reduces the column back-pressure which allows high flow rates. It is however hard to obtain column to column reproducibility given that monoliths need to be synthesized inside the column. For example, when silica monoliths are synthesized by condensation of a silica source around a porogen inside the capillary, the monolith can shrink or crack during the removal of the SDA, thus inducing a loss of efficiency. Typically monolithic columns are applied in the high-throughput separation of biomolecules and drugs and some trade names comprise Phenomenex Onyx, Merck Chromolith and Agilent Bio-Monolith.

As a last column format and in the light of continuing miniaturization of HPLC techniques, cylindrical columns have been interchanged with **chromatographic chips** to reduce solvent consumption and to allow analysis of minimal amounts of sample. For such chips microchannels (50-100 µm) are etched out of a silicon wafer and these are subsequently filled with the same spherical particles used in packed columns. Packing

3. As a guideline, typically a column is packed at 1.5 times the envisaged working pressure to ensure a stable particle bed. A stable slurry is also deemed crucial for a good packing, this can be checked beforehand by making slurries in different packing solvents or mixtures, with viscosity thereof playing an important role [258].

of the narrow channels with powder is not trivial which rises issues concerning reproducibility. Furthermore, dedicated, yet complex and expensive micro- and nanopumps are required. An elegant approach to columns-on-a-chip was described by Desmet et al., who replaced the spherical particles with an ordered array of etched micropillars having superficial porosity (**Figure 6.9**). This architecture has greatly reduced back-pressure allowing elongation of the columns. Combined with an intricate microfluidics system to distibute the mobile phase over parallel channels, extremely high efficiency is obtained (Pharmafuidics μPAC) [260, 261].

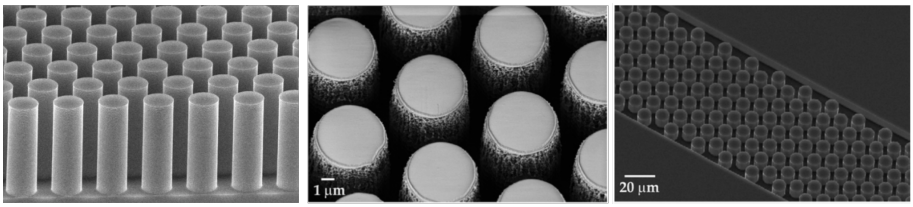

Figure 6.9: SEM images of micropillars etched from a silicon wafer with superficial porosity. Images taken from [261].

6.1.3 Separation modes

The nature of the mixture to be separated dictates which HPLC mode is the most apt for the application. Based on the type of interaction between the stationary phase and the analyte, multiple HPLC techniques are discriminated:

Normal-phase Liquid Chromatography (NP-LC)

NP-LC is historically the very first method in chromatography and was developed by Tswett as early as 1906 [262]. Employing a polar stationary phase, a polysaccharide and alumina, separation of leaf pigments into carotenes, anthophylls and chlorophylls was described using an apolar solvent, a mixture of hydrocarbons. In general, separation in NP-LC is based on the interaction of polar groups of the analyte with the polar sites of the stationary phase, typically silica, which has a hydrophilic surface arising from its silanol (Si-OH) groups. Because of the relatively high solvent cost and irreproducibility when using pure metal oxide particles (an uncontrolled water layer affecting the hydrophilic interactions may be bonded to the surface of the particles), this technique is mostly applied in TLC and lab-scale preparative chromatography on rough silica (column chromatography). However, NP-LC is quite extensively used

with polar modified silica particles bearing aminopropyl, cyanopropyl or diol functionalities instead of silanol groups (see also Section 6.2.4), which lead to more reproducible results. The mobile phase may consist of a plethora of solvents, ranging in polarity from n-hexane to methanol. The latter is considered a strong eluent in NP-LC (eluting strength $\epsilon = 0.73$) which is able to elute the most polar components, while n-hexane ($\epsilon = 0.00$) will not elute polar molecules from the polar column. For every new analyte mixture or separation problem, a new mobile phase and solvent ratio thereof needs to be optimized to obtain an adequate retention factor (k) for all analytes.

The main application of NP-LC lies in Chiral Chromatography where chiral selectors such as cyclodextrins, chiral cellulose and chiral enzymes are attached to the stationary phases allowing separation of enantiomers. Moreover, columns can be custom-made to promote highly specific interactions such as those between antigen and antibody, receptor and ligand or enzyme and substrate in Affinity Chromatography.

Reverse-phase Liquid Chromatography (RP-LC)

With an estimated market share of 44.6% RP-LC is certainly the most popular mode in HPLC [263]. As its name suggests RP-LC relies on the exact opposite interactions as NP-LC. As an apolar stationary phase is combined with polar mobile phases, this technique is very suitable for relatively hydrophobic molecules, often encountered in organic synthesis. Separation occurs through the distribution of the apolar analytes between the stationary phase and the mobile phase which typically consists of a H_2O/CH_3CN or H_2O/MeOH mixture of which the volume ratio is suitably adapted. The percentage by weight of bonded carbon of the stationary phase, often C18 or C8 modified silica, also plays a key role in the retention of analytes.

Main drawbacks are the high viscosity of water which can limit the maximum applicable flow rate before exceeding the pressure threshold and adsorption/interaction phenomena occurring between polar regions of the stationary phase, e.g. leftover silanols, and polar groups. Above this, ionic analytes are more soluble in the strong solvent, water and are thus far less retained compared to their neutral counterparts. Therefore, adsorption and interaction effects cause undesired peak tailing and peak shifting. This can be overcome (partially) by extensive passivation or deactivation of the silanols (see 6.2.4) or running experiments at a proper pH in the separation of organic acids and bases so these are not charged. For example, a common problem is base peak tailing, which arises from coulombic interactions between protonated amine-bases and negatively

charged silanol-group at neutral pH. Using popular silica-based particles however, the pH range of application is limited by its hydrolytic stability (see Section 6.2.5), making this a major field of interest for development of new chromatographic packings.[4]

As already witnessed from the above, the major benefit of RP-LC is its versatility and adaptability. Not only is the use of water cheap and environmentally benign, is allows control of pH and ionic strength (Ion-Pair Chromatography). Control on the retention factor is exerted using correct combinations of mobile phase, but can also be obtained by selection of the stationary phase. Many columns are commercially available, with variable dimensions, particle sizes and surface modifications. These latter modifications, apart from common C18 groups, are specifically developed functional groups for high performance separations of specific samples (see Section 6.2.4).

Hydrophilic interaction chromatography (HILIC)

In HILIC, an aqueous mobile phase containing high amounts of organic modifier is applied together with a polar column packing. This results in the water forming a hydrophilic water-rich layer on the surface of the polar stationary phase due to its interaction with the polar silanol groups. Retention arises from the partitioning of the analytes between the water-rich stationary phase and the water-poor mobile phase. Polar analytes will exhibit a much stronger interaction with the aqueous layer and are therefore eluted after the more hydrophobic analytes. Therefore, HILIC is mainly applied for the separation of polar analytes with high selectivity.

Other methods such as **Size exclusion Chromatography (SEC)**, separating molecules based on their size and shape with a stationary phase having a distinct porosity and **Ion-exchange Chromatography (IEC)**, where retention is obtained through coulombic interaction between the ionic stationary phase and analytes, are hardly practiced using silica-based materials and are therefore not disclosed further.

4. Also ion-pairing methods can be considered if components, especially amines, have a too high pKa to adapt for with the pH of the mobile phase. Herein, amines are separated at low pH, avoiding the high pHs which are detrimental to the stability of silica whilst separation proceeds purely on hydrophobic interactions between the ion-pair formed between the protonated amine and the acid counter-ion [264]. Also under these conditions, the acidic silanol groups are protonated, avoiding coulombic interaction between Si-O^- and the protonated amines [265].

6.1.4 Preparative HPLC [256, 266, 267]

High Performance Liquid Chromatography can roughly be subdivided in two categories: Analytical HPLC and Preparative HPLC (PREP-HPLC). The two are differentiated by their main objective. Analytical HPLC, the technique widely known and applied in academic research and R&D, focusses on qualitative and quantitative determination of compounds whereby the samples can be processed and modified, e.g. degradation or labeling, in any suitable way to generate information. The objective of PREP-HLPC, however, is to isolate and purify products independent of the amount of product to be separated. Emphasis lies on recovery of the product in the exact same composition as they entered the separation process. As a result, in preparative HPLC, columns are frequently, and sometimes heavily, overloaded with sample, causing the adsorption and partitioning process to differ significantly from the ideal case of low sample concentrations and volumes which is aimed for in analytical HPLC. Consequently, PREP separations are often optimized for either high purity, high yield or high loading, but all three together are almost never obtained.

Preparative HPLC is used for the isolation and purification of valuable products from the μg-scale in for example the screening of pharmaceutical compounds and the isolation of enzymes to the kg-scale found in the industrial synthesis of drugs or fine chemicals. The columns used can vary from a packing of cheap irregular particles for crude separations (cfr. flash chromatography) to highly customized functional columns such as chiral or molecular-imprinted polymers, metal oxide spheres or monoliths. Several operating modes such as column switching, closed-loop recycling and flip-flop chromatography have been developed to respectively deal with continuous feed introduction, column overloading or to speed up the process (**Figure 6.10**).

One important aspect in PREP-HPLC, which arises from the high mass loadings used, is washing or regenerating the column to remove highly adsorptive compounds, which can alter the separation performance in between chromatographic runs. A precolumn is often used to remove these compounds before subjecting the mixture to the main column, however, at times Cleaning in Place (CIP) of the main column is required. This step generally comprises washing the column with a strong eluens in the reversed flow direction. Of course a cost-benefit balance between CIP and replacing the column should always be taken into account. In the particular case of the industrial separation of insuline from its by-products, CIP is performed with a NaOH-solution at pH 12. During

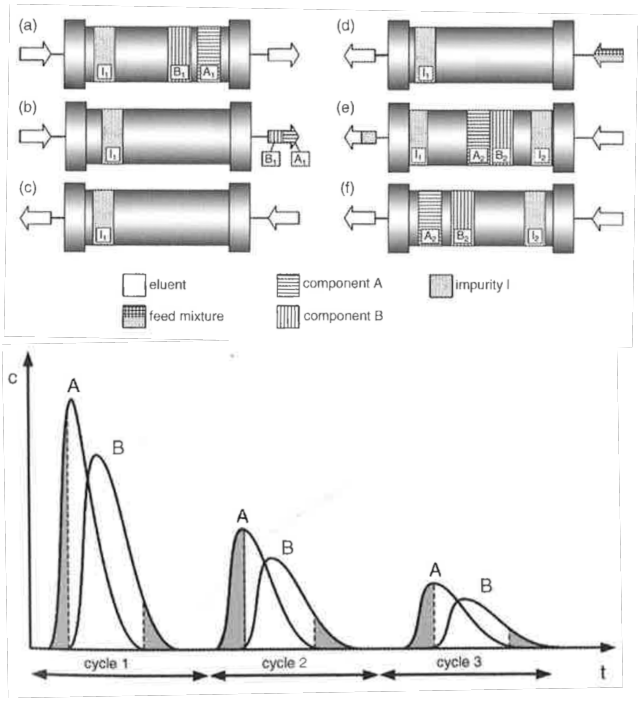

Figure 6.10: Scheme of flip-flop chromatography where a counterflow is applied to separate two components and a highly retentive impurity with minimum time loss (top). Illustration of closed-loop recycling chromatography: a mixture is cycled multiple times over the same column; after every cycle, the separated fractions (grey) are collected (bottom). Taken from [256].

the process, part of the spherical silica packing dissolves and is lost. Therefore, intermediate refilling of the column is necessary [268, 269]. A more stable packing would be capable of solving this unprofitable issue.

6.2 Particle specifications and their influence on separation performance

As suggested in previous section, silica is the material of choice for chromatography due to its high mechanical stability, chemical inertness, tuneable porosity, controlled morphology and modifiable surface. Many other metal oxides such as titania (Sachtopore, Titanosphere), alumina and zirconia have been applied for (niche) chromatographic separations [270–276]. These materials, however, show poor performance in RP-HLPC because of strong adsorption of analytes on acidic or basic sites.

Furthermore, and in contrast to silica, few chemistries exist to modify the surface of metal oxide particles with hydrophobic groups, the source of retention in RP-HPLC. Polymers are also employed in RP-HPLC, especially when harsh hydrolytic conditions are required for the separation. However, polymers suffer from low mechanical stability, swelling and low efficiency. Carbon-based media, e.g. Hypercarb, are extremely stable but, in turn, exhibit too strong adsorption for polar components which also results in inferior peak shapes.

In order to meet the ever increasing demand for high separation performance, silica-based particles for chromatography have undergone many developments and revolutions. Correspondingly, specifications and requirements for a good packing have become very stringent and all need to be fulfilled to achieve high efficiency. Silica, however being the best candidate for HPLC packings, is not perfect for all applications, implying that chemical modification of the surface is needed, not only to enhance retention, but also to increase the chemical stability of the column.

In what follows, the specifications for silica particles are reviewed with the theoretical concepts of chromatography in mind. Major improvements will be highlighted together with opportunities for further progress in silica-based technologies.

6.2.1 Morphology

Historically, separations were performed using irregular particles of porous silica or silica gel (**Figure 6.11**). Particles of 5 - 10 μm were obtained by milling of larger silica xerogel particles and size classification via air elutriation (see Section 6.2.2). Such irregular particles create a non-uniform packing and thus give rise to a high Eddy diffusion coefficient (A-term). The relatively large fraction of fine particulates still contained in the packing often causes dramatically increased back-pressure. Furthermore, rearrangement of the particles in the packed bed during separation is known to occur, which is detrimental for reproductivity [277].

Evidently, efficiency was greatly improved by shifting from such irregular shaped to spherical particles. This shape allows a more uniform packing in the column, with less voids, hence reducing the Eddy diffusion coefficient[5]. Next to the shape, dispersion on the particle size needs to be as low as possible to reduce the contribution of the A-term [278]. An overview of synthetic approaches can be found further in this work.

5. Of course the quality of the packing itself (λ) is as important as the particle size and shape to avoid voids and preferential pathways for analytes.

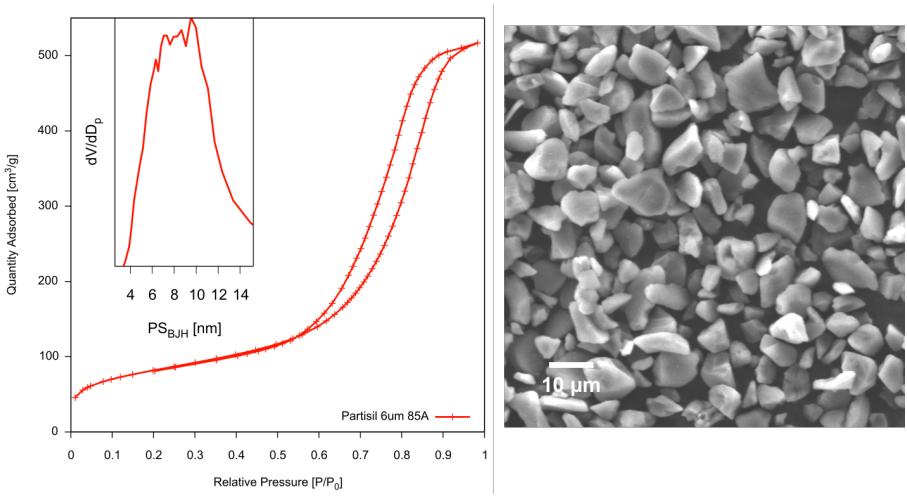

Figure 6.11: Commercial Partisil materials: N_2-sorption isotherm indicating an S_{BET} = 298 m^2/g with an average d_p = 85Å and SEM images showing irregular particles with a mean size of 6 μm.

Following the spherical particle morphology, miniaturization to smaller particles (d_p) is also proven beneficial for separation efficiency (N=L/2d_p). Small particles (< 2 μm), however, give rise to much higher back-pressure of the column given the following equation:

$$\Delta P = \frac{\eta F L}{K^0 \pi r^2 d_p^2}$$

with ΔP the change in pressure over the column, η the mobile phase viscosity, F the flow rate, L the length is the column, K^0 a column permeability term, r the column radius and d_p the mean particle size.

Therefore the smallest of particles require dedicated UHPLC equipment capable of working pressures up to 1200 bar. Since the particles are small in size, the diffusion path between the sample analytes and the stationary phase is shorter (reduction of C-term) and the paths of the analyte molecules are encouraged to be more similar in length (reduction of A-term). Therefore, the efficiency in UHPLC is higher and, given that efficiency remains unchanged at high flow rates, UHPLC allows for very fast separations as compared to the more classic 2 - 5 μm particles used in HPLC (**Figure 6.12**) [279]. At high linear velocity of the mobile phase, however, frictional heating can cause issues with separation efficiency.

Practically, < 2 μm particles are typically used for high resolution separations using longer columns, or high speed separations using shorter

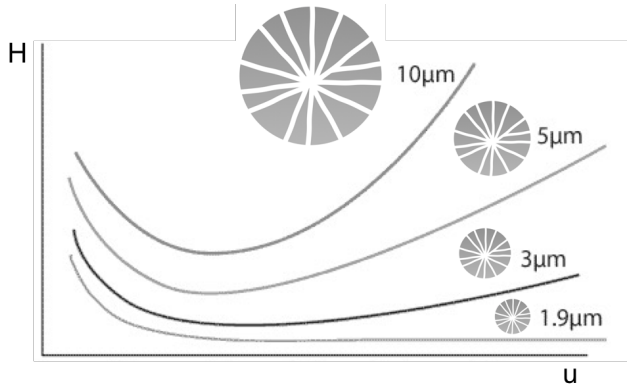

Figure 6.12: Miniaturization of spherical particles leads to reduced plate heights.

columns. Intermediate particle sizes (2 - 5 μm) are applied for complex separations of similar components where high speed is not a primary factor. 5 - 10 μm particles are used for routine analyses or for preparative chromatography where a high analyte loading is important [280].

Next to fully porous spheres, particles made up of a solid silica core and a porous shell are employed, with advantageous performance [281, 282]. In general, these core-shell particles are even more monodisperse in size compared to fully porous analogues as they are prepared starting from highly uniform solid silica spheres obtained through the classic Stöber synthesis [283] (**Figure 6.13**). In contrast with this, packings made with mixtures of different yet uniform particles sizes were also shown to have a reduced A-term [284], which somewhat refutes the previous claim. The higher surface roughness of core-shell particles (**Figure 6.14**) is also alleged to be causing a smaller A-term. Although roughness makes core-shell particles more difficult to pack, it is believed they form a more stable and uniform bed over time than fully porous particles with a smooth particle surface.

The solid core also decreases the dead volume of the column, dependent of the core to shell volume ratio [285]. This in turn reduces the B term as longitudinal diffusion is limited and the obstruction factor is higher. Mass transfer effects are also reduced using core-shell particles as fewer 'deep' pores are available. Which ever effect effectively makes an impact or has the largest influence, is however subject of debate but altogether core-shell architectures are claimed to increase separation efficiency with up to 90% for 5 μm particles and up to 20% for 1.7 μm UHPLC columns. As a result, core-shell particles can be considered as performant as fully

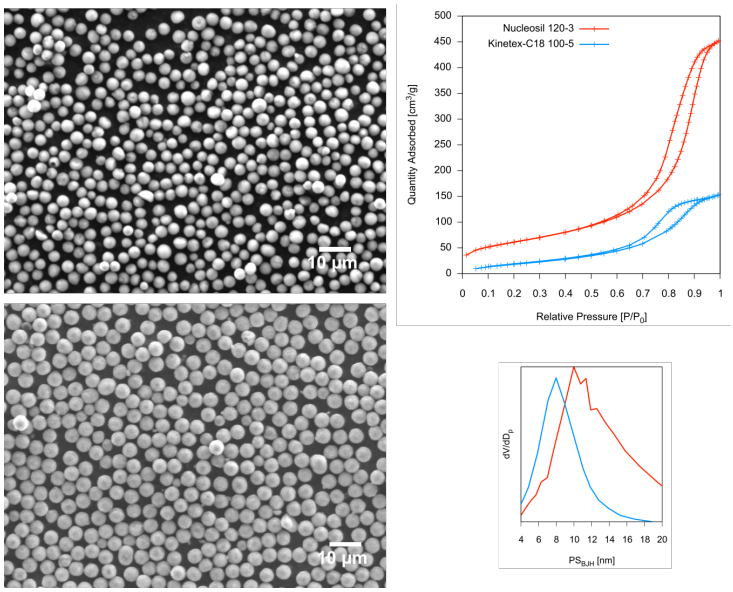

Figure 6.13: Comparison of a commercial 3 μm fully porous silica, Nucleosil 120-3 (top left) and a commercial 5 μm core-shell particle, Kinetex-C18-100Å (bottom left) visually indicating the dispersion of the particle size. N_2-sorption isotherms and pore size distribution are illustrative for commercial materials having large mesopores and few micropores. Rational comparison of both is not possible as Nucleosil is underivatized silica where Kinetex-C18 has been modified.

porous particle with smaller size, yet allowing separation with reduced back-pressure [285, 286]. Thus, core-shell particles permit separation at UHPLC-quality with standard HPLC equipment. Their reduced porosity on the contrary, means they have a lower sample capacity [287].

6.2.2 Enhancing the size dispersion: classification

Some of the synthetic approaches described further immediately manage to meet the size dispersion requirement for as-synthesized particles. Methods resulting in polydisperse particles, however, rely on a selection of particles based on size after synthesis. This so-called classification used to be done by simple sieving of the particles, however for modern chromatographic particles this technique all but suffices to separate discrete particle size ranges below 10 μm. Some more advanced elutriation methods are applied nowadays. These techniques are essentially sedi-

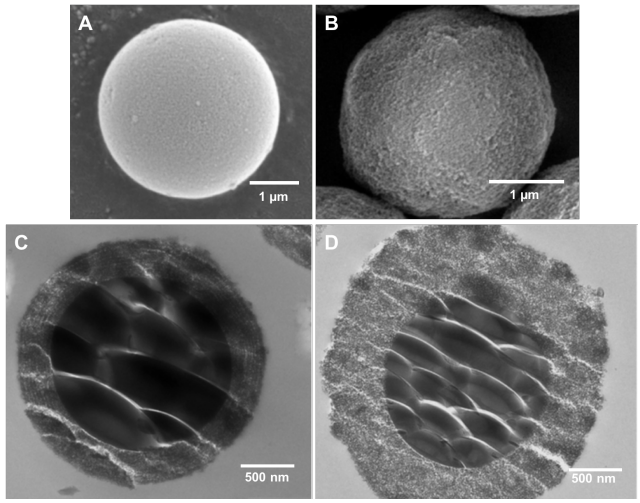

Figure 6.14: A: SEM image of fully porous commercial mesoporous silica particle (Phenomenex Luna). B: A core-shell particle (Advanced Materials Technology Halo) showing increased surface roughness. C: SEM cut of a Phenomenex Kinetex core-shell particle and D: Cross-section of a Halo core-shell particle. In the latter two stratification is witnessed, which arises from the layer by layer synthesis (see Section 6.3.2)

mentation processes, but, to achieve refined separation, a gas or liquid counterflow is applied.

Liquid elutriation [288]. For smooth spherical particles such as encountered here, Stokes' law applies:

$$F_d = 6\pi\eta R\upsilon$$

where F_d is the frictional force a particle experiences, η is the liquid's viscosity, R the particle radius and υ is the flow rate. The resulting frictional force or Stoke's drag a particle sustains is proportional to its radius. Gravitational forces acting on the spheres result from difference between the weight and buoyancy of the sphere:

$$F_g = (\rho_p - \rho_f)g\frac{4}{3}\pi R^3$$

with ρ_p and ρ_f are the mass density of the particles and the fluid respectively.

Both equations combined give an expression for the terminal velocity of the particles falling in the liquid:

$$v = \frac{2}{9}\frac{(\rho_p - \rho_f)}{\eta} g R^2$$

This means that the speed at which small particles fall in a liquid is lower than the terminal velocity of a larger particle. As a result, large particles sediment faster in a motionless liquid. Assuming all particles have the same density, selection of particle size can be reached by applying a counterflow. Hereby, particles with a terminal velocity lower than the implemented flow rate, being small particles, are removed on top of the vertical liquid column. Larger particles sediment over time as they settle against the upward current. Therefore, by controlling the flow rate of the liquid, particles of certain radius can be selected and separated from complex mixtures. Of course, next to a liquid also a directional gas stream can be applied.

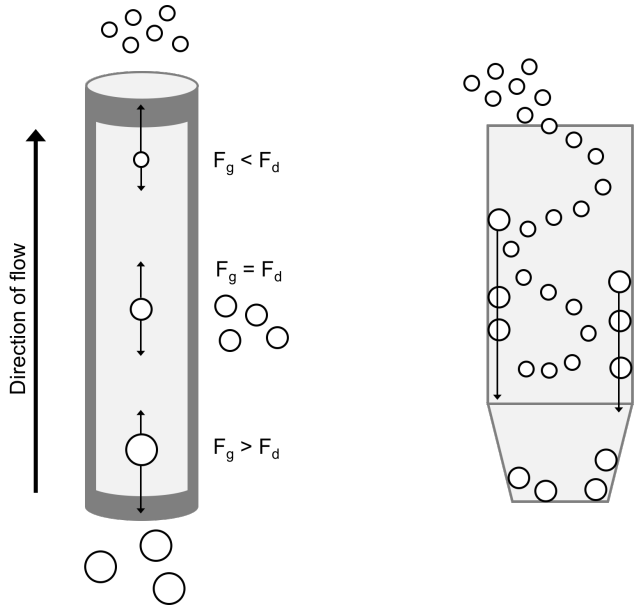

Figure 6.15: Schematic representation of elutriation (left) and cyclonic separation (right) for the classification of particles.

Cyclonic separation. For this technique, a rotating flow of air at high speed is established within a cylindrical or conical container. Separation of particles is based on inertia. Small particles easily follow the path of helical air steam in the cyclone, while large ones suffer from inertia and hit the wall of the cylinder, after which they fall to the bottom. Both

flow rate and cyclone geometry influence the classification, thus variation of these allows for selection of certain particle sizes. To protect particles from impact on the wall, a secondary flow can be applied downward along the wall of the vessel. This intercepts the large particles and smoothly brings them down.

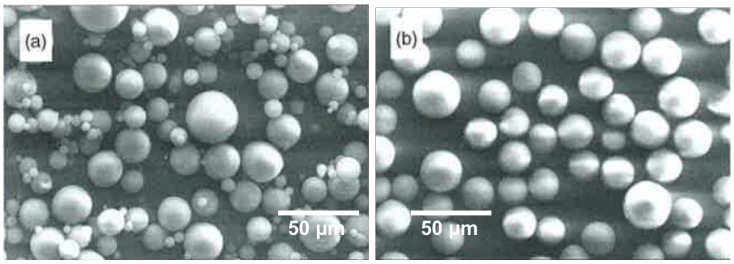

Figure 6.16: SEM images of spherical porous silica before (left) and after (right) classification. Images taken from [256].

6.2.3 Porosity and mechanical stability

For application in chromatography, silica particles should have a large surface area and pore volume to maximize the distribution of analytes between the mobile and stationary phase. Meanwhile, a large surface area ensures a large analyte capacity. A narrow pore size distribution is preferred, together with the possibility to fine-tune the size of these pores for envisaged applications. For the separation of small molecules, pore diameters of 8 - 12 nm are most frequently used, while pores of approximately 30 nm are chosen for the efficient separation of peptides and proteins [289, 290]. In both cases, using pores that are significantly larger than the analytes ensures good transport of the latter. For this same reason, micropores ($<$ 2 nm) have a negative effect on the peak shape and are highly undesired [291]. Furthermore, micropores are known to trap analytes which both reduces the signal and causes column regeneration problems.

Increase of the surface area and pore volume comes with implications on the mechanical stability. Undoubtedly, high mechanical stability for chromatographic particles is required as they are packed into columns at extremely high pressures, sometimes exceeding 1000 bar. During analyses as in RP-HPLC, although at lower pressures, particles are often more susceptible for mechanic stress due to the presence of water. Very high surface area silicas such as MCM-41 materials are known to have a low mechanical stability when water is present. This is caused by

adsorption of water to the surface silanols followed by hydrolytic cleavage of the siloxanes at elevated pressure (see also Part I). All combined, a consensus needs to be found between maximal porosity and mechanical stability.

All the above materials possess randomly ordered pores with a relatively wide pore size distribution. Widely investigated in academia, pore ordering was shown to increase retention times as compared to commercial silicas with disordered pores [292–298]. In many reports the increase in surface area is suggested to be causing this. Development of spherical silicas with sufficiently large ordered pores (> 6 nm) is troublesome and often materials suffer from poor morphology due to the increased complexity of the particle synthesis (**Figure 6.17**). Because of these issues, ordered pores have not found their way to commercialization up to today. Similar to monolithic columns, highly interconnected systems (MCM-48, SBA-16 types) are supposed to be more suited for chromatography as this pore structure should allow faster diffusion of the components because of better connectivity of the pores [294]. On the other hand, these materials consist of large spherical pores interconnected via small channels or openings, which limits application for separation of large molecules.

Post-modification of the porosity. A hydrothermal post-treatment is widely applied to further enhance the porosity of as-synthesized silica-based particles. This procedure comprises treatment of as-synthesized particles at elevated temperatures in water under autogeneous pressure. If required, a base can be added to enhance the process. When conditions are right, pores can be expanded as the (organo)silica at the surface dissolves. In some cases the dissolved silica is redeposited within micropores, thus closing these [299–305].

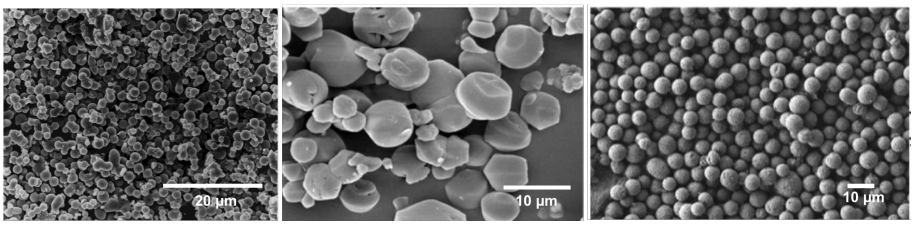

Figure 6.17: SEM images of materials applied for chromatography having ordered pores. Left: MCM-41 type material with 2.4 nm pores and an S_{BET} of 1186 m^2/g [295]. Center: SBA-15 type material with 7.6 nm pores and an S_{BET} of 811 m^2/g [296]. Right: SBA-16 type material with 8.0 nm pores and an S_{BET} of 632 m^2/g [298].

6.2.4 Modifications of the silica surface

The most applied HPLC mode, reverse-phase, requires silica particles with hydrophobic groups decorating the surface. For bare silica, this is typically performed in a second synthesis step by silanization or grafting of the superficial silanol groups using all sorts of hydrolyzable silanes [306]. For robust RP-HPLC separations C18 or C8 chains are attached to induce retention by hydrophobic interaction. Specialty stationary phases have been developed by the introduction of other functional groups such as phenyl or biphenyl groups for the separation of aromatics and pentafluorophenyl for halogenated, conjugated, isomeric, or highly polar compounds. Also highly dedicated chiral and affinity inducing groups can be attached.

High loading of the functionalities is desired, not only for high retention, but also to eliminate as many Si-OH groups as possible. As described earlier, these can have a detrimental effect on the peak shape of base analytes, one of the main issues associated with silica-based chromatography [307]. Next to ion-pairing methods [265], several surface modification methods are able to correct for this base peak tailing. A first is the use of end-capping or silanol-terminating reagents. These small and reactive molecules, such as hexamethyldisilazane (HMDS) and trimethylchlorosilane, react with silanol functionalities forming a hydrophobic trimethylsilyl group (**Figure 6.18**). This reduces the amount of free silanols that cause the base peak tailing. It is however difficult to obtain full coverage of the surface. Secondly, sterically hindered silanes with t-butyl groups covering the surface also reduce base peak tailing as they cover silanol groups that are inaccessible for end-capping reagents. Finally, base peak tailing can be prevented using polar embedded silanes, typically bearing charged groups such as carbamates, amides and ureas. [308–310]. It is believed these polar groups adsorb water molecules, which in turn protect basic analytes from interaction with the silanol groups.

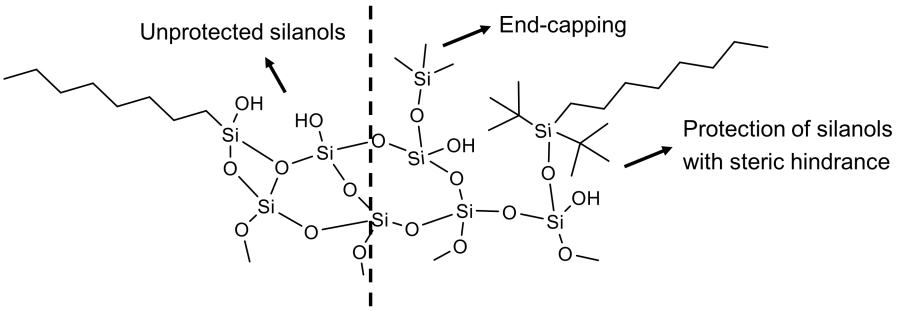

Figure 6.18: Representation of a possible silica surface: Depending on the modification and end-capping, silanol groups remain present (left) or are partially shielded from analytes (right).

6.2.5 Hydrolytic stability

The achilles heel of silica is its poor hydrolytic stability. Water molecules can easily adsorb by means of hydrogen bonding to the silanol groups of the silica surface where they may attack the labile siloxane bonds (**Figure 6.19**) [306]. Above pH 8, hydrolytic attack is very pronounced and silica readily dissolves. Modification of the silica surface with hydrophobic groups somewhat expands the use of silica-based materials to approximately pH 10 or 11 at the limit [311]. Thus, in RP-HPLC with classic silica-based materials, all conditions at high pH are ruled out as these induce structural degradation of the column with loss of efficiency, increased back pressure and bed collapse as consequences [312].

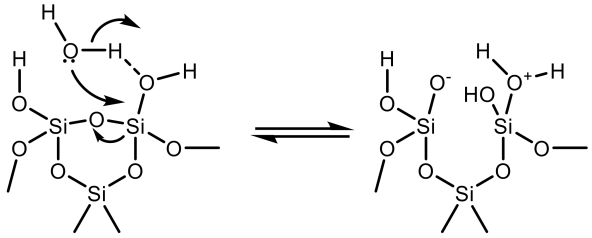

Figure 6.19: Schematic representation of the hydrolytic breakdown of silica in the presence of water.

At low pH, the siloxane framework itself is relatively stable, however surface modifications are susceptible to hydrolysis. Grafted groups are stripped from the surface below pH 2, with sterically hindered functionalities performing somewhat better [312–316]. Furthermore, end-capping groups are also removed at low pH. Removal of hydrophobic groups on the surface over time changes the retentive properties of the column

which is detrimental for reproducibility [317]. Moreover, it exposes new silanol groups, making the particles again more susceptible at high pH. This also means that all creative methods and modifications above, e.g. to overcome base tailing, are not maintained under harsh conditions.

Not only high and low pH cause hydrolytic stress, but also high temperatures are to be avoided with silica-based columns. This limits the potential of silica materials to perform ultra-fast separations using high temperatures to reduce the solvent viscosity and thereby the column back-pressure.

6.2.6 Towards ultimate chromatographic particles: opportunities for organosilica

From all the above it is clear that materials for a chromatographic packing are subjected to many stringent demands. Also there is still much room for further improvement, especially in terms of particle stability and stability of the bonded phase. An ideal particle would have the following properties:

- Spherical particles
- Monodisperse in size: $D_{90/10}$[6] < 1.6
- Available particle sizes for both analytical separations and preparative purposes: d_{part} = 2 - 5 μm and 5 - 15 μm respectively
- Large surface area: S_{BET} = 50 - 600 m^2/g
- Large pore size, tunable in the mesopore range: $d_p > 60$Å
- Limited or no micropores: $\frac{S_\mu}{S_{BET}} < 0.1$
- Mechanical stability at packing and analysis pressures
- Hydrolytic stability at pH < 2, pH > 12 and temperatures above 100°C
- Functional versatility
- Absence of metal ion impurities [318, 319]

6. $D_{90/10}$ is a statistic describing the dispersion on the particle size. Herein D_{10} is the particle diameter where the cumulative volume of the particles reaches 10%. D_{90} is the corresponding value at 90 v%. Most commercial particles have a $D_{90/10}$ below 1.3, either by a highly controlled synthesis of the particles or size classification.

Where hybrid mesoporous silica particles prepared by grafting and even co-condensation [320] do not meet these conditions, organosilicas show far more potential. Using bis-silanes instead of pure silica as the precursor for the particles, hydrolytic stability is greatly improved as appreciated from the comparison between MPS and PMOs (Part I). This allows separations in unprecedented conditions and opens possibilities toward ultra-fast chromatography at high temperatures. The latter would comprise analysis speeds encountered for UHPLC but at HPLC pressures. If temperatures could be increased up to 100 - 150°C, chromatographic analysis times can potentially be reduced to seconds. Moreover, using higher analysis temperatures, greener chromatography can be attained as the dielectric constant or relative permittivity (ϵ_r) of water decreases with elevated temperature [321]. Consequently, the eluotropic strength of the water increases with temperature, thus decreasingly smaller percentages of organic modifiers are required in the mobile phase at high temperatures [322].

High pH stability, on the other hand, would allow improved separation for most pharmaceutical compounds (of which 80% contain basic functions) as these are deprotonated from pH 10 - 11 on and higher. Low pH stability would, for example, lead to the development of better ion pairing methods for e.g. biomolecules through the use of stronger volatile acids resulting in better separation and ionization in coupled mass-spectrometers. Columns packed with organosilica particles that are stable over a wide pH range would be the first universally applicable chromatographic phases. In PREP, a packing material with enhanced hydrolytic stability would not only permit development of new separation methods, it would also tolerate far more drastic CIP processes without deterioration of the column (cfr. insuline separation).

Next to this, organosilicas are inherently more hydrophobic than silicas as they already bear groups in their silsesquioxane framework that induce retention. Moreover, base peak tailing is reduced using organosilica particles due to the lower acidity of the silanols (pKa $>$ 8) compared to pure silica (pKa = 3.5 - 6.8) [323].

The use of bis-silanes, on the other hand, makes the synthesis of particles with the same beneficial properties as silica somewhat more difficult, which limits the amount of applicable synthesis methods and ensuing materials (see Section 6.4). In what follows, typical methods to obtain silica particles with desired properties will be described. Thereafter, the applicability of these methods to obtain organosilicas with the same structural properties will be assessed and some new approaches will be described.

6.3 Synthetic approaches for spherical silica-based particles

6.3.1 Fully porous silica particles [277, 324]

Monodisperse silica particles were first described by Stöber in 1968, who performed the hydrolysis and condensation of TEOS in water using ethanol as a dispersing co-solvent and ammonia as the catalyst [283]. This delivered, depending on the reaction conditions, such as catalyst amount, temperature and co-solvent, solid particles with a controllable size between 50 and 2000 nm. Based on this groundbreaking invention, multiple pathways towards porous particles can be followed (**Figure 6.20**). In a first approach, these solid nanoparticles are fused in a controlled way to form a spherical particle with mesoporous voids between the original nanoparticles. This is done by coacervation, a technique where silica NPs are brought together during a polymerization reaction. As described by Kirkland et al., the silica nanoparticles are mixed with monomers of melamine or urea and formaldehyde [325, 326]. As polymerization takes place, the nanoparticles co-precipitate and after removal of the polymer by calcination, uniform micron-sized spheres are found.

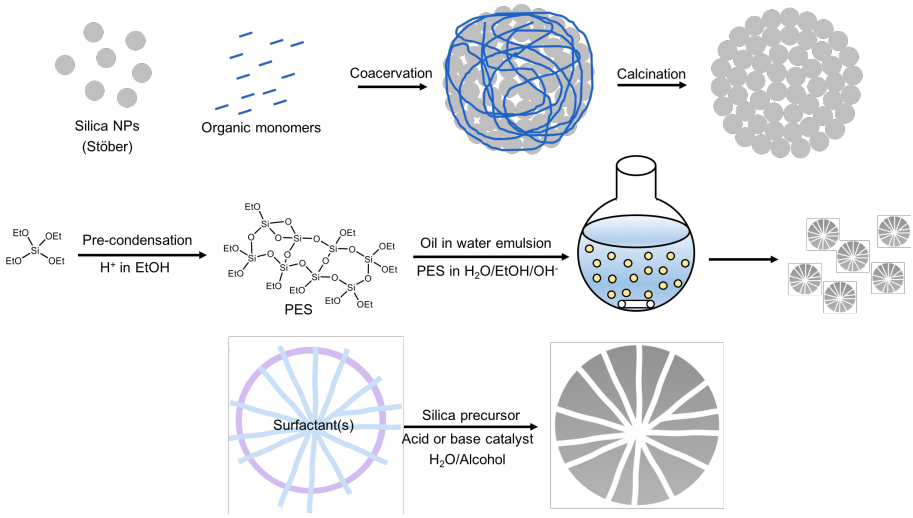

Figure 6.20: Graphical representation of the coacervation method (top), the Unger method (middle) and the adapted Stöber procedure to obtain fully porous silica spheres.

Secondly, Unger and Schick-Kalb developed a Stöber-like method in 1971, where pre-condensended TEOS, i.e. poly(ethoxysiloxane) or PES,

is used as starting point instead of a silica sol [327]. This PES is subsequently emusified in a water/ethanol mixture in which it forms microdroplets. Addition of a base catalyst starts hydrolysis of the PES, which results in the formation of porous beads. The condensation degree, measured by the viscosity of the PES, is claimed to control porosity, while the particle size is controlled by the stirring speed [328].

A third, similar option is to take the original Stöber method and add pore generating surfactants as described by the Unger group in 1997 [292, 329, 330]. Depending on the surfactant, pore size and ordering can be controlled, however it seems more practical to expand smaller pores with a post-synthetic hydrothermal treatment. This approach has further been investigated by other groups who managed to produce spheres in an acidic medium by using hydrochloric acid as a catalyst. The properties of the particles remained roughly the same except these could reach diameters up to 1 mm. [293, 331, 332]. Using NaOH instead of ammonia, spherical particles were also obtained, albeit only 1 μm in size [333]. As a main benefit for this templated method, highly monodisperse particles are obtained which do not require physical separation by means of classification. As such classification techniques to separate different size fractions are not well-suited for particles below 3 μm, this approach is preferred to obtain UHPLC particles [334]. A problem with this technique is, however, that adding a surfactant to the mixture, reduces the dispersing power of the alcohol and the final spheres can become intergrown.

In 1998, another synthesis pathway for mesoporous silica spheres was introduced by Qi et al [335]. A mixture of CTAB and the non-ionic surfactant Brij-56 combined with TEOS as silica source was used for liquid crystal templating under acidic conditions but without the addition of a co-solvent. The resulting particles reveal a particle diameter of 2 - 6 μm and all characteristic properties of the ordered mesoporous materials.

Bossière et al. expanded the field of mesoporous spherical particles as they were able to significantly enlarge the particle size [336, 337]. The reaction was accomplished in a two step Stöber method. In a first step under acidic conditions TEOS is fully hydrolyzed, while after addition of NaF, controlled nucleation in a microemulsion occurs, with the non-ionic surfactant Tergitol 15S12PEO as surfactant. Nonetheless, the pore size remained below 4 nm and, although ultrasonic treatment reduced particle agglomeration, this remained an issue.

Next to this, spherical particles of porous silica can also be obtained by employing water-in-oil emulsions [299, 338, 339] or by spray-drying

[340–342]. Both processes essentially create droplets in which xerogel particles form. Inside these spherical microdroplets, the porosity can be controlled, either by the sol-gel process occurring inside or by adding surfactants. Herein, quality of the droplet is of primordial importance as this controls the size and dispersion of the particles. With these colloid methods, it is easy to increase the particle size above those obtained in Stöber-type syntheses, while control of particle size and pore size is effectively decoupled. However, with spray drying, it seems not trivial to obtain monodisperse particles in the size range applicable for HPLC. Furthermore, considering particles with ordered porosity, an evaporating solvent (EtOH) needs to be used together with a pore generating surfactant in order to obtain porous particles. Here, gel formation takes place almost immediately after droplet formation and is induced by evaporation of EtOH [343, 344]. Due to these constraints, it remains challenging to obtain large mesopores via spray drying. Using emulsion approaches, the composition of the emulsion and the emulsifier used, have great effects on the porosity and particle size. Porosity is often non-existent or low, while particle sizes are often too small or large for an application as chromatographic packing [345–348].

Finally, another interesting procedure called pseudomorphic transformation cannot be withhold. This method highly resembles a redeposition/pore etching process that is often used to enhance the porosity of mesoporous silica particles, but now involves the addition of an SDA. Developed by Martin et al. the process starts off from commercial porous silica particles such as Nucleosil or Lichrosphere. Stirring these particles in an alkaline solution comprising sodium hydroxide, water and CTAB at elevated temperatures partly dissolves the particle. However, redeposition of this dissolved silica is believed to occur around the SDA. As a result, ordered MCM-41 type pores are obtained (CTAB inducing a pore size of approximately 4 nm), while the spherical morphology is maintained (**Figure 6.21**) [349]. Later MCM-48 type materials were also developed via this method [350].

Commercially, many columns packed with fully porous silica particles, both pure and modified, are available. Typically a whole range of particle and pore sizes are available to perfectly suit the chromatographic application. Some trade names include: Agilent Zorbax, Akzo-Nobel Kromasil, Phenomenex Luna and Aeris, Merck LiChrospher, ThermoFisher Hypersil and many others from smaller suppliers. We assume most of these particles are made similarly, according to an optimized Unger method (1971) by only few bulk suppliers such as Macherey Nagel (Nucleosil) and Fuji Silysia. Exceptions we are aware of are Kromasil, which is

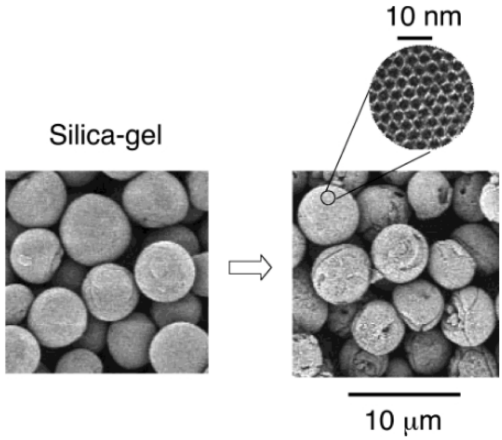

Figure 6.21: SEM images of Nucleosil 100-5 before and after its pseudomorphic transformation into a material with ordered pores (MCM-41). Images taken from [350].

an emulsion-based particle, while Nucleosil and Zorbax are prepared by coacervation of silica nanoparticles.

6.3.2 Core-shell silica particles [281, 282]

Core-shell or superficially porous particles were envisaged by Horvath and Lipsky as early as 1969 [351, 352] and subsequently developed by Kirkland et al. (**Figure 6.22**) [353, 354]. These particles were prepared by coating a glass bead with poly(diethylaminoethylmethacrylate)acetate. Thereafter, 200 nm silica nanoparticles, as prepared by Stöber, are added at pH 3.6. Coulombic attraction between silica and polymer causes a layer of nanoparticles to stick on the surface of the glass bead. After four growth rounds and a sintering step, this resulted in a stable core-shell particle. These materials were commercialized as Zipax and investigated as supports for the now abandoned technique of liquid-liquid chromatography. Bad results in the application combined with a large particle size and ongoing advantages in fully porous particles, caused reduced interest in core-shell particles for many years.

Core-shell particles were revisited in 1992, again by Kirkland, who developed a technique using simultaneously spray-drying of a mixture of large solid silica particles, obtained after sintering of monodisperse fully porous Zorbax particles, together with a sol of silica NPs [356]. The average size of the latter was 44 nm and resulted in a wide pore size distribution from 10 to 60 nm. Both this and the presence of fully

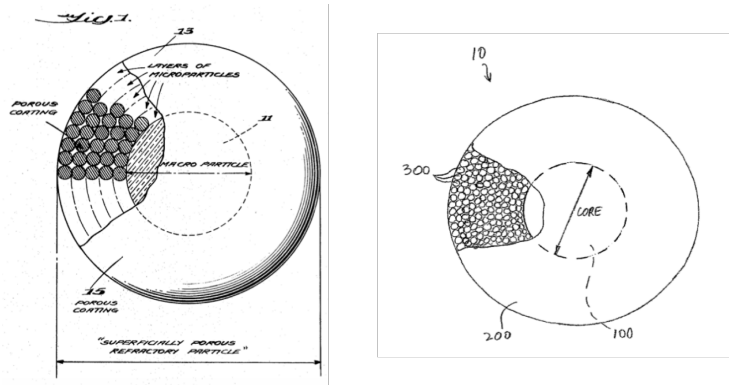

Figure 6.22: Technical drawings taken form the early core-shell particles of Kirkland [353] and their successive materials from [355].

porous aggregates, which were hard to separate, limited the use of these pioneering Poroshell particles. A major improvement was found in using a coacervation method as described for fully porous particles, but using a large core particle [357] or using a polyelectrolyte during the coating process [355, 358]. Optimization of these methods has at least led to two similar commercial materials, Agilent's Poroshell and Advanced Materials Technology's Halo, where competitors also provide core-shell particles by means of Phenomenex Kinetex, Waters Cortecs and ThermoFisher Accucore.

The Unger group, followed by others, developed another popular layer by layer (LbL) growing approach which employs a template surfactant to grow a porous shell on top of a silica core [359–361]. After one synthesis round generally, a very thin 60-75 nm layer is grown with small pore sizes. However, when suitable templates are used and pore swellers are employed one is able to boost the pore size. A shell of desired thickness is obtained after consequent growth rounds after which typically a hydrothermal pore expansion step, as described in Section 6.2.3, is performed, sometimes again using a template and/or pore expansion agents. A silica-core silica-shell particle prepared by this method is Eiroshell from University of Cork spin-off Glantreo.

Another possible method starts from a solid silica particle prepared through a two-step Stöber process to obtain a mean size up to 3.1 μm [362]. The selective etching of the particle's surface now generates superficially porous particles [363]. Furthermore, a one-pot sphere-on-sphere growth is described, but the procedure gives rise to very rough and irregularly shaped particles inapplicable for chromatography [364].

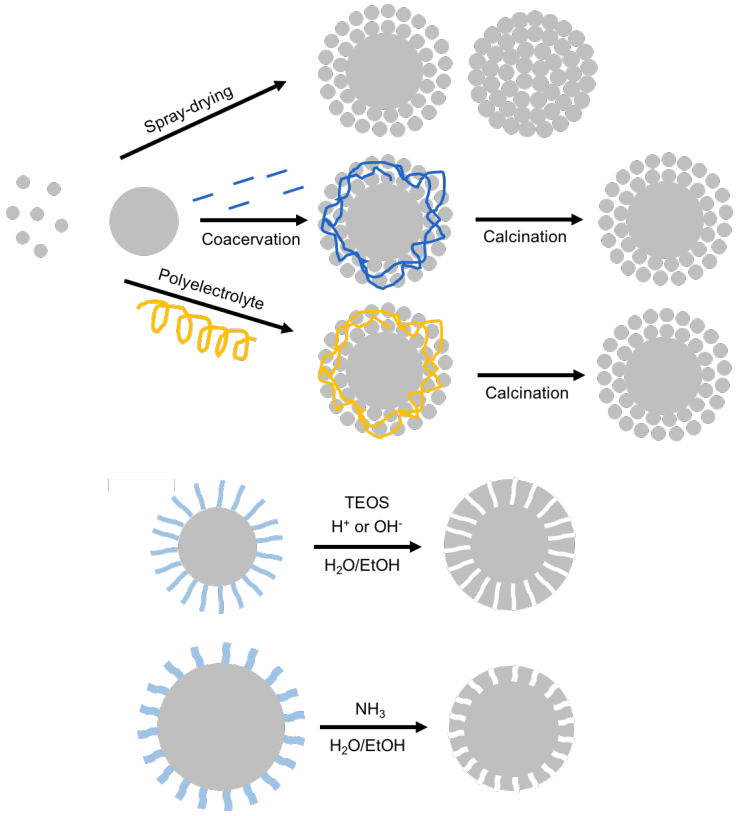

Figure 6.23: Graphic representation of synthesis methods to obtain core-shell type particles. Top: The methods of Kirkland using mixtures of large and small solid silica particles. Middle: The Unger and Eiroshell method applying surfactants to grow porous layers on top of a solid particle. Bottom: The Wei method taking advantage of selective etching in the presence of surfactants.

6.4 Hybrid silicas and organosilicas: efforts and first successes

A first effort to obtain structurally different hybrid silicas was implemented by Unger, who applied his synthesis method for silica spheres for the co-condensation of TEOS and a trialkoxysilane such as octadecyl-$Si(OEt)_3$ [320]. Morphology control was shown difficult while the materials also contained micropores. Above this, chemical stability was not increased, which is fairly logic as the structural siloxane framework remains unchanged. In a similar approach also $CH_3Si(OEt)_3$ was co-condensed with TEOS in a 1:2 ratio [365, 366]. Such materials were commercialized as Waters XTerra and were shown more stable at elevated pH as these now have a more hydrophobic surface. Still, harsh conditions could not be applied.

One of the main issues hampering the development of organosilica particles is the fact that no decent procedure, like the Stöber method for silica or the Trau method for trialkoxysilanes [367–369], is known to obtain decent monodisperse solid particles of pure organosilica without the use of TEOS; this despite some investigations [370]. Therefore, some popular methods such as coacervation are immediately ruled out if one desires to develop the ideal organosilica particle presented in Section 6.2.6.

Following the success of the Unger method for fully porous particles, research towards organosilica spheres has focussed on similar methods (**Figure 6.24**). Bis-silanes, however, are inherently hydrophobic and as a result, especially methods employing a co-solvent co-template system, basically an emulsion of oil in water, have been proven successful. Herein, it is believed that one template stabilizes a spherical morphology while the other generates the pores while the bis-silane is condensed. Using SDS and Triton X-100 in a water-ethanol mixture with base catalysis, one fully porous material (Waters X-Bridge) is marketed, which comprises of 50% ethane-bridged functionalities together with 50% of pure silica [301, 323]. Only in specific conditions, well-shaped organosilica spheres were obtained with small pores (4 nm). Classification of the particles is required and a hydrothermal post-treatment is employed to expand the pore size and reduce microporosity. For the latter, as-synthesized particles are typically treated with a 0.5 M triethylamine (TEA) at 150°C for over 24 h. As predicted, these materials show far superior hydrolytic stability compared to analogous silica materials. However, the unmodified ethane-bridged framework still shows signs of deterioration after 100 hours of testing at pH 10 and 50°C. Most likely, the presence

of 50% TEOS, assumingely a prerequisite to obtain good morphology, is the source of hydrolytic weakness. Modification of the surface with C18 chains again extends the applicable high pH range.

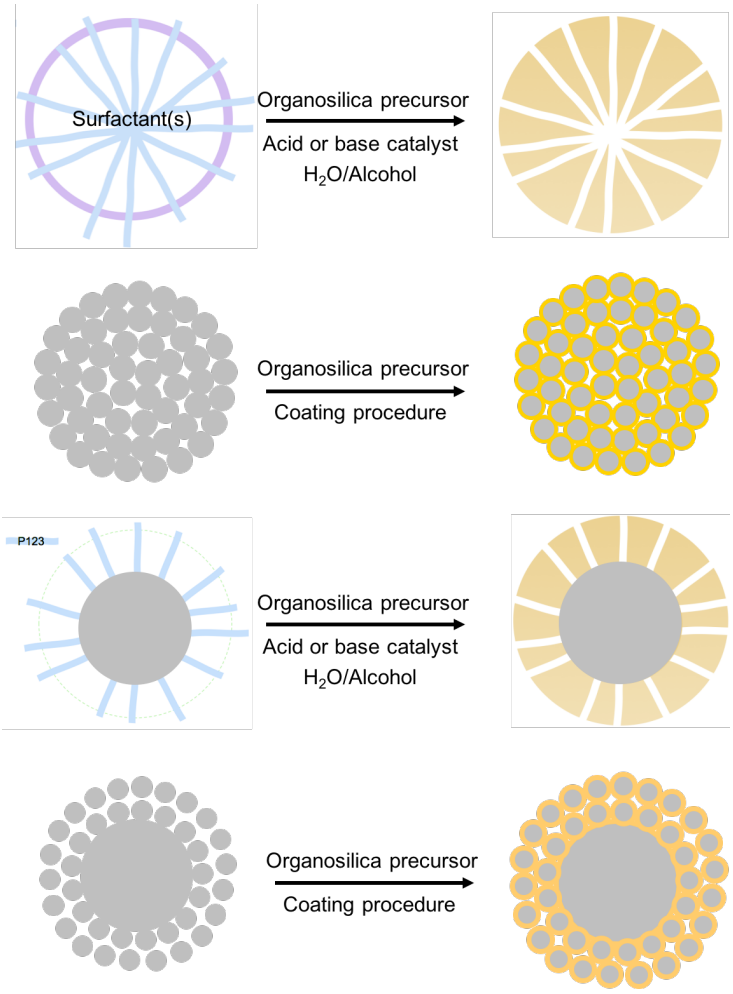

Figure 6.24: Graphic representation of synthesis methods to obtain both fully porous and core-shell organosilica particles. Generally, strategies are centered around the use of a surfactant as porogen or coating of an existing pure silica particle with a layer of organosilica.

In line with this discovery, other researchers have also employed several combinations of micellating templates, to synthesize organosilica microspheres with for example 100% ethane- [371, 372], ethene- [373] or benzene-bridges as small and rigid organic functionalities [374, 375]. Also, amine and enantioselective functionalities have been incorporated in the particle framework, albeit via co-condensation with bis(triethoxy-

silyl)ethane (BTEE) [376–378]. Although all these materials are shown to be applicable for selected HPLC experiments, the use of a template-assisted synthesis has its drawbacks, as morphology and porosity are simultaneously determined by the surfactants. As a result, the pore size does not generally exceed 40Å, particles are sometimes fused and particle size control is only achieved in few cases.

An elegant example to receive larger pores is the work of Rebbin et al. who prepared benzene-bridged PMO spheres through the use of CTAB and P123 as surfactants in a H_2O-EtOH-HCl mixture [375]. The resulting materials showed a spherical morphology with relatively broad particle size distribution centered around 10 μm, a high surface area and 5.4 nm pores. Applied in normal phase HPLC, coumarin, vanilin and caffeine were separated with significantly different affinity for the analytes as compared to pure silica particles (Nucleosil 5-10). Furthermore, aromatic compounds (benzene, naphtalene, biphenyl and phenantrene) were separated more efficiently and with longer retention times on the benzene-bridged particles (**Figure 6.25**). Later, Haffer et al. took over this concept to synthesize silica-core organosilica-shell particles by one-pot preparation of Stöber particles followed by the addition of BTEB and CTAB in basic conditions [379]. This procedure resulted in core-shell particles where the shell has pores of 4.0 nm. Unfortunately, the mean particle size only reached 600 nm as the initial solid cores were 400 nm in diameter. The researchers also observed shrinkage of the silica core when the hybrid particles were subjected to temperatures above 80°C, which resulted in yolk-shell type particles.

Xia et al. disclosed the synthesis of ethene-bridged PMO spheres using BTEEe as the precursor, dodecyltrimethylammonium bromide (DTAB) as the sole surfactant and NaOH as catalyst [373]. The particle size could easily be controlled by changing the H_2O/DTAB ratio from 600 to 225, which resulted in spheres in the range of 7.5 - 12 μm and 3 - 4.5 μm respectively. Strikingly, no ethanol or other co-solvent was used to obtain free standing spheres. The authors believe that combining high base concentrations with a relatively hydrophilic (cfr. CTAB and OTAC) alkyltrimethylammonium surfactant favors formation of spheres instead of irregular particles. The downside of this procedure is that only pores of 2.0 nm are obtained. Therefore, no application in chromatography is shown.

As a final example, Zhang et al. synthesized materials using 50 mol% BTEB and 50 mol% TEOS to receive 3.0 - 3.5 μm spheres [304]. Based on SEM images, the spheres seem to be more monodisperse than the above examples, assumingely due to the use of TEOS. Initial particles with

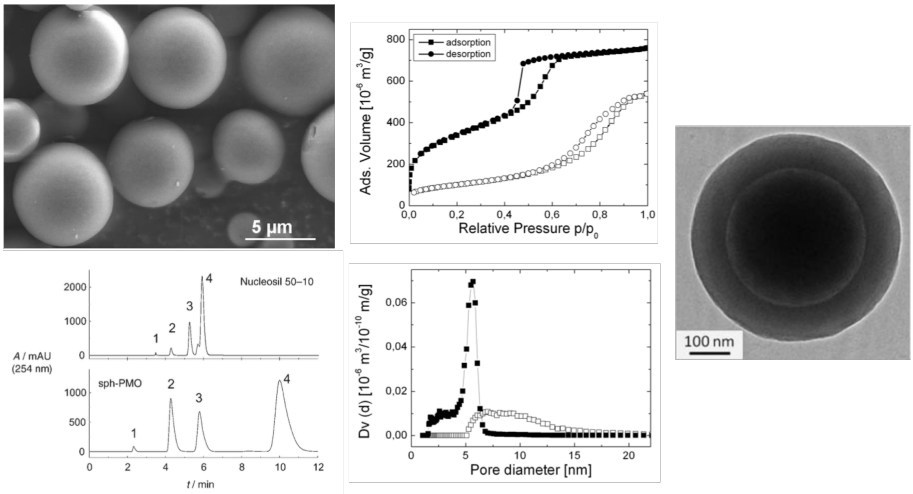

Figure 6.25: SEM image of the benzene-bridged sph-PMO of Rebbin et al. with N_2 sorption isotherms and pore size distribution (black) compared with Nucleosil 5-10 (white) as commercial counterpart and chromatograms of the NP-HPLC separation of benzene (1), naphtalene (2), biphenyl (3) and phenantrene (4) (n-hexane, 1 mL/min on Nucleosil 5-10, 2 mL/min on sph-PMO) [375]. SEM image of a benzene-bridged PMO shell silica-core particle [379].

<1.8 nm pores are prepared through condensation of the precursors in the presence of dodecylamine (DDA), CTAB and NH_3 in ethanol/H_2O as the reaction solvent. The pores were subsequently expanded with 'a swelling agent incorporation method' performed by resuspending the particles in an aqueous solution of DDA and N,N-dimethyldecylamine (DMDA) and subjecting this mixture to a hydrothermal treatment. A second expansion step is done with a tris(hydroxymethyl)aminomethane (TRIS) solution in water, again applying a hydrothermal treatment in an autoclave. This expansion increased the pore size up to 85Å with an S_{BET} of 359 m^2/g. A column packed after modification of the 50% benzene-bridged spheres by means of grafting with octadecyldimethylchlorosilane showed a H_{min} of 10 μm and was applied in the RP separation of benzene, naphthalene, biphenyl and phenanthrene. A hydrolytic stability test is carried out by purging the column with a triethylamine (TEA) solution set at pH 10. The unmodified (PHS-2c) column still displayed 100% of its original efficiency, and the C18-modified column (PHS-C18) maintained greater than 90% of its initial efficiency, while a home-C18-grafted commercial silica (S-C18) column lost over 30% of its retentive properties after 24 h of purging (**Figure 6.26**).

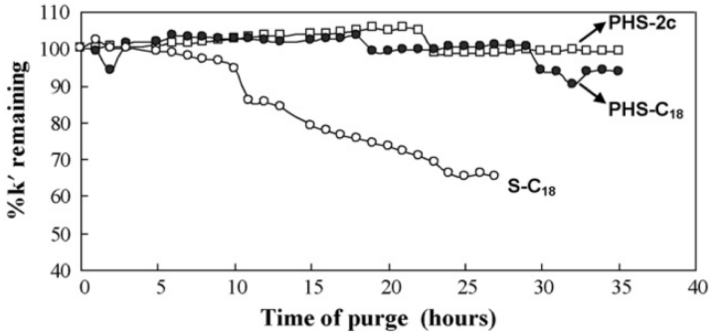

Figure 6.26: The hydrolytic evalution of Zhang et al.: Loss of retention for hybrid columns PHS-C18, PHS-2c, and a silica column, S-C18, as a function of purge time of 50 mM TEA solution: k' measured for phenanthrene.

Secondly, a recent and very popular approach is to coat a bis-silane on top of an ideal silica material, either fully porous or core-shell, thereby creating a protective layer (**Figure 6.24**). Akzo Nobel for example have developed Kromasil Eternity by modifying the surface of any Kromasil particle with $CH_3Si(OMe)_3$ or $CH_3CH_2Si(OMe)_3$, which is claimed to result in a merged hybrid top layer after a hydrothermal treatment [380]. Others have focussed on applying a coating of BTEE on existing silica particles either in aqueous media following an exchange process between pure silica and BTEE [381] or following a true grafting of BTEE in toluene [317] to obtain Poroshell HPH and Gemini Twin NX, and Kinetex EVO respectively. With these coating approaches, a perfect layer is required as failing to do so leaves the underlying silica susceptible for hydrolytic attack, which in turn can cause cavitation or the generation of macropores in the materials.

For all presented hybrid materials, modification of the organosilica surface is still performed before true application in RP-HPLC. The reason for this is assumed to be two-fold. Firstly, decorating the surface with hydrophobic groups and or end-capping, further increases the hydrothermal stability. Referring to the X-Bridge particles, such silanization pushes the base stability further from pH 10 to an alleged pH 12. This value is also given by the other manufacturers as the limit for their high pH stable packings.

Secondly, dangling C18 need to be present to obtain sufficient retention. Such groups are believed to show liquid like behaviour, leading to high differential partitioning (interaction) of the analytes, high retention and high separation power. Moieties fixed in the pore walls have a more solid

behavior, with correspondingly, a relatively low differential partitioning of the analytes, low retention and separation power (**Figure 6.27**).

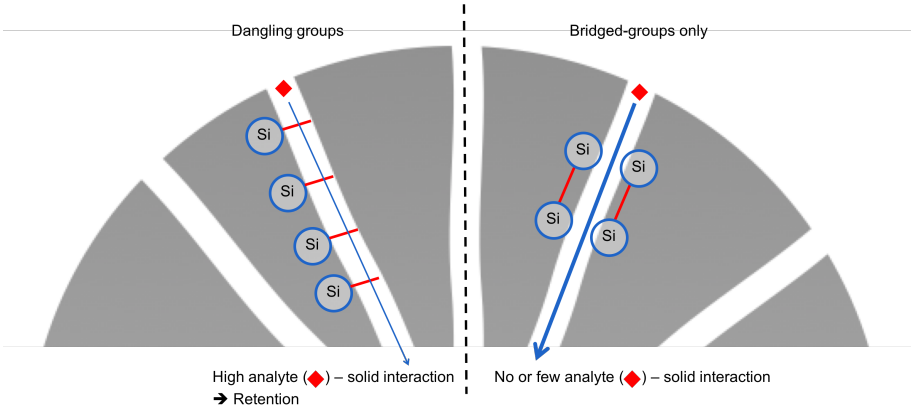

Figure 6.27: Comparison of an (organo)silica hybrid with functional groups protruding in the pore voids and a pure organosilica pore surface. The implication on the retention of analytes is illustrated.

As a consequence of the required grafting, this means that all the above efforts in spite, both as-synthesized organosilicas and bis-silane protected silicas only offer protection for harsh hydrolytic conditions at high pH. Once again, at low pH and high temperatures surface modifications are removed, which not only causes loss of retention but it also reduces the total stability of the packing [315, 317]. Therefore the above hybrid materials are close to being ideal but further improvements are still necessary to produce a 'universally' applicable chromatographic particle.

6.5 The ultimate chromatographic particle revisited: improvement of low pH stability

It is clear from the above that the last step that needs to be taken towards a completely hydrothermal and hydrolytically stable silica-based stationary phase is to get rid of functionalization of the surface through the silanol groups. Ideally, the attachment of functional groups should be irreversible in the chromatographic conditions applied. In essence, this would require replacement of the labile siloxanes with stable C-C or C-Heteroatom bonds. This is where more advanced bis-silane precursors bearing reactive groups such as AHETSCH come into play. An approach in which the retention inducing groups are irreversibly bound to the

surface is highly anticipated in industry, however few reports on this promising pathway exist.

In 2012, Yu et al. published on monodisperse 1,4-dimethoxybenzene bridged organosilica spheres having an S_{BET} of 509 m^2/g, a d_p of 63Å and a V_p of 0.8 cm^3/g [382]. This was achieved using dodecylamine and CTAB as surfactants in a water-ethanol mixture adding NH_3 as base catalyst (**Figure 6.28**). Pore expansion was performed in the presence of the initial surfactants with extra dodecylamine and N,N-dimethyldecylamine at 135°C for 24 h. Thereafter, the protective methoxy group was removed using BBr_3 leaving an hydroxyl group which was subsequently etherified using 1-bromodecane and NaH. Packed columns showed little to no loss of retention when treated with 6000 column volumes of a 1% TFA solution and 200mM TEA solution (pH 11 and 0.95 respectively) at 50°C. On the other hand, after modification of the particles with the C12 chain, the pore diameter drops to only 40Å. Furthermore, although spherical morphology is maintained after the drastic post-treatments, the etherification reaction only yields a relatively low surface coverage.

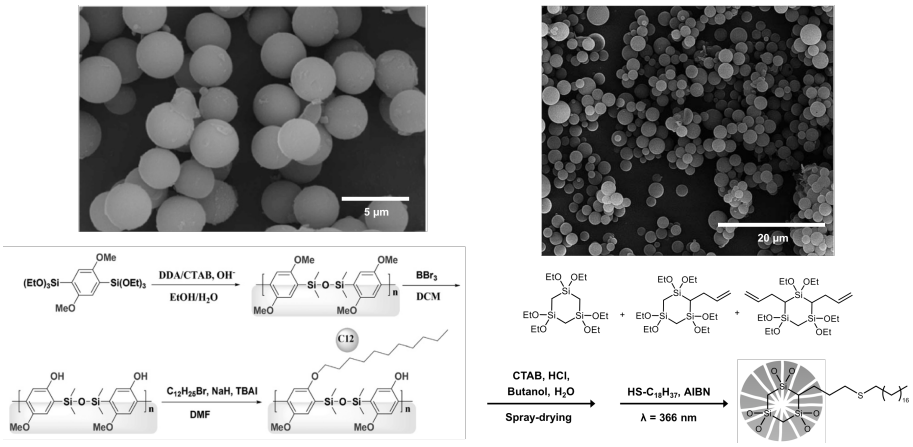

Figure 6.28: SEM image and synthetic approach of the 1,4-dimethoxybenzene bridged organosilica spheres following Yu et al. (left) [382] and allylated trisilacyclohexane spheres as described by Ide et al (right) [232].

The second example comes from our own research group as we developed spherical particles starting from a mixture of allylated HETSCH precursors through spray-drying [232]. Herein, inspired from other efforts of clicking on grafted spherical silica particles [383, 384] and co-condensed allyl-functionalized monoliths [257], the allyl group is modified by performing highly efficient thiol-ene click chemistry using octadecanethiol.

Recently, also an ethene monolith was disclosed which is modified with C18 chains for chromatography [385]. Using click-chemistry up to five times higher values are described as compared to the classical modification of Yu et al.

The results of our study showed exceptional hydrolytic stability in a pH swing experiment from pH 2 to pH 12, where separations could be performed at temperatures as high as 150°C. This not only demonstrates the framework stability of the interconnected $[Si(CH_2)]_3$-rings, it also proves the stability of the C-S bonds formed to attach retentive groups. Although spray-drying is an interesting method towards upscaling of the particle synthesis, it also comes with unsurmountable issues. The aerosol technique is not able to produce monodisperse particles, while it was also not possible to retrieve spheres with pores larger than 31Å. Moreover, the polydisperse particles with a mean size of 2 μm gave rise to extremely high back-pressure (943 bar at room temperature for 40/60 acetonitrile/water).

The practical issues in spite, the potential of AHETSCH in terms of stability and versatility is irrefutable. However, new methods need to be explored to obtain the ideal morphology and porosity.

6.6 Development of hydrolytically stable organosilica particles for HPLC

Employing the AHETSCH organosilica precursor, materials can be obtained that inherently have a high hydrolytic stability, combining unprecedented resistance against high pH and providing stability at elevated temperatures. Furthermore the incorporated allyl group grants the opportunity for stable and efficient click modification of the particle surface. Hereby, also modifications which are not easily anchored through classic chemistries (cfr. Yu paper) such as functional and chiral groups are easily accessible. The challenge remains, however, the synthesis of materials with all appropriate specifications, preferably tunable, in terms of morphology, porosity and mechanical stability to be suitable for HPLC (see Section 6.2.6).

When working with bridged organosilanes, some synthetical issues arise. First and foremost, bis-silanes are far less known and studied than classic silica precursors. Not only is the reactivity of bis-silanes more ill-described as compared to silica sources, the rate of hydrolysis and condensation varies between the organosilica precursors themselves. Optimization via trail-and-error is therefore not uncommon in organosilica

research. A second issue, as before mentioned, is that no bis-silane based dense nanoparticles or Stöber-like particles exist. As a result, at this point, coacervation and other synthesis approaches to retrieve HPLC-worthy particles are not accessible. Furthermore, calcination of as-synthesized particles to adapt or enhance their porosity and stability is not recommended, as this causes the loss of the all-important bridged functionality. As a final, and more practical issue, silica particles with all correct properties for HPLC are often marketed as packed columns provided with a bonded phase. This prevents such commercial silica particles to serve as a suitable base for bis-silane coating approaches. Although some fully porous silicas are at hand, core-shell particles are not available as bulk powders which rules out coating procedures to obtain bis-silane hybrid particles altogether.

In this work, methods are explored to obtain AHETSCH organosilica particles with the aim to be highly resemblant of current commercial materials while taking tunability, adaptability and ease of the synthesis into account. Monodisperse spherical particles of 3 to 5 μm are targeted to allow chromatographic evaluation with a common HPLC set-up, yet control of the particle size remains important for envisaged use of the same materials in UHPLC or PREP. The objective of pores exceeding 60Å is attempted using large non-ionic surfactants and pore swelling agents with 100Å pores deemed ideal.

In Chapter 7, an adapted Unger synthesis using Pluronic P123 to generate large pores is investigated to obtain fully porous AHETSCH spheres. Thereafter, in Chapter 8 a similar template-based approach is taken to generate allyl-ring type core-shell particles via layer-by-layer synthesis. Finally, a water-in-oil emulsion pathway, a novelty for organosilicas, is outlined in Chapter 9.

6.7 Industrial relevance and opportunities

The following sections summarize the industrial background of this work. Excerpts have been taken from the UGhent IOF application which has funded this work:

Since its inception in the late sixties, particle sizes in HPLC have been gradually decreasing with concomitant improvements in shape, surface area, inertness and pressure stability. The use of smaller particles allows a drastic increase the separation performance within shorter analysis time. Separations which used to be performed on workhorse 25 cm x 4.6 mm columns equipped with 5 µm particles generally take 20 -

30 min. Nowadays, such analysis can be performed by Ultra High-Performance Liquid Chromatography (UHPLC) in less than 10 minutes. This evolution, however, required the development of HPLC instrumentation allowing the utilization of $>$ 1000 bar pressure to percolate the mobile phase at the desired velocity through the column. Today?s instrumentation allows operation up to 1300 bar, yet further raising the pressure is technically challenging. The development cost of such systems might not be financially viable.

A commonly accepted solution is to reduce the viscosity of the mobile phase by increasing the temperature. High temperature HPLC offers benefits such as: (1) fundamentally faster analysis, (2) the use of longer (coupled) columns without the loss of analysis time, (3) an increased eluotropic strength of water due to the change of permittivity of water with temperature. As a result, decreasingly smaller percentages of organic modifiers are required. With an increase of the temperature up to 100-150°C, chromatographic analysis times can be reduced to seconds (almost instantaneous analysis times).

Current silica and organosilica-based columns are not stable enough for such high temperature usage due to hydrolysis of the stationary phase which in turn leads to particle degradation, column deterioration, loss of separation performance and detector fouling. Furthermore, current silica and organosilica-based columns are not stable enough for high pH applications. From pH 8 on most silica materials degrade. This is unfortunate as improved chromatography of most pharmaceutical compounds (of which 80% contain basic functions) is obtained when deprotonating them from pH 10 - 11 on and higher. Above this, current materials do not allow the use of stronger acids than 0.1% trifluoroacetic acid, especially in combination with elevated temperatures. The use of stronger volatile acids would lead to improved ion pairing of e.g. biomolecules and resulting in better separation and ionization in the MS.

The challenge to reduce analysis times by increasing the temperature of the mobile phase can only be addressed in a satisfactory way with genuinely more stable phases. More stability is also required to perform chromatography at extreme pH conditions. It should be noted that stationary phases, e.g. carbon and zirconia based, have been developed for high temperature chromatography. Unfortunately, these technologies do not provide the desired performance showing poor plate counts, irreversible adsorption of analytes, poor reproducibility, memory effects, etc., which greatly limits their use.

6.7.1 Target markets and technology impact

The liquid chromatography instrumentation market generated a revenue of 1.87 billion USD in 2011 and is estimated to further grow by 5.6% annually [386]. Together with spectroscopic identification, high performance liquid chromatography (HPLC) is the world's most employed analytical separation process (4 billion USD market; 100,000 scientific experts/buyers worldwide and 5 times more users). Liquid chromatography instruments are the 3rd most sold analytical item (after the precision balance and the pH-meter). Liquid chromatography is a critical technology for the pharmaceutical research, process and quality control in the chemical industry, environmental control, food safety, forensics and biological research (proteomics, metabolomics).

A few big houses such as Waters Corporation, Agilent Technologies, Shimadzu Scientific Company, Hitachi High Technologies Corp. and Thermo Fisher Scientific share the HPLC instrumentation market. The four largest industry players (Waters, Agilent, Shimadzu and Hitachi) hold nearly 60% of the total HPLC market share. Next to these companies, others such as Phenomenex and Advanced Materials Technology exclusively focus on column technology.

The column, which is the heart of the chromatographic setup, has a limited lifetime (maximum 2000-3000 injections except for heavy sample matrices; roughly 60% of users experience column life times of max. 12 months [263]). The columns sales value is estimated at 917 million USD in 2008 with 5.3% an annual growth rate over the period 2000-2010 [387]. Undoubtedly one of the major and most demanding segments is the pharmaceutical industry. Other demanding users are situated in the chemical and life science industry. Besides the analytical market, also the preparative HPLC market is to be considered as a possible target. Preparative liquid chromatography is impossible to perform under typical UHPLC conditions due to frictional heating. High temperature liquid chromatography on the other hand is possible on preparative scale, however the operating conditions thereby require stable stationary phases. Well-designed organosilica phases could offer a solution.

The market is driving technology towards faster analysis, reducing solvent usage, micro LC, improved resolution and sensitivity as well as improved overall productivity. With AHETSCH technology we aim at developing a hydrolytically and hydrothermally stable platform that can be further functionalized using click-chemistry. Current surface functionalization via silanol end-capping or grafting are not capable of withstanding the envisioned high operating temperatures as all currently

used strategies for functionalizing silica materials inherently involve the formation of temperature labile siloxane bonds. This is in sharp contrast to the stable covalent bond formed by click-chemistry.

6.7.2 Valorisation

The spray drying of AHETSCH particles in a Stöber-type synthesis showed auspicious properties of this technology [232], which resulted in UGhent seeking patent protection (WO2013/093022). At the time of writing, a US patent was granted, while negotiations towards a EP patent are still ongoing. Despite major interest from most column manufacturers, few action towards commercialization of the spray-dried particles was taken. We believe the particle's morphology (polydisperse particles of max. 2 μm) and porosity (max. pore size of 31Å) remains a major stumbling block to bring AHETSCH technology to the market. This work starts where the previous effort to synthesize an AHETSCH-based HPLC phase via spray-drying fell short. Three new synthesis pathways will be pursued to obtain particles with convincing properties.

Chapter 7

Fully porous particles via co-template co-solvent system

7.1 Research context: the co-template co-solvent system.

As already introduced, a synthesis employing two surfactants (co-template) in a water/EtOH mixture (co-solvent), resembling the Unger synthesis for porous silica beads [292, 329, 330], is an auspicious system to retrieve fully porous organosilica spheres (see Section 6.4). In such procedure, one surfactant is believed to generate the pores while the other stabilizes the formation of spheres during synthesis (**Figure 7.1**). Spherical morphology is further ensured by the addition of EtOH to slow down the hydrolysis and condensation rate.

A particularly appealing example is the method described by Rebbin et al. who use Pluronic P123 to generate relatively large 5.4 nm pores for benzene-bridged PMO spheres [375]. Moreover, as compared to similar approaches [372, 374, 388–390], the SEM images in this report suggest the as-synthesized particles suffer little from intergrown or fused particles, an issue which is often encountered for the co-template co-solvent method.

Based on AHETSCH, the above approach is investigated to synthesize spherical particles with a mono-allyl ring framework (sphmAR). To further expand the pore size up to a desired 100Å, the synthesis procedure is adapted using hydrophobic molecules as expanders for the non-ionic P123 template. Furthermore, a method to increase the pore size with a post-synthesis procedure is explored. In this chapter, however, only some

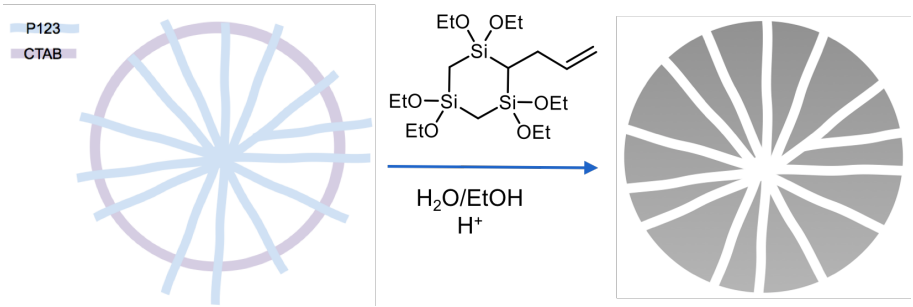

Figure 7.1: Graphical representation of the co-template co-solvent synthesis.

selected and illustrative experiments are listed which are indicative for the issues that arise when employing this synthesis method.

7.2 Experimental

Materials. Pluronic P123 (Mn = 5800, Sigma-Aldrich), Hexadecyltrimethylammoniumbromide (>98%, CTAB, Sigma-Aldrich), 1,3,5-trimethylbenzene (> 98%, TMB, Sigma-Aldrich), EtOH absolute (Fischer Scientific), HCl (37%, Carl Roth), NaOH (> 99%, Carl Roth).

Synthesis of fully porous mAR particles. For the standard procedure (sphmAR) the co-template co-solvent reaction mixture is prepared by weighing 0.226 g of P123 in a 50 ml flask together with 0.0367 g CTAB (**Figure 7.2**). Then, 6.45 ml H_2O, 1.88 ml EtOH and 0.37 ml HCl (37% solution) are added and the solution is stirred until the templates are completely dissolved. At this point, a certain amount of TMB is added as pore expander after which stirring is continued for 15 min. Thereafter, the flask is put in an oil bath set at 45°C and immediately, 0.5 g of AHETSCH is added at once. Stirring is subsequently performed at 1000 RPM for 30 min after which the cloudy mixture is transferred into a teflon-lined autoclave. The autoclave is then put in a preheated oven at 80°C for 5 h, after which the temperature is increased at a rate of 1°C/min to 130°C, which is kept for another 16 h. After cooling of the autoclave, the white precipitate is filtered and washed with 3 x 50 ml H_2O and 3 x 50 ml EtOH. To remove the templates, the particles are resuspended in 75 ml EtOH with 2.5 ml of 37% HCl and refluxed for 24 h. The porous particles are then obtained after filtration and washing with 3 x 25 ml H_2O, 3 x 25 ml EtOH and 3 x 25 ml acetone. To remove leftover solvent, the powder is dried under vacuum at 120°C for 16 h. Experimental details of some selected syntheses are listed in **Table 7.1**.

Table 7.1: Details of selected experiments in the co-template co-solvent approach for fully-porous sphmAR particles.

	V(TMB) [ml]	Co-solvent	V(Co-solvent) [ml]	CTAB [g]	HCl [ml]
sphmAR	0	EtOH	1.88	0.0367	0.37
sphmAR-PE1	0.134	EtOH	1.88	0.0367	0.37
sphmAR-HS	0.268	EtOH	1.88	0.0367	0.37
sphmAR-PE1a	0.134	EtOH	1.88	0.0367	0.185
sphmAR-PE2	0.134	EtOH	1.41	0.0367	0.37
sphmAR-PE3	0.134	EtOH	2.82	0.0367	0.37
sphmAR-PE4	0.134	MeOH	1.31	0.0367	0.37
sphmAR-PE5	0.134	EtOH	2.82	0.055	0.37

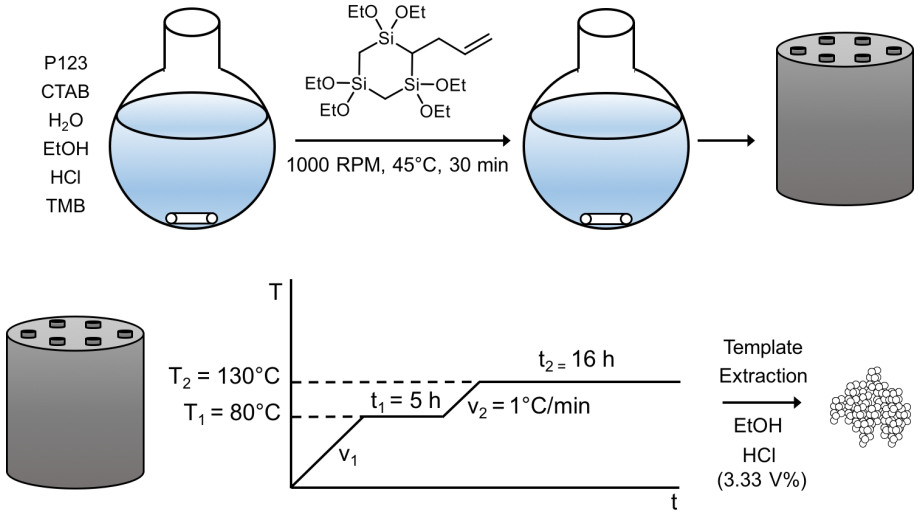

Figure 7.2: Graphical representation of the co-template co-solvent synthesis.

Procedure for post-synthetic pore expansion. 0.15 g of freshly synthesized sphmAR or sphmAR-PE particles are suspended in an aqueous NaOH-solution at pH 11, pH 12 or pH 13 in a Teflon-lined autoclave. Then, the autoclave is put in an oven at 120°C for 20 h after which, the treated particles are filtered, washed with 3 x 20 ml H_2O, 3 x 20 ml acetone and dried under vacuum for 16 h at 120°C. The samples are denoted depending on the pH of the NaOH solution used.

Characterization and analysis. A Micromeretics Tristar II is used for N_2 sorption experiments at 77 K. The specific surface area (S_{BET}) is determined via the Brunauer-Emmett-Teller theory and pore sizes (d_p) are calculated from the desorption branch following the Barrett-Joyner-Halenda theory. The mesopore volume (V_p) is obtained via the BJH theory on the adsorption isotherm, while the surface area of the micropores (S_μ) is deducted from t-plot calculations.

Diffuse Reflectance Infrared Fourier Transform Spectroscopy (DRIFTS) is performed using a Thermo Nicolett 6700 FT-IR spectrometer equipped with a Greasby-Specac diffuse reflectance cell, modified to measure samples at 20 - 300°C under vacuum.

Scanning electron microscopy (SEM) images are taken on a JEOL JSM 7600F FEG SEM and Transmission electron microscopy (TEM) images are taken on a JEOL JEM 2200-FS TEM.

X-ray powder diffractograms (XRPD) are recorded on a Thermo Scientific ARL X'TRA X-ray diffractometer using Cu Kα radiation of 40 kV and 30 mA.

7.3 Results and discussion

7.3.1 Synthesis of fully porous particles via co-template co-solvent system

To get straight to the point, by using the co-template and co-solvent procedure, we did not succeed in producing spherical particles. Moreover, it is also shown hard to obtain the desired porosity, as described in Section 6.2.6, exclusively by the particle synthesis. In what follows, examples that clarify the problems associated with this procedure are highlighted.

As witnessed from the N_2 sorption data in **Table 7.2** and the isotherms in **Figure 7.3**, the standard synthesis procedure to obtain sphmAR particles, without pore expanding agents, only yields 3.7 nm pores as determined from the desorption isotherm. The presence of small pores

can easily be rationalized by the presence of ethanol in the system. As compared to water which only dissolves the hydrophilic PEO blocks, EtOH dissolves both the PEO as well as the PPO blocks. As a result, addition of ethanol has a significant influence on the self-assembly behavior of the micelles. Here, this results in smaller micelles and thus pores [391, 392]. Therefore, despite using P123 as a large non-ionic surfactant it was not feasible to increase these values through other stoichiometries or synthesis temperatures. The particle morphology of sphmAR, on the other hand, can only be described as spheroid at best and contains a lot of aggregated and fused particles (**Figure 7.4**).

To effectively increase the pore size, TMB is added as a pore swelling agent in sphmAR-PE1. This gives rise to a type IV isotherm with H2 hysteresis, an isotherm associated with inkbottle type pores with large inner pores but with narrowed pore openings [393]. The appearance of H2 hysteresis can be ascribed to gradual phase transfer of P123 upon addition of TMB [47–50]. This is also deducted from the values in **Table 7.2**, where the adsorption $d_{p,BJH}$ indicates 7.0 nm pores with pore openings of maximally 3.9 nm determined from the desorption branch.[1] This result lies closer to the desired pore size, however, the presence of narrowed pores stays the limiting factor for mass transport of analytes in the pores. Upon addition of TMB, also the general size of the spheroid particles seems to decrease. One distinct XRD diffraction peak ([100]) is observed for sphmAR-PE1 (**A** in **Figure 7.11**), which indicates structural ordering of the pores. A very faint shoulder peak may be observed at $2\theta = 1.45$, yet deducting a pore structure from this would be over-interpretation. A similar diffractogram is found for non-expanded sphmAR.

Something particular happens when the amount of TMB is further increased to 0.268 g. As seen in the SEM images (**Figure 7.4**), 200 nm hollow nanospheres (sphmAR-HS) are formed due to complete phase transfer of the P123/CTAB system into large spherical micelles [51, 394, 395]. From SEM images, it seems that the HS material only consists of a very thin shell without structural stiffness, provided the large amount of dented spheres. The adsorption branch of the N_2 sorption furthermore indicates the presence of the inner macroporous voids, while the shell has pores of 4.0 nm. One can imagine such porous hollow materials to be

1. A steep desorption at $P/P_0 = 0.45$ is typical for the ink-bottle pores described by the Type IV H2 isotherm. At this value, capillary forces in small pores are suddenly broken, causing all N_2 contained in the pores to desorb at once. As a consequence, the narrowed pores causing this effect can only have a maximal size of 3.8 to 3.9 nm, but on average they are probably smaller.

Table 7.2: Summary of N_2 sorption experiments and particle size of sphmAR-materials.

	S_{BET} [m^2/g]	S_μ [m^2/g]	V_p [ml/g]	$d_{p,BJH}$[a] [nm]	$d_{p,BJH}$[b] [nm]	d_{part}[c] [μm]
sphmAR	806	244	0.41	ND[d]	3.7	4.0
sphmAR-PE1	783	262	0.69	7.0	3.9	3.6
sphmAR-HS	725	258	0.82[f]	-[e]	4.0	0.2
sphmAR-PE1a	635	137	0.61	8.2	4.0	4.3
sphmAR-PE2	708	231	0.68	8.5	4.0-5.2	0.9
sphmAR-PE3	801	286	0.72	7.9	4.0	2.9
sphmAR-PE4	581	162	0.50	8.3	6.0-4.0	ND[d]
sphmAR-PE5	798	283	0.53	6.9	3.9	3.9

[a]BJH pore size determined on the adsorption branch of the isotherm. [b]BJH pore size determined on the desorption branch of the isotherm, for type IV H2 isotherms, value indicates the maximal possible pore size. [c]All particles are spheroids, particle size is an estimation of the mean size as found in SEM images. [d]Not determined. [e]Adsorption isotherm typical for a macroporous void. [f] Total pore volume at $P/P_0 = 0.99$.

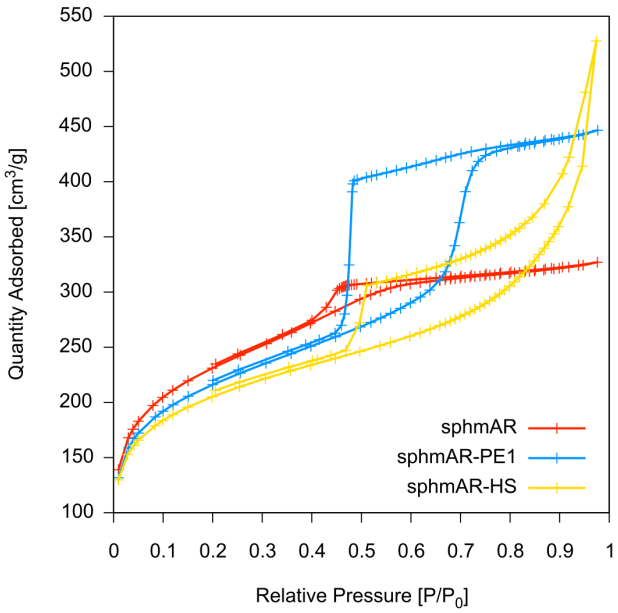

Figure 7.3: N_2 isotherms of sphmAR without addition of pore expander, with pore expander (TMB, sphmAR-PE1) and with excess pore expander leading to hollow nanospheres (sphmAR-HS)

applicable for example as nano-carriers for drug delivery, however, these are absolutely not practicable in HPLC.

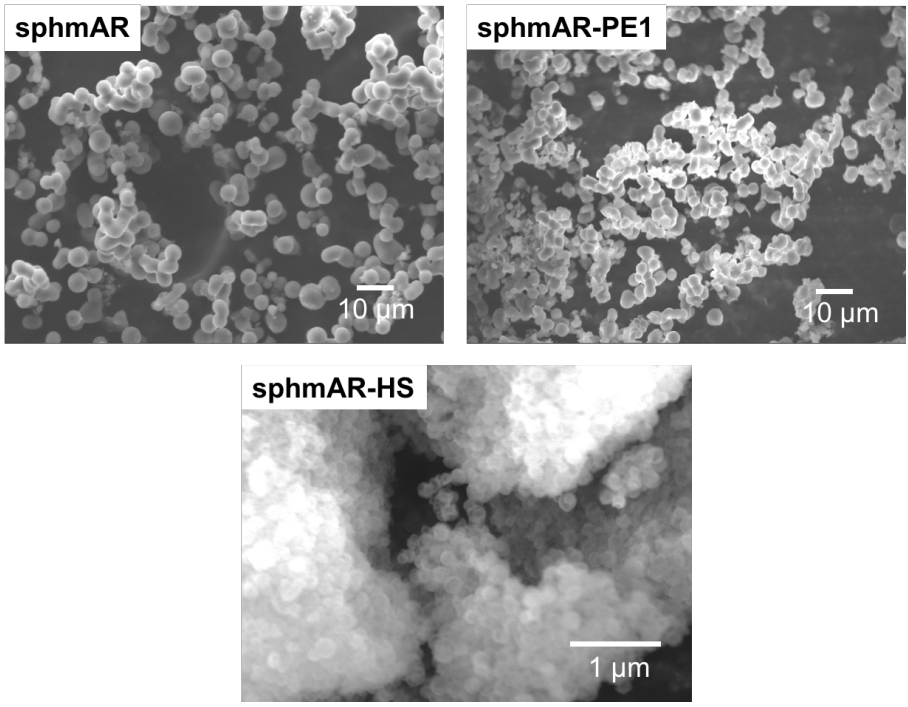

Figure 7.4: SEM images of sphmAR without addition of pore expander, with pore expander (TMB, sphmAR-PE1) and with excess pore expander leading to hollow nanospheres (sphmAR-HS).

Given the extensive influence of EtOH on the porosity, two samples are prepared using both a reduced and an increased amount of EtOH, sphmAR-PE2 and sphmAR-PE3 respectively. As expected, the desorption pore size of sphmAR-PE2 increases to 5.2 nm, however the isotherm suggests the presence of a bimodal pore system with a fraction of smaller pores centered around 4.0 nm (**Figure 7.5**). Increasing the amount of EtOH for sphmAR-PE3 does not have a significant effect on the porosity. Unfortunately, the decrease in EtOH further worsens the particle morphology of sphmAR-PE2 (**Figure 7.6**). Fewer spheroid shapes are seen in the SEM image and, with some imagination, more rod-like morphology, as expected for PMO synthesized in water, prevails.

The addition of ethanol as co-solvent decreases the rate of nucleation and growth of the mesostructured products which contributes to the formation of silica spheres [396]. As a result of the decreased reaction rate, growth becomes driven by global surface tension forces, minimizing

the surface free energy by forming the shape of a sphere [397]. During our investigations however, increasing the amount of EtOH only has a limited and certainly not a significant effect on the particle shape.

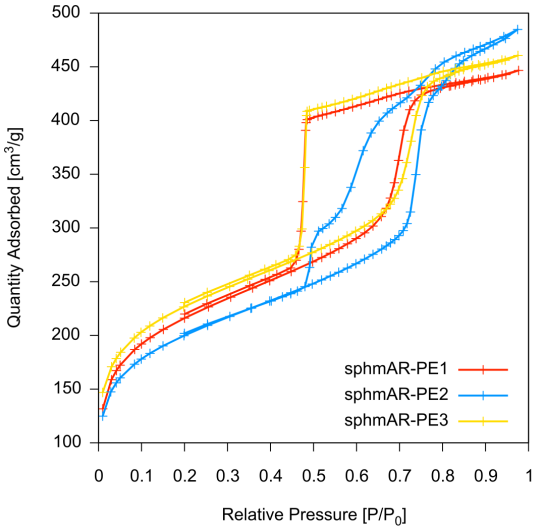

Figure 7.5: N_2 isotherms of sphmAR-PE1 and materials synthesized by the same procedure but with less (sphmAR-PE2) and more EtOH (sphmAR-PE3).

Another way to further slow down the sol-gel reaction and promote the formation of spheres, is to reduce the amount of catalyst. Therefore, the amount of HCl is halved in the synthesis of sphmAR-PE1a. This did not result in improved morphology, yet a clear increase in particle size to 4.3 μm is witnessed (**Figure 7.7**). A similar effect on the particle size has also been reported by Xia et al. who used NaOH as catalyst in the synthesis of ethene-bridged spheres [373]. Next to this, EtOH is replaced with MeOH in the synthesis of sphmAR-PE4. For this material, no spheroid particles are obtained but nanorods with uniform diameters and lenghts of around 1 μm. We assume that MeOH does not slow down the reaction as EtOH does (AHETSCH only has hydrolyzable ethoxy groups), but it must exercise some morphology control during the particle synthesis. It however lies beyond the scope of this work to further investigate this anomaly. In terms of porosity, the nanorods approximate porosities expected for PMOs, but they also show signs of a bimodal (6.0 and 4.0 nm) pore system or possibly plugged pores [393, 398], as witnessed by the Type IV H5 isotherm [399].

Morphology and porosity combined, an 'optimum' is found using increased EtOH combined with 0.055 g of CTAB and treating the as-

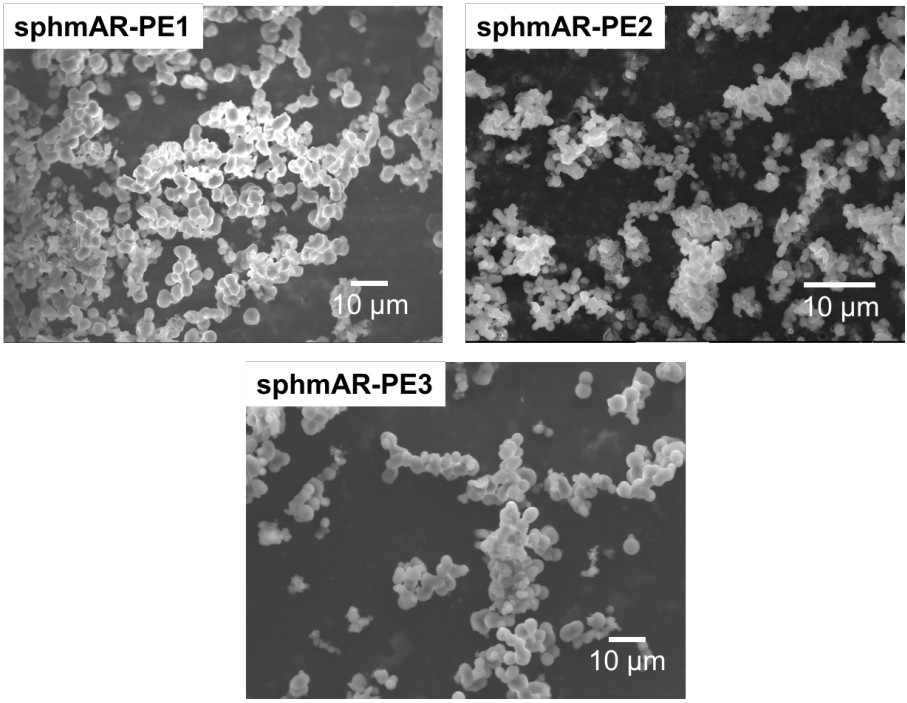

Figure 7.6: SEM images of sphmAR-PE1 and materials synthesized by the same procedure but with less (sphmAR-PE2) and more EtOH (sphmAR-PE3).

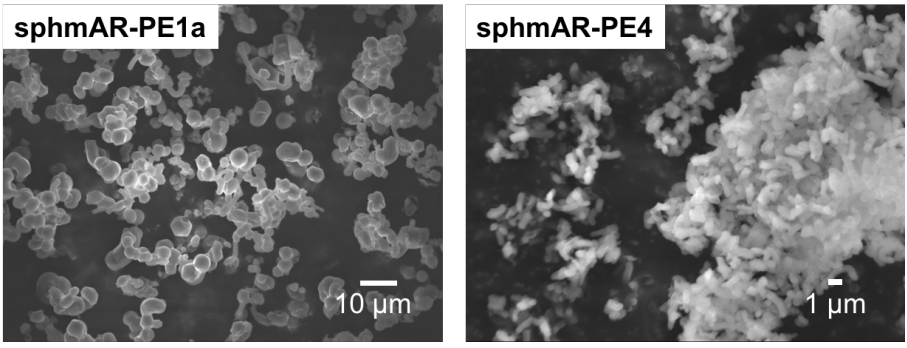

Figure 7.7: SEM images of sphmAR-PE1 but with half the amount of HCl catalyst (sphmAR-PE1a) and with MeOH instead of EtOH (sphmAR-PE4).

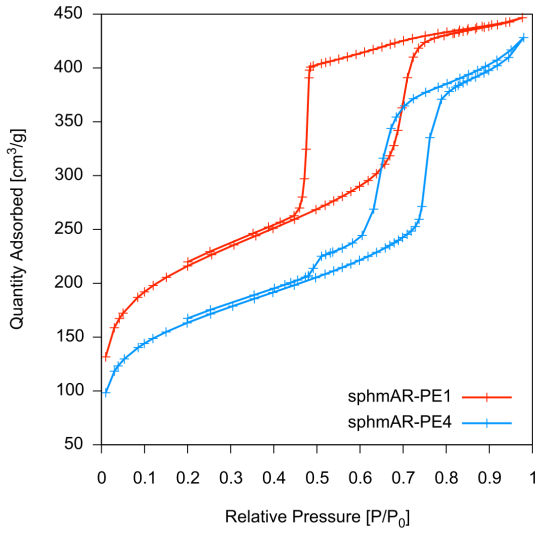

Figure 7.8: N_2 isotherms of sphmAR-PE1 and a material synthesized with MeOH instead of EtOH (sphmAR-PE4).

synthesized particles with a mechanical grinding step[2] to break up the aggregates. SphmAR-PE5 combines relatively spherical particles with pore sizes of 6.9 nm but with max. 3.9 nm openings via the adsorption and desorption isotherms, respectively (**Figure 7.9**). TEM shows the larger mesopores at the particle surface but a clear pore structure is unresolved. All together, sphmAR-PE5 is among the best we were able to produce using this procedure. However, many issues still remain such as a high microporous surface area ($S_\mu = 283\ m^2/g$) and high dispersion of the particle size, while particle morphology is still insufficiently spherical.

Various experiments, not disclosed here, further indicated the problems arisen above. Increasing the amount of EtOH yields slightly better but never close to perfect particles in terms of morphology, yet in the meantime the porosity is diminished. Vice versa, a low $EtOH/H_2O$ ratio gives rise to more attractive porosities but morphology control is lost completely. Next to this we found that the morphology also benefits from synthesizing particles at a fixed temperature of 60°C, however porosity again became far worse. Furthermore, we investigated the speed by which the precursor is added to the mixture, heating rates and the amount of CTAB[3], water and AHETSCH independently, but without

2. The particles are stirred at 1000 RPM in a flask with a magnetic stirring bar without solvent. This detaches agglomerated particles but also induces chipping of the particles.
3. If no CTAB is used during the synthesis, irregular particles are retrieved. This

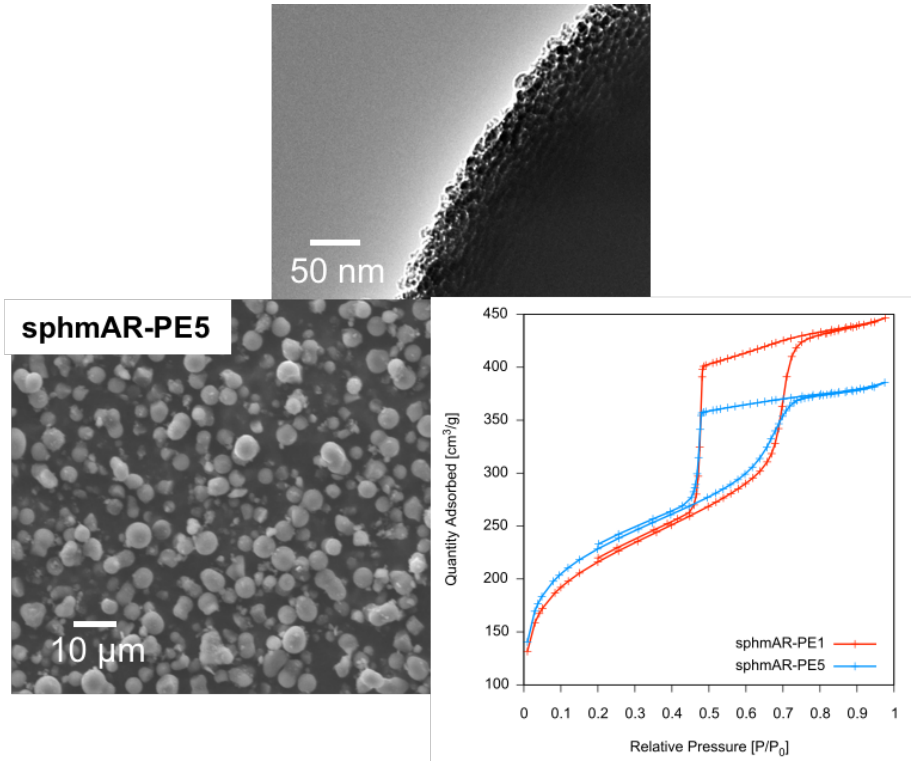

Figure 7.9: TEM images of the surface porosity of sphmAR-PE5, together with a SEM image of the optimized PE5-material and its N_2 sorption isotherm.

any improvement. Different surfactants (F127, Triton X100 and SDS), other catalysts (HNO_3, NaOH and F^-) and pore expanders (pentane) did not even yield spheroid particles.

7.3.2 Development of a pore-expanding post-treatment.

Where the particle morphology of as-synthesized sphmAR is fixed, the inadequate porosity can be enhanced by means of a second reaction step. As described in Section 6.2.3, post-modification methods are known to expand the pore size of organosilica-based materials and reduce the microporosity. To do so, the materials are often subjected to hydrolytic stress by employing an aqueous solution of an inorganic or organic base at elevated temperatures. From Part II, it is recognized that AHETSCH-based organosilicas are exceptionally stable under these conditions. Therefore, far hasher conditions are required to expand the pores.

N_2 sorption data are taken from a new batch of sphmAR which is treated at 120°C for 20 h in a NaOH solution at pH 11, pH 12 and pH 13, respectively (**Table 7.3**). Treated at pH 11, there is no significant indication of a change in porosity, except for a slight drop in S_{BET}. Starting from pH 12, however, a decrease of S_μ is witnessed and treated at pH 13, all micropores are seemingly eliminated. Furthermore, the pore size of sphmAR-pH13 has increased from 3.7 nm to 6.2 nm. At this point it is believed that partial dissolving of sphmAR occurs, thus etching out the pores, while some material is redeposited on the more curved and thermodynamically more unstable surface of the micropores [19]. This assumption is supported by an observed loss of approx. 25 w% after the pore-expansion treatment. Examining the N_2 isotherms of sphmAR-pH13 in **Figure 7.10**, a fairly broad pore size distribution is found. This might indicate a non-uniform etching process or even a restructuring of the pores into a system more similar to an organosilica xerogel.

The expansion procedure applied on TMB pore expanded sphmAR-PE1 results in a completely analogous observation, with closed micropores and mesopores that are expanded up to 8.1 nm (**Table 7.3** and **Figure 7.11**). Comparing XRD diffractograms before (A) and after treatment (B), the main [100] diffraction peak has not disappeared, indicating the preservation of pore ordering. Therefore, the hypothesis of pore restructuring is not true, thus non-uniform etching of the pores must be the reason for the broadening of the pore size distribution. Finally, the

confirms the stabilizing role of CTAB during sphere formation.

Table 7.3: Summary of N_2 sorption experiments after pore expansion treatment.

	S_{BET} [m^2/g]	S_μ [m^2/g]	$V_p{}^a$ [ml/g]	$d_{p,BJH}{}^b$ [nm]
sphmAR	827	240	0.53	3.7
sphmAR-pH11	734	234	0.46	3.7
sphmAR-pH12	635	108	0.46	3.7
sphmAR-pH13	363	0[c]	0.71	6.2
sphmAR-PE1	783	262	0.69	3.9
sphmAR-PE1-pH13	448	0[c]	1.03	8.1

[a] Total pore volume at $P/P_0 = 0.99$. [b]BJH pore size determined on the desorption branch of the isotherm, in case of type IV H2 isotherms, value indicates the maximal pore size. [c]Negative micropore volume obtained via t-plot method

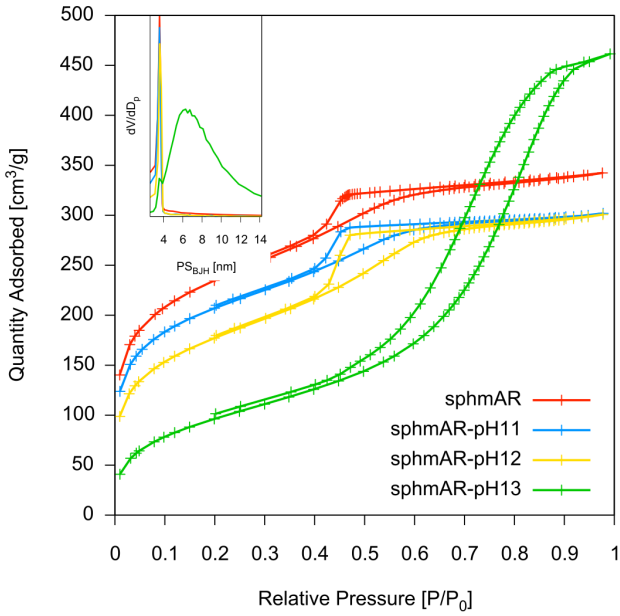

Figure 7.10: N_2 sorption isotherms of sphmAR after pore expansion treatments.

secondary diffraction peak slightly shifts to lower values for 2θ. If this secondary peak may be ascribed to the small pore openings of sphmAR-PE1, this shift confirms the pore expansion.

A more in depth investigation of this post-treatment and an extensive reasoning for these observations will be given in Section 9.6.

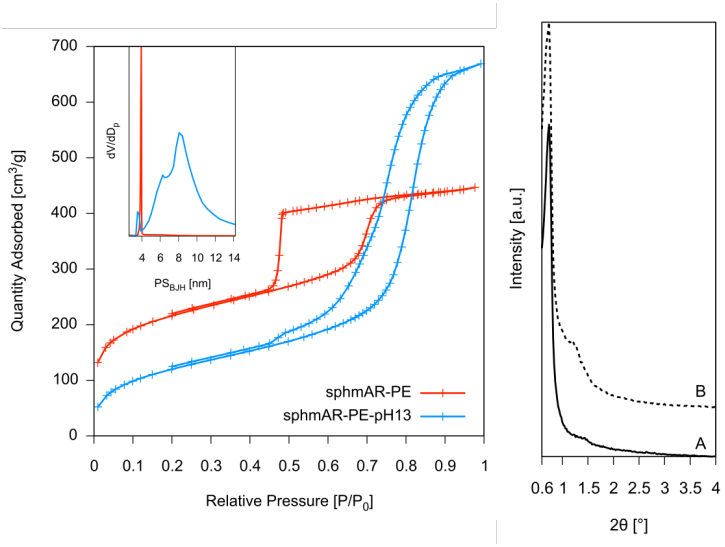

Figure 7.11: N_2 sorption isotherms and XRD diffractograms of sphmAR-PE1 before (A) and after (B) the pore expansion treatment at pH 13.

7.4 Conclusions

Employing a co-template co-solvent system, the synthesis of fully porous AHETSCH spheres is attempted, but, despite a plethora of experiments, we were not able to obtain particles that satisfy the stringent properties we have set out. Regarding porosity, as-synthesized materials, even after pore expansion using TMB, contain small pores which connect larger mesoporous voids. Provided that mass transport of molecules is determined by the diffusion through these bottlenecks, such pore architecture is believed not practicable for HPLC. However, some promising results are found in a hydrolytic post-treatment. Hereby it is possible to widen the mesopores up to 8.1 nm, but we believe a longer or harsher treatment will allow further pore expansion. The post-treatment even has a double positive effect on the porosity as next to increasing the mesopore size, it also eliminates microporosity.

Nonetheless, for all presented materials, particle morphology is troublesome. Although we have some control on the particle shape (CTAB and EtOH) and size (HCl), the system is more intricate than expected. Especially EtOH was found to play crucial role as it counteracts improved porosity with a worsened morphology and vice versa. Therefore, no optimum between the two is found and no sphmAR materials with

sufficient morphology for HPLC are found. Although we have screened some common pore-generating surfactants without retrieving a decent porosity, it is still possible that some specific template can give rise to large pores in the H_2O/EtOH system. This would, however, require an extensive screening, as from literature, we are not aware of such surfactant.

The fusing of spheroid particles we observe, was often witnessed in literature before, however there is no clear understanding nor consent of this occurrence. Presumably, a perfect balance needs to be found between all aspects of the synthesis such as micelle stabilization and dispersion, reaction rates, precursor surfactant interaction ($S^+C^-P^+$), etc. [335]. Furthermore, it seems that for BTEE based (ethane-bridge) materials less issues are witnessed, while more for complex precursors optimal reaction conditions are hardly found [371, 374, 376–378, 388–390]. This might indicate that the chemical nature of the precursor also influences the morphology.

Seen the type of the work it would require to arrive at optimal conditions, if these exist at all, we decided not to pursue further investigation of this pathway towards an allyl-ring chromatographic packing. Instead, two other methods with improved morphology control are preferred and described in the following chapters.

Chapter 8

Porous organosilica shell - Solid silica core particles

8.1 Research context: core-shell organosilica particles

To improve morphological control of mAR particles, a similar approach, using surfactants as pore generating templates, is employed to synthesize a porous organosilica shell around solid, monodisperse and spherical SiO_2 cores (**Figure 8.1**). As described in the introductory chapter, such core-shell architectures with superficial porosity have gained increased interest in the last decade as these enhance separation performance with lower back-pressure as compared to fully porous particles [285, 286].

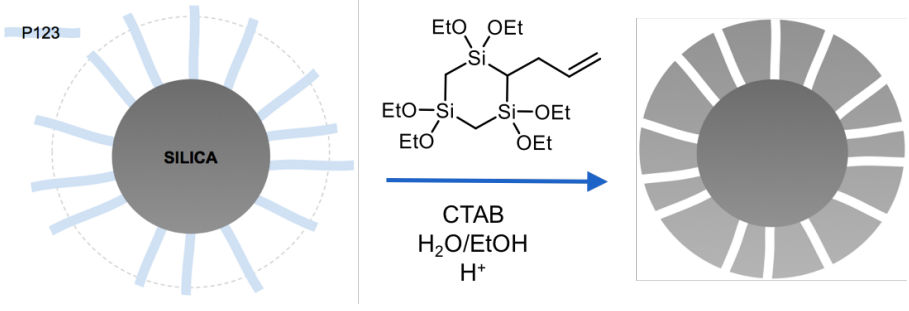

Figure 8.1: Graphical representation of the synthesis of organosilica shell - silica core particles.

Inspired from reports on silica-silica core-shell particles [360, 361, 400] and a core-shell particle having a porous benzene-bridged organosilica

shell [379], here a method is developed with AHETSCH as the precursor for a porous shell. We aspire the use of a larger silica core as compared to the 200-500 nm Stöber silica particles applied in these reports to permit application in chromatography. Such large dense silica particles are commercially available in several sizes as highly monodisperse spherical particles, presumably prepared by a two-step Stöber process (**Figure 8.2**) [362] or by thorough calcination of a porous silica particle. If an mAR layer can be exclusively grown on top of these silica spheres in a controlled way, the beneficial morphology of the cores is transferred to the hybrid core-shell particles.

To allow a reasonable loading of analyte, the porous shell should have a sufficient thickness. Commercial core-shell particles for HPLC possess a shell to core ratio of approximately 20% in diameter. Therefore, if a 2.3 μm core is used, the shell thickness should approach 250 to 300 nm, while the cited reports, only describe a shell thickness of 30 to a maximum of 75 nm per synthesis. Hence we will adopt a layer-by-layer (LbL) synthesis approach, in which multiple shell layers are subsequently deposited, to obtain the desired thickness and porosity. The development of the pore expanding, micropore reducing post-treatment in mind, initial focus lies on the synthesis of core-shell particles with decent morphology. Afterwards, we will attempt further fine-tuning of the porosity.

8.2 Experimental

Materials. Pluronic P123 (Mn = 5800, Sigma-Aldrich), Hexadecyltrimethylammoniumbromide (>98%, CTAB, Sigma-Aldrich), 1,3,5-trimethylbenzene (> 98%, TMB, Sigma-Aldrich), EtOH absolute (Fischer Scientific), HCl (37%, Carl Roth), NaOH (> 99%, Carl Roth), SOLAD PNPP3.0NAR-10 solid SiO_2 (Glantreo Ltd.).

Synthesis of porous organosilica shell - solid silica core particles (CSmAR). Prior to the growth of a porous mAR shell, 3 g of solid, spherical SiO_2 particles (SOLAD) are treated for 1 h in 50 ml of a 2M HNO_3 solution to make sure Si-OH groups are exposed on the SiO_2 surface. In an optimized synthesis, 0.2753 g of P123 is weighed in a 25 ml flask and 13.45 ml of a 2:1 H_2O:EtOH mixture containing 0.0055 g of CTAB and 0.495 ml 37% HCl are added. The contents of the flask are stirred at room temperature until complete dissolution of the P123. At this point, optionally TMB is added as a pore expander. Now, 0.3795 g of HNO_3 treated SOLAD is added after which stirring is continued for 15 min, followed by 15 min of sonication to ensure complete dispersion

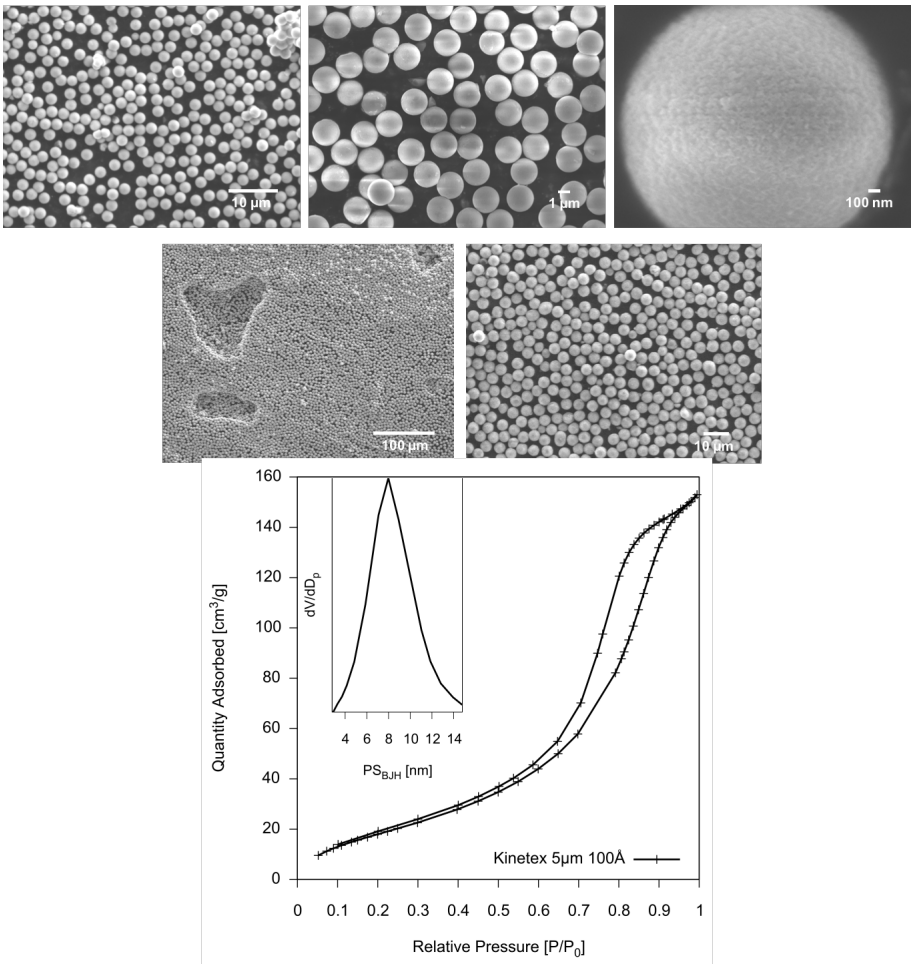

Figure 8.2: SEM images of solid SiO_2 particles used as core in this Chapter (top). Images of a commercial core-shell material, Kinetex 5-100 with C18 modification (middle). N_2 sorption isotherm of the commercial core-shell as guideline for the desired porosity.

of the SiO_2 cores. Subsequently, while stirring at 600 RPM, 0.158 g of AHETSCH is added at once, after which the flask is closed with a glass stopper and put in an oil bath at 60°C. Stirring is continued for 22 h. Thereafter, the solids are filtered and washed with 5 x 20 ml of H_2O and 5 x 20 ml acetone. We found that an explicit template removal step is not required.[1] Finally, the obtained CSmAR particles are dried under vacuum for 16 h at 120°C.

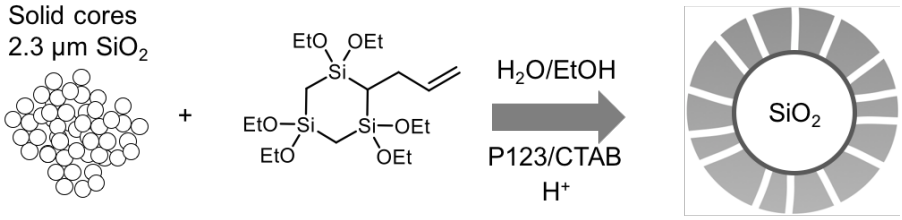

Figure 8.3: Procedure for the synthesis of organosilica shell - silica core particles.

Procedure for pore expansion and micropore reduction. 0.15 g of as-synthesized CSmAR particles are suspended in an aqueous NaOH-solution at pH 13 in a Teflon-lined autoclave. Then, the autoclave is put in an oven at 120°C for 20 h, after which the treated particles are filtered, washed with 3 x 20 ml H_2O, 3 x 20 ml acetone and dried under vacuum for 16 h at 120°C.

Characterization and analysis. A Micromeretics Tristar II is used for N_2 sorption experiments at 77 K. The specific surface area (S_{BET}) is determined via the Brunauer-Emmett-Teller theory and pore sizes (d_p) are calculated from the desorption branch following the Barrett-Joyner-Halenda theory. The total pore volume (V_p) is obtained at $P/P_0 = 0.99$, while the surface area of the micropores (S_μ) is deducted from t-plot calculations. Diffuse Reflectance Infrared Fourier Transform Spectroscopy (DRIFTS) is performed using a Thermo Nicolett 6700 FT-IR spectrometer equipped with a Greasby-Specac diffuse reflectance cell, modified to measure samples at 20 - 300°C under vacuum. Scanning electron microscopy (SEM) images are taken on a JEOL JSM 7600F FEG SEM. Focussed Ion Beam SEM was performed using a FEI Nova 600 Nanolab Dual Beam FIB-SEM.

1. No difference is observed between N_2 sorption isotherms and DRIFT spectra of a washed sample and the same sample subjected to template extraction with HCl in EtOH (reflux). Presumably, for the thin shell layer grown, the templates are efficiently removed during the washing step.

8.3 Results and discussion

8.3.1 Synthesis of porous mAR shell - solid silica core particles (CSmAR).

The solid SiO_2 cores, SOLAD PNPP3.0NAR-10, were purchased as calcined silica particles. Therefore, to ensure good attachment of the mAR-shell and enhance the reproducibility of the shell growth, the SOLAD spheres are treated with a 2M HNO_3 solution, exposing the surface Si-OH groups. SEM images before and after treatment show exactly the same monodisperse 2.3 μm particles with a distinct surface roughness, while the specific surface area (S_{BET}) is 4 m^2/g (**Figure 8.2**).[2]

After application of one mAR layer (CSmAR1-1) the difference in particle topology witnessed in the SEM images, indicate that a very thin shell of mAR is grown. No traces of possible homocondensation of AHETSCH into irregular or small spherical particles is found, which implies a 'nucleated' growth of the shell on top of the SOLAD spheres. Although no fusing of particles is observed, the organosilica shell is not perfect, as roughened patches or holes are clearly distinguished, which are indicative for the bare surface of the underlying SOLAD cores (**Figure 8.4**).

Successive layer-by-layer growth of the mAR shell is proceeded through slight adaptation of the synthesis conditions as a stepwise increase of the reaction volume was found beneficial [361] (**Table 8.1**). The SEM image of CSmAR1-5, after 5 growth rounds, shows particles free from the coating defects described above as a result of the sequential coating. On the other hand, some irregularities and fused particles are seen. Verification that truly an mAR shell is grown is found in the DRIFT spectrum of CSmAR1-5 showing the superimposed allyl-group vibrations at 3080, 1640 and 890 cm^{-1} (olefin C-H stretch, C=C stretch and olefin C-H out of plane deformation), albeit with highly reduced intensity (**Figure 8.5**).

Per growth cycle, an increase of approximately 10 m^2/g in S_{BET} is observed, which indicates the deposition of porous layers (**Table 8.1**). A corresponding increase of S_μ, however, means the micropore surface remains high at around 50% of the S_{BET}. Based on the 200 nm thick broken shells witnessed for CSmAR particles having an S_{BET} of 78 m^2/g (**Figure 8.4**, vide infra) a relation between shell thickness and porosity

2. These values slightly differ from the data provided by the manufacturer (d_{part} = 3.0 μm and $S_{BET} < 1$ m^2/g).

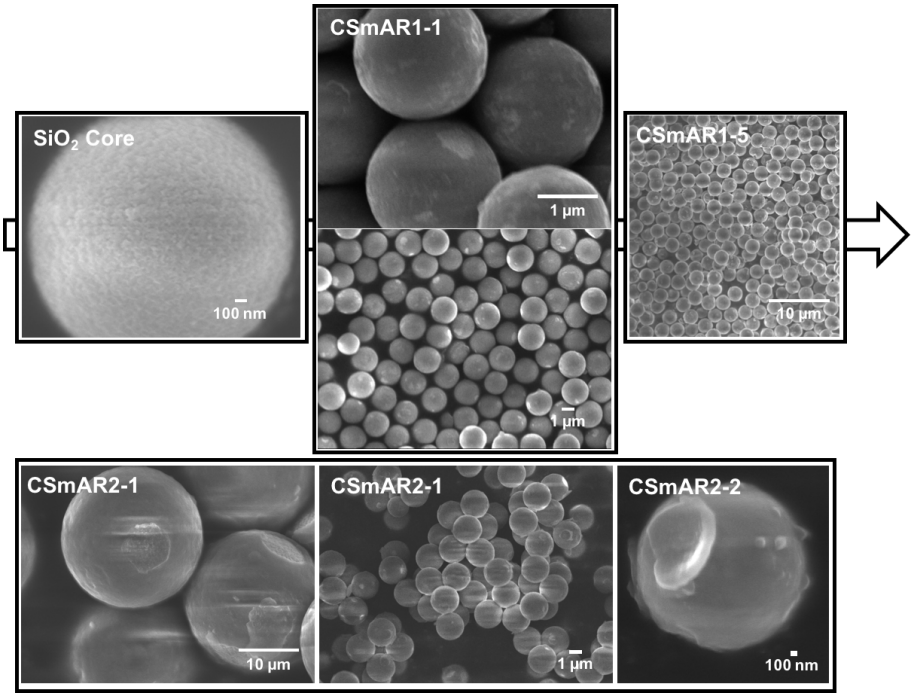

Figure 8.4: SEM images of the intial SOLAD SiO_2 core, after 1 growth cycle (CSmAR1-1) and after 5 cycles (CSmAR1-5). SOLAD coated with an alternative procedure employing a reduced reaction volume after one growth round (CSmAR2-1) and two growth rounds (CSmAR2-2), shows pronounced particle fusing. A broken shell indicates a shell thickness of 200 nm for a particle having an S_{BET} of 78 m^2/g.

Table 8.1: Layer-by-layer growth of the mAR shell: Experimental details and N_2 sorption data.

	$V(H_2O/EtOH)$ [ml]	m(CTAB) [g]	m(P123) [g]	V(37% HCl) [ml]	m(AHTESCH) [g]	S_{BET} [m^2/g]	S_μ [m^2/g]
CSmAR1-1	13.45	0.0055	0.2753	0.495	0.158	14	8
CSmAR1-2	13.87	0.0055	0.285	0.509	0.158	25	12
CSmAR1-3	14.28	0.0055	0.294	0.523	0.158	35	17
CSmAR1-4	14.70	0.0055	0.303	0.537	0.158	42	22
CSmAR1-5	15.11	0.0055	0.312	0.551	0.171	51	29

Initially 0.3795 g of SOLAD is taken, reaction temperature and time are kept constant for every growth cycle (60°C, 22 h). No pore expander is used.

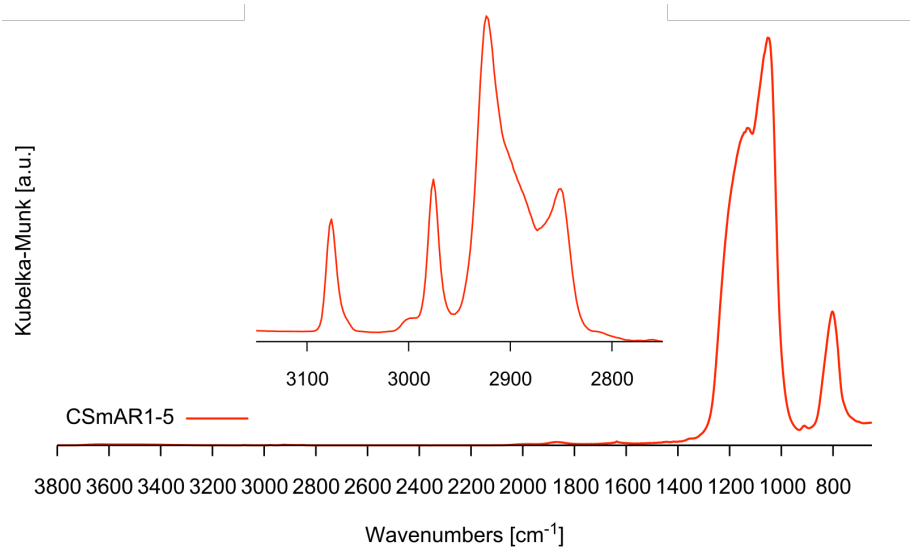

Figure 8.5: DRIFT spectrum of CSmAR1-5 after 5 growth cycles. Only the most intense characteristic vibrations (3080 cm^{-1}, 890 cm^{-1}) of the allyl-functionality of the shell are visible and are superimposed on the spectrum of the silica core.

can be estimated. For CSmAR1, it would take around 10 growth rounds to retrieve particles with a 250 nm shell, relative to an S_{BET} of 100 m^2/g and thus a shell to core diameter ratio of 20%. We deem this assessment of the shell thickness more practical than based on the SEM images, where the size increment per layer (est. 25 nm / growth round) is hardly distinguishable from the small deviation in particle size of SOLAD.

The isotherms of CSmAR1 are provided in (**Figure 8.6**). After one growth round, a Type IV H2 isotherm, similar to the isotherms for pore-expanded fully porous sphAR particles in chapter 7, is found, albeit with a significantly lower amount of nitrogen adsorbed per gram due to the presence of the solid SiO_2 core. Based on the BJH theory, 9.8 nm pores are found from the adsorption branch of the isotherm. Pore size analysis on the desorption branch indicates that these large pores are interconnected via narrow 3.9 nm openings.

Isotherms with a comparable hysteresis are found after 4 and 5 growth cycles. Herein, the size of the capillary condensation step, indicative for the mesopore volume, strikingly remains the same whereas only the Langmuir part of the isotherm is raised in between the growth cycles (no offset was applied for depiction of the isotherms). This suggests that only the micropore volume increases. Supposedly, the removal of

the templates in between the shell growth round, may cause that the mesopores generated in the previous step are filled or covered in the consecutive growth cycle. Adapted procedures to improve the mesoporosity during synthesis are discussed further.

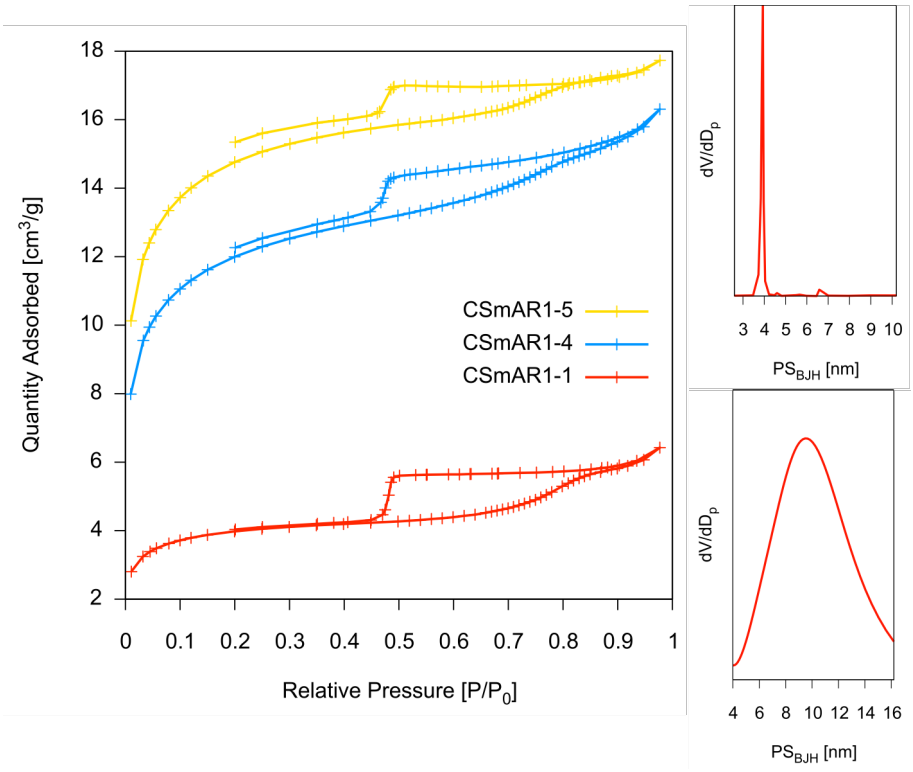

Figure 8.6: N_2 sorption isotherms of CSmAR1 after one, four and five growth rounds. No offset was applied for depiction of the isotherms. Pore size distribution of CSmAR1-1 determined from the desorption (top right) and adsorption isotherm (bottom right).

From the above results it is appreciated that CSmAR1 holds promise for application in chromatography, especially in terms of particle morphology. However, the procedure is not efficient as an estimated 10 growth cycles are required to obtain particles with the envisaged porosity. Not only is this time-consuming, each growth cycle also consumes 0.158 g of AHETSCH. Bluntly, this implies that after 10 cycles four times more precursor is used as compared to the mass of SOLAD particles to obtain only an increase of 44% in total particle volume for a hypothetical CSmAR1-10 particle. Provided this does not account for the generated pore volume, it is conceivable that the majority of precursor is lost during synthesis. Furthermore, possibilities may exist to enhance the porosity of

the as-synthesized particles, reducing the reliance on the pore expansion post-treatment.

In an attempt to improve the efficiency of the CSmAR synthesis, i.e. a thicker shell layer per cycle and/or improved porosity, adaptations to the initial procedure are applied (**Table 8.2**). As a first screened parameter, the reduction of the total reaction volume to 5 ml instead of 13.45 ml has an immediate effect provided S_{BET} increases to 45 m^2/g and 78 m^2/g after subsequent growth cycles (CSmAR2, isotherm in **Figure 8.10**). This corresponds to an estimated shell thickness of 100 and 200 nm respectively. In (**Figure 8.4**), again the coating defects are visible after one growth round (CSmAR2-1), while these disappear after the second. However, it is also clear from the SEM images that an increase in SOLAD concentration, or growth of a thicker shell, induces aggregation and fusing of the particles as the shells seem to intergrow. Although the particles themselves remain visually spherical, the formed aggregates are irregular and are thus likely to cause column packing issues. Furthermore, it seems the intergrown shells are subject to fracture.

SEM images of the other adaptations (**Figure 8.7**) show that omitting CTAB (CSmAR3) also provokes particle fusing, which in turn suggests CTAB stabilizes a colloidal suspension of SOLAD. Unfortunately, an increase in CTAB does not prevent the conjoining of the CSmAR particle when thicker layers (100 nm/cycle) are grown. Identical conclusions can be drawn from the addition of more HCl catalyst (CSmAR8) and the application of a step at higher temperature (CSmAR5). The latter method however enables the growth of a thick shell providing the particle with an S_{BET} of 79 m^2/g in one growth round (**Figure 8.10**).

From Chapter 7 it is known that both EtOH and pore expanders have a major influence on the porosity, but also on the morphology. This is also illustrated here as upon addition of TMB as pore sweller (CSmAR4) no longer a layer covering the SOLAD particle is observed. Instead roughened patches of mAR are witnessed from the SEM images. For completeness an N_2 sorption isotherm of a pore expanded sample is found in (**Figure 8.11**), showing that the pore size expansion only affects the size of the mesopores and not the connecting pore openings. On the other hand, if EtOH is absent from the reaction mixture (CSmAR6), shell growth becomes uncontrolled due to an increased hydrolysis and condensation rate of AHETSCH. Hence, large agglomerations of particles with irregular covering are found.

Finally, when the reaction volume is increased to improve the spatial

Table 8.2: Conditions and N_2 sorption data for adapted CSmAR syntheses.

	V(H_2O/EtOH) [ml]	m(CTAB) [g]	m(P123) [g]	V(37% HCl) [ml]	m(TMB) [g]	T [°C]	S_{BET} [m^2/g]	S_μ [m^2/g]
CSmAR2[a]	5.0	0.0055	0.1074	0.185	0	60	45	14
CSmAR2-2[a]	5.0	0.0055	0.1074	0.185	0	60	78	42
CSmAR3	13.45	0	0.2753	0.495	0	60	15	11
CSmAR4	13.45	0.0055	0.2753	0.495	0.195	60	13	9
CSmAR5[b]	13.45	0.0055	0.2753	0.495	0	60-90	79	26
CSmAR6	13.45[c]	0.0055	0.2753	0.495	0	60	ND[d]	ND[d]
CSmAR7	20.0	0.0055	0.4094	1.088	0	60	-[e]	-[e]
CSmAR8	13.45	0.0055	0.2753	0.725	0	60	31	18
CSmAR9	20.0	0.0055	0.4094	1.088	0	75	29	14

For all syntheses 0.3795 g SOLAD is used, reaction time = 22 h. [a]0.115 g of AHTESCH is added, all other syntheses employ 0.158 g AHETSCH. [b]3 h in the reaction the temperature was raised to a 90°aging step [c]No ethanol [d]Not determined [e]S_{BET} and S_μ identical to SOLAD.

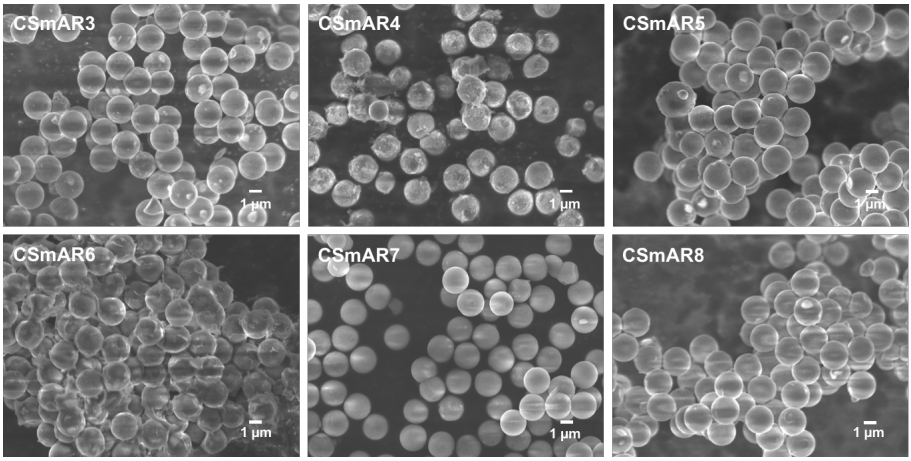

Figure 8.7: SEM images of CSmAR materials retrieved from the parameter screening study.

separation of SOLAD particles, no mAR shell is grown at 60°C. However, if the temperature is raised to 75°C to promote AHETSCH condensation (cfr. CSmAR5), independent core-shell particles are found (CSmAR9, **Figure 8.8**) with an S_{BET} of 29 m^2/g ($\sim$ 70 nm shell). After upscaling, this new procedure yielded particles with a specific surface area of 69 m^2/g after three growth cycles (**Table 8.3**). After these growth rounds, however, moderate particle fusing is observed and again it is appreciated from the N_2 isotherms that only the volume of the micropores increases after subsequent coating cycles.

Next to the pore expanding post-treatment (see Section 8.3.2), two other ideas to increase the mesopore volume of the core-shell particles are explored. In the hypothesis stated earlier, it was assumed that the existing mesopores are filled in the following growth round. Now, the exact same procedure to obtain CSmAR9-3 was investigated, without a washing step after filtration of the solids, in order not to remove the surfactants that are still present in the mesopores. In theory, this should restrict new precursor from condensing inside the mesopores [401]. To remove the templates after three growth cycles, the core-shell particles are subjected to a 24 h extraction step in 75 ml EtOH with 2.5 ml of 37% HCl under reflux conditions. Surprisingly, no difference is observed in the micropore/mesopore volume between CSmAR9-3 with intermediate removal of the surfactant and with surfactants left in place (CSmART-3, **Figure 8.12**).[3] Finally a one pot synthesis is executed in which after

3. Only for the latter, a doubling of the surface area is witnessed (S_{BET} = 126 m^2/g

Table 8.3: Upscaled synthesis of CSmAR9 and N_2 sorption data.

	$V(H_2O/EtOH)$ [ml]	m(CTAB) [g]	m(P123) [g]	V(37% HCl) [ml]	m(AHTESCH) [g]	S_{BET} [m^2/g]	S_μ [m^2/g]
CSmAR9-1	80.0	0.022	1.638	4.35	0.632	14	5
CSmAR9-2	82.5	0.022	1.692	4.47	0.632	39	15
CSmAR9-3	85.0	0.022	1.744	4.63	0.632	69	32

Initially 1.518 g of SOLAD is taken, reaction temperature and time are kept constant for every growth cycle (75°C, 22 h). No pore expander is used.

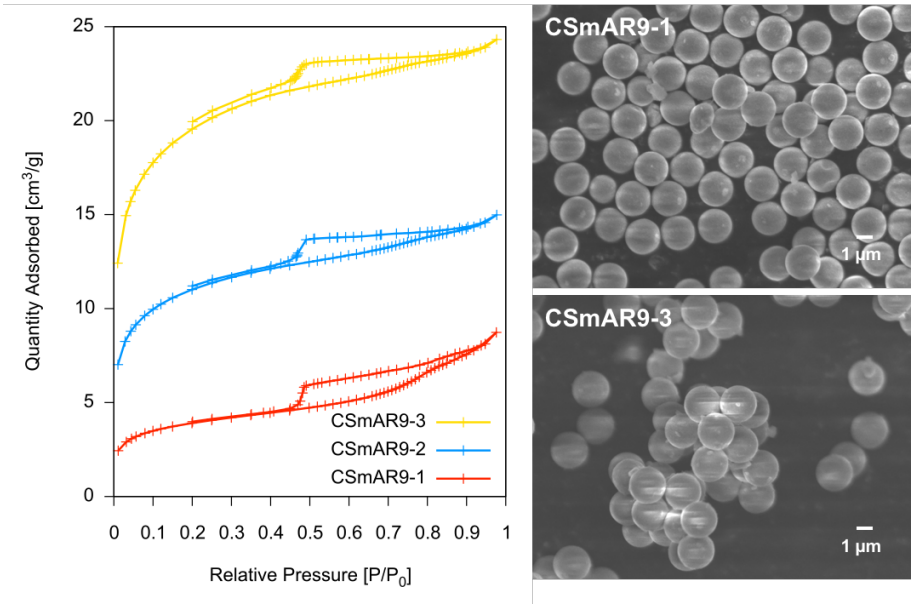

Figure 8.8: N_2 isotherms of CSmAR9 particle after upscaling and successive growth cycles (left). SEM images of the same particles after the first and third growth cycle, CSmAR9-1 and CSmAR9-3 respectively.

22 h and 44 h of reaction an extra 0.632 g of precursor is added to the initial reaction system (CSmAROP-3). After work-up of the sample, again, no significant increase in mesoporosity is noticed.[4] Because of these unexpected results, the hypothesis of pore filling is ruled out. The exact process happening is still tentative at this moment, as it can only be assumed that precursor molecules are deposited inside the mesopores through diffusion into the template containing pores. All together, it is once again clear that control of the porosity, while taking into account the particle morphology, is a demanding question to be solved.

8.3.2 Pore expansion and micropore reduction: Creation of yolk-shell particles.

Since we were not successful in obtaining a decent porosity for as-synthesized particles, the pore expansion and micropore reduction post-treatment, introduced in Chapter 7, is applied on the mAR shell - SiO_2 core materials. To probe the compatibility of the treatment with CSmAR

and $S_\mu = 55$ m^2/g).

4. Although again the total surface area has increased to 172 m^2/g with an $S_\mu = 93$ m^2/g.

particles, CSmAR5, having a sufficiently thick shell ($\sim$ 200 nm), is selected for an initial investigation. Based on the N_2 sorption isotherms before and after treatment at 120°C with a pH 13 NaOH solution, no pore size expansion nor elimination of the micropores is observed (**Figure 8.9**). Instead, a sharp increase in adsorbed N_2 at high P/P_0 values is an indication for the presence of macropores within the treated material.

This is confirmed by FIB-SEM images depicting the cross-section of an CSmAR particle after hydrolytic treatment. Clearly, in between the organosilica shell and SiO_2 core, macroporous voids are seen. Despite the relatively thick organosilica shell, the SiO_2 core has remained unprotected from hydrolytic attack, causing the core to selectively dissolve through the pores of the organosilica shell. On the other hand, it might also be noticed that the mAR shell is extremely stable as it remains unchanged after this harsh treatment.

As a control experiment, CSmAR1-5, obtained after deposition of 5 shell layers with an estimated combined thickness of 125 nm, is also subjected to the post-treatment. Afterwards, again indications of macroporosity are found. Not only does this show the lability of the silica core, this also confirms that the LbL-shell remains porous throughout and that core deterioration can take place through micropores.

Similar issues are encountered for commercialized organosilica based phases in which a bis-silane is applied on top of an ideal silica particle to create a protective layer using coating procedures. Herein, the smallest of coating defect, even within the inner regions of the particle, leaves the underlying silica exposed for hydrolysis during both post-treatments and chromatographic analyses. During column stability tests, gradually the silica is etched away forming cavitations underneath the organosilica layer which are detrimental for separation efficiency [402].

As a consequence, our pore expansion and micropore reduction procedure cannot be implemented as long as the core is made up from pure silica. Moreover, this now implies that the stability of the CSmAR particles, in all, is determined by the stability of the SiO_2 core. Thus, CSmAR materials no longer meet our stringent standards.

8.4 Conclusion

In this chapter it is proven that porous mAR shell - SiO_2 core particles benefit from the uniform morphology of the core material. Employing a rather time-consuming LbL approach, it is possible to grow 20 - 25

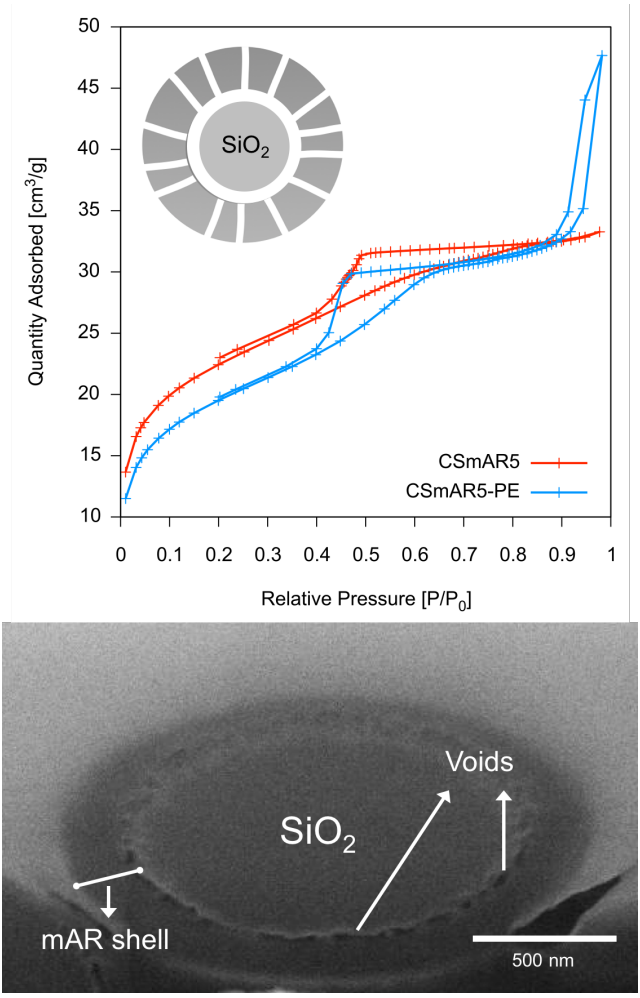

Figure 8.9: N_2 sorption isotherms of CSmAR5 before and after a hydrolytic pore expansion treatment. The generation of macropores is indicated by the N_2 adsorption at high P/P_0. FIB-SEM cross-section of a core-shell particle after the above treatment showing the macroporous voids between the silica core and the organosilica shell.

nm porous shell layers per cycle. However, if the process is accelerated, growing a thicker shell per step, problems concerning particle agglomeration and fusing arise, which is likely to cause column packing issues. Nonetheless a compromise was found between precursor and time efficiency, and clustering. In further attempts to reduce the clustering of CSmAR particles, NH_3 was used as catalyst, however no visible difference is observed.

Although the CSmAR particles show promise, at first glance, in terms of morphology, the porosity of the shell has remained troublesome. A pore structure with mesopores interconnected by small max. 3.9 nm openings is persistent, while adaptations that should be beneficial for the porosity, i.e. addition of pore expanders or reducing the amount of EtOH, have a detrimental impact on the particle morphology. Moreover, for undefinable reasons, the mesoporosity of the core-shell material seems not to increase during subsequent LbL application of the shell nor by means of a one pot synthesis. We believe, simultaneous control of porosity and morphology is troublesome due to the required presence of EtOH. A solution for the issues arising may lie in using surfactants with a lower solubility in the H_2O/EtOH solvent mixture than P123.

The porosity issues cannot be resolved with the pore expansion - micropore reduction procedure as the surface of the SiO_2 core remains exposed to hydrolytic attack. This gives rise to selective etching of the silica core and the formation of macroporous voids. Consequently, the stability of the CSmAR particles is not a function of the mAR shell, but of the silica core, which, in turn, also suggests that these materials are liable to hydrolytic stress in chromatographic conditions.

This selective removal of a silica core from a porous organosilica shell has been witnessed before [379] and has even been exploited to obtain hollow organosilica nanoparticles [403]. Although not commercially viable, this procedure can open up a different pathway towards fully porous organosilica particles. Based on a procedure to synthesize spherical mesoporous carbons [404], an inverse opal silica structure can potentially be employed as exocast for the synthesis of monodiperse PMO spheres.

It is now clear that for maximal stability, core-shell particles should consist of a core material that is at least as stable in hydrolytic conditions as the organosilica shell. Ideally, a solid mAR or HETSCH-based core should be developed as this would have a similar stability as the porous mAR shell, while it is certainly compatible with LbL growth. However, to the best of our knowledge, no Stöber procedures are known to synthesize

solid and pure[5] organosilicas, especially not given the particle size that would be required.

Next to this, we did attempt to apply a non-porous HETSCH layer on the SOLAD SiO_2 particles using several reaction conditions. Difficulties in the analysis of the very thin layers grown hampered the development of a decent procedure. Moreover, SOLAD particles we deemed completely coated, were still affected by the hydrolytic post-treatment after application of a sufficiently thick mAR shell.

In summary, we did not successfully retrieve core-shell type particles that measure up to the envisaged properties, with the instability of the SiO_2 cores and the simultaneous control of porosity and morphology (controlled layer growth) as main issues. In what follows, a water in oil emulsion is investigated to effectively decouple the control over the particle morphology and porosity in the synthesis of fully porous 100% organosilica spheres.

8.5 Appendix

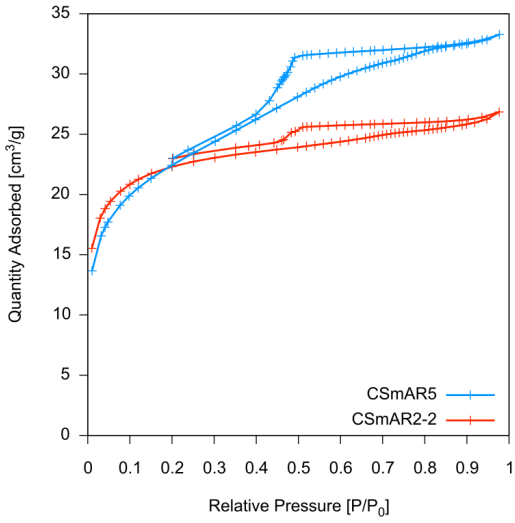

Figure 8.10: N_2 sorption isotherms of CSmAR2-2 after application of two shell layers in a synthesis with a reduced reaction volume and CSmAR5, obtained with a hydrothermal aging step (90°C) during synthesis.

5. We are aware of the manufacturing of a 50/50 TEOS/BTEE solid particle, yet the process is a business secret.

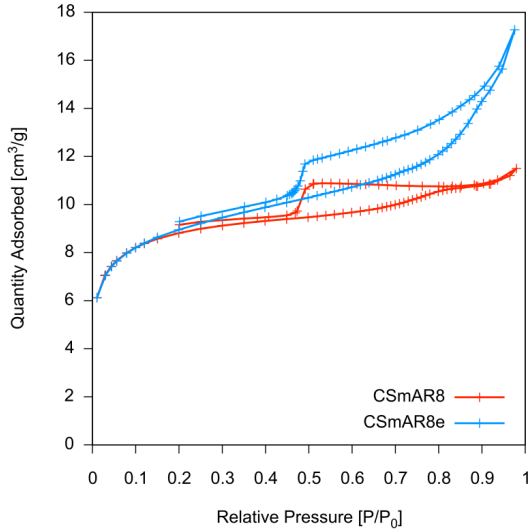

Figure 8.11: N_2 sorption isotherms of CSmAR8 and particles obtained through the same synthesis procedure but with an additional 0.195 ml TMB to expand the mesopores.

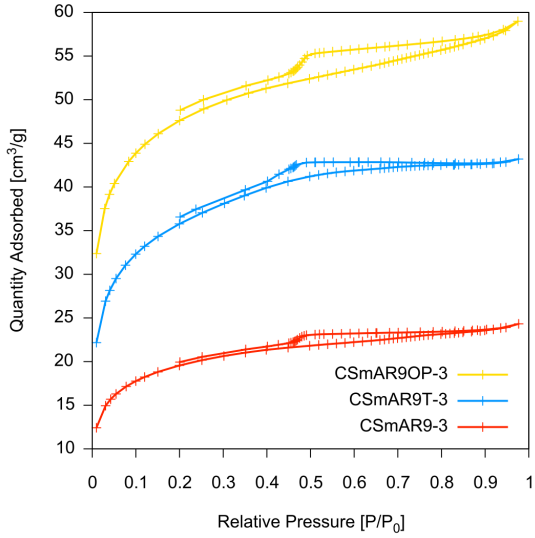

Figure 8.12: N_2 sorption isotherms of CSmAR9-3 with surfactant extracted between all shell growth cycles, of CSmAR9T-3 with minimal template removal between the steps and CSmAROP-3 prepared via a one-pot synthesis.

Chapter 9

A water-in-oil emulsion method providing robust and tunable microdroplets in the synthesis of spherical organosilica gel particles

9.1 Introduction on emulsion-based methods in materials science [405]

An emulsion is a two-phase system or colloid consisting of two (or more) immiscible liquids. Depending on the nature of the dispersed and continuous phase, two types of emulsions can be differentiated. If oil droplets are dispersed in an aqueous continuous phase, the system is deemed an oil-in-water (O/W) emulsion, whereas water droplets in an oil phase are referred to as a water-in-oil (W/O) emulsion. Double emulsions such as water-in-oil-in-water (W/O/W) and oil-in-water-in-oil (O/W/O) are also known.

Emulsions are also classified based on the size of the emulsion droplets with macro-, nano- (or mini-), and microemulsions, having droplet sizes of above 400 nm, 100 nm to 400 nm and below 100 nm respectively. Typically, emulsions are formed by the application of comminution i.e. a shear force, within the mixture by means of stirring. Nanoemulsions can also be prepared using high ultrasound power, while microemulsions on the other hand form spontaneously upon mixing of the emulsion components

as the formed microemulsion is thermodynamically stable. Emulsions are subject to light scattering at the multiple phase interphases. As a result, the droplet size determines the appearance of the emulsion with macroemulsions being white, while nano- and microemulsions are typically bluish translucent and transparent, respectively.

In order to stabilize a formed macroemulsion, i.e. protect from flocculation, creaming, sedimentation, coalescence and Ostwald ripening (**Figure 9.1**), emulsifiers, typically surfactants[1] which reduce the interfacial tension between the phases, are added. This increases the kinetic stability of the emulsion system so that the size of the droplets does not change significantly over time, while the emulsifiers also inhibit a too close approach of droplets through the formation of a mechanical, steric, and/or electrical barrier.

Also, the size of the disperse droplets is directly linked to the interfacial tension between the water and oil phases. A decrease in the interfacial tension leads to a corresponding decrease in the size of the droplets. Thus, next to the amount of shear applied to form the emulsion, the droplet size is also controlled by the emulsion parameters, namely the nature of the surfactant and solvent used, the water to surfactant ratio and the presence of a co-surfactant [406]. Furthermore, it is the emulsifier that determines which is the disperse and which is the continuous phase of an emulsion, as the Bancroft rule states: "The phase in which an emulsifier is more soluble constitutes the continuous phase." This is somewhat counter-intuitive as not only the relative percentages of oil or water determine whether a W/O or O/W emulsion is generated, but also which phase the emulsifier is more soluble in.

Immediately following the Bancroft rule, the hydrophilic-lipophilic balance (HLB) theory is commonly applied to design or describe new or existing emulsion systems. The HLB system assigns a number to the ingredient or combination of ingredients of the emulsion and links this with emulsifiers or blends of emulsifiers having the same number. These arbitrary numbers are an estimation of the hydrophilicity or lipophilicity of the emulsifiers and have been found through extensive experimental work. Lipophilic emulsifiers are assigned a low HLB number and hydrophilic ones are assigned a high HLB number. Therefore, as a rule of thumb, emulsifiers with a HLB number between 4 and 6 are typically employed for W/O emulsion while O/W emulsifiers have a HLB number between 8 and 18. These numbers, however, are a mere guideline to speed

1. Pickering emulsions are an exception as for such colloidal systems, solid particles like silica nanoparticles, stabilize the emulsion as they adsorb onto the interface between the two liquids.

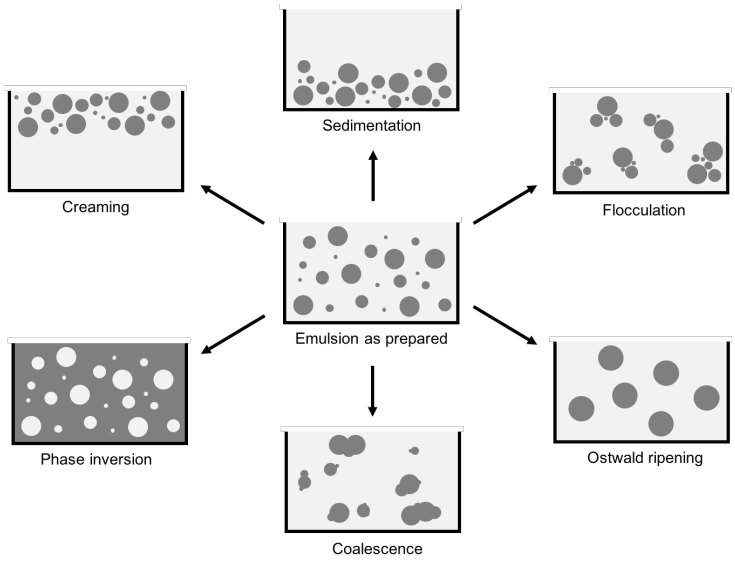

Figure 9.1: Representation of processes that may occur in an instable emulsion.

up the process of finding a good emulsion, yet in many cases, a range of HLB numbers around the theoretical one should be tested together with a screening of emulsifiers or blends with different chemical structure.[2] More insight in the HLB system and a table with HLB values can be found, for example, in the following reference [407].

In day-to-day life, emulsions are encountered in food products such as milk, mayonnaise, vinaigrette and butter. Furthermore, emulsions are also used for creams and lotions in pharmaceutics, hairstyling, personal hygiene, and cosmetics. More technically, emulsions are applied in polymer science for so-called emulsion polymerizations but they have also been used for the synthesis of metal oxides, be it as morphology controlling environment (droplets) or as macroporous template (vide infra). In materials science, control of the droplet size is of paramount importance, while for household applications generally the stability of the emulsion is more critical.

2. Emulsifiers often have a lipophilic and a hydrophilic 'version'. Illustrative examples are SPAN80 (sorbitan monooleate) and TWEEN80 (Polyethylene glycol sorbitan monooleate) which have a HLB of 4.3 and 15.0 respectively. By mixing these with various w%, all intermediate HLB values can be obtained. Other chemical families exist for these type of emulsifiers e.g. -laurate (20) or -stearate (60).

9.2 Probing the possibilities: The versatility of the W/O approach

In the synthesis approaches discussed in Chapters 7 and 8 organosilica materials are synthesized in conditions where morphology and porosity are simultaneously determined by one or multiple surfactants, with the consequence that independent control of morphology and porosity is difficult. This has lead to fused particles, limited control on the particle size and especially a reduced pore size.

Now, as described for pure silica-based predecessors, it is possible to decouple the particle morphology from the material synthesis by employing spray-drying [232] or emulsion technology [299, 406, 408, 409], both essentially providing a reactor-droplet where the sol-gel process can take place. In both approaches, the final particle adapts the size and shape of the droplet whereas porosity is generally determined by the conditions inside the droplet. From the two, emulsion technology is shown especially versatile in the synthesis of porous materials as type (W/O or O/W), composition and choice of emulsifier can be varied to obtain different particle architectures, whereas the technique for preparing the emulsion, e.g. mechanical stirring, shear rupturing [410, 411], microchannel [412] or membrane emulsification [409, 413], dictates the mean size and size dispersity of the particles.

For instance, fully porous SiO_2, ZrO_2 and TiO_2 microspheres are described through gelation inside W/O emulsions generated by mechanical stirring in the presence of a suitable emulsifier (SPAN-, TWEEN-, Brij-type or cellulose ether derivatives), and are applied as chromatographic packings [270, 299, 408, 414]. In similar reaction conditions, the monodispersity of the resulting particles is known to greatly improve by membrane emulsification [409, 415].

A second architecture, hollow SiO_2 spheres with a porous shell, are obtained using sorbitan-monooleate instead of the aforementioned emulsifiers, or by dissolving poly-ethylene glycol (PEG) in the aqueous droplets [416, 417]. Herein, formation of the hollow structures is explained by hampered diffusion of the hydrolysed silica precursor inside the water droplet. Finally, by employing O/W/O double emulsions, researchers were even able to develop macroporous silica spheres, with the inner oil droplets in the water phase acting as porogen, in a process referred to as emulsion templating.[3] [419, 420]

3. In emulsion templating, the dispersed emulsion droplets act as porogen for the material that is condensed in the continuous phase [43, 418]. Basically, this is the

Despite the advantageous properties of organosilicas, reports on emulsion-based PMOs or organosilica materials are limited to a hollow ethylene-bridged particle prepared in a H_2O/n-decane emulsion with CTAB as emulsifier [421].

Here, we will investigate the possibilities of using an W/O emulsion for the synthesis of organosilica particles that are practicable in HPLC or PREP. Of course, given the potential of AHETSCH as a precursor our final goal is to develop allyl-functionalized $[Si(CH_2)]_3$-ring particles with distinct spherical morphology. However, given the novelty of this approach in organosilica research, we will use HETSCH as a surrogate or probe molecule for AHETSCH.

The first aim of this work is to control the particle size and dispersion through adaptation of the droplet size. Thereafter we will obtain fundamental insights in the organosilica gel formation using an optimized emulsion system. Hereby, we intend to thoroughly control the final pore size of the particles in the full mesopore range (2 - 50 nm), as many packed columns are typically provided in a range of various pore sizes. To do so, we will focus on straightforward variations of the reaction formulation but without influencing the perfect spherical morphology of the particles. Then, other bis-silanes will be used in the synthesis to show the versatility of the newly developed method, which is followed by investigation of hydrothermal and hydrolytic post-treatments to further fine-tune the porosity. Finally, AHETSCH-based particles obtained with this W/O emulsion approach are evaluated as HPLC packing with focus on their exceptional stability.

9.3 Parameter study of the W/O emulsion method

9.3.1 Experimental

Materials. The following chemicals are used as received: Hexadecyltrimethylammoniumbromide (>98%, CTAB), Methyl 2-hydroxyethyl cellulose (Tylose MH300), Polyethylene glycol (20) sorbitan monooleate (TWEEN 80), Sorbitan monooleate (SPAN 80), 1-octadecanethiol ($C_{18}SH$, 98%) and 2,2-Dimethoxy-2-phenylacetophenone (DMPA, 99%) from Sigma-Aldrich; Sodiumdodecylsulphate (SDS) from TCI; Benzylalcohol (> 99%), NaOH (> 99%) and HCl (37%) from Carl Roth; Bis(triethoxysilyl)ethane (97%, BTEE), bis(triethoxysilyl)benzene (95%, BTEB) and 1,1,3,3,5,5-

phase inversed process of what will be attempted in this chapter.

hexaethoxy-1,3,5-trisilacyclohexane (95%, HETSCH) from ABCR; NH_3 (25% in H_2O) from Fisher Scientific.

General synthesis of spherical $[Si(CH_2)]_3$-interconnected ring organosilica gel (R). In a typical synthesis, 0.1 g of Tylose MH300 is weighed off and added to a 50 ml glass flask with a 25 mm long, 6 mm diameter Teflon-lined stirring bar. Hereto, 28 ml of benzylalcohol is added. Using a Pasteur pipette, a certain amount of a 8 w% HCl solution is weighed off in the flask. Then, extra H_2O is added until the aqueous phase reaches 8.23 ml. Now, the flask is closed with a glass stopper and is placed in an oil bath at 60°C and magnetic stirring is applied at a rate varying from 1000 to 1500 RPM for 30 min (for details, see Section 9.3.3). Almost immediately a white emulsion is formed (**Figure 9.2**).

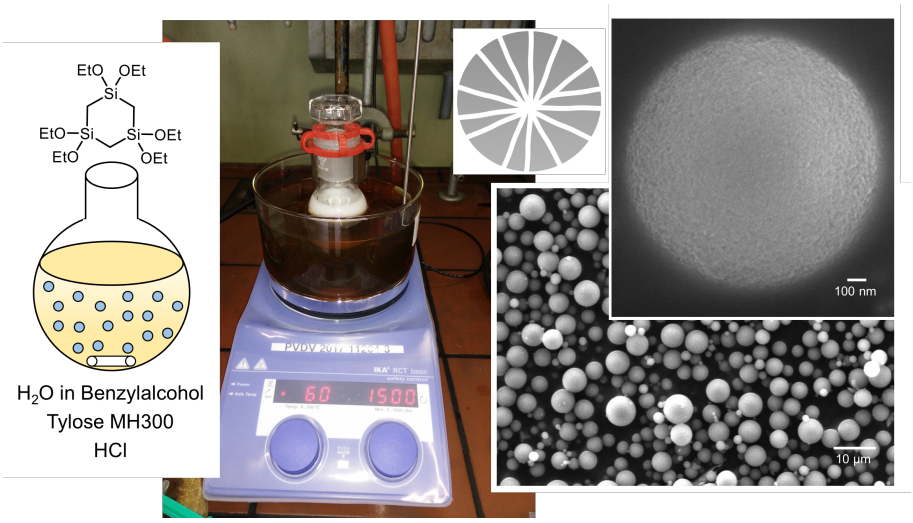

Figure 9.2: The W/O procedure with magnetic stirring for the synthesis of HETSCH-based particles in practice.

Now, a pre-weighed amount of 1,1,3,3,5,5-hexaethoxy-1,3,5-trisilacyclohexane (HETSCH), is added at once while stirring. After stirring for 1 more minute, the stirring is switched off and the flask is left under static conditions for 30 min. No change, e.g. phase separation, is observed. After this, stirring is continued at 200 RPM for a set time, maintaining a temperature of 60°C. Then, the emulsion containing the spherical organosilica particles is filtered off, and washed copiously with H_2O (5 x 100 ml) and acetone (3 x 100 ml). Finally, the white product is dried for 10 min at 120°C in air, followed by a drying step under vacuum for 16 h at 120°C.

Three sets of experiments are performed based on this procedure: first, a varying amount of HETSCH precursor (1.5 to 4 g) is added while all other parameters were kept constant with 1.8 g 8 w% HCl and 6.43 ml H_2O used (Section 9.3.4). For a second set of experiments, materials are synthesized with 2.0 g of HETSCH, although at different acidity of the emulsion droplets by adding 0.18 to 1.8 g of the 8 w% HCl and diluting this aqueous phase until it reaches 8.23 ml (Section 9.3.5). Finally, the kinetics of the organosilica formation are investigated by taking out 6 ml aliquots from the emulsion reactor at set times (see Section 9.3.6). This experiment is performed with 0.18 and 1.8 g of 8 w% HCl solution added in a reaction using 2.0 g of HETSCH.

The synthesis of organosilica particles using turrax stirring (IKA T18 ULTRA-TURRAX Basic) is identical to the description above, except that a high-speed mixer is used to prepare the water/benzylalcohol emulsion. Stirring was applied at 60°C for 15 min instead of 30 min. The precursor (2.0 g) is added during the last minute of stirring. Thereafter, the glass stopper is put in place (for stirring speeds, see Section 9.3.3).

Characterization and analysis. A Micromeretics Tristar II is used for N_2 sorption experiments at 77 K. The specific surface area (S_{BET}) is determined via the Brunauer-Emmett-Teller theory and pore sizes (d_p) are calculated from the desorption branch following the Barrett-Joyner-Halenda theory. The total pore volume (V_p) is obtained at $P/P_0 = 0.99$, while the surface area of the micropores (S_μ) is deducted from t-plot calculations.

Diffuse Reflectance Infrared Fourier Transform Spectroscopy (DRIFTS) is performed using a Thermo Nicolett 6700 FT-IR spectrometer equipped with a Greasby-Specac diffuse reflectance cell, modified to measure samples at 20 - 300°C under vacuum.

Scanning electron microscopy (SEM) images are taken on a JEOL JSM 7600F FEG SEM.

For CHNS elemental analysis, a Thermo Flash 2000 elemental analyzer is used with V_2O_5 as catalyst.

Laser diffraction particle size analysis is performed using a Sympatec HELOS/BR equipped with a RODOS dry disperser and VIBRI/L feeder.

RAMAN spectra are recorded using a Thermo-Fisher NXR RAMAN Module equipped with an InGaAs detector and Nd:YVO_4 laser operating at 1064 nm.

X-ray powder diffractograms (XRPD) are recorded on a Thermo Scientific ARL X'TRA X-ray diffractometer using Cu Kα radiation of 40 kV and 30 mA.

The solid-state NMR experiments were performed at 9.4 T, 400 MHz for ^{1}H on a Bruker BioSpin Avance II NMR spectrometer equipped with a 4 mm ^{1}H/low-γ Magic-Angle Spinning (MAS) NMR probe. The rotor was spun at the MAS frequency, υ_R = 10 kHz. The ^{29}Si isotropic chemical shifts were referenced to tetramethylsilane.

For the ^{1}H-^{29}Si cross-polarization (CP-MAS) 1D experiments, the recovery delay was τ_{RD} = 1 s, the contact time was τ_{CP} = 5 ms, the ^{29}Si radiofrequency (rf) nutation frequency was 45 kHz, and the ^{1}H rf nutation frequency was linearly ramped from 36 to 72 kHz. TPPM-15 ^{1}H decoupling of 72 kHz was applied during the acquisition of ^{29}Si spectra [422]. The number of scans was NS = 8192, which leads to nearly 2 hours experimental time.

Applied to organosilica materials, chemical shifts from a tetramethylsilane standard arise when Si-C are replaced by Si-O bonds. A silicon atom with four Si-O bonds, as found in MPS, will only show Q-sites, signals that are shifted to the region -90 to -120 ppm. PMOs derived from bissilanes, consisting of silicon atoms with three Si-O bonds and one Si-C bond, shift towards the region -50 to -70 ppm (T-sites). ^{29}Si CP-MAS NMR signals of structures with two Si-O and two Si-C bonds, as found for HETSCH and AHETSCH, are found in the region -10 to -25 (D-sites). Above this, the nature of the Si-O bond, either siloxane or silanol, allows to distinguish between more condensed sites e.g. $Si(OSi)_4$ or Q^4-site or silicon atoms with a lower degree of condensation e.g. $Si(OSi)_2(OH)_2$ or Q^2-site.

Chromatographic separations were performed using an Agilent 1100 series HPLC system equipped with a degasser, a binary pump, an autosampler with fixed injection volume of 2 μl for all experiments, a column thermostat and a variable wavelength detector (VWD) UV detector set at λ = 210 nm.

9.3.2 The emulsifier and emulsion procedure

In our first attempts to design a suitable W/O emulsion for the controlled hydrolysis and condensation of HETSCH, a screening of typical W/O systems was performed. As continuous phase, dodecane and hexadecane were selected, while mixtures of SPAN 80 and TWEEN 80 (ST80) set at a HLB of 6.0, 6.3 and 6.7 were used as emulsifiers (**Table 9.1**). After

stirring, these emulsions all showed pronounced creaming, which may be ascribed to the difference in density between the two emulsion phases. This instability makes synthesis of materials erroneous (**Figure 9.3 A-C**).

Table 9.1: Overview of preliminary W/O emulsion screening.

Continuous phase	Emulsifier	Result
Dodecane	ST80[a] (HLB: 6.0, 6.3, 6.7)	Creaming
Hexadecane	ST80[a] (HLB: 6.0, 6.3, 6.7)	Creaming
Benzylalcohol	CTAB	Coagulation
"	SDS	Coagulation
"	P123	Coagulation
"	Tylose MH300	OK

Similar W/O and continuous phase/m(emulsifier) ratios were used.
[a]Mixture of SPAN 80 and TWEEN 80 set at certain HLB.

Benzylalcohol and water have similar densities thus making such system a viable option. Indeed, the W/O emulsions prepared remained visually stable over the envisaged timespan of the organosilica synthesis. However, only emulsions employing Tylose MH300, a methyl-hydroxyethyl-cellulose-ether, delivered spherical particles within the range of application in HPLC, while using CTAB, SDS or P123 as surfactant in the optimized reaction procedure (see below) produced a combination of few very large spherical particles together with irregular ones (**Figure 9.3 D**). It seems coagulation occurs when using the latter as emulsifiers. This is due to their relative solubility in water which violates the Bancroft rule.

On the other hand, it should be recognized that the benzylalcohol/water system is an atypical emulsion as the continuous and disperse phase are partially soluble in each other. However, because of this solubility, Ostwald ripening of the emulsion droplet is believed to occur, explaining why a fairly uncontrolled manner of emulsification as magnetic stirring can deliver such relatively monodisperse droplets.

The procedure described in the experimental section, and especially the sequence of adding, was found critical to obtain satisfying $[Si(CH_2)]_3$-particles. We found that the application of a reaction step under static conditions, at least 15 min but preferably 30 min, was beneficial for the final particle size dispersion. Also, reduction of the reaction acidity had the same effect (Section 9.3.5). In both cases, the emulsion is given enough time for the ripening process to take place, eventually resulting in a significant reduction of sub-micron droplets and thus undesired fine particles (**Figure 9.3 E**).

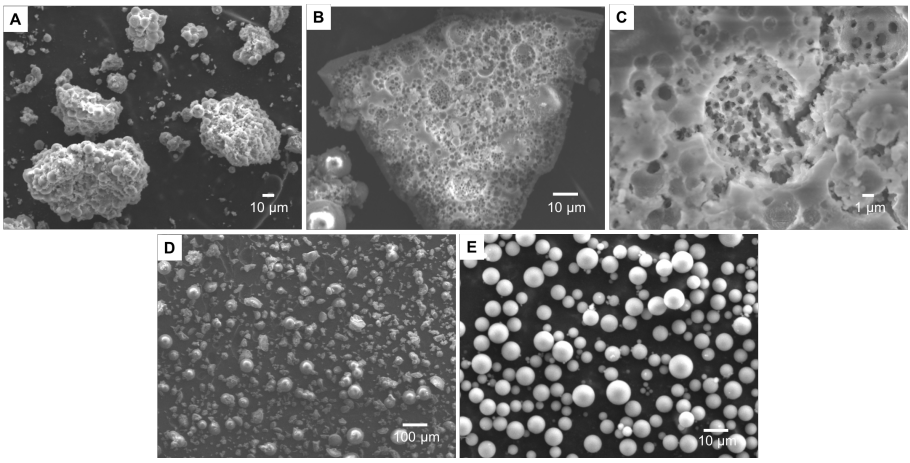

Figure 9.3: SEM images taken from HETSCH based mesoporous organosilicas synthesized in a W/O emulsion prepared with dodecane and ST80 showing the effects of creaming (A) and even phase inversion (B-C), prepared with CTAB causing coagulation (D) and following the optimized procedure (E).

9.3.3 Control of droplet size: tunable particle size

HETSCH-based organosilica spheres were synthesized under the optimal conditions described in the experimental section (9.3.1), only varying the stirring speed during emulsion formation. It is known that faster stirring induces a higher shear rate in the emulsion, causing smaller water droplets to form in the oil phase. SEM-images (**Figure 9.4**) of the obtained organosilica particles clearly show that the size of the water droplets in turn determines the size of the organosilica particles (d_{part}), as the expected decrease in particle size with increased stirring rate is observed (**Table 9.2**). Spherical morphology is maintained throughout all samples.

The stirring rate thus allows a controlled mean particle size of anywhere between 0.9 to 13.7 μm. The size dispersity of the HETSCH-particles (PSD), determined as $D_{90/10}$, is found between 2.00 and 2.89, independent of the emulsification technique and particle size. A further increase in monodispersity could not be obtained, as mechanical stirring is not known to create very monodisperse droplets, in contrast to e.g. membrane emulsification. As a note, an increase or decrease of the emulsifier amount did not give rise to significant changes in both particles size and dispersity.

To a certain extent, this W/O emulsion method resembles the use of spray drying to obtain spherical organosilica particles, as in both cases

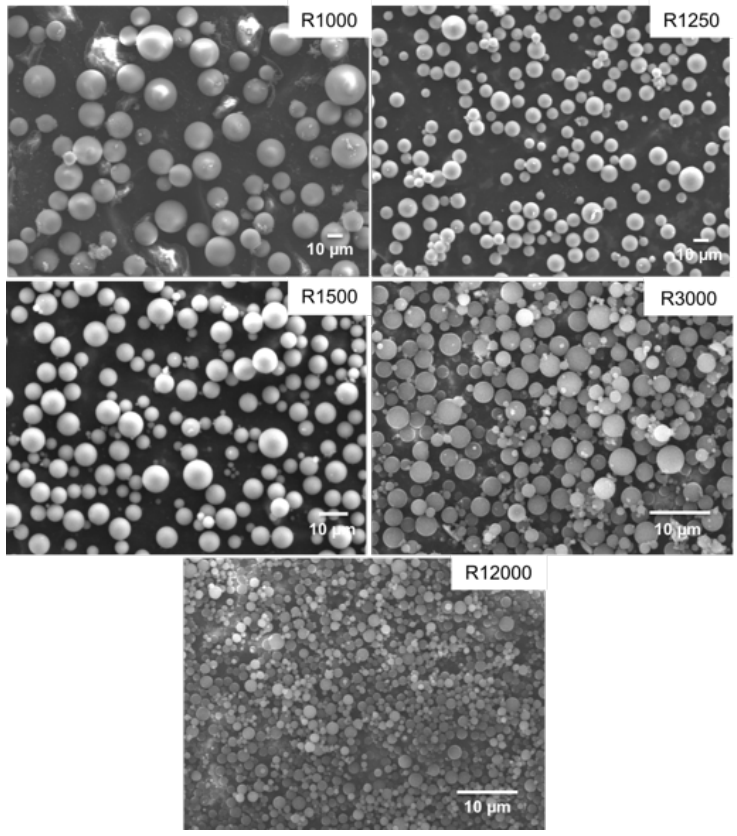

Figure 9.4: SEM images taken from HETSCH based mesoporous organosilicas (R) synthesized in a W/O emulsion prepared by stirring at 1000, 1250, 1500, 3000 and 12000 RPM.

droplets are used as the environment for reaction. However, in spray drying, an evaporating solvent (EtOH) needs to be used together with a pore generating surfactant in order to obtain porous particles, as gel formation takes place almost immediately after droplet formation. Due to these constraints, it remains challenging to obtain large mesopores, via spray drying [232].

Using the W/O emulsion method, however, N_2 sorption experiments (**Table 9.2**, **Figure 9.5**) indicate that all materials have a large specific surface area (S_{BET}) and contain large mesopores (d_{BJH}, Type IV H1 isotherms) of approx. 120Å with a relatively narrow pore size distribution. Next to this, XRD experiments yielded diffractograms without any diffraction peaks. These results point towards the formation of an organosilica gel inside the size-controlled emulsion droplets.

Table 9.2: HETSCH-based organosilicas prepared at varying stirring rate.

	$S_{BET}{}^a$ [m^2/g]	$d_{p,BJH}{}^b$ [nm]	$V_p{}^c$ [ml/g]	$d_{part}{}^d$ [μm]	$d_{part}{}^e$ [μm]	PSD^f [$D_{90/10}$]
R1000	1227	12.2	2.04	13.7	12.58	2.89[g]
R1250	1216	12.5	2.11	10.3	8.68	2.07[g]
R1500	1214	12.1	1.94	6.9	5.54	2.02[g]
R3000	1031	14.5	1.81	-	2.72	2.00[f]
R12000	836	10.4	1.22	-	0.92	2.67[f]

[a]Specific surface area determined via Brunauer-Emmett-Teller theory. [b]Pore size calculated from desorption branch following Barrett-Joyner-Halenda theory. [c]Pore volume determined at P/P_0 = 0.99. [d]D50 particle size via laser diffraction particle size analyzer. [e]Number-weighted average SEM particle size calculated from a population of at least 250 particles. [f]Particle size dispersion. [g]Based on volume-weighted distribution (laser diffraction). [f]Based on volume-weighted distribution (SEM).

9.3.4 Porosity control: amount of precursor

As a first experiment, variable amounts of HETSCH precursor (1.5, 2.0, 2.5, 3.0 and 4.0 g, corresponding to a theoretical 18.5, 25, 31, 37 and 49 w% in the H_2O droplets) are added to an identical W/O emulsion and reacted for 22 h. As clearly observed from the SEM images of R2.0 and the two most extreme cases, R1.5 and R4.0, no significant change in particle size (mostly revolving around 5.7 μm with a standard deviation of approx. 1.6 μm) or morphology occurs (**Figure 9.6**; A, B and C).

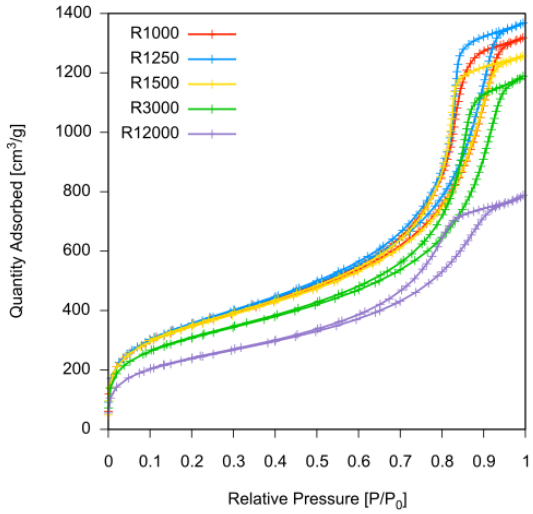

Figure 9.5: N_2 sorption isotherms of HETSCH based mesoporous organosilicas (R) synthesized in a W/O emulsion prepared by stirring at 1000, 1250, 1500, 3000 and 12000 RPM.

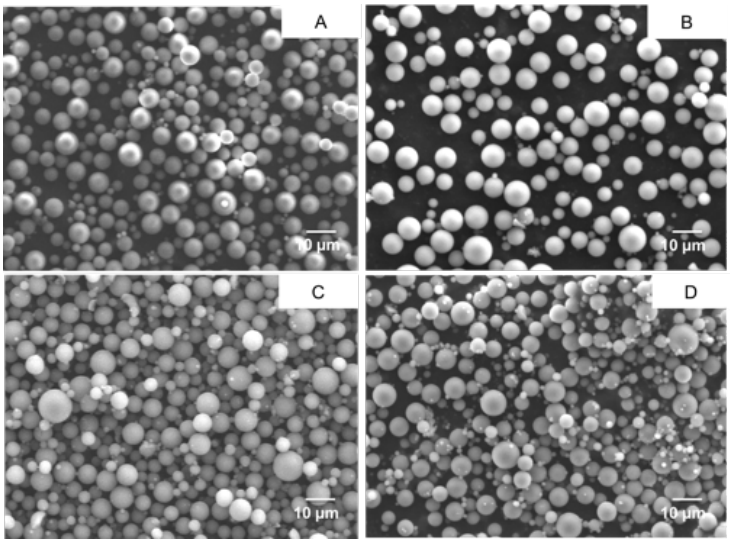

Figure 9.6: SEM images of R4.0 (A), R2.0 (B), R1.5 (C) and R2.0 using 2.4 g 8 w% HCl-sol instead of 1.8 g (D).

More interestingly, the N_2 sorption isotherms are radically influenced by the HETSCH/H_2O ratio (**Figure 9.7**, left). At high precursor to water ratio, only a Langmuir-type isotherm is observed, indicating completely microporous particles. However, when the amount of precursor is reduced, the pore size (d_p) and with it the pore volume (V_p), increases gradually towards mesopores (Type IV, H1 isotherms) of 21.2 nm and 2.48 ml/g, respectively. Additionally, the specific surface area (S_{BET}) increases from 897 m^2/g to 1165 m^2/g when the first mesopores are formed (R4.0 to R3.0), but remains constant afterwards.

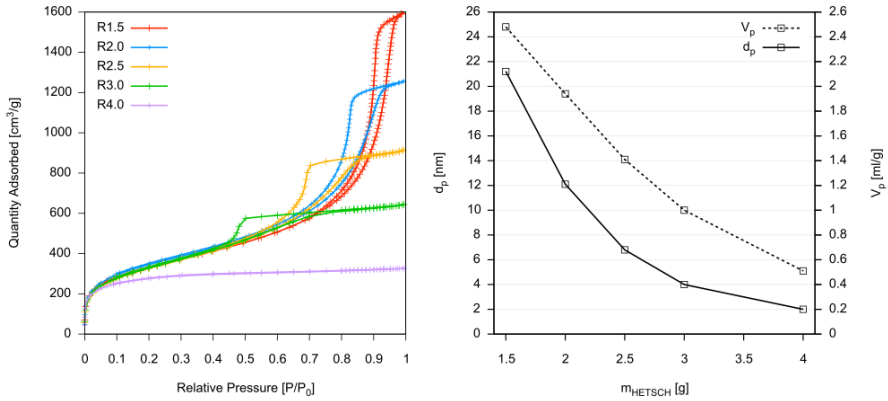

Figure 9.7: Left: N_2 sorption isotherms of materials synthesized with m_{HETSCH} = 1.5 to 4.0 g, denoted R1.5 to R4.0. Right: Pore size (d_p) and pore volume (V_p) of R-particles as a function of m_{HETSCH} used during synthesis (t = 22 h, $m_{HCl-sol}$ = 1.8 g).

As predicted, when using the same volume of aqueous droplets, of which size and shape is adopted by the organosilica gel, the material framework can only become less dense and thus more porous when fewer precursor is available. As a result, adaptation of the precursor mass allows for straightforward engineering of the particle porosity even up to large pore sizes and extreme pore volumes (**Figure 9.7**, right).

9.3.5 Porosity control: the acid catalyst

As HCl both catalyzes hydrolysis and condensation of the HETSCH precursor, here fixed at 2.0 g, we probed the effect of the droplet acidity on the gel formation. Hereby, we witnessed that d_p and V_p increase when the amount of HCl-sol added is varied from 0.18 to 1.8 g (solution pH from pH 1.32 to pH 0.32, respectively) (**Figure 9.8**). A reasoning is given below, when the kinetic study of the particle formation is considered.

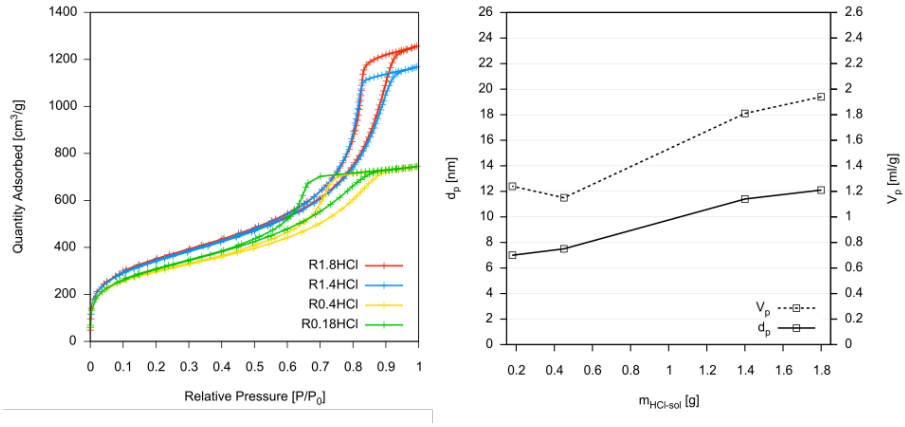

Figure 9.8: Left: N_2 sorption isotherms R-particles with $m_{HCl-sol}$ used during synthesis = 1.8 g, 1.4 g, 0.45 g and 0.18 g (t = 22 h, m_{HETSCH}= 2.0 g). Right: Pore size (d_p) and pore volume (V_p) of R-particles as a function of $m_{HCl-sol}$ used during synthesis (t = 22 h, m_{HETSCH} = 2.0 g).

Next to this, ^{29}Si CP-MAS NMR rather surprisingly indicates no significant difference in condensation degree between the different samples as proven by the unchanged ratio between D^2 ($Si(CH_2)_2(OSi)_2$; -22 ppm), D^1 ($Si(CH_2)_2(OSi)(OH)$; -17 ppm) and D^0 ($Si(CH_2)_2(OH)_2$; -7 ppm) sites (**Figure 9.9**). No T- or Q-sites are observed for these samples, implying that the $[Si(CH_2)]_3$ ring structure remains completely intact during synthesis.

Also, the particle size and shape remained unaffected in these conditions, however we found that more fine submicron particles are formed if the amount of 8 w% HCl-sol used is further increased to 2.4 g (**Figure 9.6**, D). Now, it seems that, once a pH threshold is exceeded, the rate of hydrolysis and condensation becomes too fast for the emulsion ripening process to take place. Therefore, the particles obtained at excessive acid concentration are more resembling the initial and more polydisperse W/O emulsion, which contains more submicron droplets.

9.3.6 Porosity control: reaction time

Definitive proof on the mechanism of the spherical organosilica gel formation and the generation of its pore network is found by a kinetic experiment where emulsion aliquots containing particles are removed at set times during the synthesis. All samples obtained have a similar particle morphology combined with a high specific surface area of $\sim$ 1160 m^2/g, except denoted otherwise. In contrast with templated methods

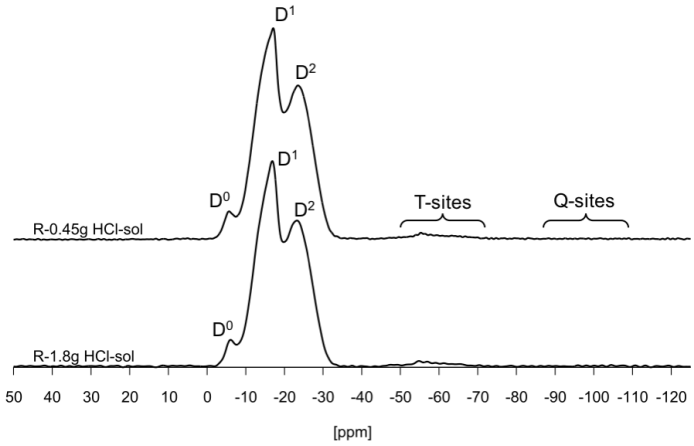

Figure 9.9: ^{29}Si CP-MAS spectrum of a sample prepared with 1.8 g of HCl 8 w% sol (bottom) and a sample with 0.45 g of HCl 8 w% sol (top) both showing D^2 ($Si(CH_2)_2(OSi)_2$; -22 ppm), D^1 ($Si(CH_2)_2(OSi)(OH)$; -17 ppm) and D^0 ($Si(CH_2)_2(OH)_2$; -7 ppm) sites.

to obtain PMOs, the organosilica in this work does not precipitate as a mesoporous material. Instead, in a synthesis with m_{HETSCH} = 2.0 g and $m_{HCl-sol}$ = 1.8 g, a first aliquot of particles, taken 0.5 h after reapplying the stirring, shows 5.4 nm pores with a volume of 0.86 ml/g (S_{BET} = 952 m^2/g) (**Figure 9.10**), whereas 0.5 h later, the pore size has increased dramatically to 9.8 nm (V_p = 1.50 ml/g). Finally, after 22 h the pore size settles at the 12.1 nm described earlier, with a pore volume of 1.91 ml/g.

A second experiment, using 10-fold less HCl, shows exactly the same trend, although the rate of pore growth is approximately ten times slower (**Figure 9.11**). Here, at t = 1 h the porosity reaches d_p = 3.9 nm and V_p = 0.51 ml/g while S_{BET} is 774 m^2/g with a t-plot micropore surface area of 314 m^2/g, while after 94 h, it settles at 9.5 nm and 1.67 ml/g with S_{BET} = 1215 m^2/g with a significantly reduced S_μ of 82 m^2/g. ^{29}Si CP-MAS NMR experiments in **Figure 9.12**, only show minor increase in condensation degree of the network between aliquots taken at t = 1 h and 94 h, which indicates that, although the difference in porosity, the organosilica network of the pore walls remains fairly unchanged after the initial precipitation of the particles.

In both experiments, following rapid hydrolysis and condensation of the precursor, supposedly a microporous gel particle is formed in the early

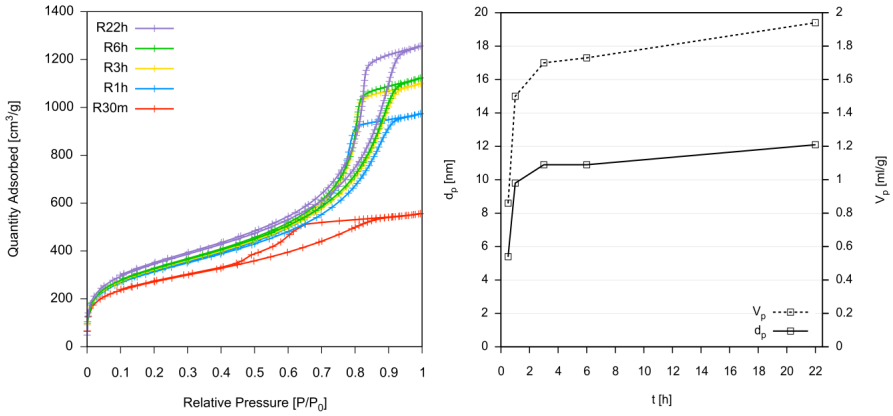

Figure 9.10: Left: N_2 sorption isotherms of R-particles with synthesis time = 30 min, 1 h, 3 h, 6 h and 22 h ($m_{HCl-sol}$ = 1.8 g, m_{HETSCH} = 2.0 g). Right: Pore size (d_p) and pore volume (V_p) of R-particles as a function of synthesis time (t) ($m_{HCl-sol}$ = 1.8 g, $m_{HETSCH)}$ = 2.0 g).

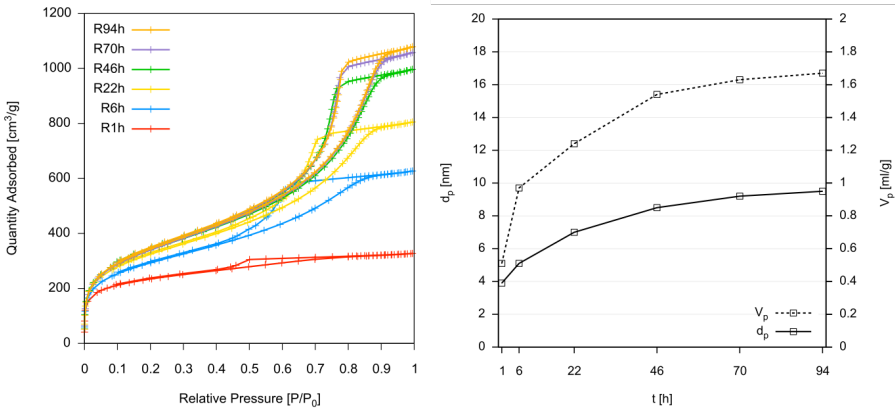

Figure 9.11: Left: N_2 sorption isotherms of R-particles with synthesis time = 1 h, 6 h, 22 h, 46 h, 70 h and 94 h ($m_{HCl-sol}$ = 0.18 g, m_{HETSCH} = 2.0 g). Right: Pore size (d_p) and pore volume (V_p) of R-particles as a function of synthesis time (t) ($m_{HCl-sol}$ = 0.18 g, $m_{HETSCH)}$ = 2.0 g).

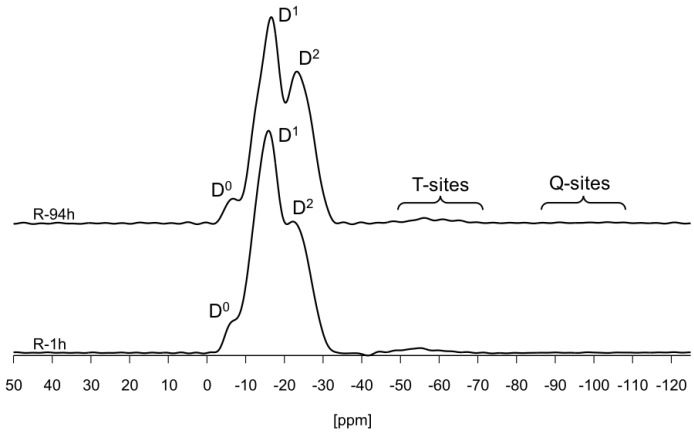

Figure 9.12: ^{29}Si CP-MAS spectrum of a ring-type organosilica sample after 1 h of reaction time (bottom) and after 94 h of reaction time (top) both showing D^2 ($Si(CH_2)_2(OSi)_2$; -22 ppm), D^1 ($Si(CH_2)_2(OSi)(OH)$; -17 ppm) and D^0 ($Si(CH_2)_2(OH)_2$; -7 ppm) sites.

stages of the synthesis, after which the pores are gradually reshaped to larger sizes under the influence of the acidic medium. It is clear that the HCl concentration not only controls the rate of this pore aging process, but also determines the final pore size. Therefore, it is conceived that the synthesis of the organosilica gel particles is initially under kinetic control, quickly forming a microporous framework. After this, the system evolves to a precursor and HCl determined solution equilibrium (thermodynamic control), which causes pore expansion as the organosilica particles partially redissolve, leaving the condensation degree of the material unchanged.

The above experiments nicely show the high flexibility of the pore size engineering throughout almost the full mesopore range. This comes on top of the established particle size control. At this point, a promising $[Si(CH_2)]_3$-material was selected for chromatographic evaluation with emphasis on mechanical stability during the packing procedure and analysis.

9.4 Application of $[Si(CH_2)]_3$-ring spheres as packing for RP-HPLC

As witnessed above, many $[Si(CH_2)]_3$ spheres not only possess large pores, they also have a high pore volume. Subjected to high pressure both during packing and analysis, packings for liquid chromatography should hold a high mechanical stability to prevent deterioration of the column. As the organosilicas prepared here have pore volumes that are easily the double of commercial columns, the mechanical stability is tested in practice.

Sedimentation pre-treatment and packing procedure. Before evaluation, the as-synthesized particles are subjected to two sedimentation steps to remove aberrantly small, large and fused or irregular particles. For this rudimentary form of classification, the material is suspended in 3 cm of isopropanol in a large beaker and ultrasound is applied for 10 min. Thereafter the beaker is left untouched until the first (largest) particles settle, typically this happens after another 5 or 10 min. The supernatant is removed with a pipette and is left to stand for 1 hour. During this period, all but the smallest particles settle, leaving a sedimented layer of 'higher quality' particles after removal of the supernatant (**Figure 9.13**).

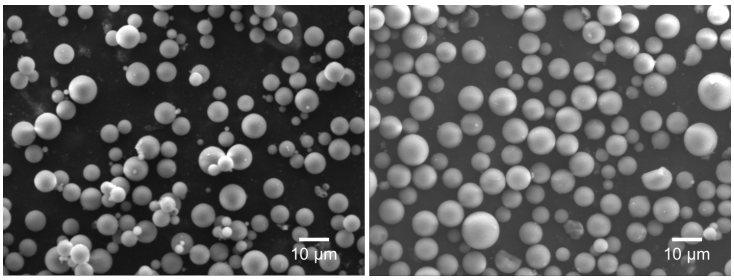

Figure 9.13: SEM images of a fairly polydisperse sample before (left) and after (right) the double sedimentation procedure.

All described columns were packed using a Haskel air driven fluid pump in a 5 cm IDEX IsoBar column with an internal diameter of 2.1 mm, equipped with Parker ports with a 2.0 μm frit at the entry and a 0.5 μm frit at the exit. The following packing procedure was adopted: 0.5 g of particles are suspended in 13 ml (i.e. the volume of the packing reservoir) of a 50:50 mixture of hexane and isopropanol and subjected to ultrasound for 15 min to ensure good dispersion of the particles. Subsequently, the slurry was attached to the high pressure pump and the columns are

packed at 700 bar for 15 min. Then the pressure was gradually released over another 15 min.

Evaluation of the mechanical stability of packed columns. In what follows, multiple columns are packed with materials having a decent morphology and possessing a V_p of around 1.90 ml/g, 10.0 nm pores and an S_{BET} of 1250 m^2/g. The slight variations between the samples make that the columns cannot be exactly compared, yet a good estimation is given for the stability of the columns over time. A good column should not show an increasing working pressure over time. This induces variability in the separations and is an indication of deterioration of the column and thus its separation efficiency.

With a first column, packed as described, we witnessed an immediate increase of the column back-pressure after an RP-HPLC analysis run, i.e. flushing the column with H_2O/CH_3CN in an 80/20 ratio, which causes a moderate to high pressure ($>$ 200 bar). SEM images after these runs clearly show that the column packing has aggregated into large clumps of particles, which block the column. Interestingly, a column packed in the same conditions but not subjected to analysis conditions does not show any signs of this, and particles are found exactly the same as before packing (**Figure 9.14**). Moreover, a column packed at 550 bar also showed significant increase of the working pressure after contact with water at elevated pressure. This indicates that only these latter conditions cause column blocking, where in the organic packing solvent, the highly porous materials are mechanically stable.

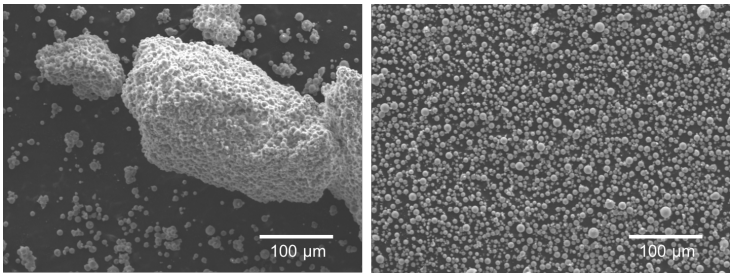

Figure 9.14: SEM images of [Si(CH$_2$)]$_3$ material taken from the column exit of a column subjected to analysis conditions (left) and a column emptied immediately after packing (right).

The mechanical stability of organosilicas is known to increase when the surface silanol groups are removed by end-capping as this decreases the adsorption of water on the surface which causes breakdown of the silicate framework. However, even after end-capping with HMDS, build-up of pressure, although somewhat less distinct, is observed over time. Also,

$[Si(CH_2)]_3$ materials of which the silanol groups are reduced via a post-treatment (see Section 9.6) do not give rise to improvement.

Finally, a column packed with unmodified particles having a V_p of 0.51 ml/g (R4.0g) was shown stable after multiple runs of analysis. Unfortunately these particles are microporous and thus unsuited for chromatographic applications. Altogether, one must conclude that the pore volume of the large pore $[Si(CH_2)]_3$-particles synthesized via this W/O procedure is too high for practical application as RP-HPLC packing.

9.4.1 Attempts to reduce V_p

Methods to significantly reduce the pore volume of the spherical $[Si(CH_2)]_3$ xerogels, while maintaining the same pore size, have been investigated. From the above experiments, it is however clear that both are inherently linked during the synthesis, as reduction of the pore volume is only witnessed together with a decrease of the pore size. Theoretically, the only way to lower V_p, whilst leaving d_p unchanged is to reduce the amount of pores within the organosilica particle, which basically comes down to a densification of the framework. Typically, this can be attained by the pre-condensation of the HETSCH precursor into its oligomeric form, similar to the pre-condensed form of TEOS, poly(ethoxysiloxane) [327]. Procedures to perform this oligomerization are described through the addition of small amounts of water and hydrochloric acid to an ethanolic solution of HETSCH. This allows for a slow hydrolysis and condensation of the silane precursor to form ethanol soluble oligomers which can be processed further [91]. Unfortunately, EtOH readily demusifies the water/benzylalcohol mixture. This rules out the above method of controlled oligomerization.

Therefore, we attempted the pre-condensation of HETSCH using both base and acid catalysts in water with varying concentration and reaction time. This, however, had either no effect on the framework density of the synthesized particles or caused premature gel formation. Based on what is known for silicates, in situ densification was practiced by starting the sol-gel reaction in the droplets in basic conditions to, in theory, first obtain dense polysilsesquioxane networks or even obtain colloidal organosilica particles [19]. After a certain time, an excess of HCl was added to fuse or cross-link these formed structures inside the droplets. Although this approach seems sound in theory, no spherical particles could be obtained, indicating at least severe incompatibility with the W/O emulsion.

All together, we found no procedure to promptly influence the framework density and thus the pore size to pore volume ratio. Given this, and the fact that the $[Si(CH_2)]_3$ has no interesting chromatographic functionality, the use of the HETSCH precursor was abandoned and the focus of our research was shifted to the application of AHETSCH and other bis-silane precursors.

9.5 Expanding the W/O method: other bis-silane precursors

Although the incorporation of methyl-, and in addition ethyl-bridges, in the siloxane framework is clearly proven to have a positive effect on the particle matrix stability [232, 323] still a retentive group e.g. C18 needs to be attached via siloxane bonds (grafting) to obtain a material suitable for reverse-phase chromatography. Since this grafted functionality is typically unstable below pH 2 [313], it would now be of utmost interest to directly incorporate a strong retentive group e.g. benzyl, during the particle synthesis. Even more appealing is the incorporation of a reactive group e.g. alkene or thiol, to covalently bind a functionality of choice via post-modification (thiol-ene 'click') of the pore surface [169, 232]. In this section we will explore the versatility in terms of functionality which is possible via the novel W/O emulsion by expanding the synthesis to other bis-silane precursors.

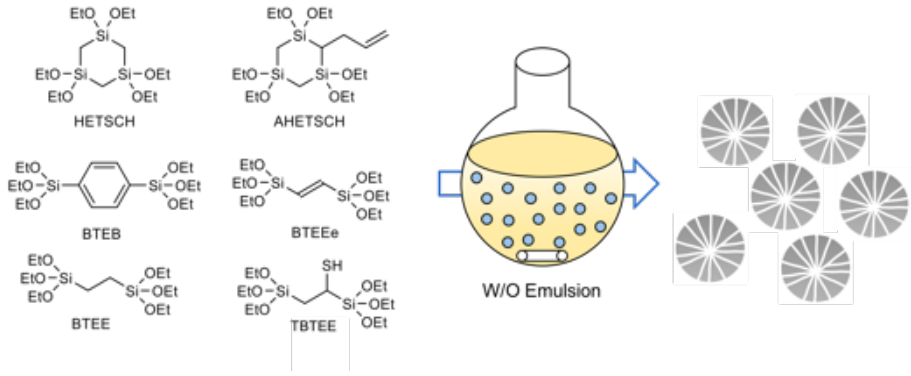

Figure 9.15: Molecular structure of the bis-silane molecules used as precursors for spherical organosilicas in a W/O-emulsion.

9.5.1 Experimental

A selection of other commercially available bis-silane precursors i.e. bis-(triethoxysilyl)ethane (BTEE), bis(triethoxysilyl)benzene (BTEB) and home-made i.e. bis(triethoxysilyl)ethene (BTEEe), 2-allyl-1,1,3,3,5,5-hexaethoxy-1,3,5-trisilacyclohexane (AHETSCH), 1-thiol-1,2-bis(triethoxysilyl)-ethane (TBTEE), (**Figure 9.15**) are employed in the same synthesis procedure as described in Section 9.3.1. All emulsions are formed at 1500 RPM. However, given the difference in hydrolysis and condensation rate of these precursors, the acidity of the water droplets was decreased to allow for the ripening process to take place. Allyl (AR) and thiol (SE)-functionalized organosilica spheres are obtained by co-condensation (50/50) of their respective precursors with HETSCH and BTEE. Synthetic details are found in **Table 9.3**.

9.5.2 The W/O emulsion as generic method for spherical polysilsesquioxane particles

For all obtained materials, DRIFT and RAMAN spectroscopy confirm the incorporation of the bridged functionalities (**Figures 9.52 to 9.58**). No significant differences are witnessed when comparing the spectra of the mesoporous organosilicas synthesized here, with their reported non-spherical counterparts [4, 5, 41, 78, 130, 133, 169, 423].

SEM images of the organosilica particles show, in all cases, spherical particles with a mean particle diameter ranging from 4.10 μm to 5.20 μm (**Figure 9.16**). As expected, particle size and shape are again determined by the droplets of the W/O emulsion, thus proving the robustness of the synthesis method. All particles possess a smooth surface, except for SE, for which spheres of varying roughness are found (**Figure 9.17**). Presumably, this is caused by propylamine impurities within the homemade thiol precursor [133].

Although the morphology of all synthesized organosilicas is similar, clear differences are observed in terms of porosity (**Table 9.3**). Firstly, the nature and reactivity of precursor used has a major influence on the porosity of the material. For example, although highly comparable synthesis conditions are used, a decrease of 50% in pore volume is observed between the two most extreme cases, R and SE. Assumingely, these differences are caused by the variation in hydrolysis and condensation rate between the precursor, or by some degree of oligomerization of the pure precursors.

Table 9.3: Overview of experiments performed with different bis-silane precursors.

	Precursor	m_{prec} [g]	$m_{8w\%HCl}$ [g]	S_{BET}[a] [m^2/g]	$d_{p,BJH}$[b] [nm]	V_p[c] [ml/g]	d_{part}[d] [μm]	PSD[e] [$D_{90/10}$]
R	HETSCH	2.0	0.45	1041[d]	7.5	1.15	5.20	1.79
AR	HETSCH + AHETSCH	1.4 + 1.4	0.45	748	5.8	0.74	4.66	2.16
AR-LP	HETSCH + AHETSCH	1.0 + 1.0	0.45	720	38.3	1.71	4.98	2.23
E	BTEE	2.0	0.45	890	7.0	0.99	4.85	2.01
SE	TBTEE + BTEE	1.0 + 1.0	0.45	514	4.5	0.60	4.31	1.81
Ee	BTEEe	2.0	0.45	928	4.5	0.95	4.10	2.00
B	BTEB	1.5	0.9	736	4.0	0.91	4.50	2.09

[a]Specific surface area determined via Brunauer-Emmett-Teller theory. [b]Pore size calculated from desorption branch following Barrett-Joyner-Halenda theory. [c]Pore volume determined at $P/P_0 = 0.99$. [d]Number-weighted average SEM particle size calculated from a population of at least 250 particles. [e]Particle size dispersion based on volume-weighted distribution.

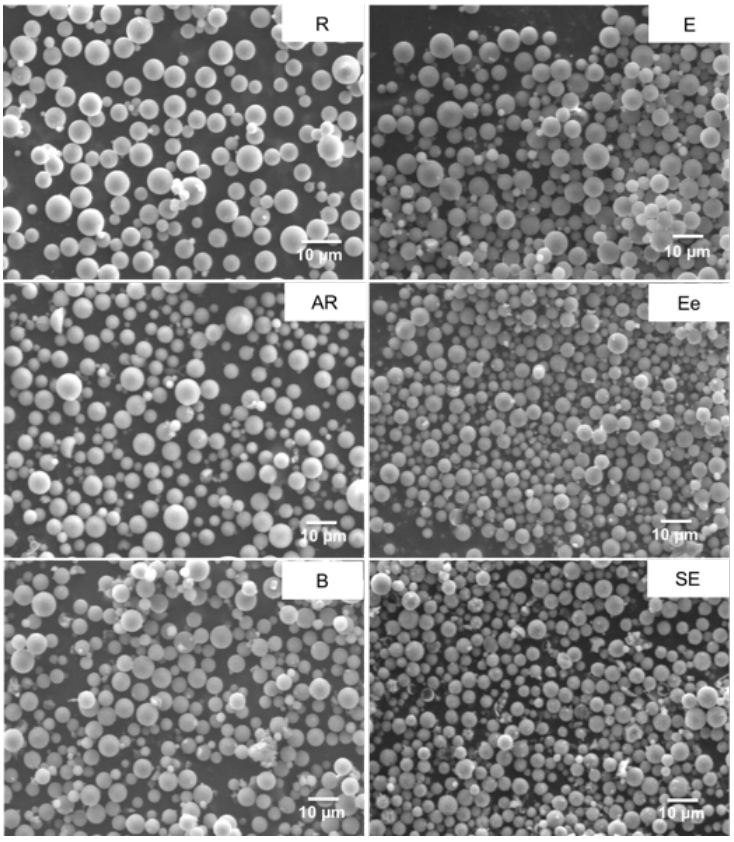

Figure 9.16: SEM images of as synthesized mesoporous organosilica particles derived from the precursors in Figure 9.15. All emulsions were formed by magnetic stirring at 1500 RPM.

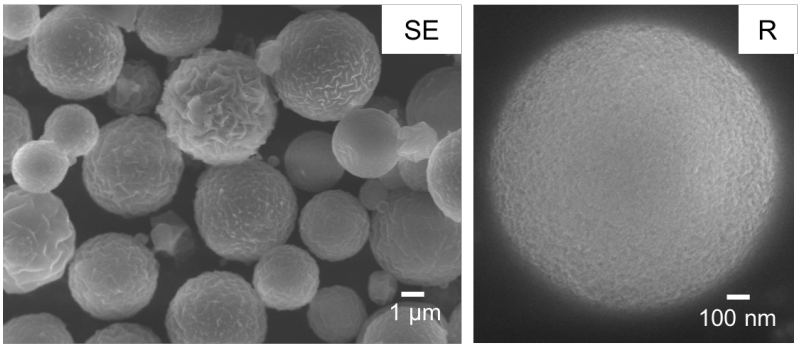

Figure 9.17: SEM images of SE particles having variable surface roughness (left) compared to a representative particle (R) for all other materials having a smooth surface.

Even more striking is the variation of N_2 isotherms when comparing R, AR, and E to B, SE and Ee (**Figure 9.18**). Here, the first materials exhibit type IV H1 hysteresis, common for silica gels, indicating a relatively uniform pore network. The latter materials, on the other hand, show type IV H2 hysteresis, indicative for large internal pores with narrowed 4.5 nm pore openings. As such more intricate porosity typically arises from syntheses using pore generating templates forming interconnected arrays of spherical micelles (SBA-16 type materials [42]), this result was unexpected. However, H2 hysteresis was persistent under various synthesis conditions (acidity, amount of precursor). Therefore, this pore blocking or an inkbottle effect must be inherent to the specific organosilane precursors.

Furthermore, there is a sharp contrast between AR (total of 2.4 g precursor used) and large pore AR (AR-LP, 2.0 g), having 5.8 nm pores (0.74 ml/g) and 38.3 nm pores (1.71 ml/g) respectively (see also Section 9.7.2). This is again a significant increase in pore size and volume when reducing the amount of precursor. As witnessed before for R, given that both materials are gelled inside the same volume of disperse phase and that both adopt the morphology of the aqueous microdroplets, it is clear that using fewer amount of precursor leaves a less dense organosilica network inside the droplets, with larger pore size and volume as a result.

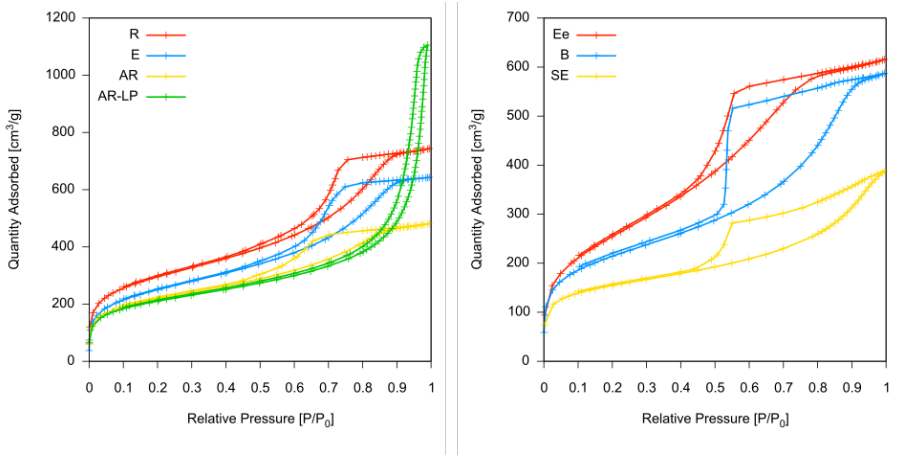

Figure 9.18: N_2 sorption isotherms (77K) of the organosilica particles. Type IV H1 hysteresis is observed for R, AR, AR-LP and E; Type IV H2 hysteresis is witnessed for B, SE and Ee.

Considering application as chromatographic packing, these results are promising given that the HETSCH precursor, apparently, gives rise to the highest V_p of all materials. The more interesting bridged function-

alities for further chemical post-modification, AR and S, show reduced pore volumes that lay more in the region of the stable microporous R material packed earlier, than the mechanically labile R particles packed in Section 9.4. Before evaluating such particles, further fine-tuning of the porosity is definitely necessary as all the above organosilicas still contain a considerable microporosity while a post-synthesis mesopore expansion might be attractive to increase the flexibility of the particle synthesis.

9.6 Organosilica stability and hydrolytic post-treatment

In this section, several post-synthesis techniques are applied to R materials, as a probe, to further fine-tune the porosity. In the meantime, these experiments provide an indication of the hydrothermal and hydrolytic stability of $[Si(CH_2]_3$-ring structured organosilicas in vitro.

9.6.1 Experimental

Hydrothermal treatment. For this post-treatment at elevated temperature, 0.15 g of porous R particles are weighed off and suspended in a Teflon-lined autoclave with 15 ml of deionized water. The closed autoclave is placed in an oven at a constant temperature ranging from 100 - 200°C for 24 h. After the autoclave is cooled in a water bath, the treated spheres are filtered, washed with 3 x 20 ml acetone and dried for 10 min at 120°C in air, followed by a drying step under vacuum for 16 h at 120°C. The samples are denoted as R-XC with X referring to the temperature used.

Thermal treatment - Autohydrophobization. In a procedure adapted from [41], 0.5 g of porous R particles are placed in an Al_2O_3 cup, which is then put in a tubular furnace with an atmosphere of controlled N_2 flow (0.25 l/min). Herein the particles are thermally treated by heating up the oven with a rate of 5°C/min to 450°C, the temperature which is kept for another 5 h. After cooling down of the oven, still under N_2, the particles are recuperated and the sample is denoted R-AH.

Hydrolytic treatment. For this post-treatment at elevated pH, 0.15 g of porous R particles are weighed off and suspended in a flat-bottomed flask with an aqueous solution of NaOH at fixed pH. Then, the particles are shaken for 24 h, except stated otherwise, at room temperature (25°C). Afterwards, the treated spheres are filtered, washed with 3 x

20 ml H_2O, 3 x 20 ml acetone and dried for 10 min at 120°C in air, followed by a drying step under vacuum for 16 h at 120°C. The samples are denoted as R-pHX, with X referring to the pH of the solution used.

Combined hydrothermal/hydrolytic treatment (HH). Both aqueous post-treatments, described above, are combined by weighing off 0.15 g of porous organosilica particles and adding these to an aqueous NH_3-solution at pH 12 in a Teflon-lined autoclave. Then, the autoclave is put in an oven at 120°C for 24 h and the treated particles are filtered, washed with 3 x 20 ml H_2O, 3 x 20 ml acetone and dried for 10 min at 120°C in air, followed by a drying step under vacuum for 16 h at 120°C. The $[Si(CH_2)]_3$, ethylene- and phenylene- bridged samples are denoted as R-HH, E-HH and B-HH respectively.

9.6.2 The hydrothermal treatment: pore size expansion, μ-pore reduction and self-hydrophobization

The N_2 sorption results of a HETSCH-based sample subjected to hydrothermal treatments at autogenous pressure for 24 h are presented in **Table 9.4** (isotherms **Figure 9.19**). From these results, grosso modo, three regimes can be noticed. Where up until 100°C in H_2O the porosity remains unaltered, a drop in specific surface area (both S_{BET} and S_μ) together with a slight increase in pore size is clear from 120°C. Up until a treatment of 160°C, however, no considerable change of porosity is seen, indicating regained hydrothermal stability. Above this temperature, the structural properties change dramatically which suggest that at these condition the hydrothermal stability is again exceeded.

Table 9.4: N_2 sorption and and elemental analysis data of an R sample hydrothermally treated at 100°C to 200°C.

	S_{BET} [m^2/g]	S_μ [m^2/g]	V_p [ml/g]	$d_{p,BJH}$ [nm]	$\%C$
R	1265	131	1.89	9.5	18.6
R-100C	1251	117	1.89	9.5	19.3
R-120C	1060	63	1.71	10.5	18.6
R-140C	1033	50	1.78	10.5	18.5
R-160C	1030	32	1.71	10.4	19.1
R-200C	608	0[a]	2.05	14.7	17.6

[a]Negative micropore volume obtained via t-plot method.

The regained hydrothermal stability is explained by comparing the DRIFT spectra of R and R-160C (**Figure 9.20**). Herein, R shows CH_2 stretch

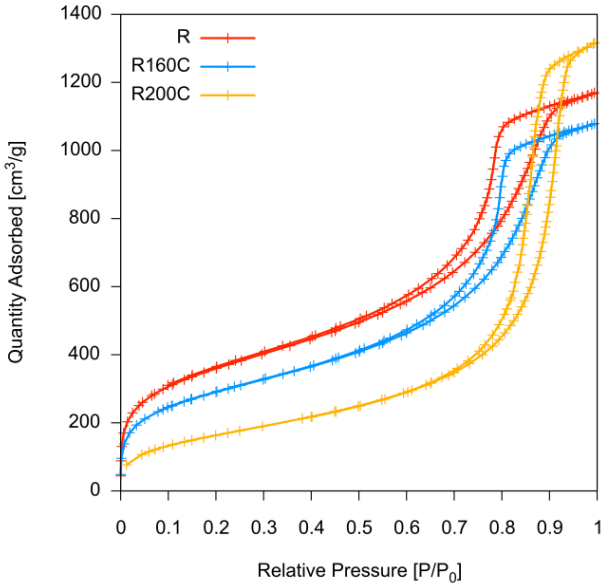

Figure 9.19: N_2 sorption isotherms of R-samples hydrothermally treated under autogeneous pressure for 24 h at 160°C (R-160C) and 200°C (R-200C).

vibrations at 2928 and 2885 cm^{-1} and a CH_2 bending vibration at 1360 cm^{-1}, characteristic for the methylene ring functionalities. A small vibration peak at 1265 cm^{-1} may be ascribed to the end-standing CH_3-group of leftover unhydrolyzed ethoxy groups of the HETSCH precursor. Now, for R-160C, the characteristic vibration of end-standing methyl-groups intensifies (CH_3 stretching at 2968 cm^{-1} and CH_3 bending at 1265 cm^{-1}) as compared to the framework CH_2-bending at 1360 cm^{-1}. Combined with a slight decrease in the Si-OH stretch vibration at 3725 cm^{-1}, this may indicate a self-hydrophobization process in which a methylene bridge reacts with a silanol group to form a Si−CH_3 functionality and a siloxane bond (**Figure 9.21**).

To confirm the occurrence of the framework rearrangement ^{29}Si CP-MAS NMR experiments (**Figure 9.22**) are performed, and indeed T^3 ($RSi(OSi)_3$; -65 ppm) and T^2 ($RSi(OSi)_2(OH)$; -56 ppm) sites are formed, which proves cleavage of a Si-C bond in benefit of a Si-O-Si bond. Furthermore, the D^2 ($Si(CH_2)_2(OSi)_2$) site at -22 ppm is now predominately present in the framework and the D^0 site ($Si(OH)_2$, -7 ppm); indicating uncondensed sites are absent. This points to a higher degree of condensation, which is reasonable after treatment at such high temperatures. Slight broadening and multiple shoulders of the D-peak are apparent and

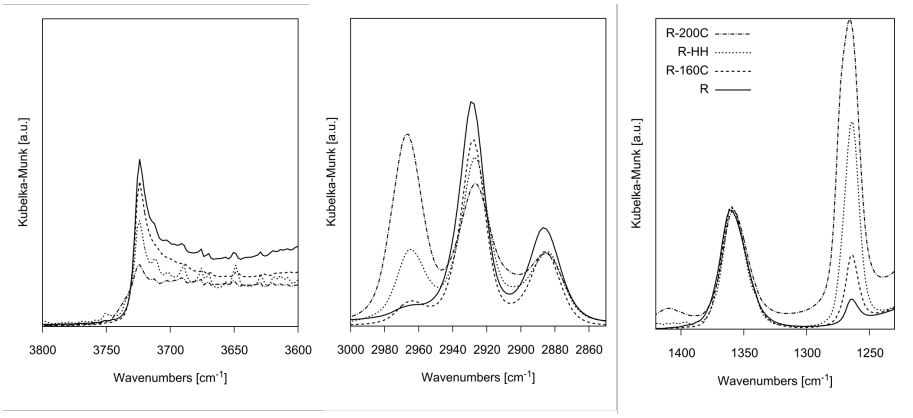

Figure 9.20: DRIFT spectra of hydrothermally post-treated R samples normalized over the framework CH_2-bending at 1360 cm^{-1}. The Si-OH stretch vibration is observed at 3725 cm^{-1}, the CH_3 stretching at 2968 cm^{-1} and the CH_3 bending at 1265 cm^{-1}. R-100C is superimposable on R, R-120C and R-140C are similar to R-160C and are omitted for clarity.

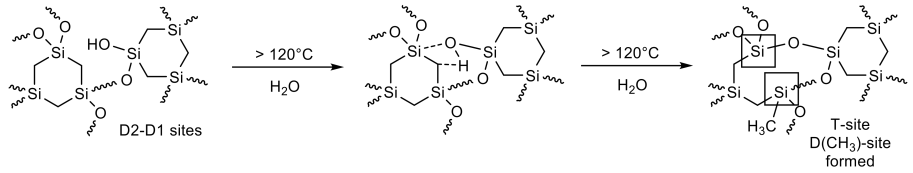

Figure 9.21: Representation of hydrothermally induced organosilica framework rearrangement leading to formation of a new T-site and a Si-CH_3 group (self-hydrophobization).

may be ascribed to D^{2*} ($Si(CH_2)(CH_3)(OSi)_2$), D^1 ($Si(CH_2)_2(OSi)(OH)$) and D^{1*} ($Si(CH_2)(CH_3)(OSi)(OH)$) at -20, -17 and -14 ppm, respectively. Some Q sites are present as well, suggesting some framework silicon atoms are no longer bound to a carbon and have thus formed two new siloxane bonds.

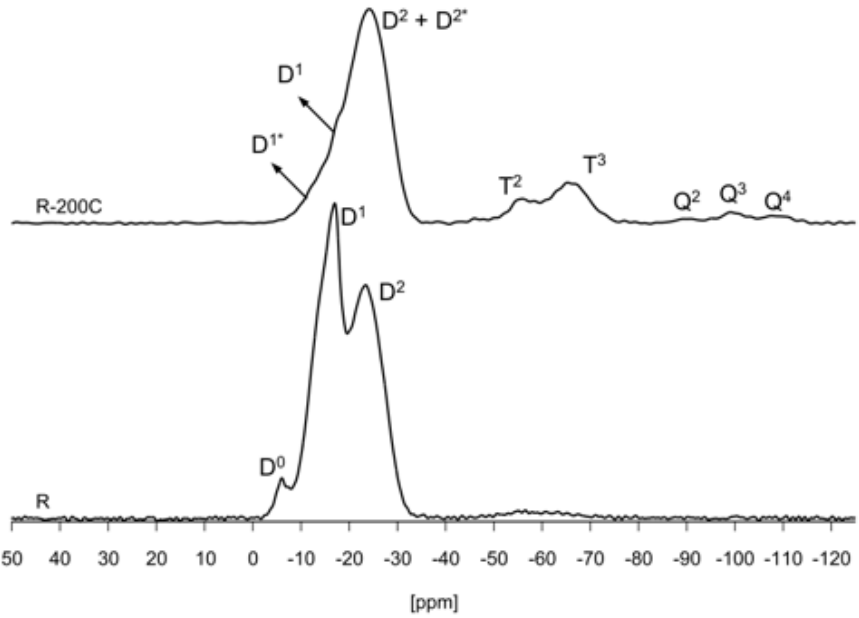

Figure 9.22: ^{29}Si CP-MAS spectrum of R and R after treatment at 200°C in H_2O (R-200C) indicating the suggested framework rearrangement. New T-sites (and Q-sites) indicate the formation of an additional siloxane bond through cleavage of a Si-C bond.

This chemical modification of the surface witnessed here, is known to improve the mechanical stability of PMOs, but up until now it was only described for materials subjected to a treatment at > 300°C in N_2 atmosphere [41, 87]. However, such reaction, starts here at 120°C (spectrum omitted for clarity) and effectively protects the material from further effects of the hydrothermal treatment up to 160°C. Although at 200°C even more of this surface reaction is observed, the material is clearly more affected by the harsh treatment expanding the pores up to 14.7 nm. However, interestingly, the micropores are eliminated completely with a 200°C treatment, assuming that the self-hydrophobization reaction closes these small pores, or that redeposition of dissolved organosilica occurs on the more curved and thus thermodynamically more unstable surface of the micropores [19].

Finally, CHNS elemental analysis of all treated samples (**Table 9.4**) indicates no significant decrease in %C as compared to the initial material R, showing that, although Si-C bonds are cleaved during rearrangement, no or few (R-200C) of the organic functionality is lost under harsh hydrothermal conditions. Finally, the morphology and size of the particles is not affected by the hydrothermal treatment (**Figure 9.23**).

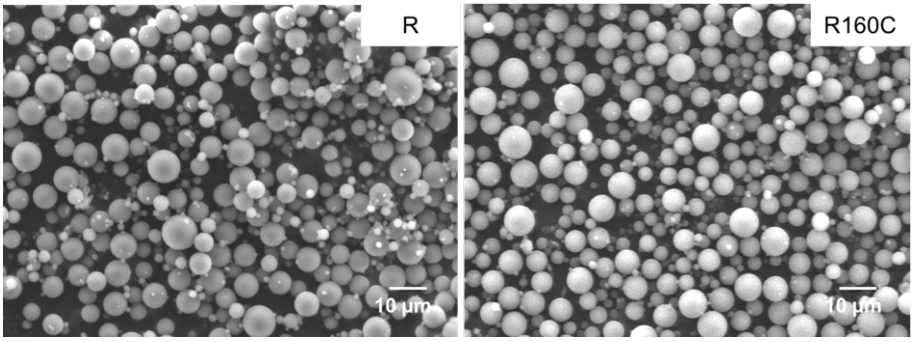

Figure 9.23: SEM-images of R before (left) and after hydrothermal treatment at 160°C (right).

9.6.3 Autohydrophobization (AH): is framework rearrangement the reason of micropore closing?

Here, we have subjected R particles to a thermal treatment at 450°C in N_2 (described in [41]) in order to determine whether the autohydrophobization witnessed above is the cause of micropores closure. For this experiment, particles synthesized using 0.45 g 8 w% HCl are treated, which explains the different porosity as compared with the samples treated hydrothermally above, however as shown in Section 9.3.5 such particles are not different in terms of chemistry nor condensation degree.

From the DRIFT spectra, the framework rearrangement that causes autohydrophobization is highly pronounced after treatment of the R-particles at 450°C. Next to the intense vibration peaks of the methyl groups, CH_3 stretching at 2968 cm^{-1} and CH_3 bending at 1265 cm^{-1}, the silanol peak is sharply reduced at 3725 cm^{-1} and the broad band between 3800 and 3200 cm^{-1}, originating from adsorbed or incorporated water molecules, has disappeared completely, hence the autohydrophobization.

Despite the drastic framework rearrangement, microporosity is not reduced to the same extent as for the hydrothermal treatment (**Table 9.5**, isotherm **Figure 9.24**). Given that S_{BET} and especially the V_p have also decreased, it is assumed that the thermal treatment has produced

a denser network in contrast to the hydrothermal treatment where the pores are expanded and an increase in V_p is observed. Therefore, both results combined, it is unlikely that the framework rearrangement causes reduction of S_μ without a redepositioning process taking place.

9.6.4 The hydrolytic treatment: pore and particle size reduction

Apart from the hydrothermal treatment, samples of R particles are subjected to a range of hydrolytic treatments in a NaOH solution at

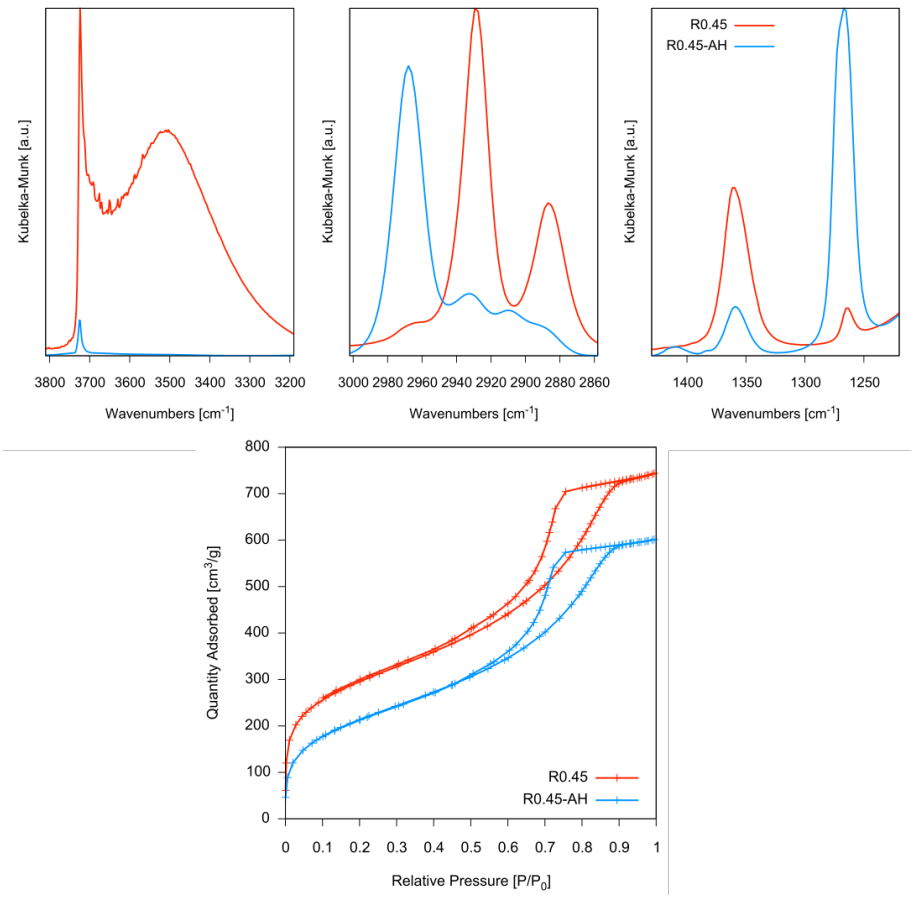

Figure 9.24: DRIFT spectra of thermally treated R samples. The Si-OH stretch vibration is observed at 3725 cm^{-1}, the CH_3 stretching at 2968 cm^{-1}, the framework CH_2-bending at 1360 cm^{-1} and the CH_3 bending at 1265 cm^{-1}. N_2 sorption isotherms of R0.45 before and after AH treatment.

room temperature (25°C). The N_2 sorption results, summarized in **Table 9.6** (isotherms **Figure 9.25**), show that the mesoporous spheres remain fairly unchanged when subjected to a 24 h treatment at pH 0, pH 12 and pH 12.5, again indicating the exceptional hydrolytic stability of the ring-structured siloxane framework. Now, when subjected to even higher hydrolytic stress (pH 13), a decrease in pore size is clearly observed from 10.7 nm to 8.8 nm after 24 h, and even to 4.0 nm after 72 h. Together with this, the pore volume drops and microporosity increases, which is exactly the opposite as witnessed for the harsh hydrothermal treatment at 200°C.

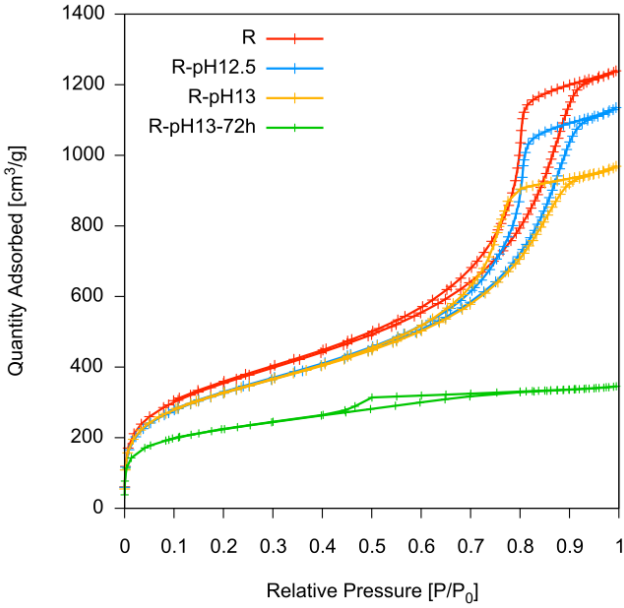

Figure 9.25: N_2 sorption isotherms of R-samples hydrolytically treated for 24 h at pH 12.5 (R-pH12.5), pH 13 (R-pH13) and treated for 72 h at pH 13 (R-pH13-72h).

Table 9.5: N_2 sorption and elemental analysis data of R samples thermally treated at 450°C in N_2 atmosphere to induce autohydrophobization.

	S_{BET} [m^2/g]	S_μ [m^2/g]	V_p [ml/g]	$d_{p,BJH}$ [nm]	%C
R0.45	1041	181	1.15	7.5	18.8
R0.45-AH	770	97	0.93	7.3	19.0

Table 9.6: N_2 sorption and elemental analysis data of R samples hydrolytically treated at pH 0 for 72 h; pH 12, 12.5 and 13 for 24 h and pH 13 for 72 h.

	S_{BET} [m^2/g]	S_μ [m^2/g]	V_p [ml/g]	$d_{p,BJH}$ [nm]	%C
R	1252	89	1.91	10.7	18.6
R-pH0-72h	1158	98	1.75	10.7	17.1
R-pH12.0	1232	123	1.86	10.3	16.6
R-pH12.5	1149	94	1.75	10.8	16.4
R-pH13.0	1044	99	1.50	8.8	16.4
R-pH13.0-72h	757	200	0.53	4.0	9.96

Now, where for the hydrothermal treatment a pore expansion arises due to partial dissolution of the organosilica, a pore size reduction at high pH is less evident as 'new' material should be deposited on the existing pore walls to densify the material. However, when comparing SEM images of R particles before and after severe treatment at pH 13 for 72 h, the particle size is also considerably decreased from 5.20 μm $\pm$ 1.67 to 3.73 μm $\pm$ 0.97 (**Figure 9.26**). Therefore, we suggest that during a purely hydrolytic treatment at room temperature, the outside of the organosilica spheres indeed dissolves, but that under these conditions, at least some of the organosilicate species in solution is redeposited inside the mesopores thus reducing the pore size.

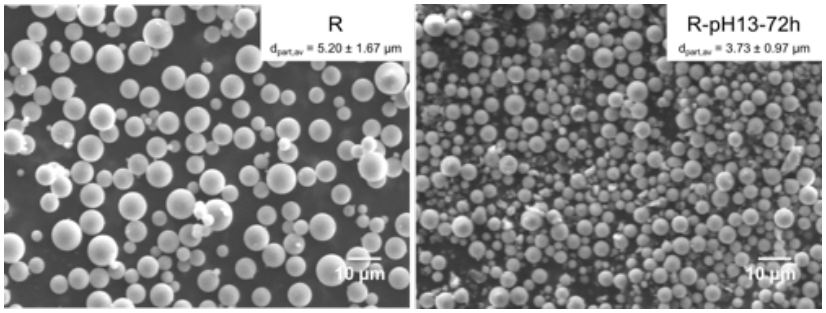

Figure 9.26: SEM images taken from R before and after hydrolytic treatment at pH 13 for 72 h. The average particle size ($d_{part,av}$) is determined from a population of 350 particles.

Finally, it must be noted that, the carbon content of the material drops significantly for R-pH13.0-72h, in contrast with a 24 h treatment, while in both cases the DRIFTS spectrum remains fairly unchanged towards the as-synthesized sample (**Figure 9.27**). This indicates gradual framework deterioration as the Si-C bonds are completely cleaved without frame-

work rearrangement. This might also contribute to the drastic pore size reduction of R-pH13.0-72h.

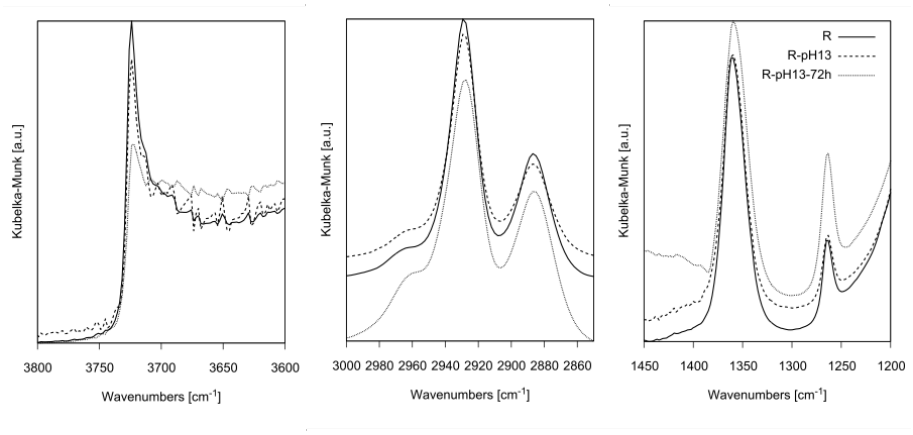

Figure 9.27: DRIFT-spectra of hydrolytically treated R-samples normalized over the framework CH_2-bending at 1360 cm^{-1} for comparison with the Si-OH stretch vibration at 3725 cm^{-1}, the CH_3 stretching at 2968 cm^{-1} and the CH_3 bending at 1265 cm^{-1}.

9.6.5 The combined HH treatment: an enhanced hydrothermal treatment inducing pore morphology changes

Both above post-treatments are combined and the N_2 sorption results of the obtained materials are given in **Table 9.7**. In this procedure, NaOH is replaced by NH_3 to avoid the possible inclusion of a metal ion in the organosilica framework, something undesired in chromatography [319]. Comparing R and R-HH, a similar effect as a harsh pure hydrothermal treatment (cfr. 200°C) is found, given that the pore size of the treated sample increases from 12.1 to 16.0 nm while S_{BET} and S_μ drop significantly. Also, in the DRIFT spectrum of R-HH, clear self-hydrophobisation is observed, which is more pronounced than for R-160C but less distinct than R-200C (**Figure 9.20**). Therefore, it seems that the addition of a base enhances the effect of the hydrothermal treatment and not vice versa.

Now the HH treatment is also applied to W/O organosilica spheres with ethylene- and phenylene- bridged siloxane networks, E and B respectively. Although DRIFT spectroscopy does not show any clear indication of framework rearrangement for both materials (**Figures 9.59 and 9.60**), the porosity is affected in a similar way as R, albeit more drastically in the case of E, indicating the latter is less stable under

Table 9.7: N_2 sorption and elemental analysis data of the organosilica samples subjected to a combined hydrothermal/hydrolytic (HH) treatment (120°C - pH 12 - 24 h).

	S_{BET} [m^2/g]	S_μ [m^2/g]	V_p [ml/g]	$d_{p,BJH}$ [nm]	%C
R	1214	127	1.94	12.1	18.6
R-HH	701	25	2.00	16.0	18.8
E	890	98	0.99	7.0	17.3
E-HH	288	0[a]	1.01	15.0	16.9
B	736	130	0.91	4.4	35.4
B-HH	522	0[a]	1.01	7.2	38.3

[a]Negative micropore volume obtained via t-plot method.

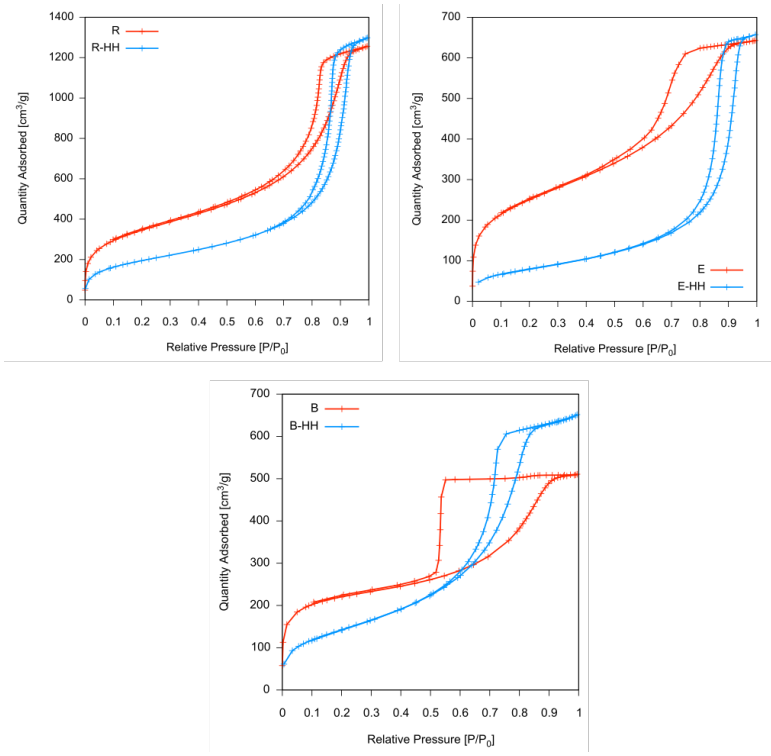

Figure 9.28: N_2 sorption isotherms of $[Si(CH_2)]_3$-brigded W/O organosilica spheres before (R) and after combined HH treatment (R-HH), of an ethyl-bridged spherical organosilica particle before (E) and after a combined hydrothermal/hydrolytic treatment (E-HH) and of phenylene-brigded W/O organosilica spheres before (B) and after combined HH treatment (B-HH).

the conditions applied. Now, where R and E (as-synthesized), both yield a mesoporous material with a Type IV H1 isotherm indicating a relatively uniform pore network (**Figure 9.28**), we found that B showed a Type IV H2 isotherm, suggesting large 11.2 nm pores (determined BJH on adsorption isotherm) with narrowed 4.4 nm openings (desorption isotherm).

Interestingly, via this HH treatment we were able to restructure this porosity of B into a Type IV H1 isotherm with uniform pores of 7.2 nm. According to what is known for silica gel, this restructuring may be due to dissolution of the organosilica where the pore walls have a larger curvature (large-narrow pore system) and redeposition of the dissolved organosilica favoring the elimination of this same curvature [19]. Eventually, such process attains thermodynamically favored cylinder-like pores as the surface of the pore walls is now minimized (**Figure 9.29**). For all HH post-treated samples, no significant loss of carbon is witnessed (**Table 9.7**), and the particle size and morphology remains unchanged (**Figure 9.30**).

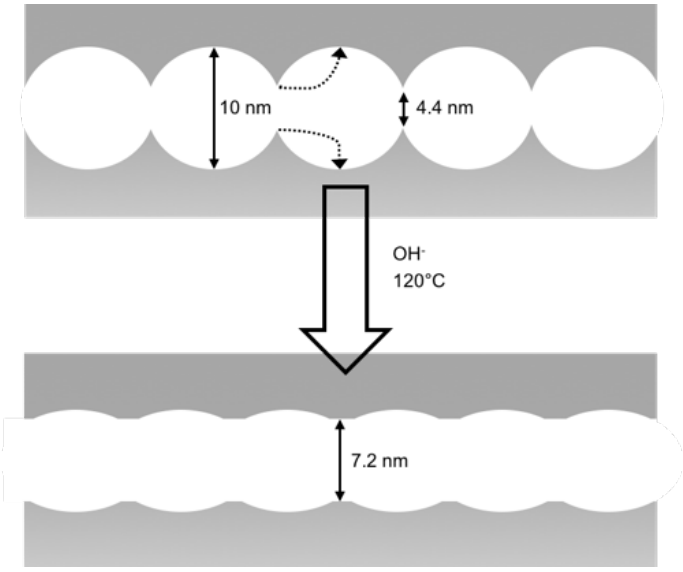

Figure 9.29: Schematic representation of the hydrolytic pore reconstruction process witnessed for a phenylene-bridged organosilica particle.

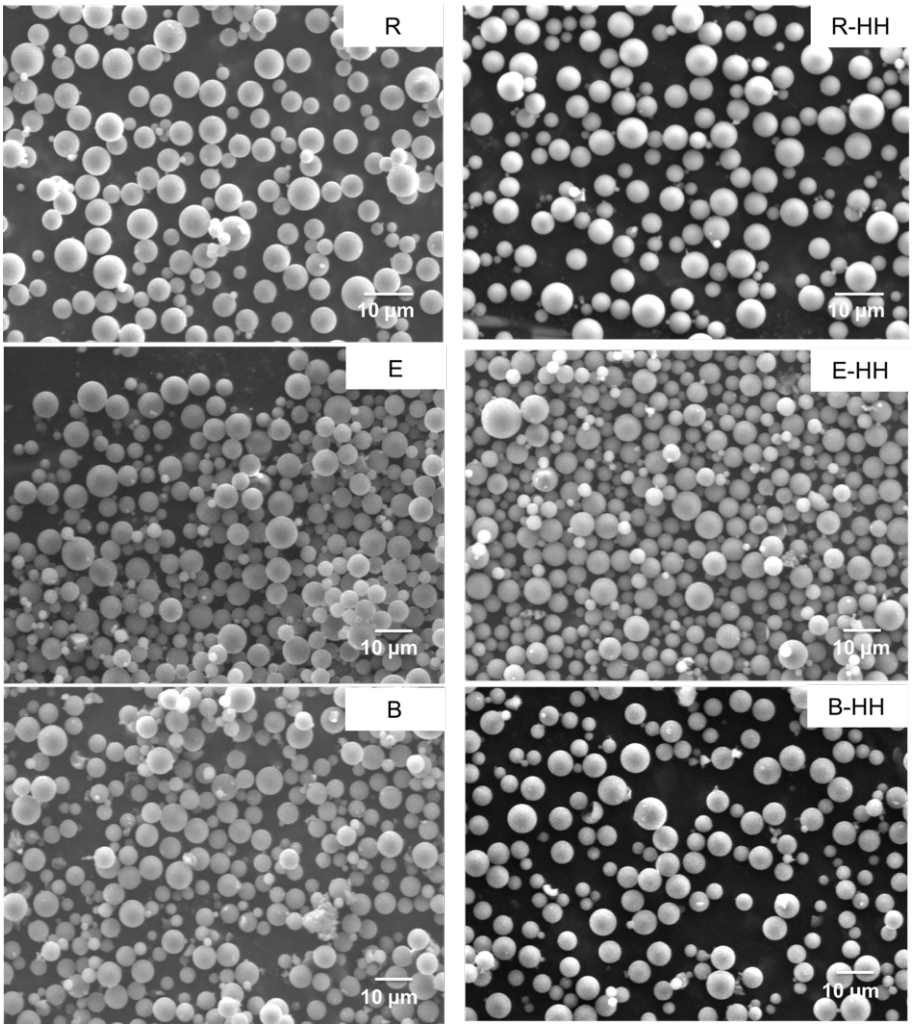

Figure 9.30: SEM images of $[Si(CH_2)]_3$ ring- (R), ethyl- (E) and benzyl- (B) functionalized spherical organosilica particles before (left) and after a combined hydrothermal/hydrolytic treatment (right, HH).

9.7 Development of AR-particles for RP-HPLC

One of the most interesting results of all the above experiments is the drastic reduction in pore volume of the spherical particles when a mixture of HETSCH and AHETSCH is employed in the W/O-based synthesis. This fortunate occurrence, most likely linked to more extended oligomerization of the precursors before the organosilica gel is formed, might remove the issues concerning mechanical stability of the particles during reverse-phase analyses. As it was our initial goal to incorporate the allyl groups as functional handle for pH stable click modification of the surface, investigation of the AR particles as chromatographic packing is highly anticipated. Combining all the knowledge generated above, an experimental procedure is developed (**Figure 9.31**).

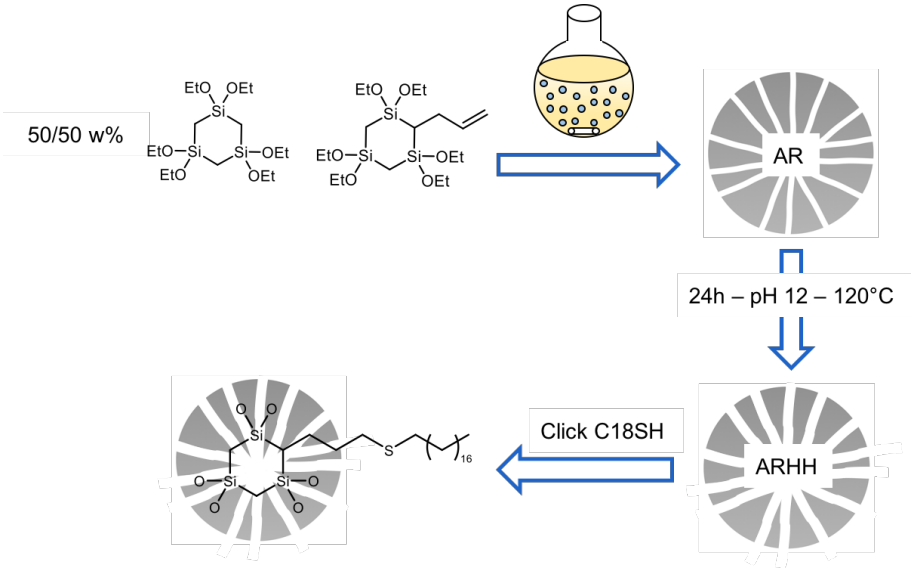

Figure 9.31: Overview of the synthesis procedure for ARHHC18.

9.7.1 Experimental

General synthesis of spherical allyl-[Si(CH$_2$)]$_3$-interconnected ring organosilica gel (AR). In a typical synthesis, 0.1 g of Tylose MH300 is weighed off and added to a 50 ml glass flask with a 25 mm long, 6 mm diameter Teflon-lined stirring bar. Hereto, 28 ml of benzylalcohol is added. Using a Pasteur pipette, 0.45 g of a 8 w% HCl solution is weighed off in the flask. Then, extra H_2O is added until the aqueous phase reaches 8.23 ml. Now, the flask is closed with a glass stopper and

is placed in an oil bath at 60°C and magnetic stirring is applied at a rate of 1500 RPM for 30 min. Almost immediately a white emulsion is formed.

Now, a pre-weighed amount 2-allyl-1,1,3,3,5,5-hexaethoxy-1,3,5-trisilacyclohexane (AHETSCH) is homogenized with 1,1,3,3,5,5-hexaethoxy-1,3,5-trisilacyclohexane (HETSCH) in a separate vessel and thereafter the mixture is added at once while stirring. After stirring for 1 more minute, the agitation is switched off and the flask is left under static conditions for 30 min. No change, e.g. phase separation, is observed. After this, stirring is continued at 200 RPM for 22 h, maintaining a temperature of 60°C. Then, the emulsion containing the spherical organosilica particles is filtered off, and washed copiously with H_2O (5 x 100 ml) and acetone (3 x 100 ml). Finally, the white product is dried for 10 min at 120°C in air, followed by a drying step under vacuum for 16 h at 120°C.

Hydrothermal/hydrolytic treatment (ARHH). Both aqueous post-treatments, described above, are combined by weighing off the porous AR particles and adding these to an aqueous NH_3-solution (1 ml / 0.1 g AR) at pH 12 in a Teflon-lined autoclave. Then, the autoclave is put in an oven at 120°C for 24 h and the treated particles are filtered, washed with 3 x 20 ml H_2O, 3 x 20 ml acetone and dried for 10 min at 120°C in air, followed by a drying step under vacuum for 16 h at 120°C. After this, classification of the particles is performed as described in Section 9.4. The obtained material is denoted as ARHH.

Click modification of the allyl-group with 1-octadecanethiol (ARHHC18). To efficiently transform the allyl-groups of ARHH into C18-chains advantageous for RP-HPLC, 0.55 g of ARHH (after sedimentation) is put into a Schlenk flask under Ar atmosphere. In a solventless procedure, 6.8 ml of 1-octadecanethiol (C18SH) is added together with 0.068 g of 2,2-dimethoxy-2-phenylacetophenone (DMPA). Then the mixture is put in an UV reactor ($\lambda = 360$ nm) where it was gently stirred for 2.5 h. The powder is filtered and washed with 6 x 50 ml of acetone. Then in a separate step to remove leftover reactants, the particles are resuspended in 100 ml of pentane and shaken for 1 h. After filtration, the obtained powder, denoted ARHHC18, is dried under vacuum at 60°C.

Column packing procedure. ARHHC18 is packed using a Haskel air driven fluid pump in a 10 cm IDEX IsoBar column with an internal diameter of 2.1 mm, equipped with Parker ports with a 2.0 μm frit at the entry and a 0.5 μm frit at the exit using the following procedure: 0.5 g of ARHHC18 is suspended in 13 ml of a 50:50 mixture of hexane and isopropanol and subjected to ultrasound for 15 min to ensure good

dispersion of the particles. Subsequently, the slurry was attached to the high pressure pump and the columns are packed at 800 bar for 15 min. Then the pressure was gradually released over another 15 min.

Chromatographic setup. All separations were performed using an Agilent 1100 series HPLC system equipped with a degasser, a binary pump, an auto-sampler with fixed injection volume of 2 μl for all experiments, a column thermostat and a variable wavelength detector (VWD) UV detector set at $\lambda = 210$ nm. Evaluation of the column stability at high temperatures was performed using a Selerity Technologies Polaratherm Series 9000 column oven. A mobile phase preheater was used with an offset of +10°C compared to the oven temperature.

Chromatographic evaluation at neutral pH of the ARHHC18 column. Using CH_3CN an water as mobile phase (v/v 30/70) the standard test mixture in **Table 9.8** is separated at 25°C.

Table 9.8: Composition of the standard test mix

	Compound	ppm
1	Uracil	20
2	Caffeine	100
3	Pyridine	2000
4	Aniline	100
5	Phenol	100
6	Acetophenone	100
7	Benzene	500
8	Propylparaben	100
9	Toluene	500

Hydrolytic stability of the ARHHC18 column at high pH. High pH column stability tests are performed using a mobile phase consisting of acetonitrile and a triethylamine (TEA) solution set at pH 12. The column, thermostatted at 60°C, was first purged with 100% acetonitrile for 30 min at a flow rate of 0.2 ml/min, followed by a 1000 min purge of the mobile phase CH_3CN/TEA-sol (v/v 30/70). After this treatment, the column is returned to neutral conditions and the standard test mix is evaluated. This cycle is performed 5 times.

Hydrolytic stability of the ARHHC18 column at low pH. For column evaluation at low pH, a test mix containing organic acids (**Table 9.9**) is separated at 25°C with a mobile phase of CH_3CN and a 0.1 v% TFA solution in water (pH 1.90). Column stability tests are performed using a mobile phase consisting of acetonitrile and a 2 v% trifluoroacetic acid (TFA) solution (pH 0.85). The column, thermostatted at 60°C,

was first purged with 100% acetonitrile for 30 min at a flow rate of 0.2 ml/min, followed by a 1000 min purge of the mobile phase CH_3CN/TFA-sol (v/v 15/85). Afterwards, the column is returned to the initial conditions for separation of the acid test mix and a new analysis run is performed (5 cycles).

Table 9.9: Composition of the acid test mix

	Compound	ppm
1	Aspirin	20
2	Salicylic acid	10
3	3,5-Nitrobenzoic acid	10
4	p-Toluic acid	20
5	Cinnamic acid	20

Hydrothermal stability of the ARHHC18 column. Using a dedicated column oven with mobile phase preheater, the ARHHC18 column is first thermostatted at 100°C while a solvent flow is maintained. Then, the isocratic separation of an adapted standard test mix (**Table 9.8**) is performed using H_2O/CH_3CN (v/v 17/83) as the mobile phase. For these experiments, phenol and aniline are omitted from the analyte mix (see Section 9.7.6). Flow rates of 0.5, 1.0 and 1.5 ml/min are applied. To assess the long term hydrothermal stability of the column, a 20 h purging step is executed at 100°C with the analytical composition of the mobile phase (flow rate: 0.3 ml/min). Thereafter, the initial experiments are repeated.

Following the evaluation of the column at 100°C, the oven temperature is increased to 120°C and the isocratic separation of the adapted standard test mix is performed using H_2O/CH_3CN (v/v 14/86) as the mobile phase, with flow rates up to 2.0 ml/min. Still at 120°C, the column is again purged for 20 h with the analytical composition of the mobile phase (flow rate: 0.3 ml/min). Then, the separation experiments are repeated. Finally, the same evaluation of the column stability is performed at 140°C (v/v 11/89).

9.7.2 Structural and chemical properties of ARHHC18

Organosilica spheres carrying allyl-functionalized $[Si(CH_2)]_3$ interconnected rings are prepared with different amounts of precursor in analogy with the unfunctionalized R materials presented earlier. The results of the N_2 sorption experiments found in **Table 9.10** again indicate that pore size control is possible through the amount of precursor added.

Compared to the results for R in Section 9.3.4, this control is more subtle for the HETSCH + AHETSCH system provided that a change of 0.2 g of precursor added already gives rise to a pore size increase from 5.8 to 17.9 nm. All materials synthesized show a similar S_{BET} combined with an increased S_{μ}, yet they possess lower pore volumes as compared to their R counterparts with a similar pore size. To obtain a promising packing for chromatography, however, the microporosity needs to be eliminated, for example with the HH-process. As this procedure also further expands the pores, the AR particles prepared with 2.8 g of precursor are selected for further processing.

Table 9.10: N_2 sorption data of AR prepared with different amounts of precursor to influence the porosity.

m_{prec} [g]	S_{BET} [m^2/g]	S_{μ} [m^2/g]	V_p [ml/g]	$d_{p,BJH}$ [nm]
1 + 1	720	164	1.71	38.3
1.3 + 1.3	704	159	1.10	17.9
1.4 + 1.4	**748**	**158**	**0.74**	**5.8**
1.5 + 1.5	620	166	0.46	4.0

In **Table 9.11** the N_2 sorption data (isotherms in **Figure 9.32**) are presented after subjecting AR to a 24 h treatment at 120°C in a pH 12 NH_3-solution. As expected this has reduced the microporous surface area significantly with approximately 100 m^2/g. Furthermore, the initial 5.8 nm pores are now expanded up to 8.9 nm which is a practicable size for common separations of small molecules. In analogy with the investigations on the framework rearrangement of R, AR is also thermally treated at 450°C in a N_2 atmosphere. This led to a similar conclusion: such treatment indeed induces autohydrophobization yet does not close the micropores. Moreover, in the case of AR, the allyl groups are lost after the high temperature treatment.

Table 9.11: N_2 sorption data of AR, ARHH and ARHHC18.

	S_{BET} [m^2/g]	S_{μ} [m^2/g]	V_p [ml/g]	$d_{p,BJH}$ [nm]	$\%C$
AR	748	158	0.74	5.8	23
ARHH	556	60	0.90	8.9	24
ARHHC18	231	0[a]	0.55	7.0	32

[a]Negative micropore volume obtained via t-plot method.

Click modification of the allyl groups with a C18-group via a stable thioether bond is confirmed with DRIFTS (**Figures 9.33 and 9.34**). Clearly more CH_2 and CH_3 functionalities are present after the at-

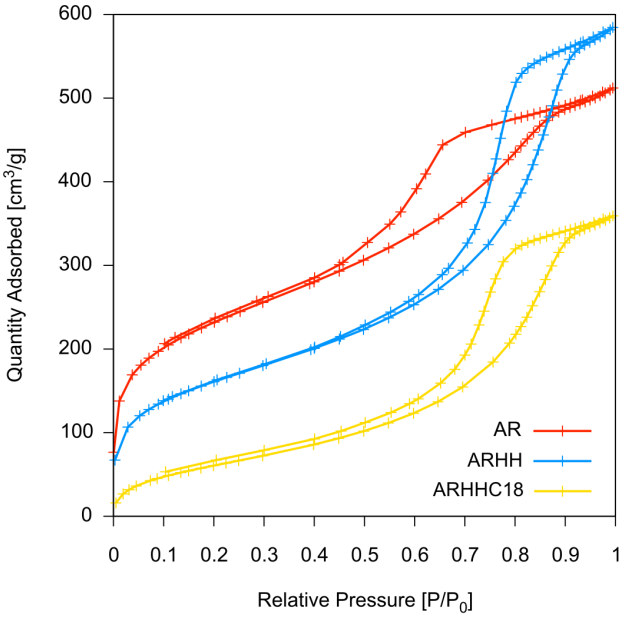

Figure 9.32: N_2 sorption isotherms of AR after the pore expansion - micropore reduction treatment (ARHH) and after subsequent modification of the allyl groups into long carbon chains (ARHHC18).

tachment C18SH with all associated vibration peaks in the aliphatic C-H stretch region (3000 cm^{-1} - 2800 cm^{-1}) and C-H bending region (1500 cm^{-1} - 1250 cm^{-1}) having a significantly increased intensity. The vibrations arising from the allyl groups, the olefin C-H stretch, C=C stretch and olefin C-H out of plane deformation at 3070, 1640 and 890 cm^{-1} respectively do not disappear completely after the click reaction. This might indicate that some allyl groups are nestled inside the organosilica framework where they cannot be reached by C18SH. Also witnessed from the DRIFT spectra is the framework rearrangement after the HH treatment with the CH_2-bending vibration at 1360 cm^{-1} of the as-synthesized material, clearly shifting to the signal for end-standing methyl groups (CH_3 bending at 1265 cm^{-1}).

The successful attachment of C18SH is also confirmed indirectly by N_2 sorption where the increased mass of the anchored C18 group causes an apparent drop of the surface area and pore volume (**Table 9.11**). Furthermore, the new hydrocarbon layer reduces the pore size slightly to 7.8 nm while the C18 chains seemingly block the remaining micropores. Whether the surface modification effectively closes off the micropores for analytes in RP-HPLC or only hamper the adsorption of nitrogen is, however, source for debate.

CHNS analysis also shows an increase from 24 w% to 32 w% in carbon content after the click reaction. Via the amount of sulphur contained by ARHHC18 the effective C18 loading is determined to be 0.37 mmol C18 per gram of ARHHC18 which is equivalent to 0.66 $\mu mol/m^2$ or 0.40 C18-chains/nm^2.[4] This loading is relatively low as compared to commercial materials bonded with grafted C18-groups that can have a loading up to 3.0 $\mu mol/m^2$ [254]. On the other hand, a similar loading is obtained as compared to the Yu paper disclosing C12-chains attached via an ether bond with the connotation that here only 50% of the material's framework contains reactive allyl groups [382].

A final parameter to be investigated before packing is the morphology and particle size of ARHHC18 (**Figure 9.35**). From the SEM image spherical particles with a mean size of 4.55 μm are found, while a dispersity on the particle size ($D_{90/10}$) of 2.16 is deducted. This latter value is the only property of ARHHC18 which, at this point, is not conform the requirements of a practicable chromatographic packing set in Section 6.2.6. Unfortunately, this is also the only parameter which is hard to control using the W/O emulsion method with mechanical

4. For the calculations of the loading per surface area, the initial S_{BET} of ARHH is taken and not S_{BET} of ARHHC18.

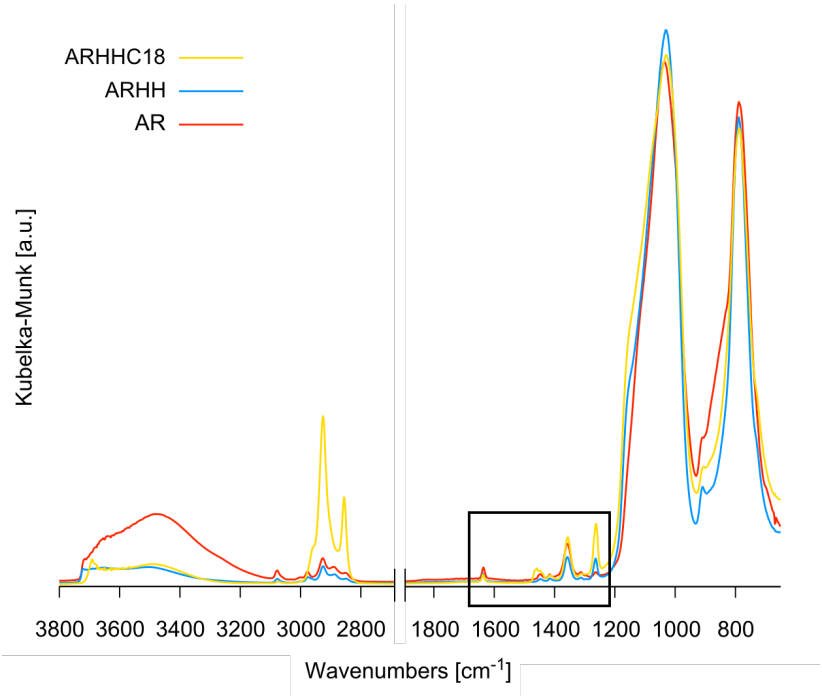

Figure 9.33: DRIFT spectra of the as-synthesized allyl-ring spheres, after hydrothermal-hydrolytic post-treatment and after modification with C18SH (AR, ARHH and ARHHC18). Characteristic C-H stretch vibrations of the aliphatic C-H bonds are found in the region 3000-2760 cm^{-1}, C-H bending vibrations are seen between 1450-1250 cm^{-1} and Si-O stretch vibrations are situated at 1100-1000 cm^{-1}. Vibrations at 3070, 1640 and 890 cm^{-1} arise from the allyl-groups (olefin C-H stretch, C=C stretch and olefin C-H out of plane deformation). The shift of the CH_2-bending vibration at 1360 cm^{-1} to a CH_3 bending vibration at 1265 cm^{-1} is testimonial for the framework rearrangement (ARHH). Clearly, after the click reaction, peak intensity of vibrations associated with C-H bonds increase (ARHHC18).

stirring. To assess the hydrolytic and mechanical stability of ARHHC18 these particles are packed and employed for separations at neutral, high and low pH and at temperatures above 100°C.

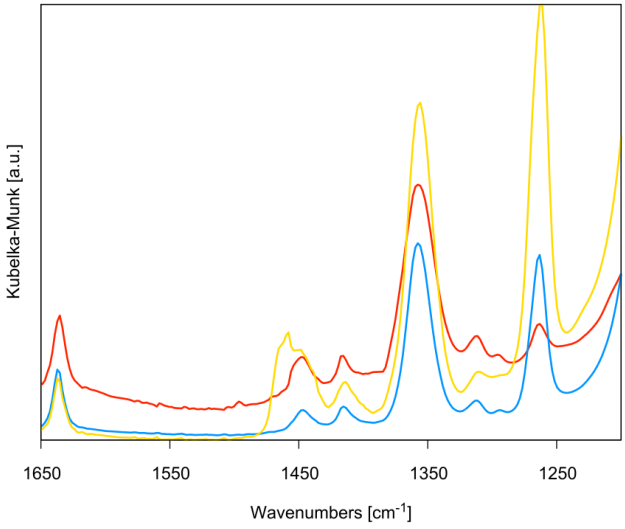

Figure 9.34: Zoom of the above DRIFT spectra (**Figure 9.33**) in the region of the C-H bending vibrations.

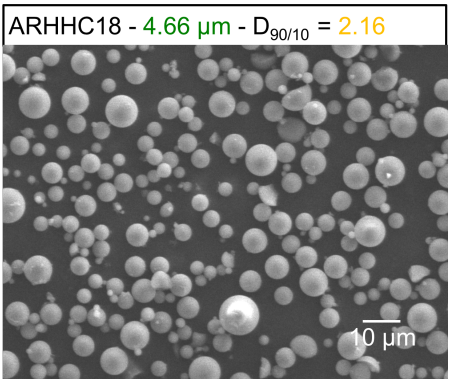

Figure 9.35: SEM image of ARHHC18 packed into a column for chromatographic assessment.

9.7.3 Column evaluation at neutral pH

Separation efficiency of the ARHHC18-column was assessed using a 9 component test mixture containing uracil (1) as unretained marker; caffeine (2), acetophenone (6), benzene (7), propylparaben (8) and toluene (9) as neutral hydrophobic compounds; pyridine (3) and aniline (4) as basic components, while phenol (5) was added as a molecule that is difficult to separate from aniline. In contrast to columns packed with emulsion-based $[Si(CH_2)]_3$-ring particles (Section 9.4), explorative chromatographic analyses in the presence of water did not result in a significant rise in column back-pressure. This is ascribed to the significantly lower pore volume of ARHH and ARHHC18 (V_p = 0.90 and 0.55 ml/g respectively) as compared to the 1.90 ml/g R particles. This again indicates the crucial role of the pore volume of the organosilica particles on the mechanical stability of the packing during analytical runs. As an indication, the ARHHC18 column back-pressure using 100% CH_3CN as mobile phase is 40 bar at a flow rate of 0.2 ml/min, while at optimal composition of the mobile phase, 30/70 CH_3CN/H_2O, a back-pressure of 107 and 212 bar is observed at flow rates of 0.2 and 0.4 ml/min.

An investigation towards the optimal linear velocity of the mobile phase, however, was indecisive as no distinct optimum for the column efficiency was found in the Van Deemter plot. Together with this, separation efficiency is poor and as a consequence significant peak broadening is observed. Plate numbers of 1782 and 1628, corresponding to a plate height of 56 and 61 μm, are determined for toluene (9) and acetophenone (6) at a flow rate of 0.2 ml/min 30/70 CH_3CN/H_2O. We believe that the reason for this five times higher plate height compared to the theoretic plate height (H_{th} = 4.55 x 2 = 9.1 μm), lies in the high dispersion on the particle size. $D_{90/10}$ of the ARHHC18 was determined at 2.16, even after a sedimentation procedure, while for commercially available, classified particles $D_{90/10}$ lies beneath 1.6 with most approaching a $D_{90/10}$ of 1.3. This has a significant influence on the packing efficiency[5] and thus Eddy diffusion coefficient (A). Furthermore, this also contributes to worsening of the C-term, as mass transfer of the analytes is less uniform. Next to this, the unoptimized packing procedure might also play a crucial role.

Nonetheless, good retention of the analytes is witnessed (**Figure 9.36**) even though the ARHHC18 particles have not been end-capped to enhance their hydrophobicity. Even aniline (4) and phenol (5) are separated using an appropriate solvent gradient (20/80 to 50/50 CH_3CN/H_2O over 30 min). Furthermore, the peaks of the basic analytes, aniline (4) and

5. No optimization of the packing procedure was performed.

especially pyridine (3), do not show peak deformation or additional base peak tailing as often witnessed for C18-grafted silica columns (**Figure 9.37**). Seen, we have not implemented any efforts to remove surface silanol groups, this is presumably due to the lower acidity of organosilica silanols (pKa $>$ 8) [323]. Next to this, the elution sequence slightly changes on our organosilica column, with the ARHHC18 column showing an increased affinity for propylparaben (8).

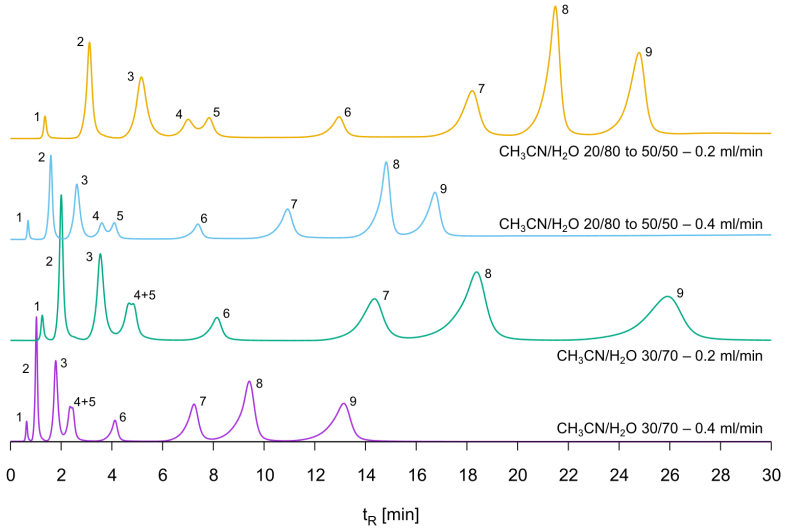

Figure 9.36: Chromatograms of the separation of the standard test mix under isocratic and gradient conditions on the home-made ARHHC18-column. (1) uracil, (2) caffeine, (3) pyridine (4) aniline, (5) phenol, (6) acetophenone, (7) benzene, (8) propylparaben, (9) toluene.

9.7.4 Hydrolytic stability of ARHHC18: high pH

Evaluation of the high pH stability of the ARHHC18 column was performed by flushing the column at 60°C with a mixture of triethylamine (TEA) in water with an effective pH of 12. It is believed that the presence of CH_3CN suspends the C18 chains in the mobile phase, leaving the surface available for hydrolytic attack, whereas for the use of 100% H_2O-phase, refolding of the dangling functionalities might protect the pore surface [315, 316]. Therefore, to ensure that the surface is subjected to the harsh hydrolytic conditions, the column stress tests were run at analytical conditions for the mobile phase, i.e. 0.2 ml/min 30/70 CH_3CN/TEA-sol. For each 1000 min, this corresponds to 925 column volumes.

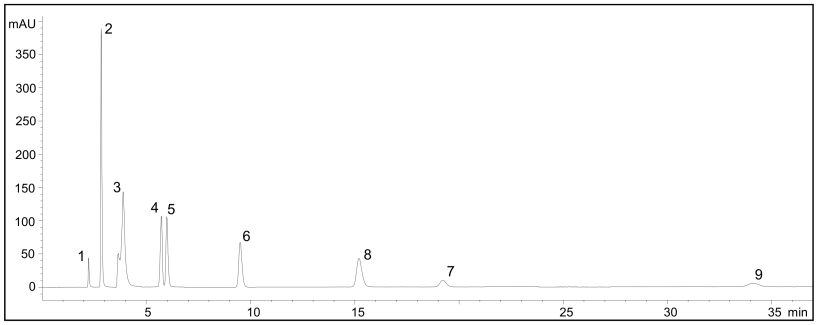

Figure 9.37: Standard test mix separation using a commercial 250 L x 4.60 mm ID x 5 μm Luna column (Phenomenex, Torrance, CA, USA), 40/60 CH_3CN/H_2O, 1.0 ml/min.

From **Figure 9.38** it is clear that no loss of retention is observed after exposing the ARHHC18 column to high hydrolytic stress. Not only does this indicate the exceptional stability of the organosilica material, it also proves that the thiol-ene click functionalization is stable at high pH. Moreover, from **Figures 9.39 to 9.41**, it is apparent that the peak shapes remain unaltered, which indicates that the analyte - stationary phase interaction, and thus the surface chemistry, remains unchanged after treatment.

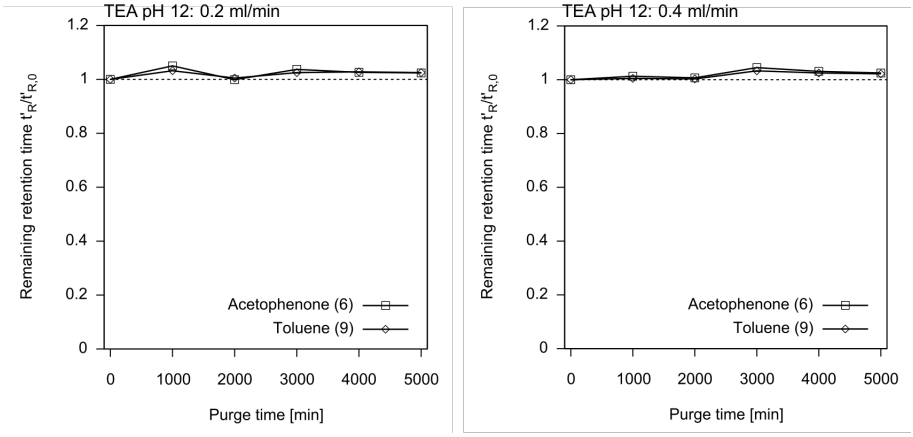

Figure 9.38: Change in the retention time t'$_R$ of acetophenone (6) and toluene (9) after purging the column at 60°C with 30/70 CH_3CN/TEA−solution set at pH 12 for up to 5000 min (4625 column volumes). Left: analysis runs at 0.2 ml/min, right: analysis runs at 0.4 ml/min.

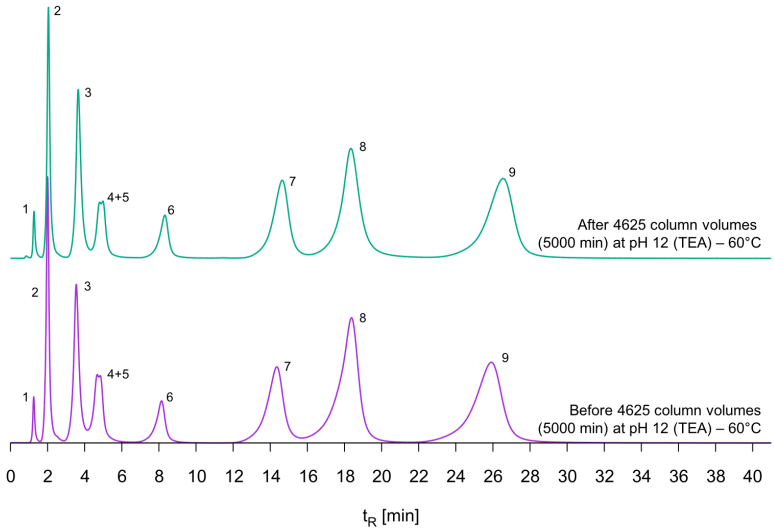

Figure 9.39: Comparison of the chromatogram of the standard test mix before and after subjecting the column to 5000 min at pH 12 and 60°C. Analysis conditions: 30/70 CH_3CN/H_2O, 25°C, 0.2 ml/min. (1) uracil, (2) caffeine, (3) pyridine (4) aniline, (5) phenol, (6) acetophenone, (7) benzene, (8) propylparaben, (9) toluene.

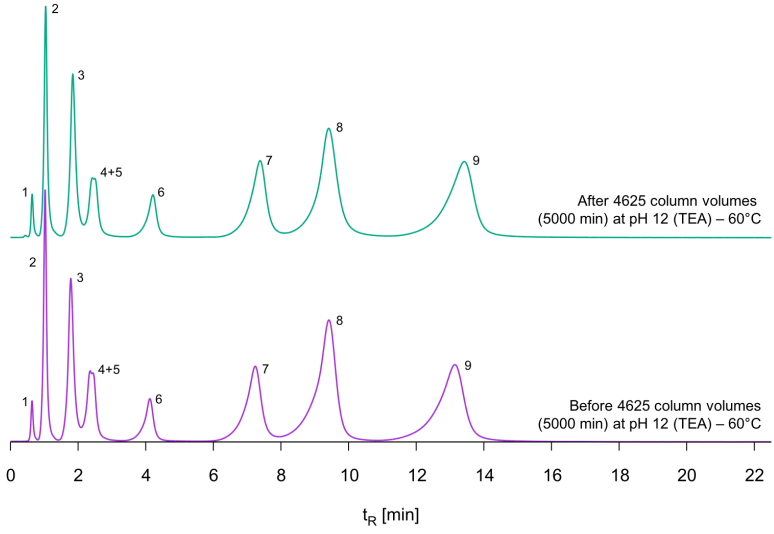

Figure 9.40: Comparison of the chromatogram of the neutral test mix before and after subjecting the column to 5000 min at pH 12 and 60°C. Analysis conditions: 30/70 CH_3CN/H_2O, 25°C, 0.4 ml/min

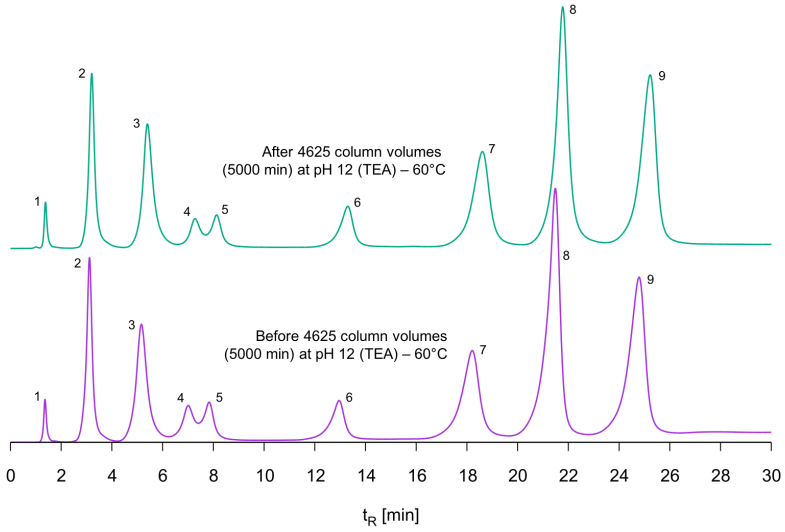

Figure 9.41: Comparison of the chromatogram of the neutral test mix before and after subjecting the column to 5000 min to pH 12 at 60°C. Analysis conditions: gradient from 20/80 to 50/50 CH_3CN/H_2O over 30 min, 25°C, 0.2 ml/min

9.7.5 Hydrolytic stability of ARHHC18: low pH

To evaluate to stability of ARHHC18 at low pH a new test mixture was developed containing organic acids as pharmaceutical mimics. The mix consists of aspirin (1), salicylic acid (2), 3,5-nitrobenzoic acid (3), p-toluic acid (4) and cinnamic acid (5) having a corresponding elution sequence (**Figure 9.61**). The importance of the mobile phase pH on the separation of organic acids is illustrated in **Figure 9.62**. At neutral pH, the components of the acid test mixture are deprotonated, which causes significantly decreased retention times and associated peak overlap due to low peak resolution. When analyzed at low pH (0.1 v% TFA in H_2O $\sim$ pH 1.90), the organic acids are in their protonated, non-ionic form, and can nicely be retained and separated.

For our stability tests, we adapted and applied a low pH procedure which has previously been used for accelerated column stability testing and for the complete stripping of a C18 grafted phase from porous silica particles [315, 316]. The ARHHC18 column was flushed with a 15/85 CH_3CN/2 v% TFA-solution in water with an apparent pH of 0.85. Purging of the column was performed at 60°C and 0.2 ml/min for a combined total of 5000 min or 4625 column volumes. Intermediate chromatographic runs were performed using 15/85 CH_3CN/0.1 v% TFA-solution in water as

the mobile phase. To make sure our investigations towards retention loss are not biased by the removal of end-capping groups[6], ARHHC18 was not treated with HMDS or trimethylchlorosilane to eliminate residual silanol groups.

Figure 9.42 again shows that the ARHHC18 column is stable under unprecedentedly harsh conditions, with no witnessed change in retention for the components of the acid test mixture after 5000 min. **Figures 9.43 and 9.44** meanwhile confirm that all component peaks preserve the same retention, and that no other interactions arise between analyte and column after treatment at low pH.

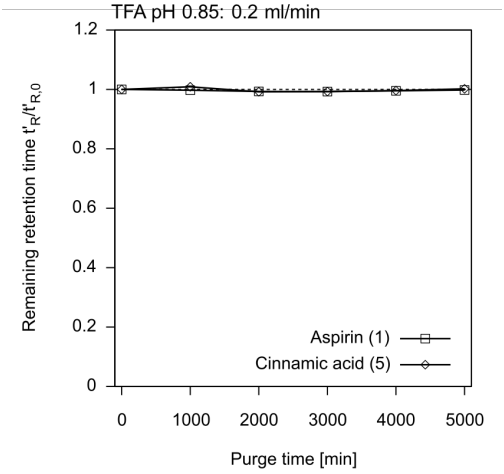

Figure 9.42: Change in the retention time t'$_R$ of aspirin (1) and cinnamic acid (5) after purging the column at 60°C with 15/85 CH_3CN/2 v% TFA-solution (pH 0.85) for up to 5 x 1000 min (4625 column volumes). Isocratic analysis runs at 0.2 ml/min 15/85 CH_3CN/0.1 v% TFA-solution (pH 1.90).

9.7.6 Hydrothermal stability of ARHHC18: Reducing analysis time

The relatively high viscosity of water at room temperature limits the flow rate of the mobile phase (u) in HPLC as high back-pressures arise, dependent of the column quality. To allow an increase of the mobile phase

6. The trimethylsilyl groups used to end-cap the silanol groups of the particle surface are bound through hydrolytically labile siloxane bonds. Therefore, when treated below pH 2, these are generally removed. Hereby, the additional surface hydrophobicity of the $(CH_3)_3Si$ group is lost, which likely causes a change in retention.

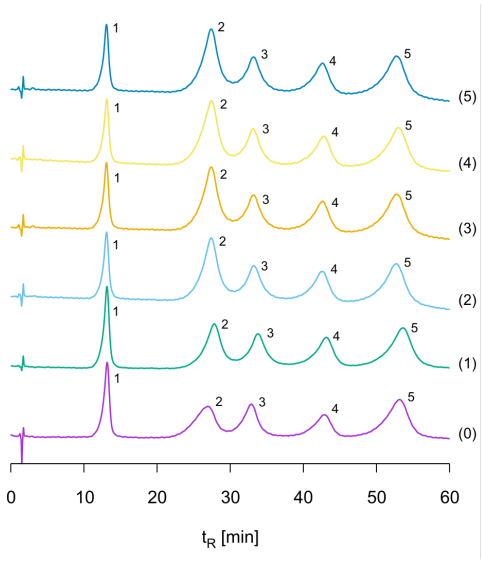

Figure 9.43: Comparison of the chromatograms of the acid test mix before and after subjecting the column to 5 x 925 column volumes at pH 0.85 and 60°C. Analysis conditions: 15/85 CH_3CN/0.1 v% TFA, 25°C, 0.2 ml/min. Aspirin (1), salicylic acid (2), 3,5-nitrobenzoic acid (3), p-toluic acid (4) and cinnamic acid (5).

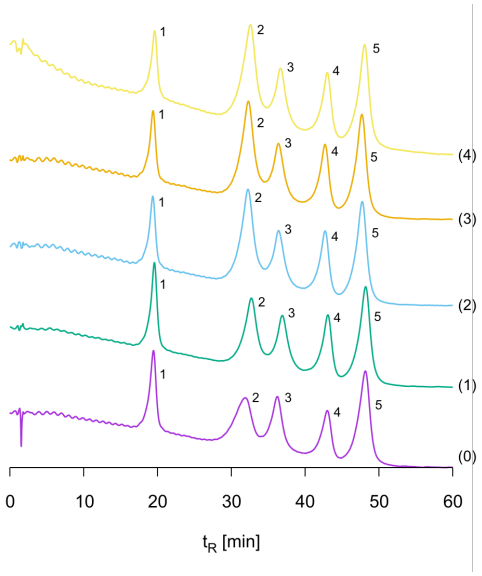

Figure 9.44: Comparison of the chromatograms of the acid test mix before and after subjecting the column to 5 x 925 column volumes at pH 0.85 and 60°C. Analysis conditions: gradient from 10/90 to 20/80 CH_3CN/0.1 v% TFA over 60 min, 25°C, 0.2 ml/min.

velocity and thus a reduced analysis time, elevated temperatures can be applied to reduce the column back-pressure. To do so, the hydrothermal stability of the stationary phase is key, hence, as a test procedure, the ARHHC18 column is subjected to high analysis temperatures using a dedicated column oven.

Firstly, it must be noted that during all performed screening experiments > 100°C, the peaks of aniline (4) and phenol (5) could not be resolved from the pyridine (3) peak. Therefore, both are omitted from the adapted test mixture. Seen in **Table 9.12**, separation of the standard test mix can be performed with a flow rate of up to u = 1.5 ml/min (327 bar), while at 120°C and 140°C, 2.0 ml/min can be attained with back-pressures of 357 and 309 bar respectively.

Table 9.12: Experimental data of the high-temperature HPLC using ARHHC18.

T [°C]	u [ml/min]	p_{in}[a] [bar]	p_{post}[b] [bar]	$t'_{R,in}$[c] [min]	$t'_{R,post}$[d] [min]
100[e]	0.5	107	104	7.691	7.649
	1.0	220	204	3.943	3.814
	1.5	327	312	2.716	2.516
120[f]	0.5	88	88	6.604	6.597
	1.0	176	177	3.305	3.330
	1.5	264	262	2.191	2.225
	2.0	357	350	1.638	1.647
140[g]	0.5	78	78	5.526	5.498
	1.0	155	159	2.807	2.873
	1.5	232	231	1.881	1.880
	2.0	310	309	1.418	1.421

[a]Column back-pressure before the 20 h flushing step, [b]Column back-pressure after the 20 h flushing step, [c]Effective retention time of toluene (9) before the 20 h flushing step, [d]Effective retention time of toluene (9) after the 20 h flushing step, [e]Mobile phase composition CH_3CN/H_2O 17/83 v/v, [f]14/86 v/v, [g]11/89 v/v

At 100°C, separation with the fewest peak overlap of the test mix is found for a mobile phase composition with 17% CH_3CN and 83% H_2O (v/v). This significant difference as compared to the separation at room temperature (30/70) is caused by the second main effect of increased solvent temperature on HPLC chromatography [322]: as the dielectric constant of water and CH_3CN/H_2O mixtures decreases with increased temperature, the elutropic strength of water increases [321]. As a result, gradually less organic modifier is required to perform the separation, allowing for increasingly green and cheap liquid chromatography. This

is further illustrated by the experiments at 120°C and 140°C, where an optimum in terms of peak resolution for the isocratic separation is found with a 14/86 v/v and a 11/89 v/v CH_3CN-H_2O mixture (**Figure 9.45**).

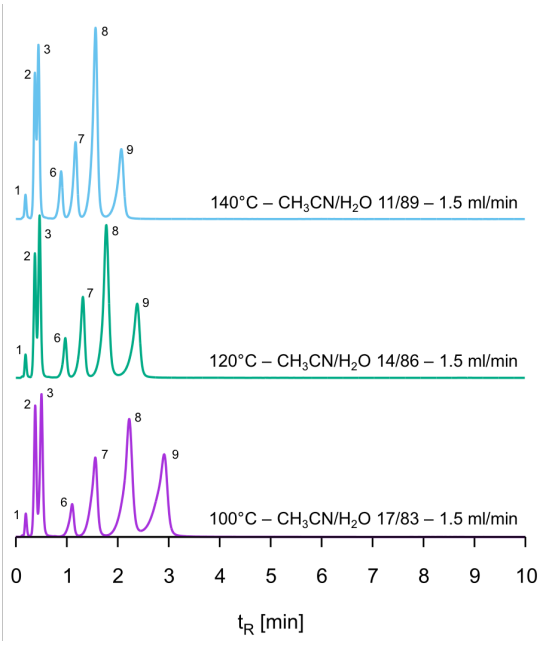

Figure 9.45: Chromatograms of the adapted standard test mix at optimal composition of the mobile phase at 100°C, 120°C and 140°C.

Figures 9.46 to 9.48, all indicate satisfactory separation of the analytes at variable conditions. At 140°C and using a flow rate of 2.0 ml/min, the test mix is evaluated in under 2 minutes, a dramatic decrease compared to analyses performed at room temperature. However, due to the poor quality of the packing and the low retention of the compounds, the caffeine and pyridine peaks progressively overlap at high flow rates.

For long-term use of the organosilica column, it is imperative that the ARHHC18 packing remains unchanged under these harsh hydrothermal conditions. To investigate this, consecutive stability tests are performed at 100°C, 120°C and 140°C. Separation is performed before and after a 20 h purging step with the mobile phase at the analysis temperature. This flushing procedure, combined with the analysis time, equilibration time and preliminary experiments, comes down to a 24 h column residence time per investigated temperature. Altogether, this is the equivalent of 432 subsequent injections (analysis time = 10 min). From **Figure 9.48**, it is appreciated that the ARHHC18 column is hydrothermally stable for 72 h, with a maximal investigated temperature of 140°C. No significant

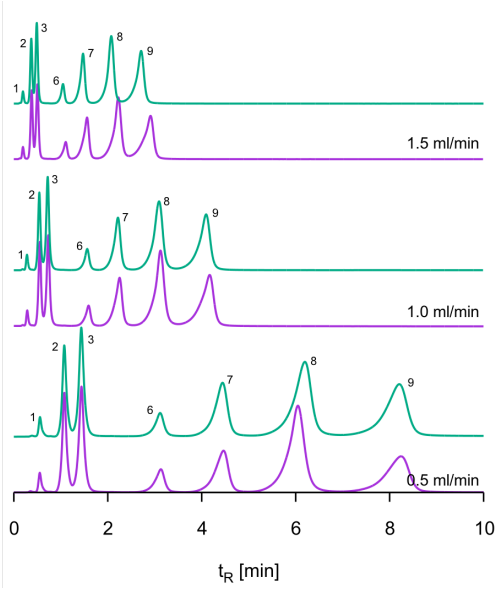

Figure 9.46: Chromatograms of the adapted standard test mix obtained with CH_3CN/H_2O 17/83 v/v at 100°C at variable flow rates before (bottom) and after (top) the hydrothermal flushing step.

changes in retention times or peak shape are observed, which, in line with the high and low pH testing, indicates that both the structural organosilica framework and the thiol-ene functionalization are conserved.

As definite proof for the overall stability ARHHC18 column, the initial standard test mix is again separated under the identical conditions described in Section 9.7.3, after being subjected to all stability tests. No noticeable reduction of the retention time is witnessed, even after the three separate, harsh treatments (**Figure 9.49**). Only the peaks of phenol (4) and aniline (5) completely overlap after all stability tests, which might point to minor peak broadening or slight loss of selectivity (**Figure 9.50**). Nonetheless, the peak shape remains similar before and after treatment. No change in column back-pressure was witnessed after all analyses. At 25°C, the initial back-pressure to separate the standard test mix was 107 bar, compared to 108 bar during the final separation . Finally, no cavitation was present at the column head when opening the ARHHC18 column after all experiments. All together, these results indicate that both the column and the particle surface are unchanged after being subjected for 4625 column volumes at pH 0.85, 4625 column volumes at pH 12, both at 60°C, and having resided for 6000 column volumes at temperatures above 100°C and up to 140°C.

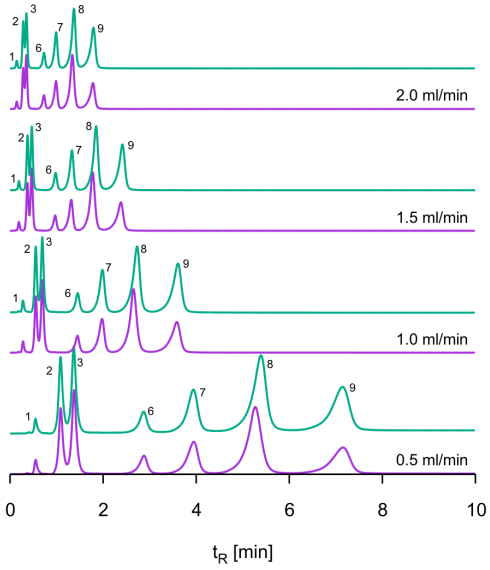

Figure 9.47: Chromatograms of the adapted standard test mix obtained with CH_3CN/H_2O 14/86 v/v at 120°C at variable flow rates before (bottom) and after (top) the hydrothermal flushing step.

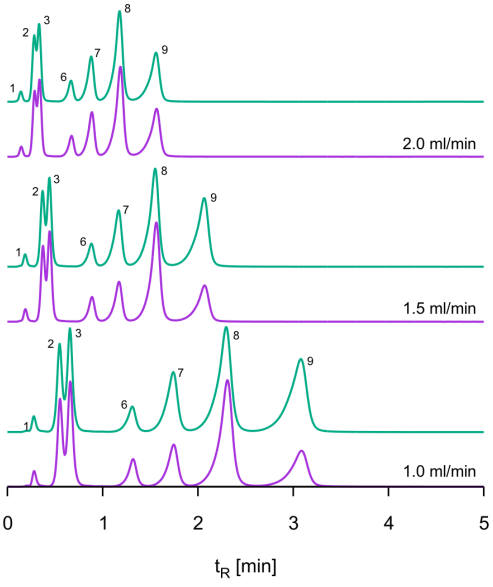

Figure 9.48: Chromatograms of the adapted standard test mix obtained with CH_3CN/H_2O 11/89 v/v at 140°C at variable flow rates before (bottom) and after (top) the hydrothermal flushing step.

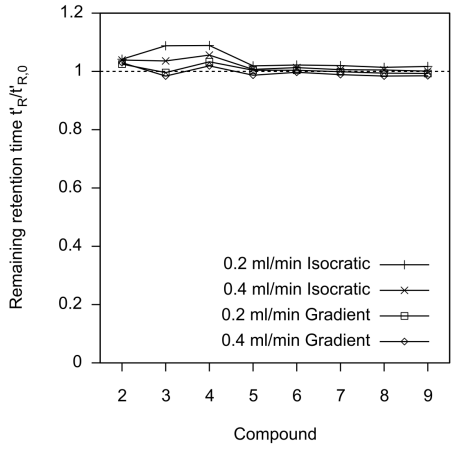

Figure 9.49: Change in the retention time t'$_R$ of the standard test mix compounds before (bottom) and after (top) all stability tests. Isocratic analysis runs 30/70 CH_3CN/H_2O, gradient from 20/80 to 50/50 CH_3CN/H_2O v/v over 30 min.

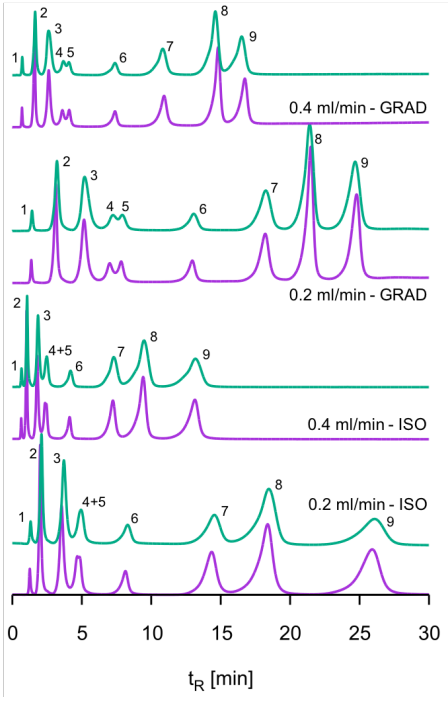

Figure 9.50: Chromatograms before (bottom) and after (top) all stability tests. Isocratic analysis runs (ISO) 30/70 CH_3CN/H_2O, gradient (GRAD) from 20/80 to 50/50 CH_3CN/H_2O v/v over 30 min.

9.8 Opportunities for improvement of the W/O method.

For these very first allyl-ring particles that are practicable in HPLC, the separation efficiency is still limited by the particle morphology and especially the dispersion on the particle size. Despite the packing being stable at extremely high temperatures, this size dispersion also limits the reduction of the analysis time, as it causes more pronounced column back-pressure.

Possibly, this morphology obtained in this work is already satisfactory for some selected applications in PREP-LC where stability is of primordial importance, and where the high surface area of the fully porous particles could allow for high sample loading. For application in analytical HPLC, however, the particle morphology needs to be improved to compete with commercial columns. Given that the particle morphology is directly influenced by the emulsion quality, synthesis of monodisperse particles requires monodisperse emulsion droplets. Mechanical stirring, whether or not combined with an Ostwald ripening step, is not considered as the most ideal method to obtain highly monodisperse emulsion droplets, however methods are described to 'purify' polydisperse emulsions via fractionation processes.

A first method is based on depletion interactions, i.e. an effective attractive force arising between colloidal particles that are suspended in a dilute solution. Described for an O/W emulsion, this is practiced by preparing the emulsion by means of mechanical stirring [424]. Thereafter, the emulsion is diluted by adding more of the continuous phase (H_2O) and leaving the emulsion until a cream layer is formed. Then, the dilute phase and cream layer are separated and more surfactant is added to the dilute phase causing new creaming to occur. After these operations have been done, a set of cream samples are retrieved with a high oil volume fraction. Each fraction is diluted again, and the process is repeated until monodisperse droplets are received [425]. This fractionated crystallization process is well-controlled and theoretically understood, however, it is quite fastidious to make use of it.

A second means of emulsion fragmentation is through shear rupturing. Herein, a premixed emulsion of large, polydisperse droplets can be ruptured into monodisperse emulsions of uniform colloidal droplets [426]. Using a specially designed shear cell or Couette cell with a controllable gap (**Figure 9.51**), the final droplet size is controlled by altering the shearing conditions and the emulsion's viscoelasticity, which depends on

its composition [410, 427]. Good results are obtained when the emulsion has a shear-thinning viscosity and if the gap of the shear cell is as narrow as 100 μm or less [411]. As residual polydispersity may be related to non-ideal flow, the applied shear rate must be well-controlled, thus a dedicated, yet commercially available setup is required [411, 428].

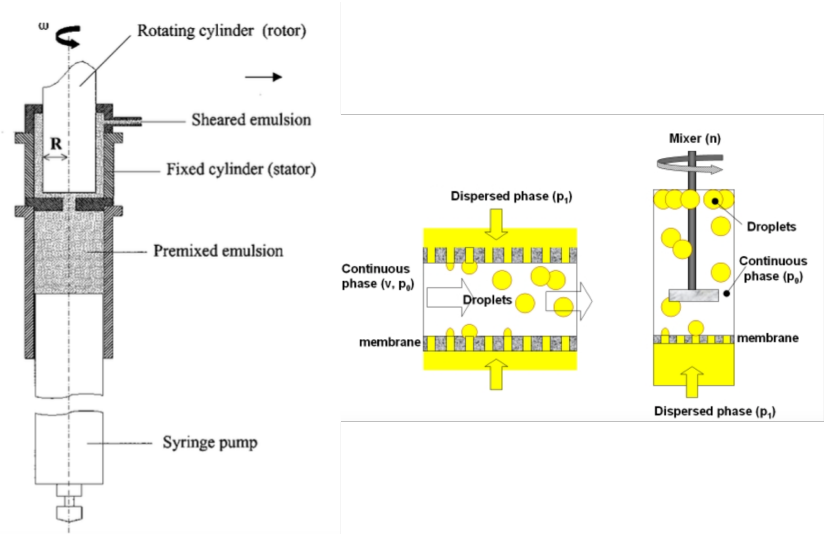

Figure 9.51: Schematical representation of a Couette cell and emulsion fragmentation by controlled shear rupturing (left, [411]). The membrane emulsification procedure using either a cross-flow of the continuous phase or stirring (right, [429]).

Alternatively, methods exist in which the dispersity of the droplets is meticulously controlled during the emulsification itself. All of these, be it membrane [413, 430–432], microchip or microchannel [412, 433] emulsification, rely on the injection of the disperse phase into the continuous phase through narrow openings with a highly uniform size. If the disperse phase is pushed through the opening at a constant rate, and if a constant shear rate along the opening is applied, all droplets detach at the same time in their growth process, thus resulting in monodisperse droplets (**Figure 9.51**). Given that all parameters, e.g. flow rate of the disperse phase and the shear force to break off the droplets, need to be highly uniform and controlled, again the technical requirements are high to realize monodisperse emulsions.[7] Using membrane emulsification,

7. We were not able to generate a monodisperse emulsion by means of a membrane using a primitive syringe adaptor and a syringe pump. This is ascribed to the insufficiently constant magnetic stirring, together with an irreproducible membrane to stirrer distance and the incompatibility of the adaptor with the acidity required

monodisperse spheres of mesoporous silica have been prepared [409, 415]. This clearly illustrates the viability of such emulsification approach to enhance the dispersion of the organosilica particles presented here.

Notwithstanding all the above methods are viable to obtain monodisperse emulsions, all of them require the optimization of a different type of W/O emulsion, extensive technical knowhow and/or dedicated setups for successful implementation. Such further developments, however, show high promise, and could finally give rise to highly competitive particles for HPLC column packings.

9.9 Appendix

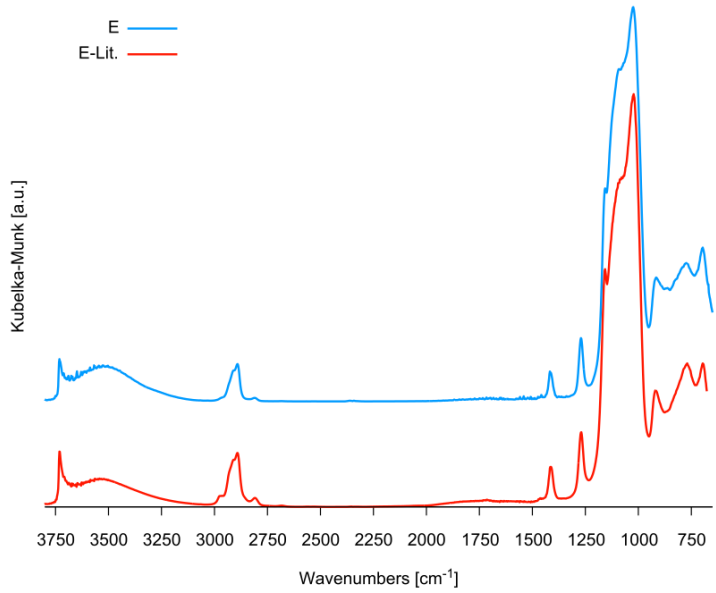

Figure 9.52: DRIFT spectra of an ethyl-bridged PMO (E-Lit.) [4, 5] and ethyl-bridged spherical mesoporous organosilica particles (E). Characteristic C-H stretch vibrations are found in the region 3000-2760 cm^{-1}, C-H bending vibrations are seen between 1450-1250 cm^{-1} and Si-O stretch vibrations are situated at 1100-1000 cm^{-1}. Vibrations lower then 1000 cm^{-1} are ascribed to typical framework vibrations for ethyl-bridged organosilicas. Silanol functionalities are present in the material given the SiO-H stretch vibration at 3740 cm^{-1}.

for the sol-gel reaction. Therefore, we could not optimize the procedure.

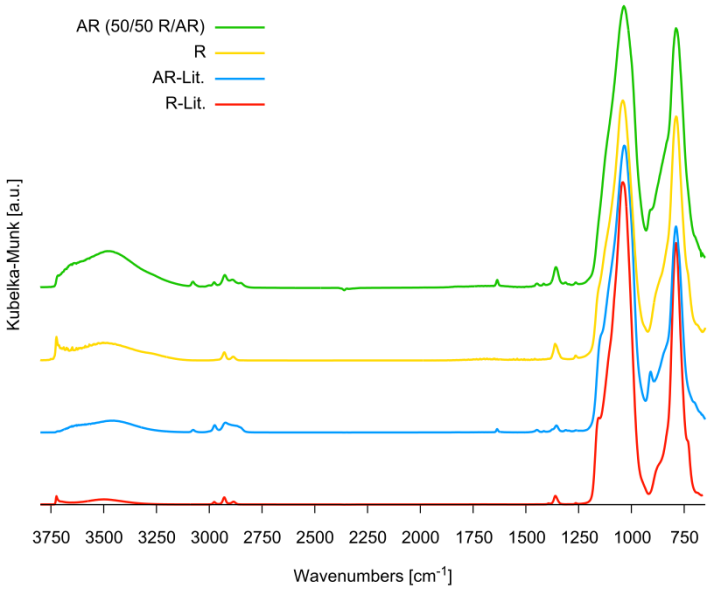

Figure 9.53: DRIFT spectra of a ring structured methyl-bridged PMO (R-Lit.) [41], an allyl functionalized ring structured methyl-bridged PMO (AR-Lit.) [423] and both materials as spherical mesoporous organosilica particles (R, AR). Characteristic C-H stretch vibrations of the methyl groups are found in the region 3000-2760 cm^{-1}, C-H bending vibrations are seen between 1450-1250 cm^{-1} and Si-O stretch vibrations are situated at 1100-1000 cm^{-1}. For the allylated material, clearly extra vibrations appear at 3070, 1640 and 890 cm^{-1} testimonial for the allyl-groups (olefin C-H stretch, C=C stretch and olefin C-H out of plane deformation). Additional C-H stretch vibrations at approx. 2900 cm^{-1} witnessed in R-Lit. and AR-Lit. are originating from leftover template used during PMO synthesis (P123). Some silanol functionalities are present in the material given the SiO-H stretch vibration at 3740 cm^{-1}.

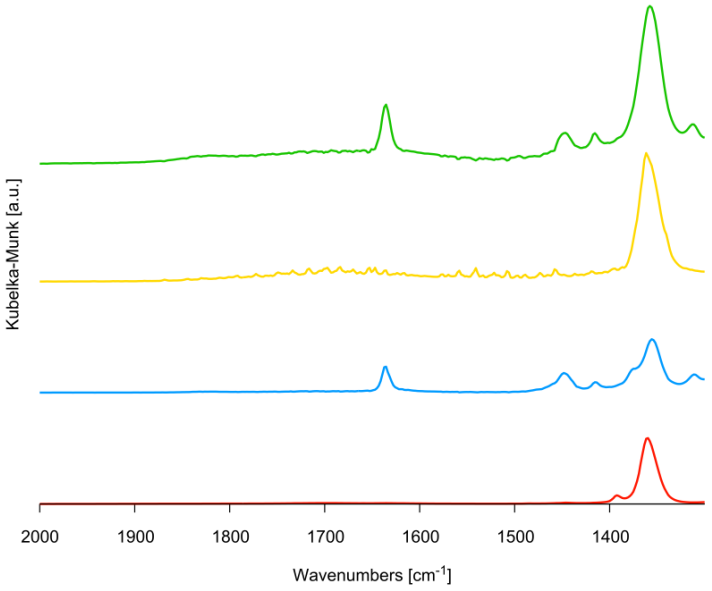

Figure 9.54: Zoom of R-Lit. (red), AR-Lit. (blue), R (yellow) and AR (green) in the 2000-1300 cm^{-1} region.

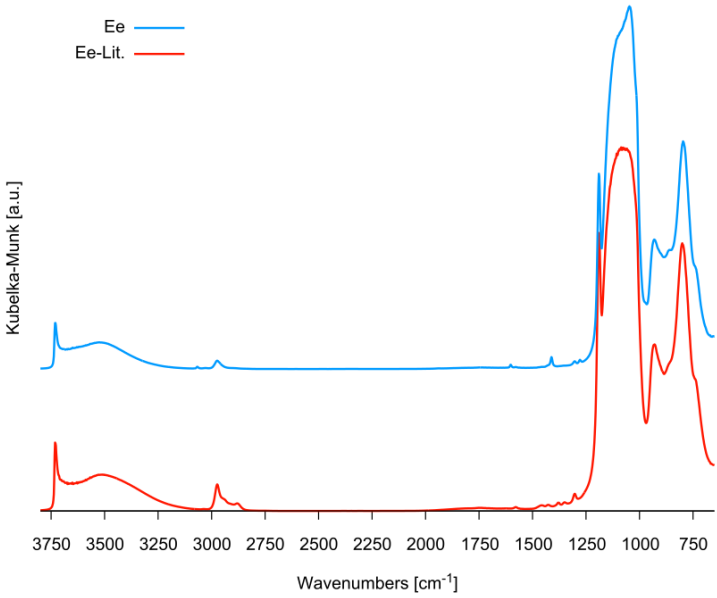

Figure 9.55: DRIFT spectra of an ethenyl-bridged PMO (Ee-Lit.) [169] and ethenyl-bridged spherical mesoporous organosilica particles (Ee). Vibrations at 3070, 1640 and 890 cm^{-1} are indicative for olefin C-H stretch and C=C stretch vibrations from the double bond. Characteristic Si-O stretch vibrations are situated at 1100-1000 cm^{-1}. Any additional C-H stretch vibrations at approx. 2900 cm^{-1} and C-H bend vibrations in the region 1500-1250 cm^{-1} in the IR spectrum of Ee-Lit. arise from leftover template used during PMO synthesis (P123). Silanol functionalities are present in the material given the SiO-H stretch vibration at 3740 cm^{-1}.

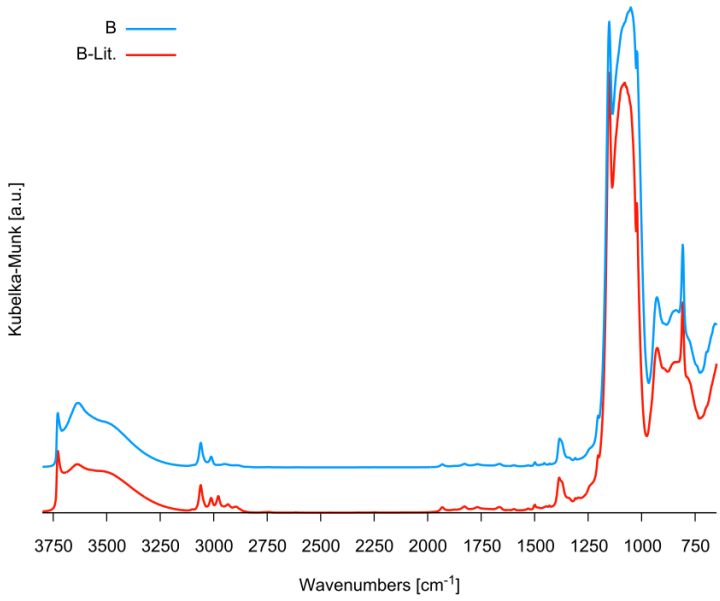

Figure 9.56: DRIFT spectra of benzyl-bridged PMO (B-Lit.) [78] and benzyl-bridged spherical mesoporous organosilica particles (B). Aromatic C-H stretch vibrations are seen between 3100-3000 cm^{-1}. Characteristic Si-O stretch vibrations and framework vibrations are situated at 1100-800 cm^{-1}. Any additional C-H stretch vibrations at approx. 2900 cm^{-1} in the IR spectrum of B-Lit. arise from leftover template used during PMO synthesis. Silanol functionalities are present in the material given the SiO-H stretch vibration at 3740 cm^{-1}.

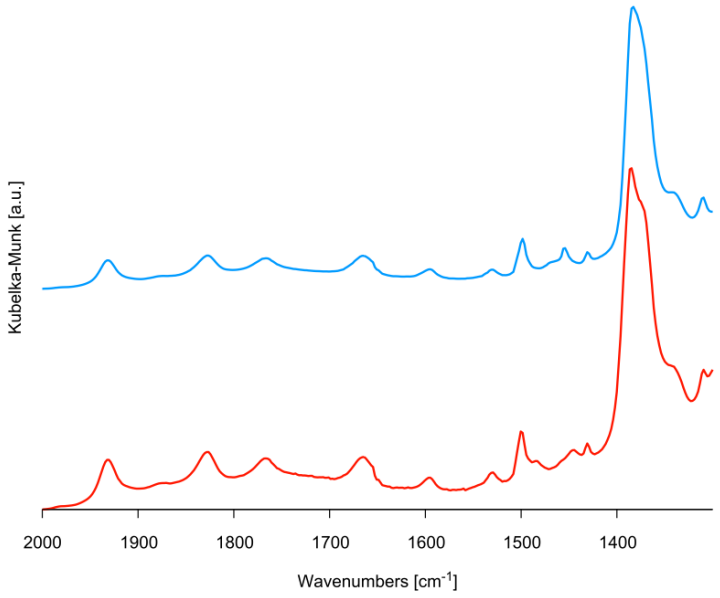

Figure 9.57: Zoom of DRIFT spectra of a benzyl-bridged PMO (red, B-Lit.) [78] and benzyl-bridged spherical mesoporous organosilica particles (blue, B) showing identical correspondence.

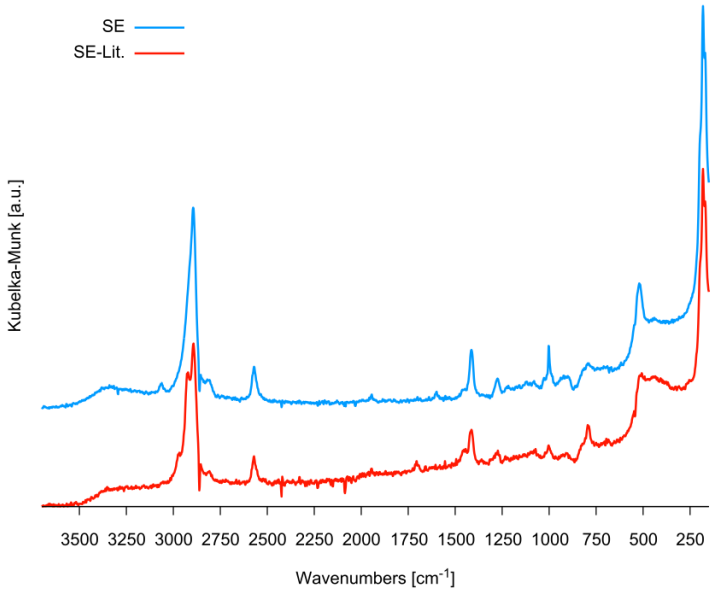

Figure 9.58: RAMAN spectra of a 50 w% ethyl - 50 w% thioethyl-bridged PMO (SE-Lit.) [133] and 50 w% ethyl - thioethyl-bridged spherical mesoporous organosilica particles (SE). C-H stretch vibrations are seen from 3000-2800 cm^{-1} and bending vibration are witnessed around 1400 cm^{-1}. At 2580 cm^{-1}, the S-H stretch vibration is observed, indicating incorporation of the thiol groups. However, at 500 cm^{-1}, also S-S stretch vibrations are present. This disulphide formation was reported and ascribed to the reaction conditions [133].

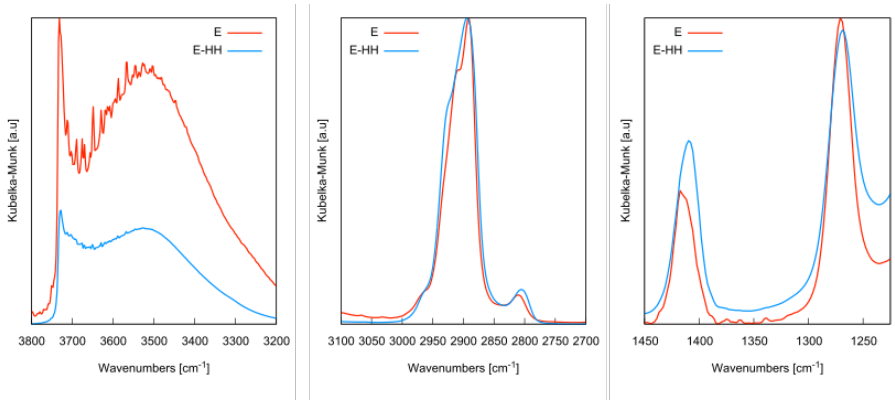

Figure 9.59: DRIFT spectra of ethyl-bridged spherical mesoporous organosilica particles before (E) and after hydrothermal/hydrolytic treatment (E-HH). Characteristic C-H stretch vibrations are found in the region 3000-2760 cm^{-1}, C-H bending vibrations are seen between 1450-1250 cm^{-1}. Silanol functionalities are present in the material given the SiO-H stretch vibration at 3740 cm^{-1}.

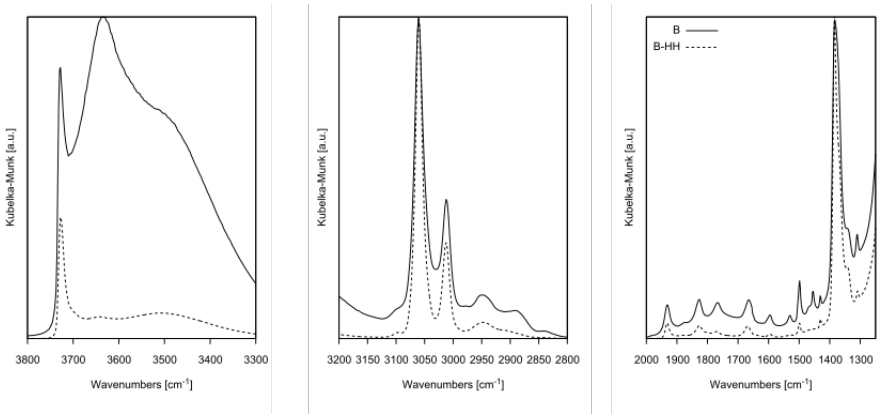

Figure 9.60: DRIFT spectra of benzyl-bridged spherical mesoporous organosilica particles before (B) and after hydrothermal/hydrolytic treatment (B-HH). Aromatic C-H stretch vibrations are seen between 3100-3000 cm^{-1}. Silanol functionalities are present in the material given the SiO-H stretch vibration at 3740 cm^{-1}. Between 2000 and 1300 cm^{-1} C=C stretch and CH-bending vibration typical for a para-substituted aromatic group are found.

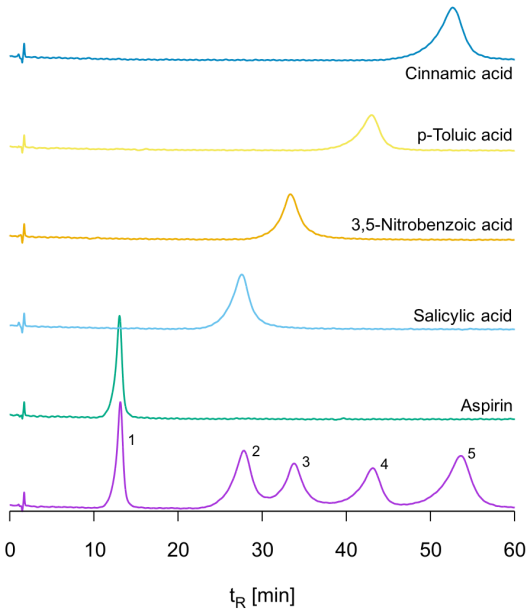

Figure 9.61: Determination of the elution sequence of the acid test mix. Conditions: 0.2 ml/min, 15/85 CH_3CN/0.1v% TFA, 25°C.

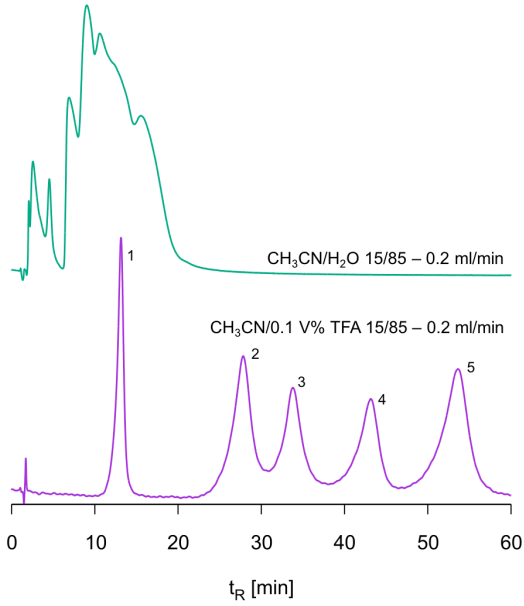

Figure 9.62: Chromatograms of the acid test mix separated at pH 1.90 (0.1v% TFA, bottom) and under neutral conditions (H_2O, top)

Chapter 10

Click modified ring-type organosilica particles for chromatography: Achievements and prospects

Despite the fairly disappointing results from template based methods, a water-in-oil emulsion method has allowed for the very versatile synthesis of highly porous spherical organosilica xerogels with multiple functionalities embedded in the polysilsesquioxane framework. Herein, it is clear that the emulsion droplet acts as a micro-environment, which controls size and shape of the synthesized particle, while an organosilica gel is formed inside the droplet. Through mechanical stirring the particle size can easily be adapted from 0.9 to 13.7 μm, while the pore size is readily tailored throughout the full mesopore range (2 - 50 nm) by means of the precursor to droplet ratio, the amount of acid catalyst and reaction time independently. Both are significant improvements compared to the spray-dry technique applied earlier, yielding small 2 μm particles with 31Å mesopores (Section 6.7.2).

Furthermore, hydrolytic post-treatments have expanded the flexibility of the synthesis and have enhanced the particle porosity, i.e. pore size expansion and elimination of micropores, for application in chromatography. It must be noted that these xerogels do not contain ordered pores. However, for emulsion based silica gels, reports are known in which the addition of an extra non-ionic surfactant (Pluronic P104) induces periodicity of the particle's pores [434].

Combining the above knowledge, we have developed a prosperous chromatographic packing using a 50-50 precursor mixture of HETSCH and AHETSCH. The embedded allyl functionalities of the latter allowed for the click modification with a C18 group commonly used for reverse phase HLPC. Separation of complex mixtures was successful and high hydrolytic stability was demonstrated up to 140°C and over an unprecedentedly broad pH range at elevated temperatures. This shows that not only the particle framework, but also the clicked surface modification is stable from at least pH 0.85 to pH 12 and up to 140°C at pH 7 under analytical column pressures. This latter high temperature has allowed the reduction of the analysis time of a standard test mixture to below 2 min. Moreover, in vitro investigations of unmodified $[Si(CH_2)]_3$-ring particles indicate that pH stability might potentially be as high as pH 0 and pH 12.5, while under neutral conditions analysis temperatures of up to 160°C might be reachable.

Click modification of the organosilica surface, on the other hand, offers the chance to create stationary phases with a plethora of different bonded functionalities, e.g. highly polar or ionic groups, chiral moieties, etc., that are unachievable through classic grafting of the silanols [384]. Given that the thioether functionality is stable under the harsh conditions applied, this might offer opportunities for the development of completely new chromatograpic methods and applications. Moreover, the silanol groups or the organosilica packing are still available for grafting, either before or after click modification.[1] Hereby, highly advanced bi-functional materials might be acquired for specialized or intricate separations. Next to this, the exceptional hydrothermal stability of the packing permits ultra-fast separation which might, in the long term, turn HPLC to an almost instantaneous analysis technique.

Returning to our initial set of required parameters for an ultimate chromatographic particle, we have achieved the following by use of the newly developed W/O emulsion method:

- **Spherical particles**

  Dependent of the emulsion quality. The aqueous W/O emulsion droplets provide confined spherical reactors for the condensation of multiple organosilica xerogels.

1. Similar to the end-capping of the free silanol groups, attachment of a bonded phase to the organosilica using a siloxane bond again turns the chromatographic phase labile at low pH.

- *Monodisperse in size*

  Dependent of the emulsion quality. Mechanical stirring, be it through magnetic agitation or high-speed turrax mixing, does not deliver monodisperse droplets. Selection of an emulsion in which Ostwald ripening takes place, improves the overall dispersion on the particle size, however not to such extent that the preset demand is met. As a consequence, the separation efficiency using the materials from this work is not yet up to the standard of commercial materials. Nonetheless, after classification or by synthesis in a monodisperse emulsion (see Section 9.8), highly attractive chromatographic packings are within reach.

- **Available particle sizes for both analytical separations and preparative purposes: d_{part} = 2 - 5 μm and 5 - 15 μm respectively**

  Dependent of the emulsion droplets or, in this work, the shear rate applied by stirring. Particle sizes from 0.9 to 13.7 μm are readily accessible.

- **Large surface area: S_{BET} = 50 - 600 m^2/g**

  The organosilica xerogels inherently possess a high porosity and a large surface area which often exceeds 600 m^2/g.

- **Large pore size, tunable in the mesopore range: $d_p > 60$Å**

  By variation of the precursor/droplet ratio pores in the complete mesopore range (2 - 50 nm) were obtained. Further fine-tuning of the porosity is attainable by adaptation of the droplet acidity or reaction time.

- **Limited or no micropores: $\frac{S_\mu}{S_{BET}} < 0.1$**

  The as-synthesized organosilica xerogels have a significant amount of micropores. Application of a hydrolytic post-treatment strongly reduces or even eliminates these, while the size of the mesopores can be expanded.

- **Mechanical stability at packing and analysis pressures**

  Dependent of the pore size, very high pore volumes are witnessed for some polysilsesquioxane frameworks, especially those derived from HETSCH. For stable application in RP-HPLC, we found that V_p needs to be sub-1.0 ml/g to avoid particle collapse under analytical conditions. Attempts to reduce the pore volume were

indecisive, however the precursors themselves exercise a significant influence on this parameter.

- **Hydrolytic stability at pH $<$ 2, pH $>$ 12 and temperatures above 100°C**

  Spherical allyl-$[Si(CH_2)]_3$-ring particles were found highly appealing as stationary phase for chromatography. After click modification with a C18-group, this packing is stable in unprecedented hydrolytic conditions. This is both owing to the highly stable organosilica framework and the firm anchoring of the bonded C18-phase.

- **Functional versatility**

  The presence of both embedded allyl functionalities and silanol groups allows the introduction of functional groups via both classic silylation as well as click chemistry. This opens up pathways towards columns with tailor-made functional groups for highly specific separations.

- **Absence of metal ion impurities**

  All experiments and reaction steps are executed without the use of metal salts or other metallic reagents.

Organic-inorganic silica hybrids have found their way into separation science since the development of RP-HPLC. User-driven demand for ever more stable and advanced stationary phases has driven research beyond what is feasible with classic fully porous silica particles, with core-shell particles being the latest big revolution in silica-based packed columns. Ever after the introduction of ethane-bridged organosilica columns, however, no further steps were taken towards a revolution in particle stability. The reason for this might be two-fold.

Firstly, organosilicas may look similar to silicas at first glance, yet in material synthesis the precursors act differently. Next to this, the precursors are fairly unstudied in terms of reactivity. For this reason, research needs to go back to the fundamentals, e.g. development of solid organosilica nanoparticles, something which is more than often left for academic research. Seen the fields of materials science and chromatography are relatively far apart, few synergies between the two exist in academia. Combined with a relatively low interest in organosilica materials, this has led to little truly progressive reports on the matter or other important advances in the field. The W/O emulsion method, however, clearly has

a great degree of inventiveness. Fixing the dispersion on the particle size might open doors towards further valorization.

As a second reason, perhaps column manufacturers are not supportive of highly stable or indestructible columns as the amount of sold columns will potentially drop. The HPLC column market, however, is highly profitable, with many users willing to invest in long-lasting, efficient columns that have the ability to fit all of their needs. Therefore, in my opinion, the customer demand for high speed separations, with highly specialized functionalities, at extreme conditions will automatically push column technology further into organosilicas. As suggested throughout the text, improvements of the organosilica packings (e.g. the generation of monodisperse emulsions or the synthesis of solid organosilica microparticles) hold high promise. The future of HPLC is without any doubt connected to advances in the stationary phase. With a general trend towards ever more demanding conditions at high temperature and extremely high pressures, organosilicas, as investigated in this work, are on the forefront of emerging technologies. Therefore, I do believe that the application of more advanced organosilicas in chromatography is no longer a question of if, but when; and that now is the time to conduct the research.

Bibliography

[1] J. M. Kim and R. Ryoo, Disintegration of mesoporous structures of MCM-41 and MCM-48 in water, *Bulletin of the Korean Chemical Society*, **1996**, 17, 1, 66–68.

[2] K. Cassiers, T. Linssen, M. Mathieu, M. Benjelloun, K. Schrijnemakers, P. Van Der Voort, P. Cool and E. F. Vansant, A detailed study of thermal, hydrothermal, and mechanical stabilities of a wide range of surfactant assembled mesoporous silicas, *Chemistry of Materials*, **2002**, 14, 5, 2317–2324.

[3] K. J. Shea, D. A. Loy and O. W. Webster, Aryl-Bridged Polysilsesquioxanes - New Microporous Materials, *Chemistry of Materials*, **1989**, 1, 6, 572–574.

[4] S. Inagaki, S. Guan, Y. Fukushima, T. Ohsuna and O. Terasaki, Novel mesoporous materials with a uniform distribution of organic groups and inorganic oxide in their frameworks, *Journal of the American Chemical Society*, **1999**, 121, 41, 9611–9614.

[5] T. Asefa, M. J. MacLachlan, N. Coombs and G. A. Ozin, Periodic mesoporous organosilicas with organic groups inside the channel walls, *Nature*, **1999**, 402, 6764, 867–871.

[6] B. J. Melde, B. T. Holland, C. F. Blanford and A. Stein, Mesoporous sieves with unified hybrid inorganic/organic frameworks, *Chemistry of Materials*, **1999**, 11, 11, 3302–3308.

[7] P. Van Der Voort, D. Esquivel, E. De Canck, F. Goethals, I. Van Driessche and F. J. Romero-Salguero, Periodic Mesoporous Organosilicas: from simple to complex bridges; a comprehensive overview of functions, morphologies and applications, *Chemical Society Reviews*, **2013**, 42, 9, 3913–3955.

[8] D. A. Loy and K. J. Shea, Bridged polysilsesquioxanes - Highly porous hybrid organic-inorganic materials, *Chemical Reviews*, **1995**, 95, 5, 1431–1442.

[9] R. J. P. Corriu and D. Leclercq, Recent developments of molecular chemistry for sol-gel processes, *Angewandte Chemie-Int. Edition*, **1996**, 35, 13-14, 1420–1436.

[10] G. Cerveau and R. J. P. Corriu, Some recent developments of polysilsesquioxanes chemistry for material science, *Coordination Chemistry Reviews*, **1998**, 178, 1051–1071.

[11] K. J. Shea and D. A. Loy, Bridged polysilsesquioxanes. Molecular-engineered hybrid organic-inorganic materials, *Chemistry of Materials*, **2001**, 13, 10, 3306–3319.

[12] P. Van Der Voort, C. Vercaemst, D. Schaubroeck and F. Verpoort, Ordered mesoporous materials at the beginning of the third millennium: new strategies to create hybrid and non-siliceous variants, *Physical Chemistry Chemical Physics*, **2008**, 10, 3, 347–360.

[13] S. Fujita and S. Inagaki, Self-organization of organosilica solids with molecular-scale and mesoscale periodicities, *Chemistry of Materials*, **2008**, 20, 3, 891–908.

[14] N. Mizoshita, T. Tani and S. Inagaki, Syntheses, properties and applications of periodic mesoporous organosilicas prepared from bridged organosilane precursors, *Chemical Society Reviews*, **2011**, 40, 2, 789–800.

[15] W. J. Hunks and G. A. Ozin, Challenges and advances in the chemistry of periodic mesoporous organosilicas (PMOs), *Journal of Materials Chemistry*, **2005**, 15, 35-36, 3716–3724.

[16] B. Hatton, K. Landskron, W. Whitnall, D. Perovic and G. A. Ozin, Past, present, and future of periodic mesoporous organosilicas - The PMOs, *Accounts of Chemical Research*, **2005**, 38, 4, 305–312.

[17] F. Hoffmann, M. Cornelius, J. Morell and M. Fröba, Silica-based mesoporous organic-inorganic hybrid materials, *Angewandte Chemie-Int. Edition*, **2006**, 45, 20, 3216–3251.

[18] F. Hoffmann and M. Fröba, Vitalising porous inorganic silica networks with organic functions-PMOs and related hybrid materials, *Chemical Society Reviews*, **2011**, 40, 2, 608–620.

[19] R. Iler, *The Chemistry of Silica*, John Wiley and Sons, **1979**.

[20] C. J. Brinker, K. D. Keefer, D. W. Schaefer and C. S. Ashley, Sol-gel transition in simple silicates, *Journal of Non-Crystalline Solids*, **1982**, 48, 1, 47–64.

[21] C. J. Brinker, K. D. Keefer, D. W. Schaefer, R. A. Assink, B. D. Kay and C. S. Ashley, Sol-gel transition in simple silicates 2, *Journal of Non-Crystalline Solids*, **1984**, 63, 1-2, 45–59.

[22] C. J. Brinker, R. Sehgal, S. L. Hietala, R. Deshpande, D. M. Smith, D. Loy and C. S. Ashley, Sol-gel strategies for controlled porosity inorganic materials, *Journal of Membrane Science*, **1994**, 94, 85–102.

[23] U. Schubert, N. Husing and A. Lorenz, Hybrid inorganic-organic materials by sol-gel processing of organofunctional metal alkoxide, *Chemistry of Materials*, **1995**, 7, 11, 2010–2027.

[24] D. A. Loy, B. Mather, A. R. Straumanis, C. Baugher, D. A. Schneider, A. Sanchez and K. J. Shea, Effect of pH on the gelation time of hexylene-bridged polysilsesquioxanes, *Chemistry of Materials*, **2004**, 16, 11, 2041–2043.

[25] G. Cerveau, R. J. P. Corriu and E. Framery, Sol-gel process-influence of ageing on the textural properties of organosilsesquioxane materials, *Journal of Materials Chemistry*, **2001**, 11, 3, 713–717.

[26] G. Cerveau, R. J. P. Corriu, E. Framery, S. Ghosh and H. P. Mutin, Hybrid materials and silica: drastic control of surfaces and porosity of xerogels via ageing temperature, and influence of drying step on polycondensation at silicon, *Journal of Materials Chemistry*, **2002**, 12, 10, 3021–3026.

[27] G. Cerveau, R. J. P. Corriu and E. Framery, Sol-gel chemistry: evidence of redistribution at silicon atom induced by NaOH as catalyst during ageing, *Comptes Rendus de l'Academie des Sciences Serie II Fascicule C - Chimie*, **2001**, 4, 2, 79–83.

[28] T. Shimizu, K. Kanamori, A. Maeno, H. Kaji and K. Nakanishi, Transparent ethylene-bridged polymethylsiloxane aerogels and xerogels with improved bending flexibility, *Langmuir*, **2016**, 32, 50, 13427–13434.

[29] T. Shimizu, K. Kanamori, A. Maeno, H. Kaji, C. M. Doherty and K. Nakanishi, Transparent ethenylene-bridged polymethylsiloxane aerogels: Mechanical flexibility and strength and availability for addition reaction, *Langmuir*, **2017**, 33, 18, 4543–4550.

[30] T. Shimizu, K. Kanamori and K. Nakanishi, Silicone-based organic-inorganic hybrid aerogels and xerogels, *Chemistry - A European Journal*, **2017**, 23, 22, 5176–5187.

[31] K. Nakanishi and K. Kanamori, Organic-inorganic hybrid poly(silsesquioxane) monoliths with controlled macro- and mesopores, *Journal of Materials Chemistry*, **2005**, 15, 35-36, 3776–3786.

[32] K. J. Shea, D. A. Loy and O. W. Webster, Arylsilsesquioxane gels and related materials - New hybrids of organic and inorganic networks, *Journal of the American Chemical Society*, **1992**, 114, 17, 6700–6710.

[33] B. Boury, P. Chevalier, R. J. P. Corriu, P. Delord, J. J. E. Moreau and M. W. Chiman, Hybrid organic-inorganic xerogel access to meso- and microporous silica by thermal and chemical treatment, *Chemistry of Materials*, **1999**, 11, 2, 281–291.

[34] B. Boury and R. J. P. Corriu, Adjusting the porosity of a silica-based hybrid material, *Advanced Materials*, **2000**, 12, 13, 989–992.

[35] H. W. Oviatt, K. J. Shea and J. H. Small, Alkylene-bridged silsesquioxane sol-gel synthesis and xerogel characterization - Molecular requirements for porosity, *Chemistry of Materials*, **1993**, 5, 7, 943–950.

[36] D. A. Loy, G. M. Jamison, B. M. Baugher, E. M. Russick, R. A. Assink, S. Prabakar and K. J. Shea, Alkylene-bridged polysilsesquioxane aerogels - Highly porous hybrid organic-inorganic materials, *Journal of Non-Crystalline Solids*, **1995**, 186, 44–53.

[37] C. T. Kresge, M. E. Leonowicz, W. J. Roth, J. C. Vartuli and J. S. Beck, Ordered mesoporous molecular-sieves synthesized by a liquid-crystal template mechanism, *Nature*, **1992**, 359, 6397, 710–712.

[38] J. S. Beck, J. C. Vartuli, W. J. Roth, M. E. Leonowicz, C. T. Kresge, K. D. Schmitt, C. T. W. Chu, D. H. Olson, E. W. Sheppard, S. B. McCullen, J. B. Higgins and J. L. Schlenker, A new family of mesoporous molecular-sieves prepared with liquid-crystal templates, *Journal of the American Chemical Society*, **1992**, 114, 27, 10834–10843.

[39] D. Y. Zhao, J. L. Feng, Q. S. Huo, N. Melosh, G. H. Fredrickson, B. F. Chmelka and G. D. Stucky, Triblock copolymer syntheses of mesoporous silica with periodic 50 to 300 angstrom pores, *Science*, **1998**, 279, 5350, 548–552.

[40] M. C. Burleigh, M. A. Markowitz, S. Jayasundera, M. S. Spector, C. W. Thomas and B. P. Gaber, Mechanical and hydrothermal stabilities of aged periodic mesoporous organosilicas, *Journal of Physical Chemistry B*, **2003**, 107, 46, 12628–12634.

[41] F. Goethals, B. Meeus, A. Verberckmoes, P. Van Der Voort and I. Van Driessche, Hydrophobic high quality ring PMOs with an extremely high stability, *Journal of Materials Chemistry*, **2010**, 20, 9, 1709–1716.

[42] D. Y. Zhao, Q. S. Huo, J. L. Feng, B. F. Chmelka and G. D. Stucky, Nonionic triblock and star diblock copolymer and oligomeric surfactant syntheses of highly ordered, hydrothermally stable, mesoporous silica structures, *Journal of the American Chemical Society*, **1998**, 120, 24, 6024–6036.

[43] Z. D. Zhang, X. X. Yan, B. Z. Tian, S. D. Shen, D. H. Chen, G. S. Zhu, S. L. Qiu and D. Y. Zhao, Synthesis of large-pore periodic mesoporous organosilica (PMO) with bicontinuous cubic structure of Ia-3d symmetry, *Chemistry Letters*, **2005**, 34, 2, 182–183.

[44] W. P. Guo, J. Y. Park, M. O. Oh, H. W. Jeong, W. J. Cho, I. Kim and C. S. Ha, Triblock copolymer synthesis of highly ordered large-pore periodic mesoporous organosilicas with the aid of inorganic salts, *Chemistry of Materials*, **2003**, 15, 12, 2295.

[45] E. B. Cho, K. W. Kwon and K. Char, Mesoporous organosilicas prepared with PEO-containing triblock copolymers with different hydrophobic moieties, *Chemistry of Materials*, **2001**, 13, 11, 3837.

[46] E. B. Cho and K. Char, Macromolecular templating approach for the synthesis of hydrothermally stable mesoporous organosilicas with high periodicity and thick framework walls, *Chemistry of Materials*, **2004**, 16, 2, 270–275.

[47] M. Kruk, Access to ultralarge-pore ordered mesoporous materials through selection of surfactant/swelling-agent micellar templates, *Accounts of Chemical Research*, **2012**, 45, 10, 1678–1687.

[48] P. Schmidt-Winkel, W. Lukens, D. Zhao, P. Yang, B. Chmelka and G. Stucky, Mesocellular siliceous foams with uniformly sized cells and windows, *Journal of the American Chemical Society*, **1999**, 121, 1, 254–255.

[49] J. Lettow, Y. Han, P. Schmidt-Winkel, P. Yang, D. Zhao, G. Stucky and J. Ying, Hexagonal to mesocellular foam phase transition in polymer-templated mesoporous silicas, *Langmuir*, **2000**, 16, 22, 8291–8295.

[50] C. Vercaemst, P. E. de Jongh, J. D. Meeldijk, B. Goderis, F. Verpoort and P. Van Der Voort, Ethenylene-bridged periodic mesoporous organosilicas with ultra-large mesopores, *Chemical Communications*, **2009**, 27, 4052–4054.

[51] A. S. Manchanda and M. Kruk, Synthesis of xylylene-bridged Periodic Mesoporous Organosilicas and related hollow spherical nanoparticles, *Langmuir*, **2016**, 32, 3, 900–908.

[52] S. Jun, S. Joo, R. Ryoo, M. Kruk, M. Jaroniec, Z. Liu, T. Ohsuna and O. Terasaki, Synthesis of new, nanoporous carbon with hexagonally ordered mesostructure, *Journal of the American Chemical Society*, **2000**, 122, 43, 10712–10713.

[53] R. Ryoo, C. H. Ko, M. Kruk, V. Antochshuk and M. Jaroniec, Block-copolymer-templated ordered mesoporous silica: Array of uniform mesopores or mesopore-micropore network?, *Journal of Physical Chemistry B*, **2000**, 104, 48, 11465–11471.

[54] A. Galarneau, H. Cambon, F. Di Renzo and F. Fajula, True microporosity and surface area of mesoporous SBA-15 silicas as a function of synthesis temperature, *Langmuir*, **2001**, 17, 26, 8328–8335.

[55] S. Z. Qiao, C. Z. Yu, Q. H. Hu, Y. G. Jin, X. F. Zhou, X. S. Zhao and G. Q. Lu, Control of ordered structure and morphology of large-pore periodic mesoporous organosilicas by inorganic salt, *Microporous and Mesoporous Materials*, **2006**, 91, 1-3, 59–69.

[56] C. Vercaemst, *Isomeric olefinic Periodic Mesoporous Organosilicas: an emerging class of versatile nanomaterials*, Ph.D. thesis, Ghent University, **2009**.

[57] C. Z. Yu, J. Fan, B. Z. Tian and D. Y. Zhao, Morphology development of mesoporous materials: a colloidal phase separation mechanism, *Chemistry of Materials*, **2004**, 16, 5, 889–898.

[58] B. D. Hatton, K. Landskron, W. Whitnall, D. D. Perovic and G. A. Ozin, Spin-coated periodic mesoporous organosilica thin films - Towards a new generation of low-dielectric-constant materials, *Advanced Functional Materials*, **2005**, 15, 5, 823–829.

[59] F. Goethals, I. Ciofi, O. Madia, K. Vanstreels, M. R. Baklanov, C. Detavernier, P. Van Der Voort and I. Van Driessche, Ultra-low-k cyclic carbon-bridged PMO films with a high chemical resistance, *Journal of Materials Chemistry*, **2012**, 22, 17, 8281–8286.

[60] M. Ide, *Ordered mesoporous silica materials in liquid chromatography: synthesis and application*, Ph.D. thesis, Ghent University, **2012**.

[61] K. A. Koyano, T. Tatsumi, Y. Tanaka and S. Nakata, Stabilization of mesoporous molecular sieves by trimethylsilylation, *Journal of Physical Chemistry B*, **1997**, 101, 46, 9436–9440.

[62] W. P. Guo, X. Li and X. S. Zhao, Understanding the hydrothermal stability of large-pore periodic mesoporous organosilicas and pure silicas, *Microporous and Mesoporous Materials*, **2006**, 93, 1-3, 285–293.

[63] W. D. Wang, D. Grozea, S. Kohli, D. D. Perovic and G. A. Ozin, Water repellent Periodic Mesoporous Organosilicas, *ACS Nano*, **2011**, 5, 2, 1267–1275.

[64] D. Esquivel, C. Jimenez-Sanchidrian and F. J. Romero-Salguero, Comparison of the thermal and hydrothermal stabilities of ethylene, ethylidene, phenylene and biphenylene bridged periodic mesoporous organosilicas, *Materials Latters*, **2011**, 65, 10, 1460–1462.

[65] X. Feng, G. E. Fryxell, L. Q. Wang, A. Y. Kim, J. Liu and K. M. Kemner, Functionalized monolayers on ordered mesoporous supports, *Science*, **1997**, 276, 5314, 923–926.

[66] N. R. E. N. Impens, P. Van Der Voort and E. F. Vansant, Silylation of micro-, meso- and non-porous oxides: a review, *Microporous and Mesoporous Materials*, **1999**, 28, 2, 217–232.

[67] S. L. Burkett, S. D. Sims and S. Mann, Synthesis of hybrid inorganic-organic mesoporous silica by co-condensation of siloxane and organosiloxane precursors, *Chemical Communications*, **1996**, 11, 1367–1368.

[68] D. J. Macquarrie, Direct preparation of organically modified MCM-type materials. Preparation and characterisation of aminopropyl-MCM and 2-cyanoethyl-MCM, *Chemical Communications*, **1996**, 16, 1961–1962.

[69] M. H. Lim, C. F. Blanford and A. Stein, Synthesis and characterization of a reactive vinyl-functionalized MCM-41: Probing the internal pore structure by a bromination reaction, *Journal of the American Chemical Society*, **1997**, 119, 17, 4090–4091.

[70] C. E. Fowler, S. L. Burkett and S. Mann, Synthesis and characterization of ordered organo-silica-surfactant mesophases with functionalized MCM-41-type architecture, *Chemical Communications*, **1997**, 18, 1769–1770.

[71] S. Inagaki, S. Guan and Y. Fukushima, Organic/inorganic complex porous materials, US6248686, **1999**.

[72] M. C. Burleigh, M. A. Markowitz, E. M. Wong, J. S. Lin and B. P. Gaber, Synthesis of periodic mesoporous organosilicas with block copolymer templates, *Chemistry of Materials*, **2001**, 13, 12, 4411.

[73] W. P. Guo, I. Kim and C. S. Ha, Highly ordered three-dimensional large-pore periodic mesoporous organosilica with Im3m symmetry, *Chemical Communications*, **2003**, 21, 2692–2693.

[74] O. Muth, C. Schellbach and M. Fröba, Triblock copolymer assisted synthesis of periodic mesoporous organosilicas (PMOs) with large pores, *Chemical Communications*, **2001**, 19, 2032–2033.

[75] C. Vercaemst, M. Ide, B. Allaert, N. Ledoux, F. Verpoort and P. Van Der Voort, Ultrafast hydrothermal synthesis of diastereoselective pure ethenylene-bridged periodic mesoporous organosilicas, *Chemical Communications*, **2007**, 22, 2261–2263.

[76] W. H. Wang, S. H. Xie, W. Z. Zhou and A. Sayari, Synthesis of periodic mesoporous ethylenesilica under acidic conditions, *Chemistry of Materials*, **2004**, 16, 9, 1756–1762.

[77] C. Yoshina-Ishii, T. Asefa, N. Coombs, M. J. MacLachlan and G. A. Ozin, Periodic mesoporous organosilicas, PMOs: fusion of organic and inorganic chemistry 'inside' the channel walls of hexagonal mesoporous silica, *Chemical Communications*, **1999**, 24, 2539–2540.

[78] S. Inagaki, S. Guan, T. Ohsuna and O. Terasaki, An ordered mesoporous organosilica hybrid material with a crystal-like wall structure, *Nature*, **2002**, 416, 6878, 304–307.

[79] M. Cornelius, F. Hoffmann and M. Fröba, Periodic mesoporous organosilicas with a bifunctional conjugated organic unit and crystal-like pore walls, *Chemistry of Materials*, **2005**, 17, 26, 6674–6678.

[80] J. Morell, G. Wolter and M. Fröba, Synthesis and characterization of highly ordered thiophene-bridged periodic mesoporous organosilicas with large pores, *Chemistry of Materials*, **2005**, 17, 4, 804–808.

[81] E. B. Cho, J. Park and M. Jaroniec, Structural Stability of Si-C Bonds in Periodic Mesoporous Thiophene-Silicas Prepared under Acidic Conditions, *Journal of Physical Chemistry C*, **2013**, 117, 41, 21441–21449.

[82] M. Kuroki, T. Asefa, W. Whitnal, M. Kruk, C. Yoshina-Ishii, M. Jaroniec and G. A. Ozin, Synthesis and properties of 1,3,5-benzene periodic mesoporous organosilica (PMO): Novel aromatic PMO with three point attachments and unique thermal transformations, *Journal of the American Chemical Society*, **2002**, 124, 46, 13886–13895.

[83] Y. Goto, K. Nakajima, N. Mizoshita, M. Suda, N. Tanaka, T. Hasegawa, T. Shimada, T. Tani and S. Inagaki, Synthesis and optical properties of 2,6-anthracene-bridged periodic mesostructured organosilicas, *Microporous and Mesoporous Materials*, **2009**, 117, 3, 535–540.

[84] O. Dag, C. Yoshina-Ishii, T. Asefa, M. J. MacLachlan, H. Grondey, N. Coombs and G. A. Ozin, Oriented periodic mesoporous organosilica (PMO) film th organic functionality inside the channel walls, *Advanced Functional Materials*, **2001**, 11, 3, 213–217.

[85] T. Asefa, M. J. MacLachlan, H. Grondey, N. Coombs and G. A. Ozin, Metamorphic channels in periodic mesoporous methylenesilica, *Angewandte Chemie-Int. Edition*, **2000**, 39, 10, 1808.

[86] T. Asefa, M. Kruk, M. J. MacLachlan, N. Coombs, H. Grondey, M. Jaroniec and G. A. Ozin, Novel bifunctional periodic mesoporous organosilicas, BPMOs: Synthesis, characterization, properties and in-situ selective hydroboration-alcoholysis reactions of functional groups, *Journal of the American Chemical Society*, **2001**, 123, 35, 8520–8530.

[87] K. Landskron, B. D. Hatton, D. D. Perovic and G. A. Ozin, Periodic mesoporous organosilicas containing interconnected $[Si(CH_2)]_3$ rings, *Science*, **2003**, 302, 5643, 266–269.

[88] C. Vercaemst, J. T. A. Jones, Y. Z. Khimyak, J. C. Martins, F. Verpoort and P. Van Der Voort, Spectroscopic evidence of thermally induced metamorphosis in ethenylene-bridged periodic mesoporous organosilicas, *Physical Chemistry Chemical Physics*, **2008**, 10, 35, 5349–5352.

[89] D. J. Brondani, R. J. P. Corriu, S. Elayoubi, J. J. E. Moreau and M. W. C. Man, Polyfunctional Carbosilanes and Organosilcon Compounds - Synthesis via Grignard Reactions, *Tetrahedron Letters*, **1993**, 34, 13, 2111–2114.

[90] K. Landskron, B. Hatton, G. A. Ozin and D. Perovic, High Organic group content Periodic Mesoporous Organosilicas (HO-PMOs), US7947799, **2005**.

[91] F. Goethals, M. R. Baklanov, I. Ciofi, C. Detavernier, P. Van Der Voort and I. Van Driessche, A new procedure to seal the pores of mesoporous low-k films with precondensed organosilica oligomers, *Chemical Communications*, **2012**, 48, 22, 2797–2799.

[92] F. Goethals, E. Levrau, G. Pollefeyt, M. R. Baklanov, I. Ciofi, K. Vanstreels, C. Detavernier, I. Van Driessche and P. Van Der Voort, Sealed ultra low-k organosilica films with improved electrical, mechanical and chemical properties, *Journal of Materials Chemistry C*, **2013**, 1, 25, 3961–3966.

[93] A. W. Wills, D. J. Michalak, P. Ercius, E. R. Rosenberg, T. Perciano, D. Ushizima, R. Runser and B. A. Helms, Block copolymer packing limits and interfacial reconfigurability in the assembly of Periodic Mesoporous Organosilicas, *Advanced Functional Materials*, **2015**, 25, 26, 4120–4128.

[94] X. Wang, D. Lu, R. Austin, A. Agarwal, L. J. Mueller, Z. Liu, J. Wu and P. Feng, Protein refolding assisted by periodic mesoporous organosilicas, *Langmuir*, **2007**, 23, 10, 5735–5739.

[95] Z. Zhou, R. N. K. Taylor, S. Kullmann, H. Bao and M. Hartmann, Mesoporous organosilicas with large cage-like pores for high efficiency immobilization of enzymes, *Advanced Materials*, **2011**, 23, 22-23, 2627.

[96] M. C. Burleigh, M. A. Markowitz, M. S. Spector and B. P. Gaber, Porous polysilsesquioxanes for the adsorption of phenols, *Environmental Science and Technology*, **2002**, 36, 11, 2515–2518.

[97] S. A. Trammell, M. Zeinali, B. J. Melde, P. T. Charles, F. L. Velez, M. A. Dinderman, A. Kusterbeck and M. A. Markowitz, Nanoporous organosilicas as preconcentration materials for the electrochemical detection of trinitrotoluene, *Analytical Chemistry*, **2008**, 80, 12, 4627–4633.

[98] C. B. Vidal, A. L. Barros, C. P. Moura, A. C. A. de Lima, F. S. Dias, L. C. G. Vasconcellos, P. B. A. Fechine and R. F. Nascimento, Adsorption of polycyclic aromatic hydrocarbons from aqueous solutions by modified periodic mesoporous organosilica, *Journal of Colloid and Interface Science*, **2011**, 357, 2, 466–473.

[99] H. L. Castricum, R. Kreiter, H. M. van Veen, D. H. A. Blank, J. F. Vente and J. E. ten Elshof, High-performance hybrid pervaporation membranes with superior hydrothermal and acid stability, *Journal of Membrane Science*, **2008**, 324, 1-2, 111–118.

[100] H. L. Castricum, A. Sah, R. Kreiter, D. H. A. Blank, J. F. Vente and J. E. ten Elshof, Hydrothermally stable molecular separation membranes from organically linked silica, *Journal of Materials Chemistry*, **2008**, 18, 18, 2150–2158.

[101] M. Nishibayashi, H. Yoshida, M. Uenishi, M. Kanezashi, H. Nagasawa, T. Yoshioka and T. Tsuru, Photo-induced sol-gel processing for low-temperature fabrication of high-performance silsesquioxane membranes for use in molecular separation, *Chemical Communications*, **2015**, 51, 49, 9932–9935.

[102] I. Agirre, P. L. Arias, H. L. Castricum, M. Creatore, J. E. ten Elshof, G. G. Paradis, P. H. T. Ngamou, H. M. van Veen and J. F. Vente, Hybrid organosilica membranes and processes: Status and outlook, *Separation and Purification Technology*, **2014**, 121, 2–12.

[103] J. H. Small, K. J. Shea and D. A. Loy, Arylene-bridged and alkylene-bridged polysilsesquioxanes, *Journal of Non-Crystalline Solids*, **1993**, 160, 3, 234–246.

[104] M. Cornelius, F. Hoffmann, B. Ufer, P. Behrens and M. Fröba, Systematic extension of the length of the organic conjugated pi-system of mesoporous silica-based organic-inorganic hybrid materials, *Journal of Materials Chemistry*, **2008**, 18, 22, 2587–2592.

[105] M. Beretta, J. Morell, P. Sozzani and M. Fröba, Towards peptide formation inside the channels of a new divinylaniline-bridged periodic mesoporous organosilica, *Chemical Communications*, **2010**, 46, 14, 2495–2497.

[106] M. Murata, M. Ishikura, M. Nagata, S. Watanabe and Y. Masuda, Rhodium(I)-catalyzed silylation of aryl halides with triethoxysilane: Practical synthetic route to aryltriethoxysilanes, *Organic Letters*, **2002**, 4, 11, 1843–1845.

[107] Y. Maegawa, Y. Goto, S. Inagaki and T. Shimada, A useful procedure for diiodination of carbazoles and subsequent efficient transformation to novel 3,6-bis(triethoxysilyl)carbazoles giving mesoporous materials, *Tetrahedron Letters*, **2006**, 47, 39, 6957–6960.

[108] S. E. Dickson and C. M. Crudden, Transformable periodic mesoporous organosilica materials, *Chemical Communications*, **2010**, 46, 12, 2100–2102.

[109] S. MacQuarrie, M. P. Thompson, A. Blanc, N. J. Mosey, R. P. Lemieux and C. M. Crudden, Chiral Periodic Mesoporous Organosilicates Based on Axially Chiral Monomers: Transmission of Chirality in the Solid State, *Journal of the American Chemical Society*, **2008**, 130, 43, 14099.

[110] M. C. Burleigh, S. Jayasundera, C. W. Thomas, M. S. Spector, M. A. Markowitz and B. P. Gaber, A versatile synthetic approach to periodic mesoporous organosilicas, *Colloid Polymer Science*, **2004**, 282, 7, 728–733.

[111] O. Olkhovyk and M. Jaroniec, Periodic mesoporous organosilica with large heterocyclic bridging groups, *Journal of the American Chemical Society*, **2005**, 127, 1, 60–61.

[112] S. Clerick, W. Libbrecht, O. van den Berg, E. De Canck, J. De Clercq and P. Van Der Voort, A novel malonamide Periodic Mesoporous Organosilica (PMO) for tuneable ibuprofen release, *Advanced Porous Materials*, **2014**, 2, 1–8.

[113] S. Parambadath, V. K. Rana, S. Moorthy, S.-W. Chu, S.-K. Park, D. Lee, G. Sung and C.-S. Ha, Periodic mesoporous organosilicas with co-existence of diurea and sulfanilamide as an effective drug delivery carrier, *Journal of Solid State Chemistry*, **2011**, 184, 5, 1208–1215.

[114] M. S. Moorthy, S.-S. Park, D. Fuping, S.-H. Hong, M. . Selvaraj and C.-S. Ha, Step-up synthesis of amidoxime-functionalised periodic mesoporous organosilicas with an amphoteric ligand in the framework for drug delivery, *Journal of Materials Chemistry*, **2012**, 22, 18, 9100–9108.

[115] S. Inagaki, O. Ohtani, Y. Goto, K. Okamoto, M. Ikai, K. Yamanaka, T. Tani and T. Okada, Light harvesting by a Periodic Mesoporous Organosilica chromophore, *Angewandte Chemie-Int. Edition*, **2009**, 48, 22, 4042–4046.

[116] N. Mizoshita, T. Tani, H. Shinokubo and S. Inagaki, Mesoporous organosilica hybrids consisting of silica-wrapped π-π stacking columns, *Angewandte Chemie-Int. Edition*, **2012**, 51, 5, 1156–1160.

[117] M. Waki, Y. Maegawa, K. Hara, Y. Goto, S. Shirai, Y. Yamada, N. Mizoshita, T. Tani, W.-J. Chun, S. Muratsugu, M. Tada, A. Fukuoka and S. Inagaki, A solid chelating ligand: Periodic Mesoporous Organosilica containing 2,2 '-bipyridine within the pore walls, *Journal of the American Chemical Society*, **2014**, 136, 10, 4003–4011.

[118] L. Grosch, Y. J. Lee, F. Hoffmann and M. Fröba, Light-Harvesting Three-Chromophore Systems Based on Biphenyl-Bridged Periodic Mesoporous Organosilica, *Chemistry - A European Journal*, **2015**, 21, 1, 331–346.

[119] N. Mizoshita, Y. Goto, M. P. Kapoor, T. Shimada, T. Tani and S. Inagaki, Fluorescence emission from 2,6-naphthylene-bridged mesoporous organosilicas with an amorphous or crystal-like framework, *Chemistry - A European Journal*, **2009**, 15, 1, 219–226.

[120] C. Baleizao, B. Gigante, D. Das, M. Alvaro, H. Garcia and A. Corma, Synthesis and catalytic activity of a chiral periodic mesoporous organosilica (ChiMO), *Chemical Communications*, **2003**, 15, 1860–1861.

[121] M. A. Gauthier, M. I. Gibson and H. A. Klok, Synthesis of functional polymers by post-polymerization modification, *Angewandte Chemie-Int. Edition*, **2009**, 48, 1, 48–58.

[122] K. A. Gunay, P. Theato and H. A. Klok, Standing on the shoulders of hermann staudinger: Post-polymerization modification from past to present, *Journal of Polymer Science A - Polymer Chemistry*, **2013**, 51, 1, 1–28.

[123] J. M. Huang, H. Chen and T. Y. Li, Improvement of proline chiral stationary phases by varying peptide length and linker, *Journal of Chromatography A*, **2006**, 1113, 1-2, 109–115.

[124] N. A. Brunelli, S. A. Didas, K. Venkatasubbaiah and C. W. Jones, Tuning cooperativity by controlling the linker length of silica-supported amines in catalysis and CO_2 capture, *Journal of the American Chemical Society*, **2012**, 134, 34, 13950–13953.

[125] S. Polarz, F. Jeremias and U. Haunz, Materials surgery - Reactivity differences of organic groups in hybrids, *Advanced Functional Materials*, **2011**, 21, 15, 2953–2959.

[126] E. De Canck, L. Lapeire, J. De Clercq, F. Verpoort and P. Van Der Voort, New ultrastable mesoporous adsorbent for the removal of mercury ions, *Langmuir*, **2010**, 26, 12, 10076–10083.

[127] E. De Canck, I. Ascoop, A. Sayari and P. Van Der Voort, Periodic mesoporous organosilicas functionalized with a wide variety of amines for CO_2 adsorption, *Physical Chemistry Chemical Physics*, **2013**, 15, 24, 9792–9799.

[128] M. Sasidharan, S. Fujita, M. Ohashi, Y. Goto, K. Nakashima and S. Inagaki, Novel synthesis of bifunctional catalysts with different microenvironments, *Chemical Communications*, **2011**, 47, 37, 10422–10424.

[129] K. Nakajima, I. Tomita, M. Hara, S. Hayashi, K. Domen and J. N. Kondo, A stable and highly active hybrid mesoporous solid acid catalyst, *Advanced Materials*, **2005**, 17, 15, 1839.

[130] D. Esquivel, E. De Canck, C. Jimenez-Sanchidrian, P. Van Der Voort and F. J. Romero-Salguero, Formation and functionalization of surface Diels-Alder adducts on ethenylene-bridged periodic mesoporous organosilica, *Journal of Materials Chemistry*, **2011**, 21, 29, 10990–10998.

[131] D. Esquivel, C. Jimenez-Sanchidrian and F. J. Romero-Salguero, Thermal behaviour, sulfonation and catalytic activity of phenylene-bridged periodic mesoporous organosilicas, *Journal of Materials Chemistry*, **2011**, 21, 3, 724–733.

[132] M. Ohashi, M. P. Kapoor and S. Inagaki, Chemical modification of crystal-like mesoporous phenylene-silica with amino group, *Chemical Communications*, **2008**, 7, 841–843.

[133] D. Esquivel, O. Van den Berg, F. J. Romero-Salguero, F. Du Prez and P. Van Der Voort, 100% thiol-functionalized ethylene PMOs prepared by "thiolacid-ene" chemistry, *Chemical Communications*, **2013**, 49, 23, 2344–2346.

[134] P. Van Der Voort, Heterogeneous Catalysis, UGhent Course Syllabus.

[135] M. Roeffaers, B. Sels, H. Uji-i, F. De Schryver, P. Jacobs, D. De Vos and J. Hofkens, Spatially resolved observation of crystal-face dependent catalysis by single turnover counting, *Nature Letters*, **2006**, 439, 572–575.

[136] G. De Cremer, M. Roeffaers, E. Bartholomeeusen, K. Lin, P. Dedecker, P. Pescarmona, P. Jacobs, D. De Vos, J. Hofkens and B. Sels, High-resolution single-turnover mapping reveals intraparticle diffusion limitation in Ti-MCM-41-catalyzed epoxidation, *Angewandte Chemie-Int. Edition*, **2010**, 49, 908–911.

[137] P. Anastas and J. Warner, *Green chemistry: Theory and practice*, Oxford University Press: New York, **1998**.

[138] J. Y. Ying, C. P. Mehnert and M. S. Wong, Synthesis and applications of supramolecular-templated mesoporous materials, *Angewandte Chemie-Int. Edition*, **1999**, 38, 1-2, 56–77.

[139] R. A. Sheldon, E factors, green chemistry and catalysis: an odyssey, *Chemical Communications*, **2008**, 29, 3352–3365.

[140] D. Gu and F. Schüth, Synthesis of non-siliceous mesoporous oxides, *Chemical Society Reviews*, **2014**, 43, 1, 313–344.

[141] D. E. De Vos, M. Dams, B. F. Sels and P. A. Jacobs, Ordered mesoporous and microporous molecular sieves functionalized with transition metal complexes as catalysts for selective organic transformations, *Chemical Reviews*, **2002**, 102, 10, 3615–3640.

[142] F. Schüth, Non-siliceous mesostructured and mesoporous materials, *Chemistry of Materials*, **2001**, 13, 10, 3184–3195.

[143] A. Zürner, J. Kirstein, M. Döblinger, C. Bräuchle and T. Bein, Visualizing single-molecule diffusion in mesoporous materials, *Nature*, **2007**, 450, 7170, 705.

[144] N. A. Brunelli and C. W. Jones, Tuning acid-base cooperativity to create next generation silica-supported organocatalysts, *Journal of Catalysis*, **2013**, 308, 60–72.

[145] J. Lauwaert, E. De Canck, D. Esquivel, J. W. Thybaut, P. Van Der Voort and G. B. Marin, Silanol-assisted aldol condensation on aminated silica: understanding the arrangement of functional groups, *ChemCatChem*, **2014**, 6, 1, 255–264.

[146] A. Corma, From microporous to mesoporous molecular sieve materials and their use in catalysis, *Chemical Review*, **1997**, 97, 6, 2373–2419.

[147] S. Jun and R. Ryoo, Aluminum impregnation into mesoporous silica molecular sieves for catalytic application to Friedel-Crafts alkylation, *Journal of Catalysis*, **2000**, 195, 2, 237–243.

[148] M. Camblor, A. Corma, P. Esteve, A. Martinez and S. Valencia, Epoxidation of unsaturated fatty esters over large-pore Ti-containing molecular sieves as catalysts: Important role of the hydrophobic-hydrophilic properties of the molecular sieve, *Chemical Communications*, **1997**, 8, 795–796.

[149] A. Corma, M. Domine, J. Gaona, J. Jorda, M. Navarro, F. Rey, J. Perez-Pariente, J. Tsuji, B. McCulloch and L. Nemeth, Strategies to improve the epoxidation activity and selectivity of Ti-MCM-41, *Chemical Communications*, **1998**, 20, 2211–2212.

[150] M. Morey, G. Stucky, S. Schwarz and M. Fröba, Isomorphic substitution and postsynthesis incorporation of zirconium into MCM-48 mesoporous silica, *Journal of Physical Chemistry B*, **1999**, 103, 12, 2037–2041.

[151] S. Liu and H. Wang, Photocatalytic generation of hydrogen on Zr-MCM-41, *International Journal of Hydrogen Energy*, **2002**, 27, 9, 859–862.

[152] M. Ferre, R. Pleixats, M. W. C. Man and X. Cattoën, Recyclable organocatalysts based on hybrid silicas, *Green Chemistry*, **2016**, 18, 4, 881–922.

[153] R. Mouawia, A. Mehdi, C. Reye and R. J. P. Corriu, Bifunctional ordered mesoporous materials: direct synthesis and study of the distribution of two distinct functional groups in the pore channels, *Journal of Materials Chemistry*, **2008**, 18, 35, 4193–4203.

[154] R. I. Kureshy, I. Ahmad, N. H. Khan, S. H. R. Abdi, K. Pathak and R. V. Jasra, Chiral Mn(III) salen complexes covalently bonded on modified MCM-41 and SBA-15 as efficient catalysts for enantioselective epoxidation of nonfunctionalized alkenes, *Journal of Catalysis*, **2006**, 238, 1, 134–141.

[155] A. R. McDonald, C. Muller, D. Vogt, G. P. M. van Klinka and G. van Koten, BINAP-Ru and -Rh catalysts covalently immobilised on silica and their repeated application in asymmetric hydrogenation, *Green Chemistry*, **2008**, 10, 4, 424–432.

[156] W. Chen, P. Li and L. Wang, Silica supported palladium-phosphine complex: recyclable catalyst for Suzuki-Miyaura cross-coupling reactions at ambient temperature, *Tetrahedron*, **2011**, 67, 2, 318–325.

[157] M. H. Lim, C. F. Blanford and A. Stein, Synthesis of ordered microporous silicates with organosulfur surface groups and their applications as solid acid catalysts, *Chemistry of Materials*, **1998**, 10, 2, 467.

[158] C. M. Crudden, M. Sateesh and R. Lewis, Mercaptopropyl-modified mesoporous silica: A remarkable support for the preparation of a reusable, heterogeneous palladium catalyst for coupling reactions, *Journal of the American Chemical Society*, **2005**, 127, 28, 10045–10050.

[159] Q. Chen, C. Xin, L.-L. Lou, K. Yu, F. Ding and S. Liu, Mesoporous SBA-15 with short mesochannels immobilized natural quinine for asymmetric michael addition of chalcones, *Catalysis Letters*, **2011**, 141, 9, 1378–1383.

[160] C. Baleizao, B. Gigante, H. Garcia and A. Corma, Chiral vanadyl Schiff base complex anchored on silicas as solid enantioselective catalysts for formation of cyanohydrins: optimization of the asymmetric induction by support modification, *Journal of Catalysis*, **2003**, 215, 2, 199–207.

[161] M. Iwamoto, T. Abe and Y. Tachibana, Control of bandgap of iron oxide through its encapsulation into SiO_2-based mesoporous materials, *Journal of Molecular Catalysis A - Chemical*, **2000**, 155, 1-2, 143–153.

[162] Y. Xu and C. Langford, Photoactivity of titanium dioxide supported on MCM41, zeolite X, and zeolite Y, *Journal of Physical Chemistry B*, **1997**, 101, 16, 3115–3121.

[163] A. M. Busuioc, V. Meynen, E. Beyers, M. Mertens, P. Cool, N. Bilba and E. F. Vansant, Structural features and photocatalytic behaviour of titania deposited within the pores of SBA-15, *Applied Catalysis A - General*, **2006**, 312, 153–164.

[164] G. Prieto, J. Zecevic, H. Friedrich, K. P. de Jong and P. E. de Jongh, Towards stable catalysts by controlling collective properties of supported metal nanoparticles, *Nature Materials*, **2013**, 12, 1, 34–39.

[165] G. Morales, G. Athens, B. F. Chmelka, R. van Grieken and J. A. Melero, Aqueous-sensitive reaction sites in sulfonic acid-functionalized mesoporous silicas, *Journal of Catalysis*, **2008**, 254, 2, 205–217.

[166] A. Karam, J. C. Alonso, T. I. Gerganova, P. Ferreira, N. Bion, J. Barrault and F. Jerome, Sulfonic acid functionalized crystal-like mesoporous benzene-silica as a remarkable water-tolerant catalyst, *Chemical Communications*, **2009**, 45, 7000–7002.

[167] W. Wang, J. E. Lofgreen and G. A. Ozin, Why PMO? Towards Functionality and Utility of Periodic Mesoporous Organosilicas, *Small*, **2010**, 6, 23, 2634–2642.

[168] C. Bispo, P. Ferreira, A. Trouve, I. Batonneau-Gener, F. Liu, F. Jerome and N. Bion, Role of acidity and hydrophobicity in the remarkable catalytic activity in water of sulfonic acid-functionalized phenyl-PMO materials, *Catalysis Today*, **2013**, 218, 85–92.

[169] J. Ouwehand, J. Lauwaert, D. Esquivel, K. Hendrickx, V. Van Speybroeck, J. W. Thybaut and P. Van Der Voort, Facile synthesis of cooperative acid-base catalysts by clicking cysteine and cysteamine on an ethylene-bridged Periodic Mesoporous Organosilica, *European Journal of Inorganic Chemistry*, **2016**, 13-14, 2144–2151.

[170] Q. Yang, J. Liu, L. Zhang and C. Li, Functionalized periodic mesoporous organosilicas for catalysis, *Journal of Materials Chemistry*, **2009**, 19, 14, 1945–1955.

[171] Q. Yang, M. Kapoor, S. Inagaki, N. Shirokura, J. Kondo and K. Domen, Catalytic application of sulfonic acid functionalized mesoporous benzene-silica with crystal-like pore wall structure in esterification, *Journal of Molecular Catalysis A - Chemical*, **2005**, 230, 1-2, 85–89.

[172] M. Kapoor, A. Bhaumik, S. Inagaki, K. Kuraoka and T. Yazawa, Titanium containing inorganic organic hybrid mesoporous materials with exceptional activity in epoxidation of alkenes using hydrogen peroxide, *Journal of Materials Chemistry*, **2002**, 12, 10, 3078–3083.

[173] S. Sisodiya, S. Shylesh and A. P. Singh, Tin incorporated periodic mesoporous organosilicas (Sn-PMOs): Synthesis, characterization, and catalytic activity in the epoxidation reaction of olefins, *Catalysis Communications*, **2011**, 12, 7, 629–633.

[174] S. Shylesh and A. P. Singh, Vanadium-containing ethane-silica hybrid periodic mesoporous organosilicas: Synthesis, structural characterization and catalytic applications, *Microporous and Mesoporous Materials*, **2006**, 94, 1-3, 127–138.

[175] A. Feliczak, K. Walczak, A. Wawrzynczak and I. Nowak, The use of mesoporous molecular sieves containing niobium for the synthesis of vegetable oil-based products, *Catalysis Today*, **2009**, 140, 1-2, 23–29.

[176] A. Bhaumik, M. Kapoor and S. Inagaki, Ammoximation of ketones catalyzed by titanium-containing ethane bridged hybrid mesoporous silsesquioxane, *Chemical Communications*, **2003**, 4, 470–471.

[177] Q. Yang, Y. Li, L. Zhang, J. Yang, J. Liu and C. Li, Hydrothermal stability and catalytic activity of aluminum-containing mesoporous ethane-silicas, *Journal of Physical Chemistry B*, **2004**, 108, 23, 7934–7937.

[178] B. Rac, P. Hegyes, P. Forgo and A. Molnar, Sulfonic acid-functionalized phenylene-bridged periodic mesoporous organosilicas as catalyst materials, *Applied Catalysis A - General*, **2006**, 299, 193–201.

[179] D. Dubé, M. Rat, W. Shen, B. Nohair, F. Beland and S. Kaliaguine, Perfluorinated alkylsulfonic acid functionalized periodic mesostructured organosilica: A new acidic catalyst, *Applied Catalysis A - General*, **2009**, 358, 2, 232–239.

[180] D. Dubé, M. Rat, F. Beland and S. Kaliaguine, Sulfonic acid functionalized periodic mesostructured organosilica as heterogeneous catalyst, *Microporous and Mesoporous Materials*, **2008**, 111, 1-3, 596–603.

[181] M. I. Lopez, D. Esquivel, C. Jimenez-Sanchidrian, F. J. Romero-Salguero and P. Van Der Voort, A "one-step" sulfonic acid PMO as a recyclable acid catalyst, *Journal of Catalysis*, **2015**, 326, 139–148.

[182] S. El Hankari, B. Motos-Perez, P. Hesemann, A. Bouhaouss and J. J. E. Moreau, Pore size control and organocatalytic properties of nanostructured silica hybrid materials containing amino and ammonium groups, *Journal of Materials Chemistry*, **2011**, 21, 19, 6948–6955.

[183] J. Alauzun, A. Mehdi, C. Reye and R. J. P. Corriu, Mesoporous materials with an acidic framework and basic pores. A successful cohabitation, *Journal of the American Chemical Society*, **2006**, 128, 27, 8718–8719.

[184] S. Shylesh, A. Wagener, A. Seifert, S. Ernst and W. R. Thiel, Mesoporous organosilicas with acidic frameworks and basic sites in the pores: An approach to cooperative catalytic reactions, *Angewandte Chemie-Int. Edition*, **2010**, 49, 1, 184–187.

[185] F.-X. Zhu, W. Wang and H.-X. Li, Water-medium and solvent-free organic reactions over a bifunctional catalyst with Au nanoparticles covalently bonded to HS/SO_3H functionalized Periodic Mesoporous Organosilica, *Journal of the American Chemical Society*, **2011**, 133, 30, 11632–11640.

[186] J. Hong and F. Zaera, Interference of the surface of the solid on the performance of tethered molecular catalysts, *Journal of the American Chemical Society*, **2012**, 134, 31, 13056–13065.

[187] J. Y. Shi, C. A. Wang, Z. J. Li, Q. Wang, Y. Zhang and W. Wang, Heterogeneous organocatalysis at work: Functionalization of hollow Periodic Mesoporous Organosilica Spheres with MacMillan catalyst, *Chemistry - A European Journal*, **2011**, 17, 22, 6206–6213.

[188] S. Hudson, J. Cooney, B. K. Hodnett and E. Magner, Chloroperoxidase on periodic mesoporous organosilanes: Immobilization and reuse, *Chemistry of Materials*, **2007**, 19, 8, 2049–2055.

[189] N. Yu, Y. Ding, A.-Y. Lo, S.-J. Huang, P.-H. Wu, C. Liu, D. Yin, Z. Fu, D. Yin, C.-T. Hung, Z. Lei and S.-B. Liu, Gold nanoparticles supported on periodic mesoporous organosilicas for epoxidation of olefins: Effects of pore architecture and surface modification method of the supports, *Microporous and Mesoporous Materials*, **2011**, 143, 2-3, 426–434.

[190] J. Liu, H. Q. Yang, F. Kleitz, Z. G. Chen, T. Y. Yang, E. Strounina, G. Q. Lu and S. Z. Qiao, Yolk-shell hybrid materials with a Periodic Mesoporous Organosilica shell: Ideal nanoreactors for selective alcohol oxidation, *Advanced Functional Materials*, **2012**, 22, 3, 591–599.

[191] R. A. Garcia, R. van Grieken, J. Iglesias, V. Morales and D. Gordillo, Synthesis of chiral periodic mesoporous silicas incorporating tartrate derivatives in the framework and their use in asymmetric sulfoxidation, *Chemistry of Materials*, **2008**, 20, 9, 2964–2971.

[192] P. Wang, X. Liu, J. Yang, Y. Yang, L. Zhang, Q. Yang and C. Li, Chirally functionalized mesoporous organosilicas with built-in BINAP ligand for asymmetric catalysis, *Journal of Materials Chemistry*, **2009**, 19, 42, 8009–8014.

[193] P. Borah and Y. Zhao, beta-Diketimine appended periodic mesoporous organosilica as a scaffold for immobilization of palladium acetate: An efficient green catalyst for Wacker type reaction, *Journal of Catalysis*, **2014**, 318, 43–52.

[194] B. Karimi, D. Elhamifar, J. H. Clark and A. J. Hunt, Ordered mesoporous organosilica with ionic-liquid framework: An efficient and reusable support for the palladium-catalyzed Suzuki-Miyaura coupling reaction in water, *Chemistry - A European Journal*, **2010**, 16, 27, 8047–8053.

[195] B. K. Bahuleyan, B. R. Jermy, I. Y. Ahn, H. Suh, D.-W. Park, C. S. Ha and I. Kim, One-pot synthesis of spherical periodic mesoporous organosilica supported catalyst bearing Ni(II) alpha-diimine complexes for ethylene polymerization, *Catalysis Communications*, **2009**, 11, 4, 252–256.

[196] T. P. Nguyen, P. Hesemann, P. Gaveau and J. J. E. Moreau, Periodic mesoporous organosilica containing ionic bis-aryl-imidazolium entities: Heterogeneous precursors for silica-hybrid-supported NHC complexes, *Journal of Materials Chemistry*, **2009**, 19, 24, 4164–4171.

[197] E.-Y. Jeong, A. Burri, S.-Y. Lee and S.-E. Park, Synthesis and catalytic behavior of tetrakis(4-carboxyphenyl) porphyrin-periodic mesoporous organosilica, *Journal of Materials Chemistry*, **2010**, 20, 48, 10869–10875.

[198] V. Dufaud, F. Beauchesne and L. Bonneviot, Organometallic chemistry inside the pore walls of mesostructured silica materials, *Angewandte Chemie-Int. Edition*, **2005**, 44, 22, 3475–3477.

[199] T. Zhang, C. Gao, H. Yang and Y. Zhao, Synthesis of a ferrocene-containing ordered mesoporous organosilica and its catalytic activity, *Journal of Porous Materials*, **2010**, 17, 5, 643–649.

[200] P. Borah, X. Ma, K. T. Nguyen and Y. Zhao, A Vanadyl Complex Grafted to Periodic Mesoporous Organosilica: A Green Catalyst for Selective Hydroxylation of Benzene to Phenol, *Angewandte Chemie-Int. Edition*, **2012**, 51, 31, 7756–7761.

[201] M. A. O. Lourenco, L. Carneiro, A. Mayoral, I. Diaz, A. R. Silva and P. Ferreira, Chiral periodic mesoporous copper(II) bis(oxazoline) phenylene-silica: A highly efficient and reusable asymmetric heterogeneous catalyst, *Journal of Catalysis*, **2014**, 320, 63–69.

[202] H. Yang, X. Han, G. Li, Z. Ma and Y. Hao, Mesoporous ethane-silicas functionalized with a bulky N-heterocyclic carbene for Suzuki-Miyaura coupling of aryl chlorides and benzyl chlorides, *Journal of Physical Chemistry C*, **2010**, 114, 50, 22221–22229.

[203] T. Seki, K. McEleney and C. M. Crudden, Enantioselective catalysis with a chiral, phosphane-containing PMO material, *Chemical Communications*, **2012**, 48, 51, 6369–6371.

[204] X. Yang, F. Zhu, J. Huang, F. Zhang and H. Li, Phenyl@Rh(I)-bridged Periodic Mesoporous Organometalsilica with high catalytic efficiency in water-medium organic reactions, *Chemistry of Materials*, **2009**, 21, 20, 4925–4933.

[205] A. Kuschel, M. Luka, M. Wessig, M. Drescher, M. Fonin, G. Kiliani and S. Polarz, Organic ligands made porous: Magnetic and catalytic properties of transition metals coordinated to the surfaces of mesoporous organosilica, *Advanced Functional Materials*, **2010**, 20, 7, 1133–1143.

[206] M. Waki, N. Mizoshita, T. Tani and S. Inagaki, Periodic Mesoporous Organosilica derivatives bearing a high density of metal complexes on pore surfaces, *Angewandte Chemie-Int. Edition*, **2011**, 50, 49, 11667–11671.

[207] H. C. Kolb, M. G. Finn and K. B. Sharpless, Click chemistry: Diverse chemical function from a few good reactions, *Angewandte Chemie-Int. Edition*, **2001**, 40, 11, 2004.

[208] C. E. Hoyle and C. N. Bowman, Thiol-ene click chemistry, *Angewandte Chemie-Int. Edition*, **2010**, 49, 9, 1540–1573.

[209] Y. Li, H. Su, X. Feng, Z. Wang, K. Guo, C. Wesdemiotis, Q. Fu, S. Z. D. Cheng and W.-B. Zhang, Thiol-Michael click chemistry: another efficient tool for head functionalization of giant surfactants, *Polymer Chemistry*, **2014**, 5, 21, 6151–6162.

[210] C. E. Hoyle, Y. Tai and T. Roper, Thiol–enes: Chemistry of the past with promise for the future, *Journal of Polymer Science A - Polymer Chemistry*, **2004**, 42, 21, 5301–5338.

[211] J. Nakazawa, B. J. Smith and T. D. P. Stack, Discrete Complexes Immobilized onto Click-SBA-15 Silica: Controllable Loadings and the Impact of Surface Coverage on Catalysis, *Journal of the American Chemical Society*, **2012**, 134, 5, 2750–2759.

[212] A. Schlossbauer, D. Schaffert, J. Kecht, E. Wagner and T. Bein, Click chemistry for high-density biofunctionalization of mesoporous silica, *Journal of the American Chemical Society*, **2008**, 130, 38, 12558.

[213] J. Gao, X. Zhang, S. Xu, F. Tan, X. Li, Y. Zhang, Z. Qu, X. Quan and J. Liu, Clickable Periodic Mesoporous Organosilicas: Synthesis, click reactions, and adsorption of antibiotics, *Chemistry - A European Journal*, **2014**, 20, 7, 1957–1963.

[214] A. Schachtschneider, M. Wessig, M. Spitzbarth, A. Donner, C. Fischer, M. Drescher and S. Polarz, Directional materials: Nanoporous organosilica monoliths with multiple gradients prepared using click chemistry, *Angewandte Chemie-Int. Edition*, **2015**, 54, 36, 10465–10469.

[215] O. Bortolini, L. Caciolli, A. Cavazzini, V. Costa, R. Greco, A. Massi and L. Pasti, Silica-supported 5-(pyrrolidin-2-yl)tetrazole: development of organocatalytic processes from batch to continuous-flow conditions, *Green Chemistry*, **2012**, 14, 4, 992–1000.

[216] J. Gehring, B. Trepka, N. Klinkenberg, H. Bronner, D. Schleheck and S. Polarz, Sunlight-triggered nanoparticle synergy: teamwork of reactive oxygen species and nitric oxide released from mesoporous organosilica with advanced antibacterial activity, *Journal of the American Chemical Society*, **2016**, 138, 9, 3076–3084.

[217] A. K. Tucker-Schwartz, R. A. Farrell and R. L. Garrell, Thiol-ene click reaction as a general route to functional trialkoxysilanes for surface coating applications, *Journal of the American Chemical Society*, **2011**, 133, 29, 11026–11029.

[218] J. Gehring, D. Schleheck, B. Trepka and S. Polarz, Mesoporous organosilica nanoparticles containing superacid and click functionalities leading to cooperativity in biocidal coatings, *ACS Applied Materials and Interfaces*, **2015**, 7, 1, 1021–1029.

[219] I. E. Marko, P. R. Giles, M. Tsukazaki, S. M. Brown and C. J. Urch, Copper-catalyzed oxidation of alcohols to aldehydes and ketones: An efficient, aerobic alternative, *Science*, **1996**, 274, 5295, 2044–2046.

[220] T. Mallat and A. Baiker, Oxidation of alcohols with molecular oxygen on solid catalysts, *Chemical Reviews*, **2004**, 104, 6, 3037–3058.

[221] Z. Shi, C. Zhang, C. Tang and N. Jiao, Recent advances in transition-metal catalyzed reactions using molecular oxygen as the oxidant, *Chemical Society Reviews*, **2012**, 41, 8, 3381–3430.

[222] S. E. Davis, M. S. Ide and R. J. Davis, Selective oxidation of alcohols and aldehydes over supported metal nanoparticles, *Green Chemistry*, **2013**, 15, 1, 17–45.

[223] I. E. Marko, P. R. Giles, M. Tsukazaki, I. Chelle-Regnaut, C. J. Urch and S. M. Brown, Efficient, aerobic, ruthenium-catalyzed oxidation of alcohols into aldehydes and ketones, *Journal of the American Chemical Society*, **1997**, 119, 51, 12661–12662.

[224] W. H. Fung, W. Y. Yu and C. M. Che, Chemoselective oxidation of alcohols to aldehydes and ketones by tert-butyl hydroperoxide catalyzed by a ruthenium complex of N,N ',N "-trimethyl-1,4,7-triazacyclononane, *Journal of Organic Chemistry*, **1998**, 63, 9, 2873–2877.

[225] A. Hanyu, E. Takezawa, S. Sakaguchi and Y. Ishii, Selective aerobic oxidation of primary alcohols catalyzed by a $Ru(PPh_3)_3Cl_2$/hydroquinone system, *Tetrahedron Letters*, **1998**, 39, 31, 5557–5560.

[226] K. Yamaguchi, K. Mori, T. Mizugaki, K. Ebitani and K. Kaneda, Creation of a monomeric Ru species on the surface of hydroxyapatite as an efficient heterogeneous catalyst for aerobic alcohol oxidation, *Journal of the American Chemical Society*, **2000**, 122, 29, 7144–7145.

[227] A. Dijksman, A. Marino-Gonzalez, A. M. I. Payeras, I. W. C. E. Arends and R. A. Sheldon, Efficient and selective aerobic oxidation of alcohols into aldehydes and ketones using ruthenium/TEMPO as the catalytic system, *Journal of the American Chemical Society*, **2001**, 123, 28, 6826–6833.

[228] G. Csjernyik, A. Ell, L. Fadini, B. Pugin and J. Backvall, Efficient ruthenium-catalyzed aerobic oxidation of alcohols using a biomimetic coupled catalytic system, *Journal of Organic Chemistry*, **2002**, 67, 5, 1657–1662.

[229] K. Yamaguchi and N. Mizuno, Supported ruthenium catalyst for the heterogeneous oxidation of alcohols with molecular oxygen, *Angewandte Chemie-Int. Edition*, **2002**, 41, 23, 4538.

[230] B. Karimi, D. Elhamifar, O. Yari, M. Khorasani, H. Vali, J. H. Clark and A. J. Hunt, Synthesis and characterization of alkyl-imidazolium-based Periodic Mesoporous Organosilicas: A versatile host for the immobilization of perruthenate (RuO_4^-) in the aerobic oxidation of alcohols, *Chemistry - A European Journal*, **2012**, 18, 42, 13520–13530.

[231] S. Ganesamoorthy, M. M. Tamizh, K. Shanmugasundaram and R. Karvembu, Immobilization of Ru(III) complex on silica: a heterogenized catalyst for selective oxidation of alcohols in water at room temperature, *Tetrahedron Letters*, **2013**, 54, 51, 7035–7039.

[232] M. Ide, E. De Canck, I. Van Driessche, F. Lynen and P. Van Der Voort, Developing a new and versatile ordered mesoporous organosilica as a pH and temperature stable chromatographic packing material, *RSC Advances*, **2015**, 5, 8, 5546–5552.

[233] T. Koiwa, Y. Masuda, J. Shono, Y. Kawamoto, Y. Hoshino, T. Hashimoto, K. Natarajan and K. Shimizu, Synthesis, characterization, and detailed electrochemistry of binuclear ruthenium(III) complexes bridged by bisacetylacetonate. Crystal and molecular structures of [Ru(acac)(2)(2)(tae)] (acac=2,4-pentanedionate ion, tae=1,1,2,2-tetraacetylethanate dianion), *Inorganic Chemistry*, **2004**, 43, 20, 6215–6223.

[234] M. J. Frisch and G. W. Trucks and H. B. Schlegel and G. E. Scuseria and M. A. Robb and J. R. Cheeseman and G. Scalmani and V. Barone and B. Mennucci and G. A. Petersson and H. Nakatsuji and M. Caricato and X. Li and H. P. Hratchian and A. F. Izmaylov and J. Bloino and G. Zheng and J. L. Sonnenberg and M. Hada and M. Ehara and K. Toyota and R. Fukuda and J. Hasegawa and M. Ishida and T. Nakajima and Y. Honda and O. Kitao and H. Nakai and T. Vreven and Montgomery, Jr., J. A. and J. E. Peralta and F. Ogliaro and M. Bearpark and J. J. Heyd and E. Brothers and K. N. Kudin and V. N. Staroverov and R. Kobayashi and J. Normand and K. Raghavachari and A. Rendell and J. C. Burant and S. S. Iyengar and J. Tomasi and

M. Cossi and N. Rega and J. M. Millam and M. Klene and J. E. Knox and J. B. Cross and V. Bakken and C. Adamo and J. Jaramillo and R. Gomperts and R. E. Stratmann and O. Yazyev and A. J. Austin and R. Cammi and C. Pomelli and J. W. Ochterski and R. L. Martin and K. Morokuma and V. G. Zakrzewski and G. A. Voth and P. Salvador and J. J. Dannenberg and S. Dapprich and A. D. Daniels and O. Farkas and J. B. Foresman and J. V. Ortiz and J. Cioslowski and D. J. Fox, Gaussian09 Revision D.01, Gaussian Inc. Wallingford CT 2009.

[235] C. Lee, W. Yang and R. Parr, Development of the Colle-Salvetti correlation-energy formula into a functional of the electron-density, *Physical Review B*, **1988**, 37, 2, 785–789.

[236] A. Becke, A real-space model of nondynamical correlation, *Journal of Chemical Physics*, **2003**, 119, 6, 2972–2977.

[237] J. Perdew, K. Burke and M. Ernzerhof, Generalized gradient approximation made simple, *Physical Review Letters*, **1996**, 77, 18, 3865–3868.

[238] J. Perdew, K. Burke and M. Ernzerhof, Generalized gradient approximation made simple (vol 77, pg 3865, 1996), *Physical Review Letters*, **1997**, 78, 7, 1396.

[239] N. Handy and A. Cohen, Left-right correlation energy, *Molecular Physics*, **2001**, 99, 5, 403–412.

[240] W. Hoe, A. Cohen and N. Handy, Assessment of a new local exchange functional OPTX, *Chemical Physics Letters*, **2001**, 341, 3-4, 319–328.

[241] F. Weigend, Accurate Coulomb-fitting basis sets for H to Rn, *Physical Chemistry Chemical Physics*, **2006**, 8, 9, 1057–1065.

[242] F. Weigend and R. Ahlrichs, Balanced basis sets of split valence, triple zeta valence and quadruple zeta valence quality for H to Rn: Design and assessment of accuracy, *Physical Chemistry Chemical Physics*, **2005**, 7, 18, 3297–3305.

[243] S. Grimme, J. Antony, S. Ehrlich and H. Krieg, A consistent and accurate ab initio parametrization of density functional dispersion correction (DFT-D) for the 94 elements H-Pu, *Journal of Chemical Physics*, **2010**, 132, 15.

[244] S. Grimme, S. Ehrlich and L. Goerigk, Effect of the damping function in dispersion corrected Density Functional Theory, *Journal of Computational Chemistry*, **2011**, 32, 7, 1456–1465.

[245] L. Goerigk and S. Grimme, A thorough benchmark of density functional methods for general main group thermochemistry, kinetics, and noncovalent interactions, *Physical Chemistry Chemical Physics*, **2011**, 13, 14, 6670–6688.

[246] S. Boys and F. Bernardi, Calculation of small molecular interactions by differences of separate total energies - Some procedures with reduced errors, *Molecular Physics*, **1970**, 19, 4, 553.

[247] M. Swart, A. Ehlers and K. Lammertsma, Performance of the OPBE exchange-correlation functional, *Molecular Physics*, **2004**, 102, 23-24, 2467–2474.

[248] T. Bogaerts, S. Wouters, P. Van Der Voort and V. Van Speybroeck, Mechanistic investigation on oxygen transfer with the manganese-salen complex, *ChemCatChem*, **2015**, 7, 17, 2711–2719.

[249] Y. Minenkov, A. Singstad, G. Occhipinti and V. R. Jensen, The accuracy of DFT-optimized geometries of functional transition metal compounds: a validation study of catalysts for olefin metathesis and other reactions in the homogeneous phase, *Dalton Transactions*, **2012**, 41, 18, 5526–5541.

[250] J. Zhang, Q. Jiang, D. Yang, X. Zhao, Y. Dong and R. Liu, Reaction-activated palladium catalyst for dehydrogenation of substituted cyclohexanones to phenols and H-2 without oxidants and hydrogen acceptors, *Chemical Science*, **2015**, 6, 8, 4674–4680.

[251] C. Li, H. Yang, X. Shi, R. Liu and Q. Yang, Synthesis of SBA-15 type mesoporous organosilicas with diethylenebenzene in the framework and post-synthetic framework modification, *Microporous and Mesoporous Materials*, **2007**, 98, 1-3, 220–226.

[252] U. Neue, *HPLC Columns: Theroy, Technology and Practice*, John Wiley and Sons, **1997**.

[253] C. Poole and S. Schuette, *Contemporary practice of chromatography*, Elsevier Science BV, **1984**.

[254] The Ultimate Guide to HPLC/UHPLC Reversed Phase Selectivity, https://www.phenomenex.com/Info/WebDocumentServe/reversedguide.pdf.

[255] F. Lynen, Analytical Separation Methods, UGhent Course Syllabus.

[256] H. Schmidt-Traub, M. Schulte and A. Seidel-Morgenstern, *Preparative Chromatography*, Wiley-VCH, **2012**.

[257] H. Colon, X. Zhang, J. Murphy, J. Rivera and L. Colon, Allyl-functionalized hybrid silica monoliths, *Chemical Communications*, **2005**, 22, 2826–2828.

[258] M. Wahab, D. Patel, R. Wimalasinghe and D. Armstrong, Fundamental and practical insights on the packing of modern high-efficiency analytical and capillary columns, *Analytical Chemistry*, **2017**, DOI: 10.1021/acs.analchem.7b00931.

[259] K. Nakanishi and N. S., Inorganic porous material and process for making same, US5624875.

[260] W. De Malsche, H. Eghbali, D. Clicq, J. Vangelooven, H. Gardeniers and G. Desmet, Pressure-driven reverse-phase liquid chromatography separations in ordered nonporous pillar array columns, *Analytical Chemistry*, **2007**, 79, 15, 5915–5926.

[261] R. M. Tiggelaar, V. Verdoold, H. Eghbali, G. Desmet and J. G. E. Gardeniers, Characterization of porous silicon integrated in liquid chromatography chips, *Lab on a Chip*, **2009**, 9, 3, 456–463.

[262] M. Tswett, Adsorptionsanalyse und chrematographische Methode. Anwendung auf die Chemie des Chlorophylls, *Berichte der Deutschen botanischen Gesellschaft*, **1906**, 24, 316–323.

[263] R. Majors, Current Trends in HPLC Column Technology, *LCGC*, **2012**, 25, 31–39.

[264] U. Neue, T. Wheat, J. Mazzeo, C. Mazza, J. Cavanaugh, F. Xia and D. Diehl, Differences in preparative loadability between the charged and uncharged forms of ionizable compounds, *Journal of Chromatography A*, **2004**, 1030, 123–134.

[265] D. McCalley, Comparative evaluation of bonded-silica reversed-phase columns for high-performance liquid chromatography using strongly basic compounds and alternative organic modifiers buffered at acid pH, *Journal of Chromatography A*, **1997**, 769, 2, 169–178.

[266] R. Fredriksson, Analytical versus Preparative and Production-Scale HPLC: Some Considerations, *Innovations in Pharmaceutical Technology*, **2012**, 40, 16–18.

[267] U. Huber and R. Majors, Principles in preparative HPLC, chem.agilent.com.

[268] W. Sievers, R. Bicker, D. Desch, J. Von Eysmondt, R. Keller and F. Richard, Procedure for the chromatographic purification of insulins, US6710167.

[269] R. Dickhardt, B. Unger and C. Grafe, Chromatographic process for purification of insulin, US5621073.

[270] U. Trudinger, G. Muller and K. K. Unger, Porous zirconia and titania as packing materials for High-Performance Liquid-Chromatography, *Journal of Chromatography*, **1990**, 535, 1-2, 111–125.

[271] H. Matsuda, H. Nakamura and T. Nakajima, New ceramic titania - Selective adsorbent for organic-phosphates, *Analytical Sciences*, **1990**, 6, 6, 911–912.

[272] M. Kawahara, H. Nakamura and T. Nakajima, Titania and Zirconia as new Ceramic Column Packing Materials for High-Performance Liquid-Chromatography, *Analytical Sciences*, **1989**, 5, 4, 485–486.

[273] J. Winkler and S. Marme, Titania as a sorbent in normal-phase liquid chromatography, *Journal of Chromatography A*, **2000**, 888, 1-2, 51–62.

[274] J. Nawrocki, C. Dunlap, J. Li, J. Zhao, C. McNeff, A. McCormick and P. Carr, Part II. Chromatography using ultra-stable metal oxide-based stationary phases for HPLC, *Journal of Chromatography A*, **2004**, 1028, 1, 31–62.

[275] J. Nawrocki, C. Dunlap, A. McCormick and P. Carr, Part I. Chromatography using ultra-stable metal oxide-based stationary phases for HPLC, *Journal of Chromatography A*, **2004**, 1028, 1, 1–30.

[276] K. Engholm-Keller and M. R. Larsen, Titanium dioxide as chemo-affinity chromatographic sorbent of biomolecular compounds - Applications in acidic modification-specific proteomics, *Journal of Proteomics*, **2011**, 75, 2, 317–328.

[277] K. Unger, D. Kumar, M. Grün, G. Buchel, S. Ludtke, T. Adam, K. Schumacher and S. Renker, Synthesis of spherical porous silicas in the micron and submicron size range: challenges and opportunities for miniaturized high-resolution chromatographic and electrokinetic separations, *Journal of Chromatography A*, **2000**, 892, 1-2, 47–55.

[278] D. Cabooter, A. Fanigliulo, G. Bellazzi, B. Allieri, A. Rottigni and G. Desmet, Relationship between the particle size distribution of commercial fully porous and superficially porous high-performance liquid chromatography column packings and their chromatographic performance, *Journal of Chromatography A*, **2010**, 1217, 45, 7074–7081.

[279] J. Kirkland, Ultrafast reversed-phase high-performance liquid chromatographic separations: An overview, *Journal of Chromatographic Science*, **2000**, 38, 12, 535–544.

[280] S. Fekete, J. Schappler, J.-L. Veuthey and D. Guillarme, Current and future trends in UHPLC, *Trends in Analytical Chemistry*, **2014**, 63, 2–13.

[281] G. Guiochon and F. Gritti, Shell particles, trials, tribulations and triumphs, *Journal of Chromatography A*, **2011**, 1218, 15, 1915–1938.

[282] R. Hayes, A. Ahmed, T. Edge and H. Zhang, Core-shell particles: Preparation, fundamentals and applications in high performance liquid chromatography, *Journal of Chromatography A*, **2014**, 1357, SI, 36–52.

[283] W. Stöber, A. Fink and E. Bohn, Controlled Growth of Monodisperse Silica Spheres in Micron Size Range, *Journal of Colloid and Interface Science*, **1968**, 26, 1, 62.

[284] F. Gritti, T. Farkas, J. Heng and G. Guiochon, On the relationship between band broadening and the particle-size distribution of the packing material in liquid chromatography: Theory and practice., *Journal of Chromatography A*, **2011**, 1218, 45, 8209–8221.

[285] A. C. Sanchez, G. Friedlander, S. Fekete, J. Anspach, D. Guillarme, M. Chitty and T. Farkas, Pushing the performance limits of reversed-phase ultra high performance liquid chromatography with 1.3 mu m core-shell particles, *Journal of Chromatography A*, **2013**, 1311, 90–97.

[286] J. J. DeStefano, T. J. Langlois and J. J. Kirkland, Characteristics of superficially-porous silica particles for fast HPLC: Some performance comparisons with sub-2-mu m particles, *Journal of Chromatographic Science*, **2008**, 46, 3, 254–260.

[287] A. Fanigliulo, D. Cabooter, G. Bellazzi, D. Tramarin, B. Allieri, A. Rottigni and G. Desmet, Comparison of performance of high-performance liquid chromatography columns packed with superficially and fully porous 2.5 μm particles using kinetic plots, *Journal of Separation Science*, **2010**, 33, 23-24, 3655–3665.

[288] C. Scott, Continuous separation of ion-exchange resin into size fractions by elutriation with water, *Analytical Biochemistry*, **1968**, 24, 2, 292.

[289] S. A. Schuster, B. M. Wagner, B. E. Boyes and J. J. Kirkland, Wider pore superficially porous particles for peptide separations by HPLC, *Journal of Chromatographic Science*, **2010**, 48, 7, 566–571.

[290] S. Fekete, R. Berky, J. Fekete, J.-L. Veuthey and D. Guillarme, Evaluation of a new wide pore core-shell material (Aeris^{TM} Widepore) and comparison with other existing stationary phases for the analysis of intact proteins, *Journal of Chromatography A*, **2012**, 1236, 177–188.

[291] A. Rodrigues, Z. Lu, J. Loureiro and G. Carta, Peak Resolution in Linear Chromatography - Effects of Intraparticle Convection, *Journal of Chromatography A*, **1993**, 653, 2, 189–198.

[292] G. Buchel, M. Grün, K. Unger, A. Matsumoto and K. Tsutsumi, Tailored syntheses of nanostructured silicas: Control of particle morphology, particle size and pore size, *Supramolecular Science*, **1998**, 5, 3-4, 253–259.

[293] H. Yang, G. Vovk, N. Coombs, I. Sokolov and G. Ozin, Synthesis of mesoporous silica spheres under quiescent aqueous acidic conditions, *Journal of Materials Chemistry*, **1998**, 8, 3, 743–750.

[294] K. Schumacher, M. Grün and K. Unger, Novel synthesis of spherical MCM-48, *Microporous and Mesoporous Materials*, **1999**, 27, 2-3, 201–206.

[295] K. Gallis, J. Araujo, K. Duff, J. Moore and C. Landry, The use of mesoporous silica in liquid chromatography, *Advanced Materials*, **1999**, 11, 17, 1452–1455.

[296] M. Mesa, L. Sierra, B. Lopez, A. Ramirez and J. Guth, Preparation of micron-sized spherical particles of mesoporous silica from a triblock copolymer surfactant, usable as a stationary phase for liquid chromatography, *Solid State Sciences*, **2003**, 5, 9, 1303–1308.

[297] M. Mesa, L. Sierra, J. Patarin and J. Guth, Morphology and porosity characteristics control of SBA-16 mesoporous silica. Effect of the triblock surfactant Pluronic F127 degradation during the synthesis, *Solid State Sciences*, **2005**, 7, 8, 990–997.

[298] L. Yang, Y. Wang, G. Luo and Y. Dai, Preparation and functionalization of mesoporous silica spheres as packing materials for HPLC, *Particuology*, **2008**, 6, 3, 143–148.

[299] M. Nystrom, W. Herrmann and B. Larsson, Silica particles, a method for preparation of silica particles and the use of the particles, EP0298062.

[300] A. Sayari, Unprecedented expansion of the pore size and volume of periodic mesoporous silica, *Angewandte Chemie-Int. Edition*, **2000**, 39, 16, 2920–2922.

[301] Z. Jiang, R. P. Fisk, J. E. O'Gara, T. H. Walter and K. D. Wyndham, Porous inorganic/organic hybrid particles for chromatographic separations and process for their preparation, US6686035.

[302] Y. Goto, K. Okamoto and S. Inagaki, The formation of periodicity within the pore walls of mesoporous organosilica by post-synthesis treatment, *Bulletin of the Chemical Society of Japan*, **2005**, 78, 5, 932–936.

[303] G. Zhu, H. Zhong, Q. Yang and C. Li, Chiral mesoporous organosilica spheres: Synthesis and chiral separation capacity, *Microporous and Mesoporous Materials*, **2008**, 116, 1-3, 36–43.

[304] Y. Zhang, Y. Jin, H. Yu, P. Dai, Y. Ke and X. Liang, Pore expansion of highly monodisperse phenylene-bridged organosilica spheres for chromatographic application, *Talanta*, **2010**, 81, 3, 824–830.

[305] L. Guan, B. Di, M. Su and J. Qian, Immobilization of beta-glucosidase on bifunctional periodic mesoporous organosilicas, *Biotechnology Letters*, **2013**, 35, 8, 1323–1330.

[306] E. F. Vansant, P. Van Der Voort and K. Vrancken, *Characterization and chemical modification of the silica surface*, Elsevier Science BV, **1995**.

[307] J. Nawrocki, The silanol group and its role in liquid chromatography, *Journal of Chromatography A*, **1997**, 779, 1-2, 29–71.

[308] J. O'Gara, B. Alden, T. Walter, J. Petersen, C. Niederlander and U. Neue, Simple Perparation of a C8 HPLC Stationary-Phase with an Internal Polar Functional Group, *Analytical Chemistry*, **1995**, 67, 20, 3809–3813.

[309] T. Czajkowska, I. Hrabovsky, B. Buszewski, R. Gilpin and M. Jaroniec, Comparison of the retention of organic-acids on alkyl and alkylamide chemically bonded phases, *Journal of Chromatography A*, **1995**, 691, 1-2, 217–224.

[310] T. Czajkowska and M. Jaroniec, Selectivity of alkylamide bonded-phases with respect to organic acids under reversed-phase conditions, *Journal of Chromatography A*, **1997**, 762, 1-2, 147–158.

[311] S. W. Pettersson, E. Collet and U. Andersson, Chemical stability of reversed phase high performance liquid chromatography silica under sodium hydroxide regeneration conditions, *Journal of Chromatography A*, **2007**, 1142, 1, 93–97.

[312] H. Claessens and M. van Straten, Review on the chemical and thermal stability of stationary phases for reversed-phase liquid chromatography, *Journal of Chromatography A*, **2004**, 1060, 23–41.

[313] N. Sagliano, T. R. Floyd, R. A. Hartwick, J. M. Dibussolo and N. T. Miller, Studies on the stabilization of reversed phases for liquid chromatography, *Journal of Chromatography*, **1988**, 443, 155–172.

[314] J. Kirkland, J. Adams, M. van Straten and H. Claessens, Bidentate silane stationary phases for Reversed-Phase High-Performance Liquid Chromatography, *Analytical Chemistry*, **1998**, 70, 20, 4344–4352.

[315] B. C. Trammell, C. A. Boissel, C. Carignan, D. J. O'Shea, C. J. Hudalla, U. D. Neue and P. C. Iraneta, Development of an accelerated low-pH reversed-phase liquid chromatography column stability test, *Journal of Chromatography A*, **2004**, 1060, 1-2, 153–163.

[316] H. Y. Song, G. Desmet and D. Cabooter, Evaluation of the kinetic performance differences between Hydrophilic-Interaction Liquid Chromatography and Reversed-Phase Liquid Chromatography under conditions of identical packing structure, *Analytical Chemistry*, **2015**, 87, 24, 12331–12339.

[317] I. M. Rustamov, M. C. Chitty, T. Farkas, L. Loo and E. Welch, pH stable chromatographic media using templated multilayer organic/inorganic grafting, US7563367.

[318] J. Kirkland, C. Dilks and J. DeStefano, Normal-phase High-Performance Liquid-Chromatography with highly purified porous silica microspheres, *Journal of Chromatography*, **1993**, 635, 1, 19–30.

[319] H. Engelhardt and T. Lobert, Chromatographic determination of metallic impurities in reversed-phase HPLC columns, *Analytical Chemistry*, **1999**, 71, 9, 1885–1892.

[320] K. K. Unger and J. Schick-Kalb, Preparation of organically modified silicon dioxides, US4017528.

[321] Y. Yang, M. Belghazi, A. Lagadec, D. Miller and S. Hawthorne, Elution of organic solutes from different polarity sorbents using subcritical water, *Journal of Chromatography A*, **1998**, 810, 1-2, 149–159.

[322] T. Greibrokk and T. Andersen, High-temperature liquid chromatography, *Journal of Chromatography A*, **2003**, 1000, 1-2, 743–755.

[323] K. D. Wyndham, J. E. O'Gara, T. H. Walter, K. H. Glose, N. L. Lawrence, B. A. Alden, G. S. Izzo, C. J. Hudalla and P. C. Iraneta, Characterization and evaluation of C18HPLC stationary phases based on ethyl-bridged hybrid organic/inorganic particles, *Analytical Chemistry*, **2003**, 75, 24, 6781–6788.

[324] K. K. Unger, *Porous Silica*, Elsevier Scientific Publishing, **1979**.

[325] J. J. Kirkland, Completely porous microspheres for chromatographic uses, US3782075.

[326] R. Iler and H. J. McQueston, Uniform oxide microspheres and a process for their manufacture, US3855172.

[327] K. K. Unger and J. Schick-Kalb, Spherical porous silicon dioxide produced from polyalkoxysiloxanes, DE2155281.

[328] K. K. Unger and J. Schick-Kalb, Verfahren zur Herstellung von organisch modifizierten Siliciumdioxiden, DE2357184.

[329] M. Grün, I. Lauer and K. Unger, The synthesis of micrometer- and submicrometer-size spheres of ordered mesoporous oxide MCM-41, *Advanced Materials*, **1997**, 9, 3, 254.

[330] M. Grün, K. Unger, A. Matsumoto and K. Tsutsumi, Novel pathways for the preparation of mesoporous MCM-41 materials: control of porosity and morphology, *Microporous and Mesoporous Materials*, **1999**, 27, 2-3, 207–216.

[331] Q. Huo, J. Feng, F. Schüth and G. Stucky, Preparation of hard mesoporous silica spheres, *Chemistry of Materials*, **1997**, 9, 1, 14.

[332] H. Yang, N. Coombs and G. Ozin, Morphogenesis of shapes and surface patterns in mesoporous silica, *Nature*, **1997**, 386, 6626, 692–695.

[333] K. Yano and Y. Fukushima, Particle size control of mono-dispersed super-microporous silica spheres, *Journal of Materials Chemistry*, **2003**, 13, 10, 2577–2581.

[334] J. Holmes, M. Morris, J. Hanrahan, D. Keane and M. Copley, Method for synthesising microparticles, US20100272996.

[335] L. Qi, J. Ma, H. Cheng and Z. Zhao, Micrometer-sized mesoporous silica spheres grown under static conditions, *Chemistry of Materials*, **1998**, 10, 6, 1623–1626.

[336] C. Boissiere, A. van der Lee, A. El Mansouri, A. Larbot and E. Prouzet, A double step synthesis of mesoporous micrometric spherical MSU-X silica particles, *Chemical Communications*, **1999**, 20, 2047–2048.

[337] C. Boissiere, A. Larbot, A. van der Lee, P. Kooyman and E. Prouzet, A new synthesis of mesoporous MSU-X silica controlled by a two-step pathway, *Chemistry of Materials*, **2000**, 12, 10, 2902–2913.

[338] M. Le Page, R. Beau and J. Duchene, Chromatographic separation with porous silica, FR1473240.

[339] S. Imrich and I. Halazs, Verfahren zur Herstellung von Kugelformigen porösen SiO_2 Teilchen, DE2155045.

[340] H. Bergna and S. FA, Molded amorphous silica bodies and molding powders for manufacture of same, US3301635.

[341] A. Kiselev, K. GL, B. Lipkind and N. JS, Chromatographic adsorption agent by hydrothermal treatment of silicon dioxide xerogel, DE2225452.

[342] M. Ide, E. Wallaert, I. Van Driessche, F. Lynen, P. Sandra and P. Van Der Voort, Spherical mesoporous silica particles by spray drying: Doubling the retention factor of HPLC columns, *Microporous and Mesoporous Materials*, **2011**, 142, 1, 282–291.

[343] Y. Lu, H. Fan, A. Stump, T. Ward, T. Rieker and C. Brinker, Aerosol-assisted self-assembly of mesostructured spherical nanoparticles, *Nature*, **1999**, 398, 6724, 223–226.

[344] G. Rao, G. Lopez, J. Bravo, H. Pham, A. Datye, H. Xu and T. Ward, Monodisperse mesoporous silica microspheres formed by evaporation-induced self assembly of surfactant templates in aerosols, *Advanced Materials*, **2002**, 14, 18, 1301.

[345] S. Schacht, Q. Huo, M. Voigt, G. Stucky and F. Schüth, Oil-water interface templating of mesoporous macroscale structures, *Science*, **1996**, 273, 5276, 768–771.

[346] L. Yang, Y. Wang, Y. Sun, G. Luo and Y. Dal, Synthesis of micrometer-sized hard silica spheres with uniform mesopore size and textural pores, *Journal of Colloid and Interface Science*, **2006**, 299, 2, 823–830.

[347] R. Pal and D. Kundu, Sol-gel synthesis of porous and dense silica microspheres, *Journal of Non-Crystalline Solids*, **2009**, 355, 1, 76–78.

[348] R. Schiller, C. K. Weiss, J. Geserick, N. Husing and K. Landfester, Synthesis of Mesoporous Silica Particles and Capsules by Miniemulsion Technique, *Chemistry of Materials*, **2009**, 21, 21, 5088–5098.

[349] T. Martin, A. Galarneau, F. Di Renzo, F. Fajula and D. Plee, Morphological control of MCM-41 by pseudomorphic synthesis, *Angewandte Chemie-Int. Edition*, **2002**, 41, 14, 2590.

[350] A. Galarneau, J. Iapichella, K. Bonhomme, F. Di Renzo, P. Kooyman, O. Terasaki and F. Fajula, Controlling the morphology of mesostructured silicas by pseudomorphic transformation: A route towards applications, *Advanced Functional Materials*, **2006**, 16, 13, 1657–1667.

[351] C. Horvath, B. Preiss and S. Lipsky, Fast liquid chromatography - An investigation of operating paramters and separation of nucleotides on pellicular ion exchangers, *Analytical Chemistry*, **1967**, 39, 12, 1422–&.

[352] C. Horvath and S. Lipsky, Column design in High Pressure Liquid Chromatography, *Journal of Chromatographic Science*, **1969**, 7, 2, 109–&.

[353] J. J. Kirkland, Superficially porous supports for chromatography, US3505785.

[354] J. Kirkland, Controlled surface porosity supports for high speed gas and liquid chromatography, *Analytical Chemistry*, **1969**, 41, 1, 218.

[355] J. Kirkland and L. TJ, Porous microparticles solid cores, WO2007095162.

[356] J. Kirkland, Superficially porous silica microspheres for the fast High-Performance Liquid-Chromatography of macromolecules, *Analytical Chemistry*, **1992**, 64, 11, 1239–1245.

[357] J. Kirkland, F. Truszkowski, C. Dilks and G. Engel, Superficially porous silica microspheres for fast high-performance liquid chromatography of macromolecules, *Journal of Chromatography A*, **2000**, 890, 1, 3–13.

[358] J. Kirkland and L. TJ, Process for prepairing substrates with a porous surface, US2009297853.

[359] G. Buchel, K. Unger, A. Matsumoto and K. Tsutsumi, A novel pathway for synthesis of submicrometer-size solid core/mesoporous shell silica spheres, *Advanced Materials*, **1998**, 10, 13, 1036.

[360] S. Yoon, J. Kim, H. Jung, Y. Park, K. Yoon, S. Park and J. Yu, Synthesis of monodisperse spherical silica particles with solid core and mesoporous shell: mesopore channels perpendicular to the surface, *Journal of Materials Chemistry*, **2007**, 17, 1758–1761.

[361] J. Glennon and J. Omamogho, A process for preparing silica particles, WO2010061367.

[362] K. K. Unger, H. Giesche and J. Kinkel, Spherical SiO_2 particles, US4911903.

[363] T. Wei, W. Chen and W. Barber, Superficially porous metal oxide particles, methods for making them, and separation devices using them, US2010051877.

[364] A. Ahmed, H. Ritchie, P. Myers and H. Zhang, One-Pot Synthesis of Spheres-on-Sphere Silica Particles from a Single Precursor for Fast HPLC with Low Back Pressure, *Advanced Materials*, **2012**, 24, 45, 6042.

[365] U. Neue, T. Walter, B. Alden, Z. Jiang, R. Fisk, J. Cook, K. Glose, J. Carmody, J. Grassi, Y. Cheng, Z. Lu and R. Crowley, Use of high-performance LC packings from pH 1 to pH 12, *American Laboratory*, **1999**, 31, 36.

[366] Z. Jiang, R. P. Fisk, J. E. O'Gara, T. H. Walter and K. D. Wyndham, Porous inorganic/organic hybrid particles for chromatographic separations and process for their preparation, US2002070168.

[367] J. Choi, C. Kim and D. Kim, Formation and characterization of monodisperse, spherical organo-silica powders from organo-alkoxysilane-water system, *Journal of the American Ceramic Society*, **1998**, 81, 5, 1184–1188.

[368] M. Trau and A. Johnston, Synthesis and use of organosilica particles, US20030124564.

[369] C. Miller, R. Vogel, P. Surawski, K. Jack, S. Corrie and M. Trau, Functionalized organosilica microspheres via a novel emulsion-based route, *Langmuir*, **2005**, 21, 21, 9733–9740.

[370] K. D. Wyndham, B. W. Muriithi, M. F. Morris and N. L. Lawrence, Superficially porous materials comprising a substantially nonporous core having narrow particle size distributions; process for the preparation thereof; and use thereof for chromatographic separations, WO2012018598.

[371] D. J. Kim, J. S. Chung, W. S. Ahn, G. W. Kam and W. J. Cheong, Morphology control of organic-inorganic hybrid mesoporous silica by microwave heating, *Chemistry Letters*, **2004**, 33, 4, 422–423.

[372] V. Rebbin, M. Jakubowski, S. Potz and M. Fröba, Synthesis and characterisation of spherical periodic mesoporous organosilicas (sph-PMOs) with variable pore diameters, *Microporous and Mesoporous Materials*, **2004**, 72, 1-3, 99–104.

[373] Y. D. Xia, Z. X. Yang and R. Mokaya, Molecularly ordered ethylene-bridged periodic mesoporous organosilica spheres with tunable micrometer sizes, *Chemistry of Materials*, **2006**, 18, 5, 1141–1148.

[374] M. P. Kapoor and S. Inagaki, Synthesis of phenylene bridged mesoporous silsesquioxanes with spherical morphology in ammonia solution, *Chemistry Letters*, **2004**, 33, 2, 88–89.

[375] V. Rebbin, R. Schmidt and M. Fröba, Spherical particles of phenylene-bridged periodic mesoporous organosilica for high-performance liquid chromatography, *Angewandte Chemie-Int. Edition*, **2006**, 45, 31, 5210–5214.

[376] G. Zhu, D. Jiang, Q. Yang, J. Yang and C. Li, trans-(1R,2R)-diaminocyclohexane-functionalized mesoporous organosilica spheres as chiral stationary phase, *Journal of Chromatography A*, **2007**, 1149, 2, 219–227.

[377] C. Li, B. Di, W. Q. Hao, F. Yan and M. X. Su, Aminopropyl-functionalized ethane-bridged periodic mesoporous organosilica spheres: Preparation and application in liquid chromatography, *Journal of Chromatography A*, **2011**, 1218, 3, 408–415.

[378] L. T. Wang, S. Q. Dong, F. Han, Y. W. Zhao, X. Zhang, X. L. Zhang, H. D. Qiu and L. Zhao, Spherical beta-cyclodextrin-silica hybrid materials for multifunctional chiral stationary phases, *Journal of Chromatography A*, **2015**, 1383, 70–78.

[379] S. Haffer, M. Tiemann and M. Fröba, Periodic Mesoporous Organosilica (PMO) materials with uniform spherical core-shell structure, *Chemistry - A European Journal*, **2010**, 16, 34, 10447–10452.

[380] J. Ekeroth, Silica Based Material, WO2007070001.

[381] T. Wei, W. Chen and W. Barber, Inorganic/organic hybrid totally porous metal oxide particles, methods for making them and separation devices using them, US2010055000.

[382] H. Yu, C. Y. Jia, H. B. Wu, G. J. Song, Y. Jin, Y. X. Ke and X. M. Liang, Highly stable high performance liquid chromatography stationary phase based on direct chemical modification of organic bridges in hybrid silica, *Journal of Chromatography A*, **2012**, 1247, 63–70.

[383] C. Chu and R. Liu, Application of click chemistry on preparation of separation materials for liquid chromatography, *Chemical Society Reviews*, **2011**, 40, 5, 2177–2188.

[384] A. Marechal, R. El-Debs, V. Dugas and C. Demesmay, Is click chemistry attractive for separation sciences?, *Journal of Separation Science*, **2013**, 36, 13, 2049–2062.

[385] C. Wu, Y. Liang, K. G. Yang, Y. Min, Z. Liang, L. H. Zhang and Y. K. Zhang, Clickable Periodic Mesoporous Organosilica Monolith for Highly Efficient Capillary Chromatographic Separation, *Analytical Chemistry*, **2016**, 88, 3, 1521–1525.

[386] *Global laboratory analytical instrumentation market*, Frost and Sullivan, **2015**.

[387] *Industry Analysis, Size, Share, Growth, Trends and Forecast*, Global Chromatography Systems Market, **2013-2019**.

[388] A. Katiyar, S. Yadav, P. G. Smirniotis and N. G. Pinto, Synthesis of ordered large pore SBA-15 spherical particles for adsorption of biomolecules, *Journal of Chromatography A*, **2006**, 1122, 1-2, 13–20.

[389] E. Cho, D. Kim and M. Jaroniec, Periodic mesoporous organosilicas with multiple bridging groups and spherical morphology, *Langmuir*, **2007**, 23, 23, 11844–11849.

[390] D.-D. Jiang, Q. Wei, S.-P. Cui, W.-Y. Chen, Z.-R. Nie, X.-Y. Yue and Q.-Y. Li, Controllable morphology and pore structure of micron-sized organic-inorganic hybrid silica spheres derived from silsesquioxane, *Journal of Sol-Gel Science and Technology*, **2016**, 78, 1, 40–49.

[391] J. Armstrong, B. Chowdhry, J. Mitchell, A. Beezer and S. Leharne, Effect of cosolvents and cosolutes upon aggregation transitions in aqueous solutions of the poloxamer F87 (Poloxamer P237): A high sensitivity differential scanning calorimetry study, *Journal of Physical Chemistry*, **1996**, 100, 5, 1738–1745.

[392] S. S. Soni, G. Brotons, M. Bellour, T. Narayanan and A. Gibaud, Quantitative SAXS analysis of the P123/water/ethanol ternary phase diagram, *Journal of Physical Chemistry B*, **2006**, 110, 31, 15157–15165.

[393] C. Vercaemst, H. Friedrich, P. E. de Jongh, A. V. Neimark, B. Goderis, F. Verpoort and P. Van Der Voort, Periodic Mesoporous Organosilicas consisting of 3D hexagonally ordered interconnected globular pores, *Journal of Physical Chemistry C*, **2009**, 113, 14, 5556–5562.

[394] J. Liu, S. Bai, H. Zhong, C. Li and Q. Yang, Tunable assembly of organosilica hollow nanospheres, *Journal of Physical Chemistry C*, **2010**, 114, 2, 953–961.

[395] J. G. Croissant, X. Cattoen, M. W. C. Man, J. O. Durand and N. M. Khashab, Syntheses and applications of periodic mesoporous organosilica nanoparticles, *Nanoscale*, **2015**, 7, 48, 20318–20334.

[396] Y. Ma, L. Qi, J. Ma, Y. Wu, O. Liu and H. Cheng, Large-pore mesoporous silica spheres: synthesis and application in HPLC, *Colloids and Surfaces A-Physicochemical and Engineering Aspects*, **2003**, 229, 1-3, 1–8.

[397] S. Liu, P. Cool, O. Collart, P. Van Der Voort, E. Vansant, O. Lebedev, G. Van Tendeloo and M. Jiang, The influence of the alcohol concentration on the structural ordering of mesoporous silica: Cosurfactant versus cosolvent, *Journal of Physical Chemistry B*, **2003**, 107, 38, 10405–10411.

[398] P. Van Der Voort, P. Ravikovitch, K. De Jong, A. Neimark, A. Janssen, M. Benjelloun, E. Van Bavel, P. Cool, B. Weckhuysen and E. Vansant, Plugged hexagonal templated silica: a unique micro- and mesoporous composite material with internal silica nanocapsules, *Chemical Communications*, **2002**, 9, 1010–1011.

[399] M. Thommes, K. Kaneko, A. Neimark, J. Olivier, F. Rodriguez-Reinoso, J. Rouquerol and K. Sing, Physisorption of gases, with special reference to the evaluation of surface area and pore size distribution (IUPAC Technical Report), *Pure and Applied Chemistry*, **2015**, 87, 9-10, 1051–1069.

[400] J. H. Kim, S. B. Yoon, J.-Y. Kim, Y. B. Chae and J.-S. Yu, Synthesis of monodisperse silica spheres with solid core and mesoporous shell: Morphological control of mesopores, *Colloids and Surfaces A-Physicochemical and Engineering Aspects*, **2008**, 313, 77–81.

[401] F. Goethals, E. Levrau, E. De Canck, M. R. Baklanov, C. Detavernier, I. Van Driessche and P. Van Der Voort, Pore narrowing of mesoporous silica materials, *Materials*, **2013**, 6, 2, 570–579.

[402] B. Muriithi, Solid core particles for high pH chromatographic separations, Lecture, 5th International Conference on Multifunctional, Hybrid and Nanomaterials, Lisbon, Portugal, **2017**.

[403] Y. Chen, P. Xu, H. Chen, Y. Li, W. Bu, Z. Shu, Y. Li, J. Zhang, L. Zhang, L. Pan, X. Cui, Z. Hua, J. Wang, L. Zhang and J. Shi, Colloidal HPMO nanoparticles: silica-etching chemistry tailoring, topological transformation, and nano-biomedical applications, *Advanced Materials*, **2013**, 25, 22, 3100–3105.

[404] Z. Sun, Y. Liu, B. Li, J. Wei, M. Wang, Q. Yue, Y. Deng, S. Kaliaguine and D. Zhao, General synthesis of discrete mesoporous carbon microspheres through a confined self-assembly process in inverse opals, *ACS Nano*, **2013**, 7, 10, 8706–8714.

[405] M. Rosen and J. Kunjappu, *Surfactants and interfacial phenomena - Fourth edition*, John Wiley and Sons, **2012**.

[406] C. Barbé, J. Bartlett, L. Kong, K. Finnie, H. Lin, M. Larkin, S. Calleja, A. Bush and G. Calleja, Silica particles: A novel drug-delivery system, *Advanced Materials*, **2004**, 16, 21, 1959–1966.

[407] I. A. Inc., The HLB system: a time-saving guide to emulsifier selection, http://www.firp.ula.ve/archivos/historicos/76_Book_HLB_ICI.pdf.

[408] M. Nystrom, W. Herrmann and B. Larsson, Method for prepartion of silica particles, US5256386.

[409] M. M. Dragosavac, G. T. Vladisavljevic, R. G. Holdich and M. T. Stillwell, Production of Porous Silica Microparticles by Membrane Emulsification, *Langmuir*, **2012**, 28, 1, 134–143.

[410] T. Mason and J. Bibette, Shear rupturing of droplets in complex fluids, *Langmuir*, **1997**, 13, 17, 4600–4613.

[411] C. Mabille, V. Schmitt, P. Gorria, F. Calderon, V. Faye, B. Deminiere and J. Bibette, Rheological and shearing conditions for the preparation of monodisperse emulsions, *Langmuir*, **2000**, 16, 2, 422–429.

[412] I. Kobayashi, S. Mukataka and M. Nakajima, Effect of slot aspect ratio on droplet formation from silicon straight-through microchannels, *Journal of Colloid and Interface Science*, **2004**, 279, 1, 277–280.

[413] S. Omi, Preparation of monodisperse microspheres using the Shirasu porous glass emulsification technique, *Colloids and Surfaces A-Physicochemical and Engineering Aspects*, **1996**, 109, 97–107.

[414] J. Arika, E. Shiota and K. Yamamote, Spherical micro-porous silica gel and a production process thereof, US4554211.

[415] M. Ipponmatsu, M. Nishigaki, H. Akira and T. Tsurutani, Uniform inorganic microspheres and production thereof, US5376347.

[416] J. Park, C. Oh, S. Shin, S. Moon and S. Oh, Preparation of hollow silica microspheres in W/O emulsions with polymers, *Journal of Colloid and Interface Science*, **2003**, 266, 1, 107–114.

[417] W. Li, X. Sha, W. Dong and Z. Wang, Synthesis of stable hollow silica microspheres with mesoporous shell in nonionic W/O emulsion, *Chemical Communications*, **2002**, 20, 2434–2435.

[418] A. Imhof and D. Pine, Ordered macroporous materials by emulsion templating, *Nature*, **1997**, 389, 6654, 948–951.

[419] C. Oh, S. Chung, S. Shin, Y. Kim, S. Im and S. Oh, Distribution of macropores in silica particles prepared by using multiple emulsions, *Journal of Colloid and Interface Science*, **2002**, 254, 1, 79–86.

[420] H. Zhang, G. Hardy, M. Rosseinsky and A. Cooper, Uniform emulsion-templated silica beads with high pore volume and hierarchical porosity, *Advanced Materials*, **2003**, 15, 1, 78.

[421] N. Ma, Y. Deng, W. Liu, S. Li, J. Xu, Y. Qu, K. Gan, X. Sun and J. Yang, A one-step synthesis of hollow periodic mesoporous organosilica spheres with radially oriented mesochannels, *Chemical Communications*, **2016**, 52, 17, 3544–3547.

[422] A. Bennett, C. Rienstra, M. Auger, K. Lakshmi and R. Griffin, Heteronuclear decoupling in rotating solids, *Journal of Chemical Physics*, **1995**, 103, 6951–6958.

[423] S. Clerick, E. De Canck, K. Hendrickx, V. Van Speybroeck and P. Van Der Voort, Heterogeneous Ru(III) oxidation catalysts via click bidentate ligands on a periodic mesoporous organosilica support, *Green Chemistry*, **2016**, 18, 22, 6035–6045.

[424] J. Bibette, D. Roux and F. Nallet, Depletion interactions and fluid-solid equilibrium in emulsions, *Physical Review Letters*, **1990**, 65, 19, 2470–2473.

[425] J. Bibette, Depletion interactions and fractionated crystallization for polydisperse emulsion purification, *Journal of Colloid and Interface Science*, **1991**, 147, 2, 474–478.

[426] K. Min and W. Goldburg, Nucleation of a binary-liquid mixture under steady-state shear, *Physical Review Letters*, **1993**, 70, 4, 469–472.

[427] T. Mason and J. Bibette, Emulsification in viscoelastic media, *Physical Review Letters*, **1996**, 77, 16, 3481–3484.

[428] J. Bibette and T. Mason, Emulsion manufacturing process, US5938581.

[429] M. G. Buonomenna, Membrane processes for a sustainable industrial growth, *RSC Advances*, **2013**, 3, 17, 5694–5740.

[430] S. Joscelyne and G. Tragardh, Membrane emulsification - a literature review, *Journal of Membrane Science*, **2000**, 169, 1, 107–117.

[431] T. Nakashima, M. Shimizu and M. Kukizaki, Particle control of emulsion by membrane emulsification and its applications, *Advanced Drug Delivery Reviews*, **2000**, 45, 1, 47–56.

[432] E. Piacentini, E. Drioli and L. Giorno, Membrane emulsification technology: Twenty-five years of inventions and research through patent survey, *Journal of Membrane Science*, **2014**, 468, 410–422.

[433] I. Kobayashi, M. Nakajima, H. Nabetani, Y. Kikuchi, A. Shohno and K. Satoh, Preparation of micron-scale monodisperse oil-in-water microspheres by microchannel emulsification, *Journal of the American Oil Chemists Society*, **2001**, 78, 8, 797–802.

[434] N. Andersson, B. Kronberg, R. Corkery and P. Alberius, Combined emulsion and solvent evaporation (ESE) synthesis route to well-ordered mesoporous materials, *Langmuir*, **2007**, 23, 3, 1459–1464.